XPS and STM studies of simple and complex molecules at Cu(110) and Ag(111) surfaces

Darran Richards

School of Chemistry
University of Wales, Cardiff
September 2007

ProQuest LLC
789 East Eisenhower Parkway
P.O. Box 1346
Ann Arbor, MI 48106-1346

Declaration/Statements

CANDIDATE'S ID NUMBER	0232638
CANDIDATE'S SURNAME	**Please circle appropriate value** **Mr / ~~Miss~~ / ~~Ms~~ / ~~Mrs~~ / ~~Rev~~ / ~~Dr~~ / Other please specify .....**
CANDIDATE'S FULL FORENAMES	DARRAN RICHARDS

DECLARATION

This work has not previously been accepted in substance for any degree and is not concurrently submitted in candidature for any degree.

Signed ..... (candidate)

Date 19/5/18

STATEMENT 1

This thesis is being submitted in partial fulfillment of the requirements for the degree of .....(insert MCh, Md, MPhil, PhD etc, as appropriate)

Signed ..... (candidate)

Date 19/5/18

STATEMENT 2

This thesis is the result of my own independent work/investigation, except where otherwise stated.
Other sources are acknowledged by footnotes giving explicit references.

Signed ..... (candidate)

Date 19/5/18

STATEMENT 3

I hereby give consent for my thesis, if accepted, to be available for photocopying and for inter-library loan, and for the title and abstract to be made available to outside organisations.

Signed ..... (candidate)

Date 19/5/18

Abstract

The adsorption of aniline at a clean and oxidised Cu(110) surface has been studied using STM and XPS at 295K. Adsorption at a partially oxidised surface results in formation of a phenyl imide. Co-adsorption of aniline and oxygen resulted in a closer packed surface. Concentrations calculated using XPS were twice that of concentrations calculated using unit cells determined by STM. Two models were proposed to account for this discrepancy. The first involved alternating parallel and perpendicular phenyl rings with respect to the surface. The favoured proposal on a basis of the steric hindrance involves parallel pi-stacking of the phenyl rings.

The interaction of gaseous malonyl dichloride ($C_3H_2Cl_2O_2$) with clean Cu(110) and partially oxidised Cu(110) surface has been studied. At low temperatures, malonyl dichloride physisorbed at the surface. Malonyl dichloride will only adsorb at a Cu(110) surface in the presence of oxygen at room temperature. This indicates that oxygen activates a reaction with malonyl dichloride at the Cu(110) surface.

The interaction of melamine with clean and oxidised Cu(110) and clean Ag(111) has been studied. Melamine adsorption at a Cu(110) and Ag(111) surface resulted in molecular adsorption. Adsorption of melamine and malonyl dichloride at a Cu(110) surface resulted in a reaction occurring leading to Cl adsorption but no effect on melamine. The binding energies do suggest that melamine is adsorbed molecularly at the surface but chlorine was also present. A co-adsorption of melamine and malonyl dichloride at an Ag(111) surface produced a surface with melamine molecularly adsorbed and also chlorine present. Pre-adsorbed melamine was exposed to cesium. Cesium atoms adsorbed on the supramolecular network created by melamine at an Ag(111) surface.

The interaction of biphenyl dicarboxylic acid (BPDCA) with clean and oxidised Cu(110) and Ag(111) surfaces has been studied. Chemisorption occurred at a clean Cu(110) surface. Predominantly, the substrate-adsorbate interaction was too strong for any supramolecular structures to be formed. The adsorption of BPDCA at an Ag(111) surface resulted in various structures that were affected by concentration. Both the

carboxylic groups and the phenyl rings played a part in the creation of the various supramolecular structures at the surface. The weaker substrate decreased the adsorbate-substrate interactions and allowed more freedom for intermolecular interactions.

Acknowledgements

The following people played a very important part in my project and without them none of the project would have been achievable. My very sincere thanks go to the following -

Dr Phil Davies for allowing me to undertake this project and for the help and enthusiasm throughout the project.

Dr David Morgan for all his help in every part of surface science. All his teachings have been invaluable.

Dr Dyfan Edwards for all his help at the beginning and constant patience.

Dr Albert Carley for his XPS expertice.

To all those who constantly had to help me take the covers on and off.

To my wife, without you this would not have been possible
Thank you

Glossary

All gas exposures are expressed in Langmuirs, L, defined as 10^{-6} torr s.

A chemisorbed oxygen monolayer at Cu(110) surfaces is defined as 5.5×10^{14} atoms cm^{-2}.

AES . . . . . Auger Electron Spectroscopy
ARUPS . . . . . Angle Resolved Ultraviolet Photoelectron Spectroscopy
ARXPS . . . . . Angle Resolved X-ray Photoelectron Spectroscopy
EELS . . . . . Electron Energy Loss Spectroscopy
HREELS . . . . . High Resolution Electron Energy Loss Spectroscopy
IR . . . . . Infrared
LEED . . . . . Low Energy Electron Diffraction
RAIRS . . . . . Reflection Absorption Infrared Spectroscopy
SES . . . . . Secondary Electron Spectroscopy
SEXAFS . . . . . Surface Extended X-ray Absorption Fine Structure
SPM . . . . . Scanning Probe Microscopy
STM . . . . . Scanning Tunnelling Microscopy
STS . . . . . Scanning Tunnelling Spectroscopy
TPD . . . . . Temperature Programmed Desorption
VEELS . . . . . Vibrational Electron Energy Loss Spectroscopy
XPS . . . . . X-ray Photoelectron Spectroscopy
UHV . . . . . Ultra-High Vacuum
UPS . . . . . Ultraviolet Photoelectron Spectroscopy

Contents

Chapter 4
Instrumentation

Chapter 5
Aniline

Chapter 6
Malonyl dichloride

Chapter 7
Melamine

Chapter 1

Introduction

1.1 Surface Science

Technologies that are used everyday such as heterogeneous catalysis, molecular electronics, functional coatings and nanotechnology are fundamentally connected to surface science. To improve the technologies it is important to study the chemistry of the interactions of molecules with surfaces. The chemistry of a system can be altered using various adsorbates. Using STM it is possible to calculate the structure of adsorbates at the surface. XPS allows us to determine what chemical groups are present.

Heterogeneous catalysis is a very important aspect of technology. It is much easier to study heterogeneous catalysis in model systems. In this case the model systems involve adsorption of gaseous substances on single crystals. Catalysis aims to control the rate of a

chemical reaction. In order to achieve this it is important to understand the mechanism in which molecules interact with the surface. Heterogeneous catalysis depends on at least one reactant being physisorbed or chemisorbed.

Using molecular assemblies for a variety of electronic applications is more relevant to the experiments that took place at copper and silver surfaces. An important feature that was looked at throughout the thesis was the self assembly fabrication technique. This involves the self assembly of molecules into higher order structures. STM is incredibly useful in studying molecular devices such as molecular wires, once they have been fabricated.

Nanostructured materials can be defined as those materials whose structured elements have dimensions in the 1 to 100nm range. Nanotechnology involves the use of nanoscale systems to guide the placements of reactive materials. A molecular template can be created and used to position various metal clusters. The focus of this thesis is the interaction between template molecules and the interaction these template molecules have with the surface.

1.2 Single Crystal Metal Surfaces

To discuss surface processes, the type of surface on which that adsorption is taking place must first be considered. Much of the work in this study considers two surfaces, Cu(110) and Ag(111) single crystals. Crystal planes are defined by their Miller indices [1]. The surface is defined as a section cleaved from a crystalline solid. This forms a well defined crystal plane. Different planes may be yielded through cleaving the solid at varying angles.

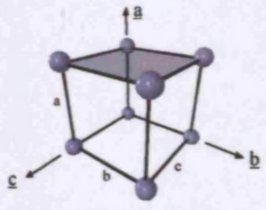

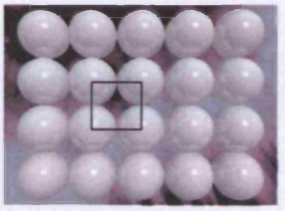

$$\left(\frac{a}{a},\frac{b}{\infty},\frac{c}{\infty}\right)\rightarrow(100)$$

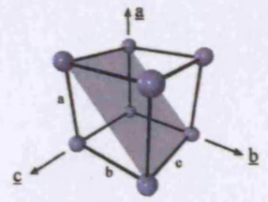

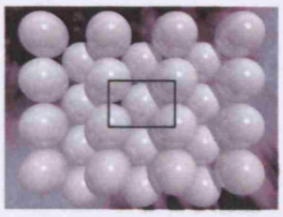

$$\left(\frac{a}{a},\frac{b}{b},\frac{c}{\infty}\right)\rightarrow(110)$$

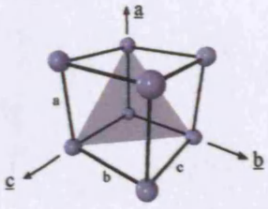

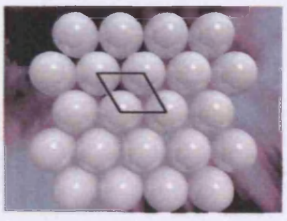

$$\left(\frac{a}{a},\frac{b}{b},\frac{c}{c}\right)\rightarrow(111)$$

Figure 1.1. Identification of the low-index crystal lattice planes using Miller indices.

Figure 1.1 indicates how Miller indices are based on the points of intersection of the surface plane with a lattice unit cell. For the (110) surface, the crystal plane intersects the **a** axis of the unit cell at a distance a and intersects the **b** axis at a distance b from the origin while extending infinitely along the and **c** axis (i.e. a, b, ∞). The fractional indices are removed by multiplying the whole indice. It has been demonstrated numerous times that characterising the crystal plane is important due to the fact that surface reactivity is related to the crystal plane. Somorjai *et al* [2] for example reported three low index surfaces of iron exhibited contrasting reactivity to ammonia.

In practice, atomically smooth surfaces are impossible to achieve. This is because defect structures can be created in a number of ways and are always present. These defect structures can have a large effect on surface reactivity as they can provide an initial reaction site for adsorption of diffusing gas molecules. The defective sites can offer more substrate interaction due to more area of substrate available. Some of the topographical features are shown below in figure 1.2. It must be noted that atoms at defect sites are of low co-ordination and are less strongly bound to the bulk than those at the flat surface making them more reactive.

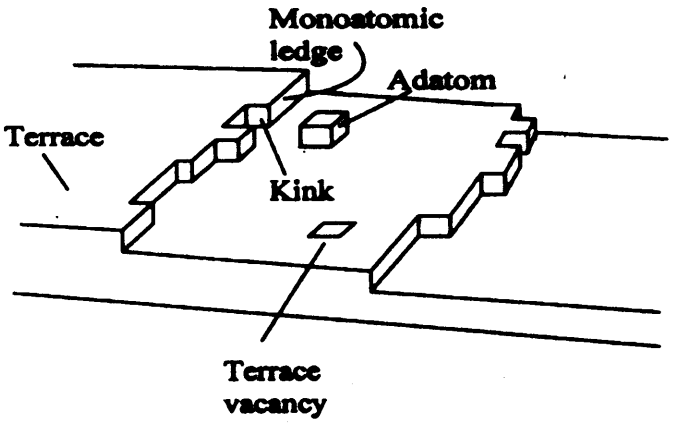

Figure 1.2. Surface Defects [3]

1.3 Adsorption

It is possible to classify most solid-gas reactions according to one of four types; physical adsorption, chemical adsorption, solution (or absorption), or bulk compound formation. All experiments contained in this thesis are only concerned with surface reactions therefore only physical and chemical adsorption will be discussed.

1.3(a) Physisorption and Chemisorption

Molecules impinging onto a surface can either undergo elastic collisions, and therefore be reflected from the surface with no net change in total energy, or undergo inelastic collisions and lose energy. If the loss of energy (lost from the molecule by diffusing across the surface) is large enough to prevent it being reflected from the surface then it will become bound to the surface [4].

For physical adsorption the molecule is held only weakly to the surface by weak long range Van der Waals type forces, and there is no significant redistribution of electron density in either the molecule or the substrate surface. The heat of adsorption (ΔH^0_{AD}) associated with physisorption is of the order of the enthalpy of condensation, < 35 kJ

mol^{-1}. Physisorption is non-dissociative and reversible. There is no significant limit to the saturation coverage and the surface structure has no effect on the physisorption.

Unlike physical adsorption, chemical adsorption involves a chemical bond, thereby resulting in substantial rearrangement of electron density between the adsorbate and substrate. Chemisorption involves a high degree of specificity dependent upon the structure and chemical nature of the surface. This specificity is shown in the varied heats of adsorption for chemisorbed molecules. The enthalpy of chemisorption is far greater than that of physisorption, typically ~ 200 kJ mol^{-1}. As with ordinary chemical reactions chemisorption proceeds until a definite surface stoichiometry is reached, and then stops at a point corresponding to a monolayer. Chemisorption can be either molecular or dissociative, and the nature of the resulting bond may lie anywhere between the extremes of ionic or covalent behaviour.

1.3(b) Physical Adsorption

A physisorbed molecule retains its identity, due to the fact that Van der Waals forces are weak long range interactions. Distortion of the adsorbed molecule due to the interaction with the surface may occur. The surface can adsorb the small amounts of energy released through physisorption as vibrations of the lattice and dissipate the energy as thermal motion. The vibrational energy depends on the surface temperature. As the surface temperature increases, this can cause the vibrational energy to increase above the desorption energy (E_D) enabling the molecule to escape from the surface. The residence time (τ) of a physisorbed molecule will depend on the surface temperature and is given by the Frenkel equation.

$$\tau = \tau_0 \exp\left(\frac{E_D}{KT}\right) \ldots 1.1$$

Where, τ_0 is the period of oscillation of the molecule at the surface, typically 10^{-13} seconds at 300K and E_D is the desorption energy.

1.3(c) Chemical adsorption

Chemisorption can be separated into two categories; molecular chemisorption, and dissociative chemisorption. The potential energy curves are shown below. It must be noted that chemisorption shows deeper potential energy wells than physisorption. As the incoming molecule approaches the surface it becomes physisorbed into a chemisorption precursor state. A potential energy barrier exists between this precursor and the chemisorbed state due to the deformation of the adsorbate bond (often leading to dissociation) and rearrangement of the substrate atoms.

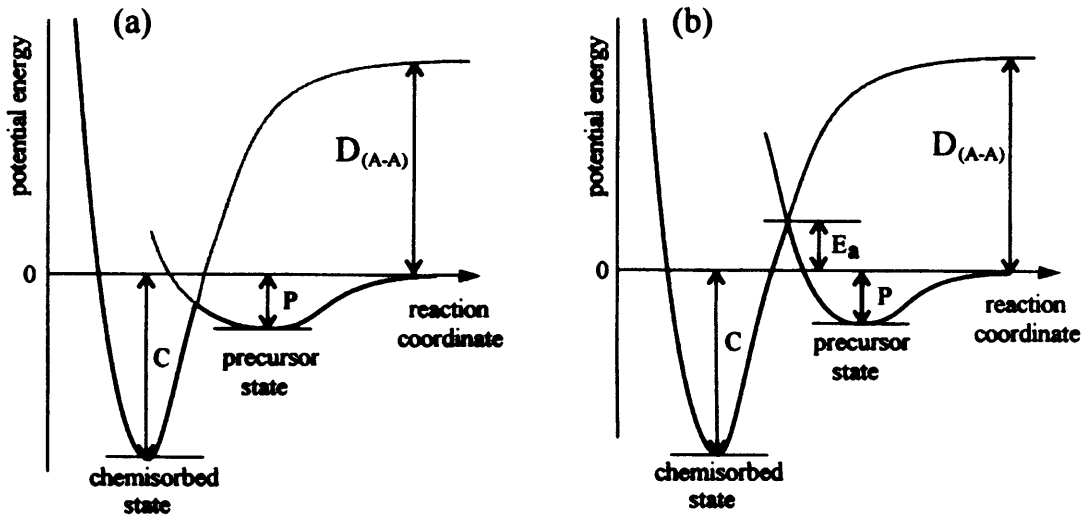

Figure 1.3. Potential energy diagrams for non-activated (a) and activated (b) chemisorption processes [5].

1.4(a) Kinetics of adsorption

The rate of adsorption is controlled by two main factors. These are the arrival rate of molecules at the surface and the proportion of these molecules adsorbing onto the surface (the sticking probability).

Rate of adsorption (R_{ads}) = Sticking probability (S) x incident flux (F)

These quantities can be expressed as follows:

The incident flux is given by the Hertz-Knudsen equation:

$$F = \frac{P}{(2\pi.m.k.T)^{\frac{1}{2}}} \quad (1.2)$$

Where P = pressure
m = mass of gas atom/molecule
k = Boltzman constant
T = temperature

The sticking probability has a value between 0 and 1, and depends on the presence and magnitude of an activation barrier to adsorption, and the concentration of previously adsorbed atoms or molecules, n_a, this can be expressed as follows:

$$S = f(n_a).\exp^{\left(-\frac{E_a}{RT}\right)} \quad (1.3)$$

Where $f(n_a)$ is a term taking into account the effect previously adsorbed atoms or molecules may have on there further adsorption. E_a is the activation energy for adsorption.

Combining the equations yields the following equation for the rate of adsorption:

$$R = \frac{f(n_a).P}{\sqrt{2.\pi.m.k.T}} \exp^{\left(-\frac{E_a}{RT}\right)} \quad (1.4)$$

1.4(b) Thermodynamics of adsorption

The Gibbs-Helmholtz equation (equation 1.5) states that for a reaction to be spontaneous, ΔG must be negative.

$$\Delta G = \Delta H - T\Delta S \quad (1.5)$$

Chemisorption is usually accompanied by an entropy decrease (since the translational freedom of the gas molecule is significantly reduced upon adsorption), so the process must be exothermic.

1.5 References

[1] P. W. Atkins, *Physical Chemistry 4th edition,* Oxford University Press (1990).

[2] N. D. Spencer, R. C. Schoonmaker and G. A. Somorjai, *J. Catal.* 74 (1982) 643.

[3] P. W. Atkins, *Physical Chemistry 4th edition,* Oxford University Press (1990).

[4] D.O. Hayward and B.M.W. Trapnell in *Chemisorption*, Butterworths, London (1964).

[5] P. H. Holloway, *J. Vac. Sci. Technol.*, 18 (1981) 653.

Chapter 2

Photoelectron Spectroscopy

2.1 X-Ray Photoelectron Spectroscopy

Originally discovered by Wilhelm Roetgen in the nineteenth century, X-rays have become one of the most useful applications of spectroscopy in science. XPS originated in 1887 with the discovery of the photoelectric event by H. Hertz [1]. X-ray spectroscopy is an analytical technique with a broad range of applications, particularly in determining crystal structure and elemental analysis of solid samples.

X-Ray Photoemission Spectroscopy (XPS, formerly known as ESCA - Electron Spectroscopy for Chemical Analysis) was developed at Uppsala University, Sweden in the 60's by a group headed by Kai Siegbahn, who in 1981 won the Nobel Prize for Physics for his work in developing the technique. Kai Siegbahn developed a high resolution spectrometer which allowed the measurement of accurate binding energies of photoelectron peaks [2]. This finding realised the goal for using XPS for electronic structure investigation. The same group observed a chemical shift for binding energy of core electrons [3]. This lead to the development of the whole field of electron spectroscopy for chemical analysis.

2.2 Fundamentals

The phenomenon of X-ray photoelectron spectroscopy is based upon the photoelectric effect outlined by Einstein in 1905 [4]. This involved exposing a metallic surface and causing adsorption of electromagnetic radiation that is above the threshold frequency (particular to each type of surface). A current is then produced. No electrons are emitted for radiation below the threshold frequency, as they cannot gain sufficient energy to overcome their atomic bonding. The electrons that are emitted are often termed photoelectrons.

The energy of a photon is given by Einsteins equation –

$$E = h\nu \quad (1)$$

Where h - Planck constant (6.62×10^{-34} J s) and ν - frequency (Hz) of the radiation. Although X-ray photoelectron spectroscopy can be used for chemical analysis, it is fundamentally a surface technique, and cannot provide completely reliable analytical data for bulk samples.

The photon is adsorbed by an atom in a molecule or solid. Absorption of these photons causes ejection of an electron. There is a threshold frequency needed to eject an electron, which is based on the work function (f) for the material: $n_c = ef/h$ ($f \sim$ 2-6 eV). This amount of energy is needed to take an electron from the Fermi level to remove it to the vacuum. Therefore, photons with frequency $n > n_c$ are needed.

Adsorption of a photon and ejection of an electron is known as the photoelectric effect. X-ray photoelectron spectroscopy requires radiation which is energetic enough to eject core electrons.

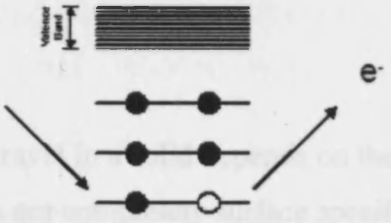

Figure 2.1: The photoemission process for XPS

Although core electrons are not generally involved in chemical bonding, electron binding energies are affected by the local environment and the intensities of the resulting peaks provide information on the composition of a sample. The electron emitted will have a characteristic binding energy given by Einstein's equation – 2

$$E_{kin} = h\nu - E_B \quad (2)$$

$h\nu$ represents the photon energy and E_B represents the binding energy of the electron in the solid [5].

2.3 Koopmans' Theorem

Koopmans' theorem is an approximation used to interpret photoelectron spectra. According to Koopmans' theorem the binding energy measured by XPS should be equal to the calculated orbital energy [6]. This assumption is known as "The Frozen orbital approximation" [7]. For this to be true the orbital that the electron came from cannot undergo any transformations while the electron departs. Also the photoelectron cannot interact with the cloud of electrons surrounding the atom as it exits. If there is any electronic relaxation (a change in the molecular orbitals of an ionized molecule because of a change in electronic repulsions), or if there is a change in correlations, then the Koopmans' theorem breaks down.

Screening does occur when a photoelectron exits an inner orbital. Therefore Einstein's equation can be more accurately written as –

$$(E\ final - E\ initial) = hv\text{-}Ek \quad (3)$$

2.4 Surface sensitivity

The distance an electron can travel in a solid depends on the material and the kinetic energy of the electron. XPS is not completely surface specific. Most of the signal comes from within a few atomic layers of the surface; however a small part of the signal comes from deeper depths of the solid.

The soft X-rays employed in XPS penetrate a substantial distance into the sample (~μm). Therefore, this excitation conveys no surface sensitivity at the required atomic scale. The surface sensitivity arises from the emission and detection of the photoemitted electrons. There are two factors that can prevent an emitted electron from being detected; if it was captured before reaching the surface or if it lost energy before reaching the surface, i.e. if it escaped from the solid and reached the detector. The process in which an electron can lose energy as it travels through the solid is known as "inelastic scattering". The probability of an electron leaving the surface decreases with depth. This can be described by the inelastic free path.

The inelastic scattering can be quantified by the parameter λ. This is referred to as the inelastic mean free path. The inelastic mean free path is the average distance travelled by an electron through a solid before it is inelastically scattered; it is dependent upon

- The initial kinetic energy of the electron.
- The nature of the solid

The inelastic mean free path can be calculated from the following equation.

$$P(d) = \exp (- d / \lambda) \quad (4)$$

The equation gives the probability of the electron travelling a distance, d, through the solid without undergoing scattering. λ is the inelastic mean free path for the electrons of energy E.

XPS is therefore a surface sensitive technique as the mean free path of photoelectrons is of the order of a few nanometres in a solid. Electrons originating further below the surface suffer energy loss through collisions and may not even escape the surface. Scattered electrons contribute to the continuous background situated at lower kinetic energy.

It has been shown experimentally [8] that the mean free path of electrons for inelastic scattering depends on the kinetic energy of the emitted electrons. This can be shown graphically in the form of a curve.

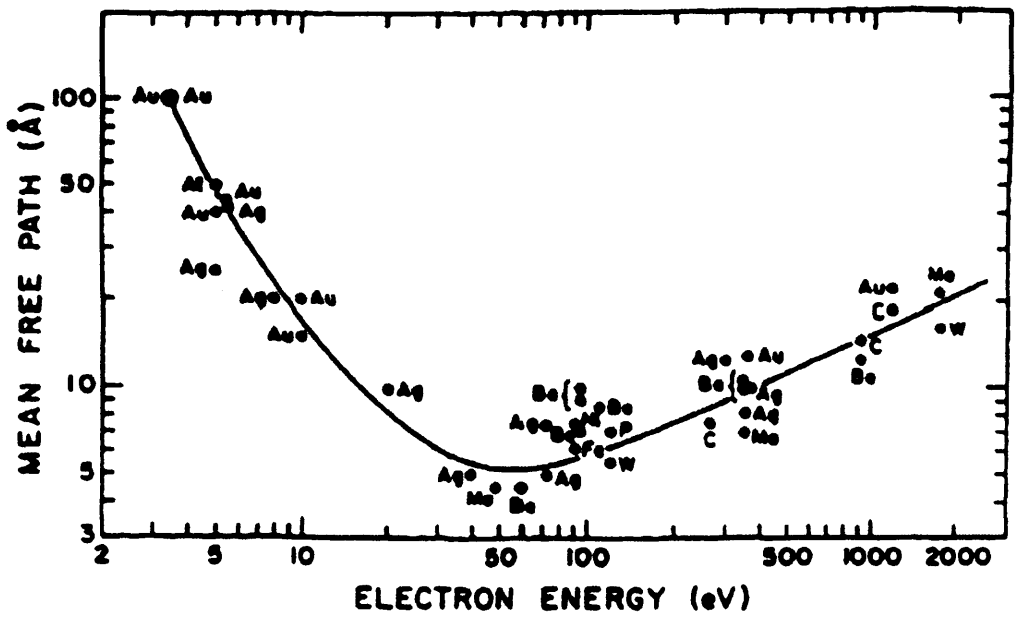

Fig 2.2; "Universal curve" of electron *inelastic mean free path* l (IMFP) versus KE (eV)

2.5 Final State effects

Final state effects are those factors that influence the charge state of an atom after the photon has hit it, or affect the photoelectron while is it leaving. This affects the kinetic energy of the photoelectron and therefore can result in a change in the binding energy. The following factors are final state effects.

2.5 (a) Relaxation

The photoemission event leaves a hole in the core level. The localized hole can dissipate and become delocalized due to inflow (diffusion) of charge. The process of charge diffusion is called relaxation. There are two different types of relaxation. During a process known as intra-atomic the core hole is delocalized due to rearrangement of electrons in the orbitals of the excited atom. Inter-atomic relaxation involves the core hole being delocalized due to movement of electrons from the surrounding atoms in the material.

As relaxation causes the localized core hole to become more diffuse, the leaving electron can escape at a higher kinetic energy. This therefore increases the extent of

relaxation and causes the binding energy of the electron to decrease. The effect of increasing relaxation causes a shift in peak position to a lower binding energy [8]. Relaxation will not cause an extra peak to appear in the spectra. It can only be observed by comparing cases with and without relaxation.

2.5 (b) The Shake up process

In the simple case of photo ejection, a core electron leaves the atom, having had the entire energy of the photon. It is focused by the spectrometer and appears as a single spectra line at kinetic energy KE. The loss of a core electron by photoemission increases the nuclear charge. This major perturbation gives rise to substantial reorganization of the valence electrons. It can involve excitation of one of the electrons to a higher unfilled level, and lose an amount of kinetic energy equal to the excitation energy [9]. This is referred to the shake up process.

2.5 (c) The shake off process

In a process similar to shake up, valence electrons can be completely ionized. The departing photoelectron has transferred sufficient energy to the valence electron to move it entirely from the atom. This process referred to as shake off, leaves an ion with vacancies in both the core level and the valence level. Shake off electrons are ejected into an unbound continuum state and consequently fall into the region corresponding to the broad inelastic tail.

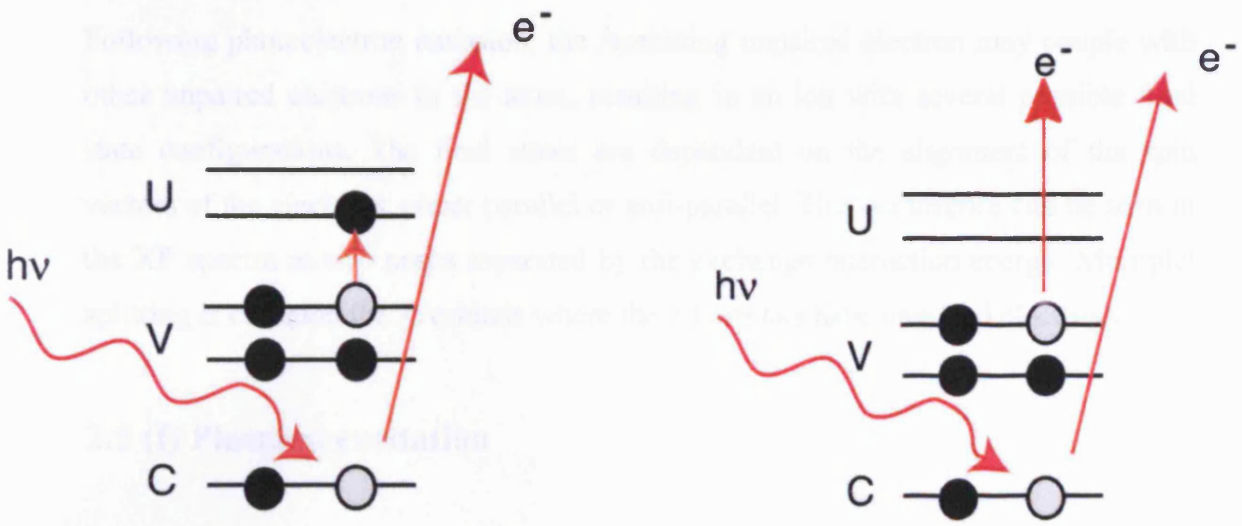

Fig. 2.3 The shake up and shake off process.

2.5 (d) Spin orbit coupling

The removal of an electron caused by the photoelectric process can lead to changes in the configuration of the final state. Spin orbit coupling arises from the magnetic interaction between an electron's spin and the angular momentum and only occurs if there is an unpaired electron within an atom's sub-shell.

Spin-orbit coupling is any interaction of a particle's spin with its motion. spin-orbit interaction causes shifts in an electron's atomic energy levels (detectable as a splitting of spectral lines), due to an electromagnetic interaction between the electron's spin and the nucleus's electric field through which it moves. Spin orbit coupling does not give rise to a single photoemission peak, but a closely spaced doublet. The inner core electronic configuration of the initial state of palladium is $(1s)^2\ (2s)^2\ (2p)^6\ (3s)^2\ (3p)^6\ (3d)^{10}$. All the sub-shells are completely full. The removal of an electron from the $3d$ sub-shell by photo-ionization leads to a $(3d)^9$ configuration for the final state. As the d-orbitals ($l = 2$) have non-zero orbital angular momentum, there will be coupling between the unpaired spin and orbital angular momenta. This results in a closely spaced doublet seen in the XP spectra.

2.5 (e) Multiplet splitting

Following photoelectron emission, the remaining unpaired electron may couple with other unpaired electrons in the atom, resulting in an ion with several possible final state configurations. The final states are dependant on the alignment of the spin vectors of the electrons, either parallel or anti-parallel. This occurrence can be seen in the XP spectra as two peaks separated by the exchange interaction energy. Multiplet splitting is common for 3s orbitals where the 3d orbitals have unpaired electrons.

2.5 (f) Plasmon excitation

An outgoing photoelectron can impart some of its kinetic energy as it passes through a solid. This results in collective oscillations within the conduction band of electrons. Plasmons have a fixed frequency (ω) that is characteristic of a solid. Plasmons can also occur at multiples of this frequency (2ω, 3ω etc). Plasmon loss features appear in the XP spectrum as a series of regularly spaced discrete loss features ($h\omega$) of decreasing intensity. They are common for samples with s or p type valence density at or near the Fermi edge. However, d type valence density is not advantageous for plasmon losses. Al^0 has the configuration $3s^2\ 3p^1$ and exhibits extensive plasmon loss, both from surface and bulk plasmons. Most transition metals with large d-state densities such as Cu^0 with the configuration $4s^1\ 3d^{10}$ show little or no plasmon loss features.

There are two different types of plasmon features; bulk and surface plasmons. As the solid lattice terminates at the surface a localised oscillation occurs. This appears as a lower intensity peak adjacent to that for the bulk plasmon.

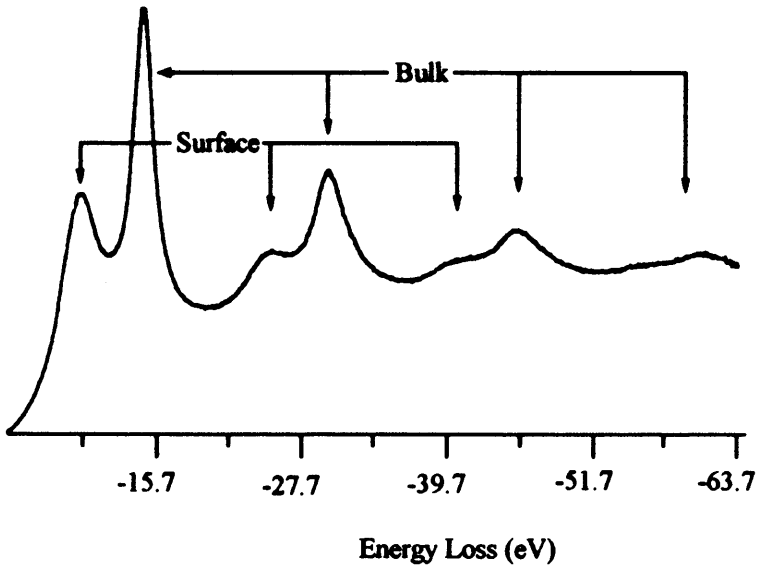

Figure 2.4 Plasmon dominated loss pattern for Al^0 (10).

2.6 The fate of the core hole and techniques that arise from its decay

As discussed previously a core-hole is formed as a consequence of the initial photoelectric event and results in a short lived ionic state. This can be denoted by (M^+). The core hole results in a high energy, ionic system. The system will rearrange itself to neutralise the core hole by filling this hole with an electron from the outer shell. It is able to do this in two ways.

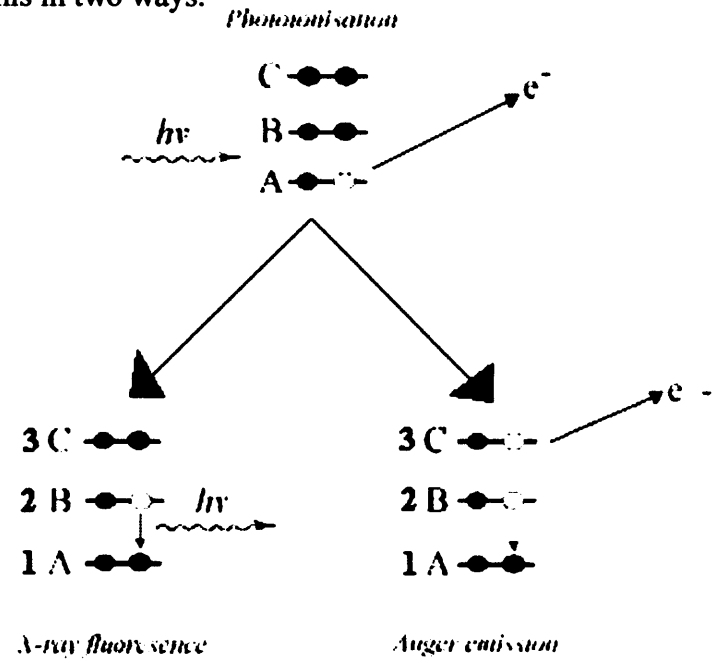

Fig. 2.5 Neutralising the core hole

(i) X-ray Fluorescence - An electron from an outer shell drops into the unoccupied orbital, to fill the hole left behind by the photoelectric process. This transition gives off an X-ray of fixed, characteristic energy that can be detected by a fluorescence detector. The energy needed to eject a core electron is characteristic of each element, and so is the energy emitted by the transition.

(ii) Auger transition – Auger electrons are emitted at discrete energies that allow the atom of origin to be identified. The Auger process involves three steps. These are; excitation of the atom causing emission of an electron, an electron drops down to fill the vacancy created in the first step, and the energy released in the second step causes the emission of an Auger electron. Auger electron energies are independent of the incident photon energy and depend only on the energy difference between the levels concerned. This can be shown by the equation –

$$E_{Auger} = E_1 - (E_2 + E_3) \qquad (5)$$

Auger electrons are analysed along with the photoelectric signal and appear as discrete lines on the spectrum. Auger electrons are easily distinguishable from photoelectrons due to the fact that changing the kinetic energy will have no effect on the Auger electron energy.

Both decay processes are very fast and depend on atomic number (z). Auger decay is more dominant at smaller atomic numbers. X-ray Fluorescence is more likely to occur as the atomic number increases.

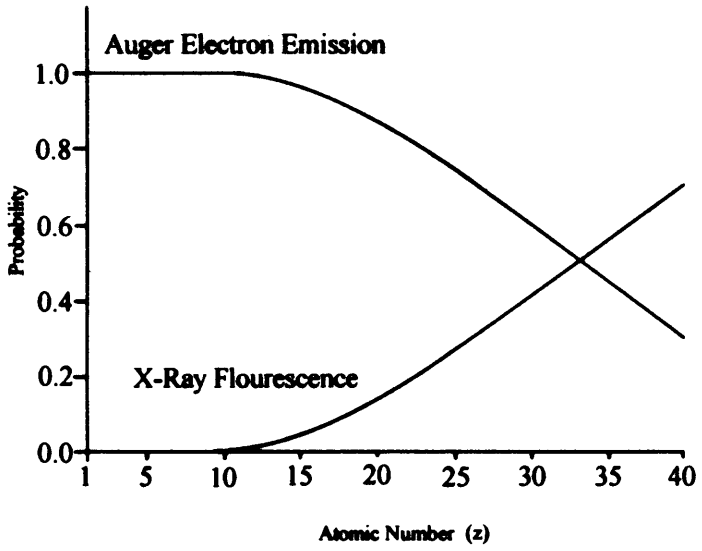

Fig. 2.6 Relative yields of X-ray fluorescence and Auger electron emission as a function of atomic number.

2.7 Chemical Shift

XPS is a useful tool in chemical analysis. The exact binding energy of an electron depends not only upon the level from which photoemission is occurring, but also upon the formal oxidation state of the atom and the local chemical and physical environment. Changes in either factor will give rise to small shifts in the peak positions in the spectrum. This important feature is known as chemical shift - the measurable binding energy difference between two or more inequivalent chemical environments of the same element.

For an electron tightly held in a positively charged species, the binding energy will be higher. Similarly, as the positive charge in the system increases so the binding energy increases, as more energy is required to remove the electron.

Siegbahn *et al* first observed how changes in electron density resulted in a chemical shift. This led to development of the whole field of electron spectroscopy named ESCA (electron spectroscopy for chemical analysis) (11). Sodium thiosulphate was used to show how the different electrical environments can affect XP spectra.

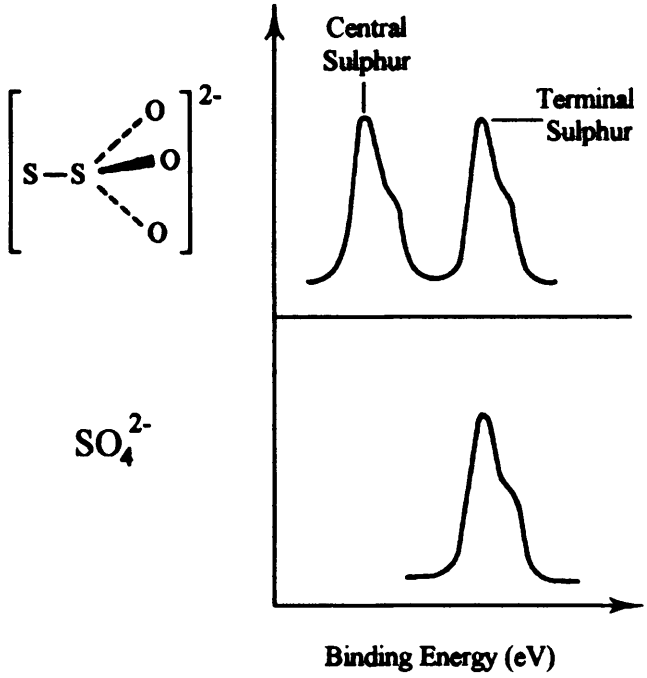

Fig 2.7 S (2p) XPS signals of sodium thiosulphate and sodium sulphate, illustrating the chemical shift (12).

There is a discrete double peak structure attributed to the chemical states of the sulphur atoms. The central sulphur atom is more electro-positive due to the electron withdrawing nature of the oxygen atoms. Chemical shift is charge dependant. Core level spectroscopy can be used to obtain information on the charge distribution in molecules.

2.8 The Reference level

A reference level is required to make accurate comparisons between experimental binding energies. This is due to the fact that photoelectron spectra can involve studying bands that are separated by several tens of electrovolts to small chemical shifts that may only be a few electronvolts apart. Einstein's relationship must therefore be modified in order to account for the spectrometer work function.

$$E_B^F = h\nu - E_K^V - \phi_{sp} \quad (6)$$

For clean metal samples the obvious choice is the Fermi level.

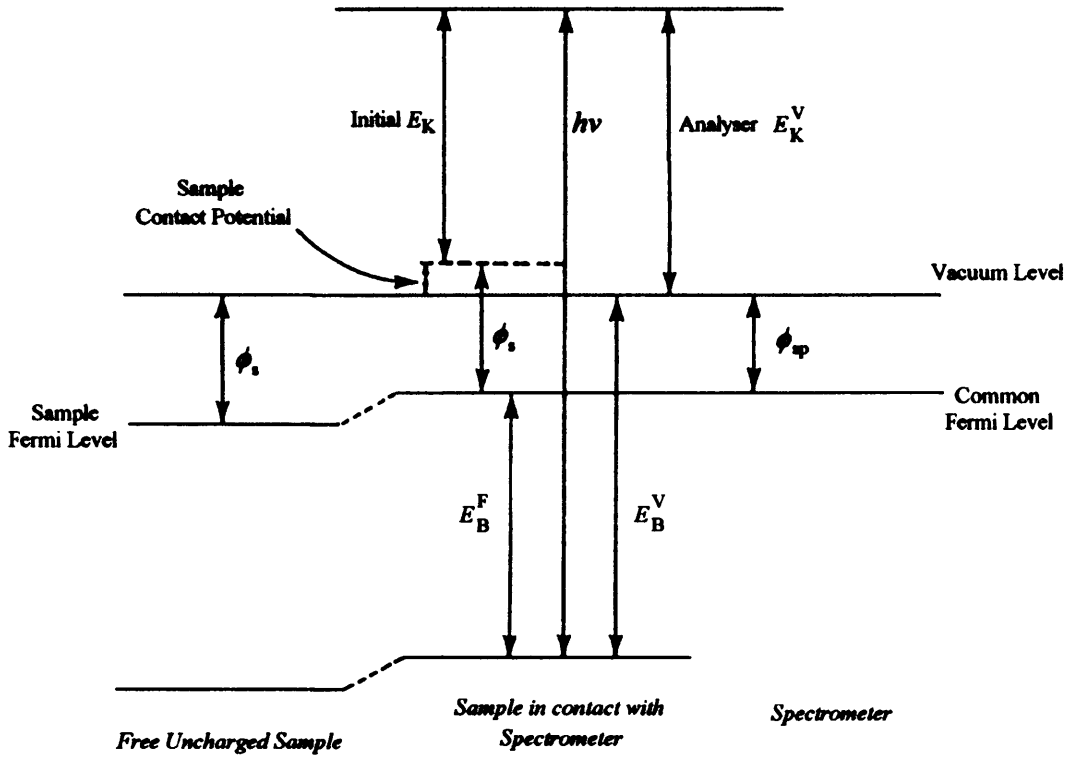

Fig. 2.8 The energy level diagram for a conducting sample in contact with the spectrometer

Once the relationship between K.E. and B.E. is established, it is a matter of calibrating future spectra by reference of the main metal peaks. All the reported binding energies contained in this thesis have been calibrated to the main peak of the clean metal substrate. The case for non-conducting or semi-conducting samples is different. XPS measurements will suffer from charging effects arising from electron deficiency at the surface due to the photoionisation process. However all samples used in the following work are metallic and therefore these will not be discussed here.

2.9 Line broadening effects

As energy levels within atoms are quantised the ideal XP spectra should ideally consist of series of discrete lines. However, in reality these exist as broad peaks. There are a number of factors that contribute to line broadening. The peak width (ΔE)

defined as the full width at half maximum (FWHM) is given by equation 7 assuming a Gaussian distribution of each component:

$$\Delta E = (\Delta E^2_n + \Delta E^2_p + \Delta E^2_a) \qquad (7)$$

Where ΔE_n is the inherent line width of the core level, ΔE_p is the width of the x-ray line, ΔE_a is the resolution of the analyser.

The lifetime of the core hole produced during photoemission is related to the natural width of the photoelectron peak (ΔE_n). This relationship is expressed in terms of the Heisenberg Uncertainty Relationship.

$$\Delta E_n = \frac{h}{\tau} \quad eV \qquad (8)$$

ΔE_o = Natural Line Width (eV)

h = Planck's Constant (6.582×10^{-16} eVs)

τ = Core Hole lifetime (secs)

The inverse relationship between the line-width and the core-hole lifetime results in core-holes with the shortest lifetimes give rise to more significant broadening. The narrowest peaks produced are therefore for the longest lived core holes. The decay of the core hole is dependant on the rate with which x-ray fluorescence or Auger emission occurs.

Phonon broadening can also occur due to the coupling between the core-hole and the nuclei within a solid lattice. Lattice vibrations or phonons are induced and this can be seen as Gaussian broadening of the photoelectron peak. As this phenomenon is vibrational dependant it is therefore temperature dependant. It can result on a broadening of 0.1eV and is therefore negligible. A more detailed review is given by Peter Minnhagen (13).

The greatest contribution to broadening is the analyser resolution (ΔE_a). Broadening of up to 2 eV may occur.

The line width of the ionising radiation also effects broadening. Table 2.1 displays the energy and line widths of some common ionisation sources.

Line	Energy (eV)	Associated width (eV)
Y$M\xi$	132.2	0.47
Zr$M\xi$	151.4	0.77
Mo$M\xi$	192.3	1.53
Cu$L\alpha$	929.7	3.8
Mg$k\alpha$	1253.6	0.7
Al$k\alpha$	1486.6	0.85
Cr$k\alpha$	5417.0	2.1
Cu$k\alpha$	8084.0	2.6

Table 2.1 Energies and associated linewidths of X-ray line sources used in XPS (14).

A compromise between the energy and the associated width results in the use of Mg$k\alpha$ and Al$k\alpha$. The fact that they have reasonable high energies and low associated widths means that they are the two most commonly used. Al$k\alpha$ was used exclusively as the X-ray source in this study.

Instrumental broadening can be minimised by fitting a quartz monochromator to the X-ray source. This generates a well defined photon source and therefore decreases the associated line width.

2.10 Photoionisation Cross-section μ

This can be defined as the total probability of removing an electron from an occupied orbital of an atom with a photon of energy. This is assuming that photoionisation is a process that consists of one photon in and one electron out.

The photoionisation cross-section varies according to the type of orbital. A sperical s-orbital has a greater interaction with a photon than with a p-orbital.

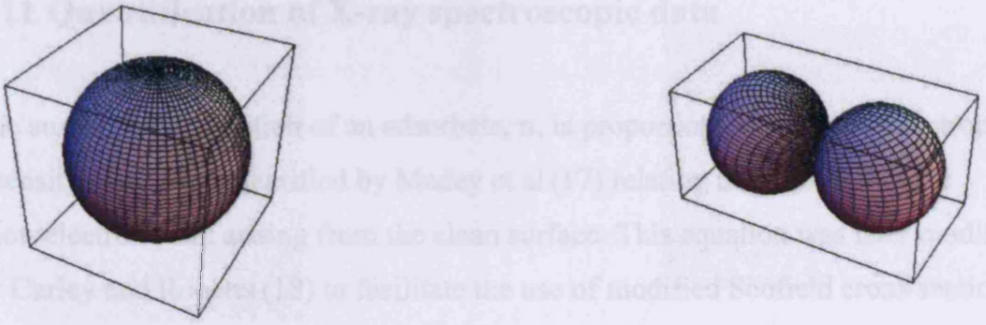

Fig. 2.9 A comparison of an s-orbital and a p-orbital.

The element and the wavelength of radiation also affect the cross-section. The longer the wavelength of radiation, the larger the photoionisation cross-section will be. Therefore peaks arising from UV excitation will be more intense than those arising from x-ray excitation. Scofield has calculated values of μ for all elements with an atomic mass of 96 or less for Al*kα* and Mg*kα* x-ray sources (15).

.

The photoelectron intensity depends on the angle between the incoming photons and the detector. The photoelectron intensity is proportional to;

$$I \propto \left(1+\frac{\beta}{4}\right) \qquad (9)$$

β is termed the asymmetry factor and ranges between -1 and +2 depending on the incident photon energy and nature of the photoemitting atomic orbital. β values for s-

orbitals are always equal to to 2. β values for other orbitals have been tabulated by Reilman et al (16). Taking the angular variation into account results in a modification of the photoionisation cross-secton which is termed μ', which is given by the following equation where μ is the original cross section value (15).

$$\mu` = \mu\left(1 + \frac{\beta}{4}\right) \qquad (10)$$

2.11 Quantification of X-ray spectroscopic data

The surface concentration of an adsorbate, σ, is proportional to its photoelectron peak intensity. This was quantified by Madey et al (17) relating the intensity of the photoelectron peak arising from the clean surface. This equation was later modified by Carley and Roberts (18) to facilitate the use of modified Scofield cross-sections.

$$\sigma_a = \frac{I_a}{I_s} \times \frac{E_a \mu_s}{E_s \mu_a} \times \frac{\rho_s N_A \lambda Cos\Phi}{M_s} \qquad (11)$$

σ = Surface atom coverage (atoms cm^{-2})
I = Integrated area of photoelectron peak
M = Relative atomic mass of the substrate (kg)
λ= Mean free path of photoelectrons through the substrate.
μ = Adjusted photo ionisation cross section of the peak
E = Kinetic energy of the photoelectron peak (e V)
ρ= Density of the substrate peak (g cm^{-3})
ϕ = Take-off angle. Measured between the surface normal and the analyser
N_A = Avagadro number (6.022×10^{23} mol^{-1})

The equation may be used accurately for coverages up to a monolayer since the attenuation of the photoelectron signal by this concentration is negligible. For greater coverages the attenuation of the substrate peak by the adlayer causes an underestimation of the surface concentration.

From the experimentally determined mean free path equation, there is a 5% error. This therefore corresponds to a 5% error in calculated concentrations.

Data analysis

Raw photoelectron data is analysed using in house software developed by Carley (20).This data analysis software allows spectra to be manipulated in such ways as background removal, spike removal, spectral subtraction, and peak area calculation.

2.12 Background removal

Inelastically scattered electrons produce a background while scanning regions. Removal of this background gives a greater accuracy in peak quantification. A linear background subtraction can be obtained by the removal of a straight line drawn from either side of the peak. This method is only used when photoelectron peaks have a small rising background. It is not related to the factors that contribute to the background intensity. Spectral regions which have a large rising background a non linear removal is used. This is based on the method developed by Shirley (21). The background is assumed to arise by the scattering of higher kinetic energy electrons. It is therefore proportional to the integrated photoelectron intensity at higher kinetic energy. The area between two selected points is repeatedly integrated until a converged background value is obtained, which can then be subtracted from the peak intensity.

The peak area can be calculated accurately after removal of the background. This is done by the software by integrating the intensity above a baseline drawn between two points either side of the photoelectron peak as shown in figure 2.10.

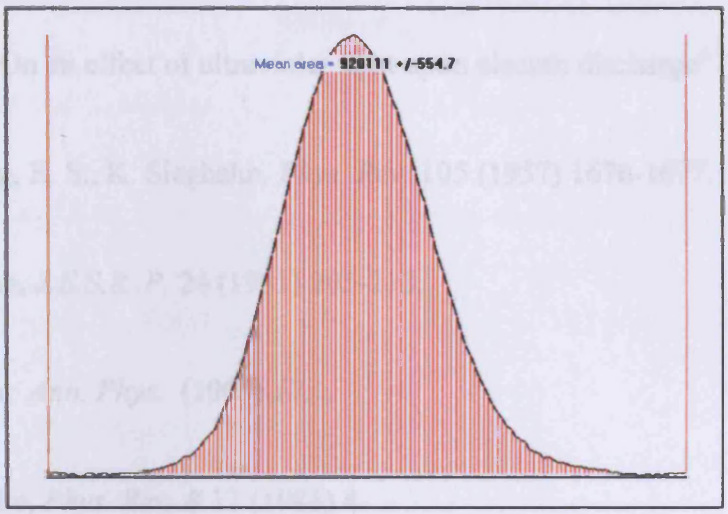

Fig. 2.10 : Peak area measurement

The peak area is used to calculate the surface concentration.

2.13 References

(1) Hertz, H. "On an effect of ultraviolet light upon electric discharge" (1877).

(2) C. Nordling, E. S., K. Siegbahn. *Phys. Rev.* 105 (1957) 1676-1677.

(3) K. Siegbahn, *J.E.S.R..P.* 24 (1981) 205-213.

(4) A. Einstein, *Ann. Phys.* (1905) *17.*

(5) C. R. Bundle, *Phys. Rev. B* 12 (1981) 4.

(6) T. Koopmans, *Phys. 1* (1933) 104-113.

(7) C. R. Brundle, 11 (1974) 212-214.

(8) D. B. Riviere, "Practical Surface Analysis by Auger and X-ray photoelectron Spectroscopy" J. Wiley and Sons, 1983.

(9) T Hayaishit, Y Morioka, H Aksela, S Aksela and E. Yagishita, 25 (1992) 4119-4124.

(10) J. C. Fuggle, D. J. Fabian, L. M. Watson, *J. Elec. Spec. Relat. Phenom,* 9 (1976) 99.

(11) S. Hagstrom, C. Nordling, K. Siegbahn, *Phys Lett 9* (1964) 235-236.

(12) K. Siegbahn, *Nova Acta Regiae Sci. Ups. Ser.* IV 20 (1967).

(13) P. Minnhagen, *J. Phys. Chem* 6 (1976) 1789-1800.

(14) J. C. Rivière, "*Practical surface analysis by Auger and X-ray photoelectron spectroscopy*" Wiley and Sons, 1983.
(15) J. H. Scofield, *J. Elec. Spec.* 1976, *Volume 8*, Pages 129-137.

(16) R. Reilman and S. Manson, *J. Elec. Spec.* 8 (1976) *8*, 389.

(17) T. Madey, J. Yates, N. Erickson, *Chem. Phys. Lett.* 19 (1973) 487.

(18) A. F. Carley, M. W. Roberts, *Proc. R. Soc. Lond.* A. 363 (1978) 403.

(19) D. Penn, *J. Elect. Spec. Rela. Phen.* 9 (1976) 29.

(20) A. F. Carley, PhD Thesis, University of Bradford (1980).

(21) D A Shirley, *Phys. Rev. B*, 5 (1972) 4709.

Chapter 3

Scanning Tunnelling Microscopy

3.1 Introduction

The scanning tunneling microscope or STM was invented in 1981 by Gerd Binnig and Heinrich Rohrer of IBM's Zurich Lab in Zurich, Switzerland. The invention acquired the two a Nobel Prize in Physics in 1986 [1]. The STM allows scientists to visualize regions of high electron density and hence gather the position of individual atoms, where previously studies of diffraction patterns from prior methods lead to much debate as to the real, spatial lattice structure of the item in question.

3.2 Fundamentals

The technique is based upon scanning a probe (the tip), just above a surface whilst monitoring some interaction between the probe and the surface. The interaction that is monitored is the tunnelling current between a metallic tip and a conducting substrate which are in very close proximity but not actually in physical contact. In order for the technique to provide atomic resolution the position of the tip with respect to the surface must be very accurately controlled (to within about 0.1 Å) by moving either the surface or the tip. Also the tip must ideally terminate to a single atom.

The name of the technique arises from the quantum mechanical tunnelling-type mechanism by which the electrons can move between the tip and substrate. Quantum tunnelling is the quantum-mechanical effect of transitioning through a classically-forbidden energy state.

The STM has higher resolution than the atomic force microscope (AFM). Both the STM and the AFM fall under the class of scanning probe microscopy instruments. This invention was quickly followed by the development of a whole family of related techniques which, together with STM, may be classified in the general category of Scanning Probe Microscopy (SPM) techniques.

3.3 Tunnelling current

The tunnelling current originates from the wavelike properties of particles in quantum mechanics. These waves don't end abruptly at a wall or barrier, but taper off quite quickly. If the barrier is thin enough, the probability function may extend into the next region.

Tunnelling is a quantum mechanical effect. A tunnelling current occurs when electrons move through a barrier that they classically shouldn't be able to move though. When an electron is incident upon a vacuum barrier with potential energy larger than the kinetic energy of the electron, there is still a non-zero probability that it may traverse the forbidden region and reappear on the other side of the barrier. It is shown by the leak out electron wave function.

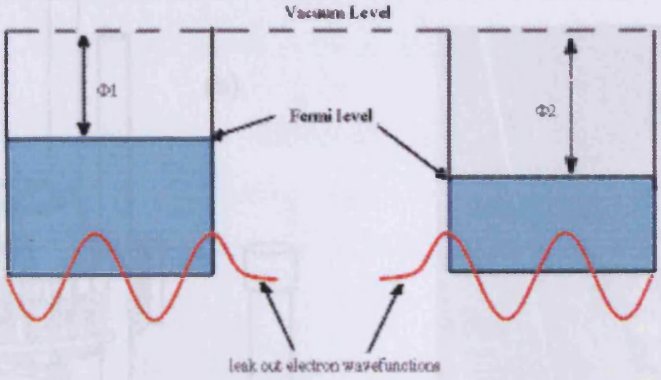

Fig. 3.1: The tunnelling current.

If the two conductors are very close (within a few Angstroms) then their electron wavefunctions overlap and tunnelling can occur. A characteristic exponential inverse decay length K is given by

$$K = \frac{\sqrt{2m\Phi}}{\hbar} \qquad (1)$$

m is mass of electron, Φ is the local tunnelling barrier height or the average work function of the tip and sample. When a small voltage, V is applied between the tip and the sample, the overlapped electron wavefunction permits quantum mechanical tunnelling and a current, I will flow across the vacuum gap.

3.4 Instrumentation

The system used was a custom UHV variable temperature STM. It is equipped with cooling and heating facilities which cover a temperature range of 40 – 1400K. Figure 3.2 (a) shows a schematic of the STM stage and figure 3.2 (b) shows an actual image of the stage.

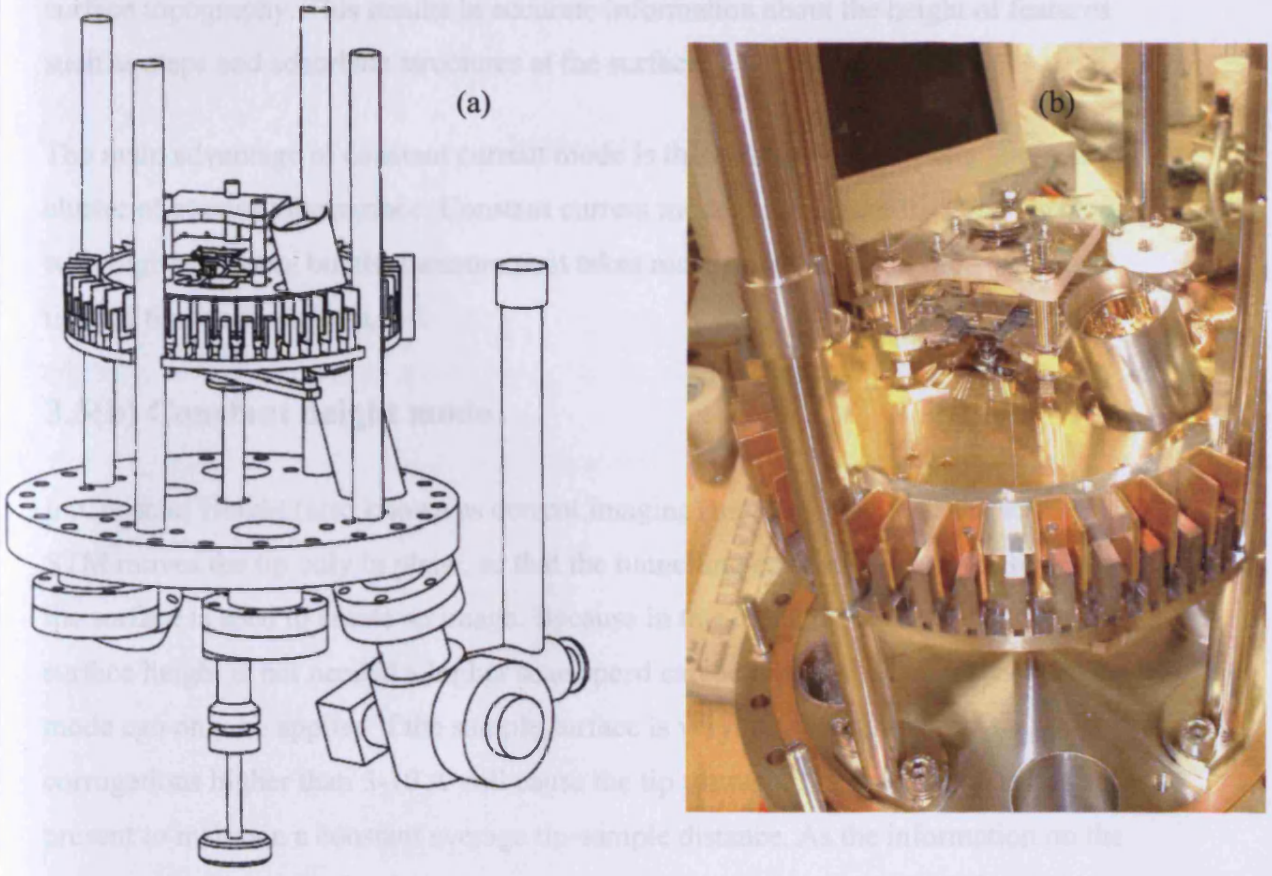

Figure 3.2: (a) Side view of the VT STM [2], (b) photograph of the VT STM.

3.5 Scanning modes

There are two different types of scanning modes. These are constant height and constant tunnelling modes. The different modes can be used when dealing with different surfaces.

3.5(a) Constant current mode

In constant-current mode, the current is used as the input to a feedback circuit that moves the scanner together with the tip up and down in the height direction. With an applied potential, the tip is brought close to the sample surface until the tunnelling current set-point is detected, at which point the constant-current feedback loop is locked. When the tip moves laterally to a new position, any subtle sample-tip distance variation will lead to the fluctuation of the tunnelling current. Consequently, the feedback circuit will move the tip up and down until the current keeps the set-point value. As a result, the moving tip keeps the constant sample-tip distance, tracing the

surface topography. This results in accurate information about the height of features such as steps and adsorbate structures at the surface.

The main advantage of constant current mode is that the tip will not crash into a large cluster of atoms at the surface. Constant current mode can measure irregular surfaces with high precision, but the measurement takes more time due to the finite response time of the feedback loop.

3.5(b) Constant height mode

In Constant Height (also known as current imaging) mode of operation the scanner of STM moves the tip only in plane, so that the tunnelling current between the tip and the surface is used to create an image. Because in this mode the adjusting of the surface height is not needed a higher scan speed can be obtained. Constant height mode can only be applied if the sample surface is very flat, because surface corrugations higher than 5-10 A will cause the tip to crash. The weak feedback is still present to maintain a constant average tip-sample distance. As the information on the surface structure is obtained via the current, a direct gauging of height differences is not possible.

An advantage of constant height mode is that it can be used at high scanning frequencies (up to 10 kHz). The increase in scanning speeds is useful as reactions in real time can be observed.

3.6 Piezoelectric scanner

The piezoelectric effect is a phenomena resulting from a coupling between the electric and mechanical properties of a material. When mechanical stress is applied to a piezoelectric material, an electric potential will be produced. Likewise, when an electric potential is applied to the material a mechanical change will occur. Piezo tubes are useful devices for fine control of an object in space. By sectioning the surface of a tube into four regions and connecting them, as well as one end of the tube to electrodes, it becomes possible to apply voltages to the tube in various directions. By applying voltages perpendicular to the tubes cross-section, it becomes possible to control the position of one end of the tube in two dimensions (x and y), while

applying a voltage along the length of the tube; it becomes possible to control the position in the third dimension (z).

The system used in the Omicron VT-STM mounts the tip onto a piezoelectric cylinder. The cylinder is rigid and therefore has a high resonant frequency. Voltages applied between the pairs of opposing electrodes on the outside of the cylinder result in the tip scanning in the *x* and *y* plane. Voltages applied between inside and outside surfaces expand and contract the cylinder to vary the *z* direction.

The Omicron VT-STM utilises a single scanner with a maximum range of $15\mu m^2$ wit a z-travel of 2 μm.

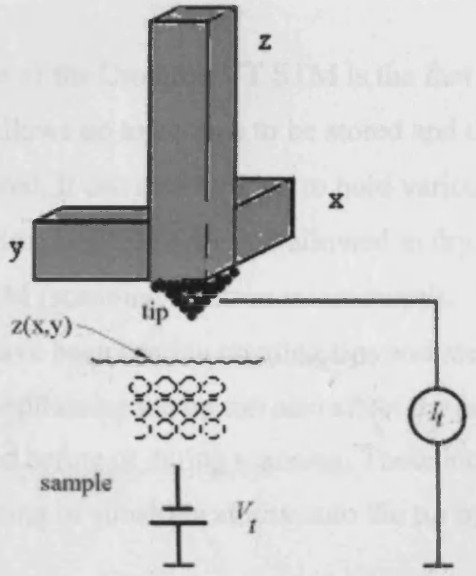

Figure 3.3: Piezo electric scanner.

3.7 Tip Preparation

The size, shape and cleanliness of an STM tip are very important for the resolution of the STM images. The tips should have a minimal radius of curvature at the end, they should have a narrow diameter to penetrate into holes, but they should also be thick enough to keep the resonance frequency high. The tip material should be stable in high electric fields and, when operated in air, chemically stable. Tips have been made out of wires of tungsten, platinum-iridium, platinum, gold, and nickel.

The most common method which was also used to etch all tips used in the following experiments is electrochemical etching. A more detailed method was written by Olivier L. Guise *et al* [4]. The method used in creating tips for the experiments in the following experiments involved cutting a length of Tungsten (W) wire (ideally 0.38 mm diameter) to approximately 3.6 mm and clamping it in a specially designed tip holder. A solution of 0.6 M KOH is poured into a beaker just covering a tungsten ring electrode (approximately 300 mm in diameter) which is connected to the tip. The circuit is completed as the tip is lowered into the solution and a current applied (15 V AC, 150 mA) between the electrodes. It is known when the etching process is completed as the current ceases to flow (checked with ammeter) whereby any part of the tip immersed in the solution has been etched away to leave a sharp v-shaped tip.

A useful design feature of the Omicron VT STM is the fact that it contains a tip holder carousel. This allows up to six tips to be stored and therefore changed without losing vacuum if required. It can also be used to hold various other samples. This tip must them be rinsed with distilled water and allowed to dry. Tips can then be characterised using SEM (scanning electron microscopy).
Many other methods have been used in creating tips and are discussed by Inger Ekvall *et al* [4]. Cleaning or conditioning the tip can also affect the performance. There are many different techniques used before or during scanning. These include heating tips, ion-gun sputtered tips and stripping of substrate atoms onto the tip by a 'softly' crashing the tip into the surface.

3.8 Vibration dampening

As STM is sensitive to surroundings due to the fact that it relies upon the tip coming within angstroms of the surface and remaining a constant tunnelling current, vibrations are an important factor to consider. There are three main sources of vibration to consider when using the STM.

- Acoustic room vibrations
- Internally generated resonance
- External vibrations

Loud noises can cause degradation of the image while scanning. Internally generated resonance is kept to a minimum due to the fact that the tip/sample unit is made as light and rigid as possible in order to raise the resonant frequency and therefore the scan frequency of the system. External vibrations are the greatest cause for concern as without it high resolution STM would be impossible. In order to minimise external vibrations the spectrometer is placed in the basement of the building. However a more extensive method is used to remove the external vibrations; eddy current damping. This uses eddy currents to damp motion. A ring of copper plates are mounted on the STM stage and a ring of permanent magnets are fixed at the columns of the spring suspension as a counterpart.

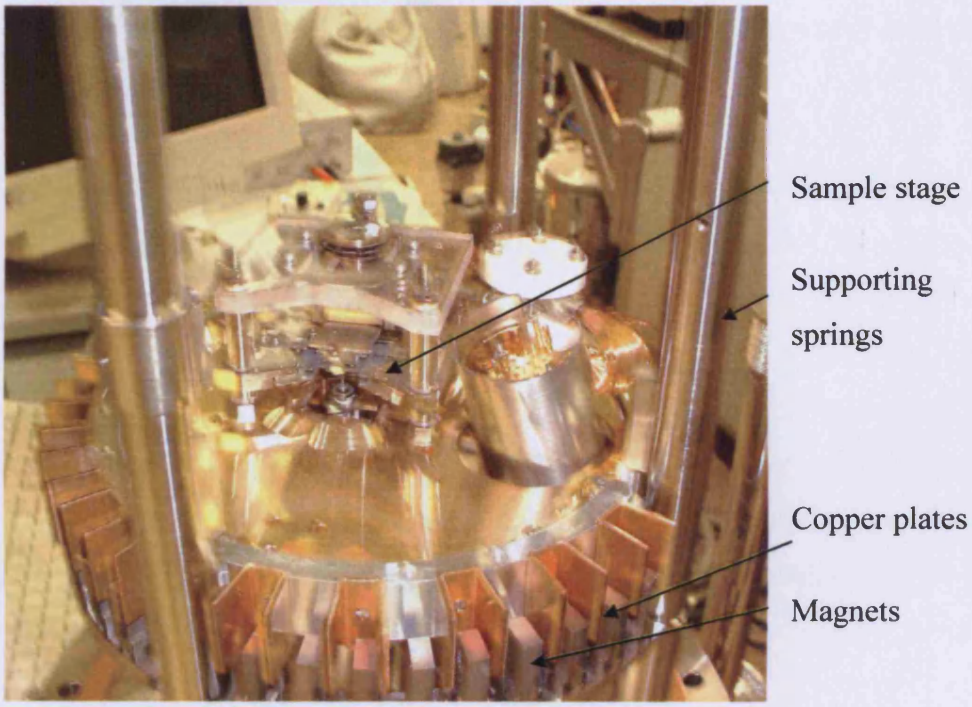

Fig. 3.4: Vibration dampening instrumentation.

3.9 Sample preparation

The crystal used in the experiments is held into position by a specially designed sample holder.

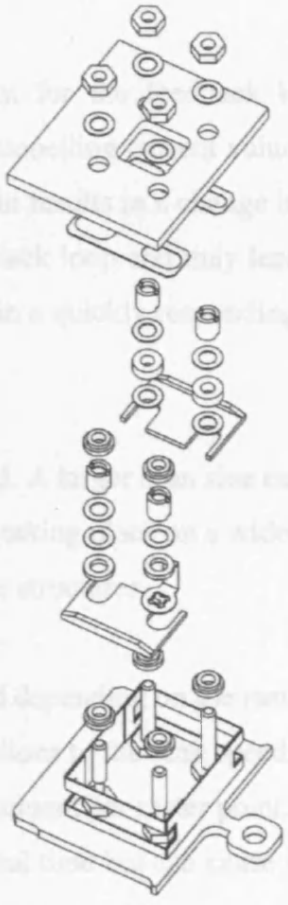

Fig. 3.5 : sample holder.

It consists of a molybdenum base plate and a ceramic plate. The ceramic plate is coated with pure tungsten at a layer thickness of about 100 nm to avoid electro-static charges when using XPS. The molybdenum base plate engages in the carousel and the manipulator, which is used to transfer the sample between the STM and XPS chambers. The sample itself is fixed to the ceramic plate that engages in the sample stage.

3.10 Scanning Parameters

There are a number of parameters to consider when using the STM. The gap voltage sets the voltage bias applied to the surface for STM measurements. This is normally set between 1 and 2 volts. Changing the polarity of the bias voltage reverses the flow of the tunnelling electrons.

The feedback sets the point for the feedback loop. This feedback source is the tunnelling current. Typical tunnelling current values used are in the range of 0.5 - 2.5 nA. A change in the loop gain results in a change in the feedback loop. Low loop gain values result in a slow feedback loop and may lead to a flattened signal output while high loop gain values result in a quickly responding feedback loop and may lead to tip oscillations.

The scan size can be changed. A larger scan size can be useful when observing reactions and reconstruction taking place on a wide scale. A close up of the surface is useful in determining smaller structures.

The scan speed can be varied depending on the raster size and scanner capabilities. There are a number of limitations to the scan speed. The upper limit cannot scan faster than one topographic measurement per raster point. Fast scan speeds can be useful to see an experiment occur in real time but can cause image quality degradation. The next slower scan speed will correspond to two topographic measurements per raster point.

3.11 Data Analysis

There are a number of processing techniques that can be applied to improve the image. Noisy images can be filtered. This involves software smoothing the images [5].

The linear background of the z image can be removed. This is done by removing the background in the x and y directions by fitting the average slopes for both directions. This allows a better display of corrugation at the surface.

3.12 References

(1) G. Binnig and D. P. Smith, *Rev. Sci. Instrum.* 57 (1986) 1688.

(2) Omicron User's Guide, Omicron Vakumphysik GmbH, Germany.

(3) O. Guise, M. Jung, P. Goughnour, and J. Yates, *J. Vac. Sci. Technol.* 15 (2002) 191-193.

(4) I. Ekvall, D. Claesson, H. Olin and E. Olsson, *Chem. Phys. Lett,* 206 1999, 18.

(5) R. J. Colton, A. Engel, J. E. Fromer, H. E. Gaub, A. A. Gerwith, R. Gukenberger, J. Robe, W. M. Heckl and B. Parkinson "*Procedures in Scanning Probe microscopes*", John Wiley and Sons, New York, 1998

Chapter 4

Instrumentation

4.1 Introduction

All experiments were completed using an Omicron Variable temperature STM (VT-STM). This instrument consists of two chambers. The first chamber is used for cleaning and acquiring XP spectra. Scanning tunnelling microscopy takes place in the second chamber.

4.2 The requirement for a vacuum

Successful XP spectra require a vacuum. This is for two reasons. As discussed in chapter 2 the photoelectrons released in a molecule or a solid surface must reach the electron energy analyser. This must be achieved with minimal collisions. Therefore a pressure of $10^{-5} - 10^{-6}$ torr is required.

Prevention of electrical discharge between the X-ray anode and electron energy analyser is also a necessity. Again a base pressure of $10^{-5} - 10^{-6}$ torr is required to prevent this.

An atomically clean surface is a necessity for successful XP spectra and scanning tunnelling microscopy. This adds a greater demand on the base pressure. Pressures of 10^{-10} torr (ultra high vacuum, UHV) are required to avoid contamination build up on the surface. One of the crucial factors in determining how long a surface can be maintained clean (or, alternatively, how long it takes to build-up a certain surface concentration of adsorbed species) is the number of gas molecules impacting on the surface from the gas phase. The rate of impingement (z) of a gas on a surface is governed by the Hertz-Knudsen equation,

$$Z = \frac{P}{(2\pi MKT)^{\frac{1}{2}}} \text{ cm}^2 \text{ s}^{-1} \quad (1)$$

where P = pressure, M = molecular mass, K = Boltzmann constant, T = Temperature (K).

Assuming a sticking probability of unity (i.e. all molecules that strike the surface will stick to it), then a surface consisting of approximately 1.5×10^{15} atoms cm^{-2} at a pressure of 10^{-6} torr at 300K will be covered with a monolayer of surface contamination in only 4 seconds.

By comparison the same surface for the same gas at 10^{-10} torr and 300K will not become contaminated for approximately eight hours. However, in practice these sticking probabilities can vary and experiments have shown that the time taken for an atomically clean surface to become contaminated can be much greater than eight hours.

4.3 Obtaining UHV

In order to achieve pressures of 10^{-10} torr, four different pumps are used. These are rotary, turbo, diffusion and ion molecular pumps. Each pump is used to achieve a certain pressure. A description and pressure each pump can deliver is discussed below.

4.3(a) Rotary pumps

Rotary pumps (also known as roughing) cover a pressure range from 10^2 to 10^{-2} Torr. In these pumps oil provides the seal between the vacuum and atmosphere sides of the pump. Because of their construction it is relatively easy for oil vapour to enter the vacuum system leading to contamination of samples with hydrocarbons which is of course undesirable. Even if hydrocarbon contamination did not exist, the density of gas molecules is only reduced to about 10^{15} per cubic centimetre which is insufficient to keep a sample clean.

The pump consists of a wheel with blades on its perimeter lubricated with oil. Rotation of the wheel causes the blades to trap air molecules from the vacuum vessel between the wheel and pump wall and then transports them to an exhaust port of the pump via a one way valve.

Gas ballasting helps to prolong pump life because it removes the main source of pump contamination, condensable vapours. The gas ballast is a vented exhaust that admits a small amount of air at atmospheric pressure to the compression side of the pump, thus permitting most condensable vapours to pass through the pump without condensing.

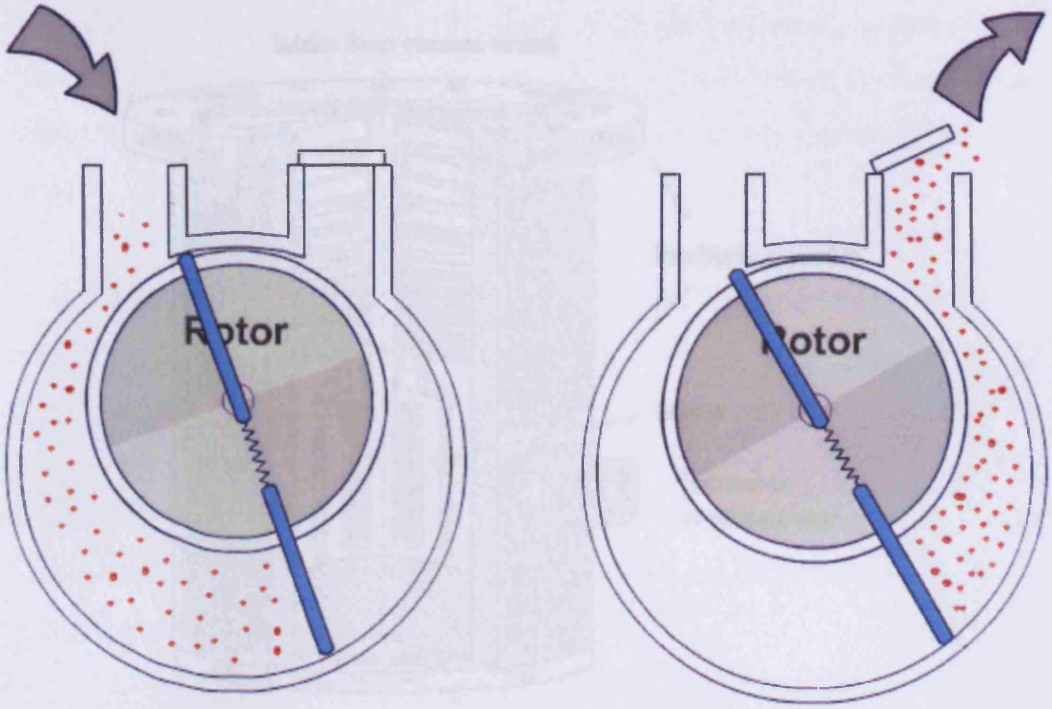

Fig. 4.1: Schematic of a rotary pump.

4.3(b) Turbo molecular pump

To achieve a vacuum of 10^{-1} to 10^{-6} a turbomolecular pump is used. These are basically high speed fans, whose blades are moving at a speed comparable to the speed of gas molecules. As the blades spin and hit gas molecules they are driven towards the pump exhaust and then into the intake of the rotary pump. Turbo pumps are capable of sustaining very high compression ratios, the ratio of the gas pressure at the output to that at the input. This low outlet pressure is maintained by a rotary pump, which acts as both a roughing pump for the system and a backing pump for the turbo.

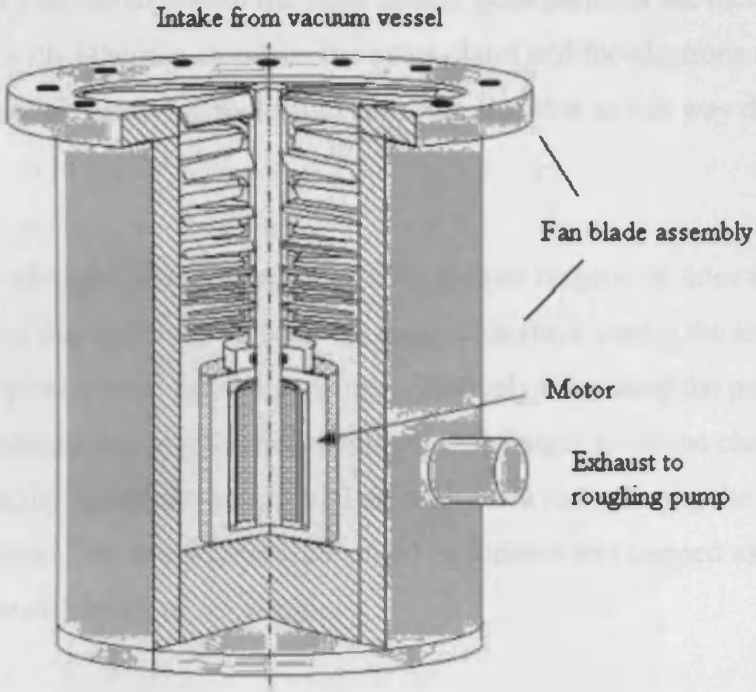

Fig. 4.2: Schematic of an ion pump.

A turbo pump is assembled from several wheels in series, with each wheel having different blade geometries. Each wheel then can be regarded as a single pump. As the wheel turns, gas molecules are reflected from the blades into the exhaust. Affixed to the intake port of a roughing pump, turbo pumps work as turbochargers, increasing the number of air molecules present at the roughing pump's intake port.

4.3(c) Ion pump

Ion pumps are effective from 10^{-5} to 10^{-12} torr. Instead of mechanically removing the air molecules from inside the chamber, an ion pump captures and traps air molecules. Physically, the ion pump consists of two parallel titanium plates with an electrically insulated titanium cell structure in the middle. Titanium is chosen because it readily interacts and bonds with ions. To complete the structure, a magnet is placed on either side of the outer titanium plates, creating a magnetic field perpendicular to the plates. A high voltage (5 kV) is applied to the cell structure in the middle. This voltage creates an electric field between the plates and the middle cell. As neutral air molecules inside the chamber randomly enter the ion pump, the electric field ionizes them. Once ionized, the free electrons travel towards the positively charged middle

cell while the ions move toward the outer plates. Both particles are then captured, the ions binding with Titanium atoms on the outer plates and the electrons collecting on the central anode. Removing molecules from the chamber in this way decreases the air pressure.

As the newly charged particles begin to move to their respective sides they feel a magnetic force due to the noted magnetic field. This force causes the ions and electrons to spiral around inside the pump, effectively increasing the path length the ions travel before becoming trapped. A longer path length gives the charged particles more opportunity to collide with neutral air molecules just entering the pump. If such a collision occurs, the neutral molecule could be ionized and trapped as well, increasing the efficiency of the pump.

An electric current proportional to the number of electrons collected by the middle cell is used as a measure of vacuum quality. This is because the number of electrons collected is proportional to the number of ions created, which in turn is proportional to the number of air molecules inside the chamber. If this electric current gets too high, the ion pump turns itself off as a precaution. The high voltage components are not made to work in high-pressure environments where electrical sparking could damage the pump.

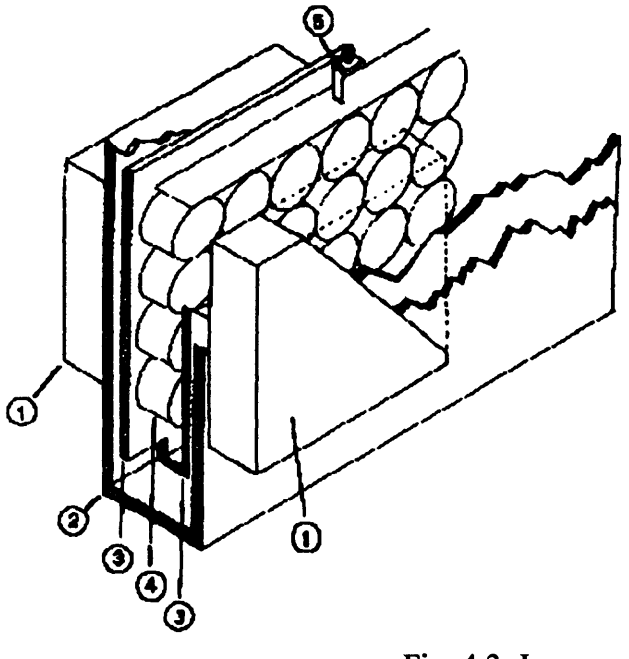

1. Permanent magnets
2. Pump envelope
3. titanium cathode
4. anode cell array
5. positive high voltage lead

Fig. 4.3: Ion pump titanium plate.

4.4 The Gas line

The purpose of the gas line is to be able to dose gasses into the main chamber. These gasses have to be free of atmospheric contamination. The gas line consists of two pumps; rotary and diffusion. This results in a pressure of approximately 10^{-7} to 10^{-8} torr. The gas line can be pumped down using the pumps, isolated, and then the various gasses can be dosed into the main chamber via a leak valve. This results in a dosage free from atmospheric contamination.

4.5 Diffusion pump

A diffusion pump is used on the gas line as they are ideal where there is a through-put for heavy gas loads. Diffusion pumps work by heating oil to its boiling point. The oil must have a high resistance to thermal degradation, a vapour pressure at 298K of 10^{-9} torr minimum and must not react with gasses passing through the pump to form volatile products. The oil used was polyphenyl ether oil. This had a vapour pressure at 298K of 4×10^{10}torr[1].

The vapours travel upward inside the jet assembly and are accelerated out and downward through the jet nozzles. As it rises, it is directed into a funnel-shaped set of baffles and jetted as a supersonic vapor towards the sides, which are kept cool by cold water tubing that surrounds the upper part of the pump. Air molecules that diffuse into this portion of the pump collide with the vapor molecules and are trapped. The oil vapor cools and condenses, dragging air molecules down as it sinks to the bottom of the pump. At the bottom, the heater reboils the oil, releasing the air molecules, which are pumped away by the mechanical pump. The diffusion pump produces a working pressure in the sample chamber of about 1×10^{-5} Torr.

Diffusion pumps cannot begin to work in atmosphere. A roughing pump is used to bring the gas line down to a pressure of 10^{-3} Torr. As a diffusion pump cannot vent directly to atmosphere, the roughing pump is also used to maintain proper discharge conditions.

One major disadvantage of diffusion pumps is the tendency to backstream oil into the vacuum chamber. This oil can contaminate surfaces inside the chamber or upon contact with hot filaments or electrical discharges may result in carbonaceous or siliceous deposits.

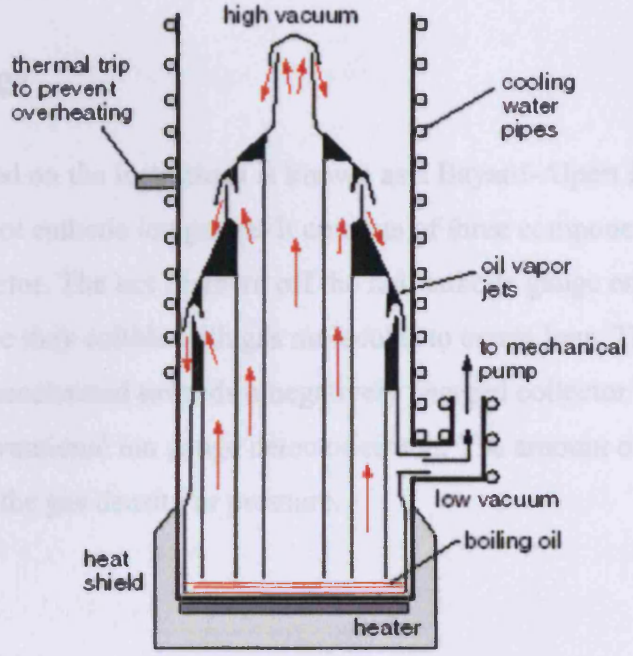

Fig. 4.4: A diffusion pump.

4.6 Pressure measurement

Two different gauges are used to measure the pressure of the chamber and the gas line. Pirani gauges are used to measure pressures of $0.5\text{-}10^{-3}$ torr. Ion gauges are used to measure lower pressures of $10^{-3} - 10^{-11}$ torr.

4.6(a) Pirani gauge

The Pirani gauge is a roughing pressure vacuum gauge. It uses the thermal conductivity of gases to measure pressure. The Pirani gauge head is based around a heated wire placed in a vacuum system. The electrical resistance of the wire is proportional to its temperature. At atmospheric pressure, gas molecules collide with

the wire and remove heat energy from it. This cools the wire. As gas molecules are removed (i.e. the system is pumped down) there are fewer molecules and therefore fewer collisions. Fewer collisions mean that less heat is removed from the wire and so it heats up. As it heats up its electrical resistance increases. A simple circuit can detect the change in resistance and once calibrated can directly correlate the relationship between pressure and resistance.

4.6(b) Ion gauge

The ion gauge used on the instrument is known as a Bayard-Alpert ion gauge. It is also known as a hot cathode ion gauge. It consists of three components; filament, grid (anode) and collector. The hot filament off the hot-cathode gauge emits electrons into the vacuum, where they collide with gas molecules to create ions. These positively charged ions are accelerated towards a negatively charged collector where they create a current in a conventional ion gauge detector circuit. The amount of current formed is proportional to the gas density or pressure.

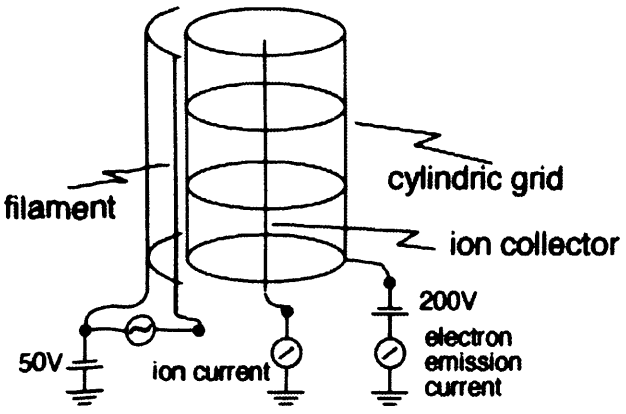

Figure 4.5 Schematic of a Bayard-Alpert ion gauge.

4.7 Baking

In order to maintain UHV conditions regular heating of the system to 150°C is required. The system is heated for at least 16 hours in order to increase the outgassing

rate of the systems internal surface. The heating causes a fast removal of the impurities adsorbed on the walls of the vacuum system. The need for baking systems means working with UHV chambers can be time-consuming. It also requires that the system is build only of components which can withstand high temperatures for a long period of time. For this reason the chamber is made up of stainless steel. The only part of the instrument that is made of a different material is the analyser chamber.

4.8 The chambers and gas line handling

The VT-STM consists of two chambers; one for XPS analysis and a second for STM. The system also incorporates facilities for LEED. The STM chamber is equipped with a manipulator to allow transfer of STM scanning tips and sample plates between the sample probe and the STM stage. The liquids are dosed into the chamber via a leak valve. They are purified by freezing using liquid nitrogen and then pumping out contamination using a diffusion pump. While dosing, the purity is monitored using in-situ mass spectrometry. Solids are dosed using a k-cell. This involes heating the solid in a closed furnace and then focusing the cell at the surface. The furnace is then opened and a beam of gaseous molecules hit the surface. Again this is monitored using mass spectroscopy.

4.9 Instrumentation for X-ray photoelectron spectroscopy

4.9(a) X-ray source design

The X-ray source was designed specifically to be used in photoelectron spectroscopy. It has a twin anode that allows either Mg Kα or Al Kα radiation to be selected. This is useful due to the fact that both photoelectron and Auger peaks can appear in the same XP spectra. Therefore some interference between the lines is possible. As there is a twin anode source changing the ionizing radiation will result in a change of kinetic energy of the ejected photoelectron. However the energy of the Auger electron will remain unchanged. This means that they are distinguishable. Below shows a schematic diagram of the x-ray source and a description of how photoelectron spectroscopy is achieved.

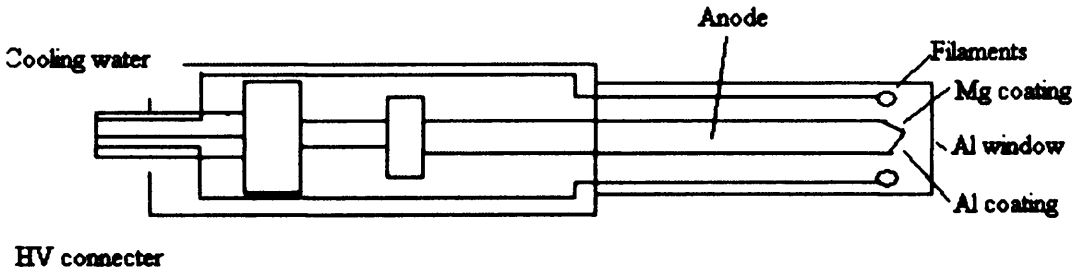

Figure 4.6: Schematic of a dual anode x-ray source.

Electrons are extracted from a heated filament to bombard the selected surface of an anode at a high positive potential. At the tip of the anode there are two tapered copper faces. One face is covered in a film of aluminum and the other is covered in a film of magnesium. Application of a high positive potential to the anode (15kV) accelerates the electrons from the filament to the nearest face. This causes the ejection of X-ray photons. The focus electrode and the shape of the nose cone ensure that the electrons hit the anode in the correct area. Water is used to cool the centre of the anode and this prevents it from getting to hot. X-rays generated in the surface of the anode pass through a thin aluminium window to the sample under analysis. The aluminium window forms a partial vacuum barrier between the source and the sample region. This allows the source to be differentially pumped if required. The aluminium window also protects the sample from stray electrons, heating effects and contamination from X-ray source degassing.

4.9(b) Electron energy analyser and electron multiplier

Ejected photoelectrons energies are measured by a concentric hemispherical analyser (CHA). The kinetic energy of the photoelectron is calculated from its velocity. As electrons from the analyser do not generate enough current to be measured, an electron multiplier is used to amplify the signal. Electrons that enter the multiplier through the entrance cone collide with the interior wall producing secondary electrons. These are accelerated towards the channeltron anode producing a cascade of electrons which undergo more collisions and therefore produce more electrons.

4.10 Sample preparation

The crystals used in the studies were cleaned using repeated cycles of argon-ion bombardment. This was achieved using a cold cathode argon ion gun. This cleans the surface by shooting high energy argon ions (20μA) to remove contamination from the surface. The way in which this is achieved involves argon gas being admitted into the ionisation chamber continuously from an attached cylinder (Argo. LTD, purity 99.999%). A high voltage is applied between the cathode and anode to induce an electrical discharge ionising the argon to form Ar^+ ions. These ions are focused into a beam, accelerated and then directed towards the sample at earth potential. This results in the contamination being sputtered off.

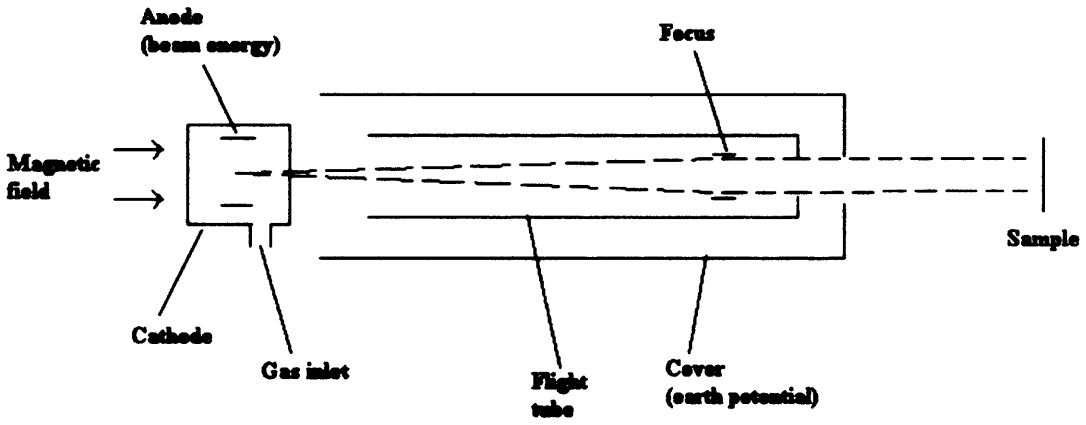

Fig. 4.7: Schematic of an ion gun.

Bombarding is a destructive technique and as is it necessary to have an atomically flat surface, annealing is required. Annealing consists of heating the material and then cooling it very slowly and uniformly. The result is an atomically flat surface suitable for STM and XPS analysis.

The single crystal metal sample is held into position in a specially designed sample holder. This consists of a base made out of molybdenum and a ceramic plate. The sample is attached to the ceramic plate. This engages in the sample stage of the STM. The molybdenum plate engages in the probe and the carousel of the STM tip and sample holder. The probe is used to transfer the sample between the XPS and STM chambers.

Pure tungsten coats the ceramic plate (~ 100nm thick) and this has the effect of avoiding electrostatic charges during XPS. This plate has been tested by Omicron to exhibit no shift in binding energy.

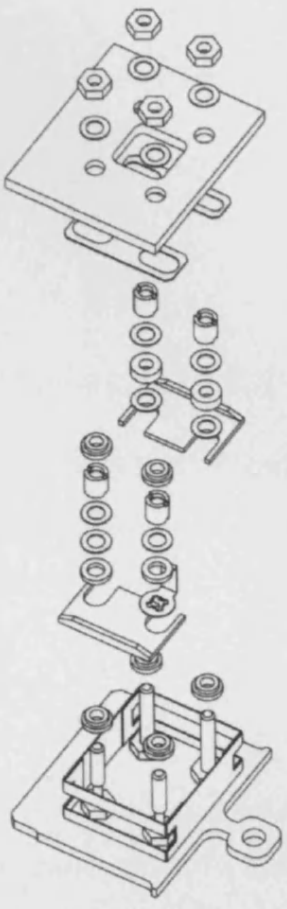

Figure 4.8: Sample plate assembly [2].

4.11 References

(1) http://www.sisweb.com/vacuum/sis/satovc5p.htm, 03/11/2005.

(2) Omicron Users guide, Omicron Vakumphysik GmbH, Germany

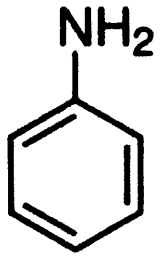

Chapter 5

Interaction of Aniline with clean and oxidised Cu(110) surfaces

5.1 Introduction

The interaction of aniline with clean Cu(110) and partially oxidised Cu(110) has been studied using XPS and STM. The investigation focuses on the change in structures present at the surface due to the presence of oxygen. All experiments took place at room temperature.

5.2 Chemisorption of aniline at metal surfaces

Previous studies at Cardiff University of ammonia [1-3] and pyridine [4, 5] with clean and oxidised surfaces makes aniline an interesting alternative model due to the associated phenyl ring and differing basicity from that of ammonia or pyridine. Due to the delocalisation of the lone pair into the phenyl ring aniline is a significantly weaker base than ammonia or pyridine.

Molecule	pKb [6]	Gas phase basicity [7]
Pyridine	8.75	898.1
Aniline	9.37	850.6
Ammonia	4.75	819.0

Table 5.1 Differing basicity.

Previous studies of aniline adsorption at a Cu(110) surface [8] showed aniline desorbing from a weakly-bound multilayer state at 195K. It chemisorbed at 300K. Studies using HREELS concluded that the aromatic ring of the aniline molecule is orientated approximately parallel to the surface. At 100K HREELS showed the presence of two NH stretching modes in the multilayer state. However, there was only one chemisorbed state at 300K. TPD showed that above temperatures of 300K, products were from a dissociative process. This was further proven by the fact that temperatures for the desorption of benzene and ammonia are 270K and 255K respectively. At 300K it was concluded that the interaction with Cu(110) resulted in adsorption of C_6H_5NH. Nitrogen bonded to the surface but there was also a weak interaction between the aromatic ring and the surface.

ARUPS (angle resolved UV photoemission spectroscopy) was used to study adsorption of aniline at a Pd(110) surface [9]. It was found that a phenyl-imide was formed at the surface which adsorbed almost parallel to the surface. LEED results showed that a densely packed c(4x2) structure was formed. A separate study using STM also reported the same c(4x2) structure formed at a Si(100) surface [10].

Aniline adsorption has also been investigated at both Ag(111) [11] and Ag(110) [12] surfaces. At an Ag(111) surface, TPD studies show that aniline adsorbs molecularly at a temperature below 250K. HREELS indicates the aniline molecules lie at an angle of approximately 13°. The saturation coverage was approximately 1.5×10^{14} molecules cm^{-2}.

At an Ag(110) surface, TPD showed a small desorption peak at 450K when background oxygen was present in the system. This indicates that aniline will react with surface oxygen. Aniline was found to desorb from a multilayer state at 195K, a

chemisorbed monolayer at 325K, as well as another state at 250K. Saturation was reached at a surface concentration of 2.3×10^{14} molecules cm^{-2}. This is twice the maximum coverage found for benzene and phenol. The authors concluded that aniline forms two layers on Ag(110), and that desorption of the second layer is responsible for the peak at 250K in the TPD spectrum.

Amines have many applications in heterogeneous catalysis. Amines are used as reactants and catalyst modifiers [13-15]. Amine surface interactions also play an important role in corrosion inhibition [16-18]. The following study looks at the interaction of aniline with a clean and oxygen modified Cu(110) surface. The differing basicity of the molecule and the associated phenyl ring will alter its behaviour compared to ammonia and pyridine. How it alters is the question that is addressed in the current study.

5.3 Experimental

STM images were obtained using a variable temperature STM (VT STM) developed by Omicron Vakuumphysik GmbH with XPS capability. Al Kα (1486.6eV) radiation was used as an X-ray source. The Cu(110) crystal was cleaned by repeated cycles of Ar^+ bombardment. Following the bombardment, the Cu crystal would be annealed at 900K for 1 hour and the Ag crystal would be annealed at 850K for 1 hour. The cleanliness of the sample was checked using XPS.

The aniline (99.5%, Aldrich) was subjected to several freeze-pump-thaw cycles using a dry ice/acetone mixture, and the purity was monitored with in situ mass spectrometry. The oxygen (99.998%) was obtained from Argo Ltd and used as received.

5.4(a) Aniline ($C_6H_5NH_2$) adsorption at clean Cu(110) at 295K: XPS results

A clean Cu(110) surface was exposed to various doses of aniline, up to a maximum exposure of 120L. This gave rise to a C(1s) peak at 283.7 eV. Adsorption does occur but it is very limited. Due to the fact that as the XP spectra showed little increase in coverage between a dose of 20L and 120L, the maximum concentration was calculated to be 5.2 x 10^{14} atoms cm^{-2} after this final dose.

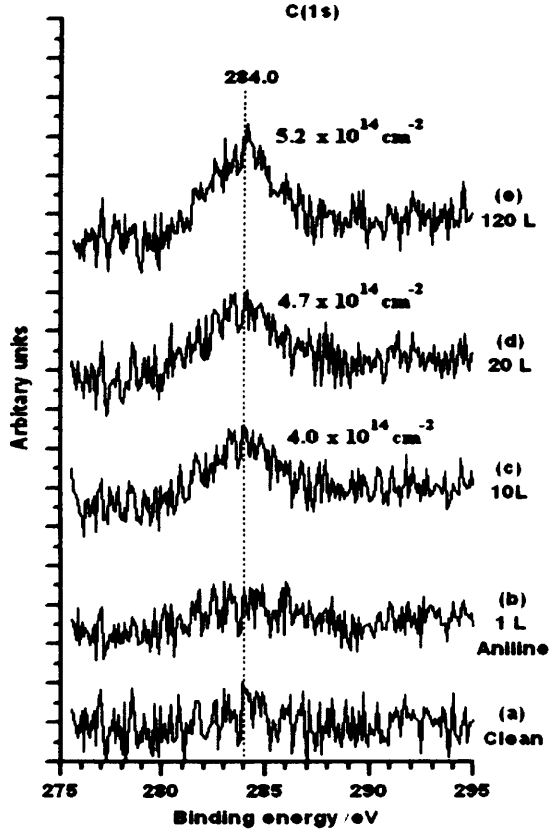

Fig. 5.1: The adsorption of aniline at a clean Cu(110) surfaces at 295K. (a) Clean, (b) 1L exposure, (c) 10L exposure, (d) 20L exposure, (e) 120L exposure.

5.4(b) Aniline ($C_6H_5NH_2$) adsorption at clean Cu(110) at 295K: STM results

STM images of a clean Cu(110) surface exposed to 120L aniline showed no evidence of an adsorbed species. Due to the low concentration present, what ever species is present at the surface may be mobile and therefore not imaged.

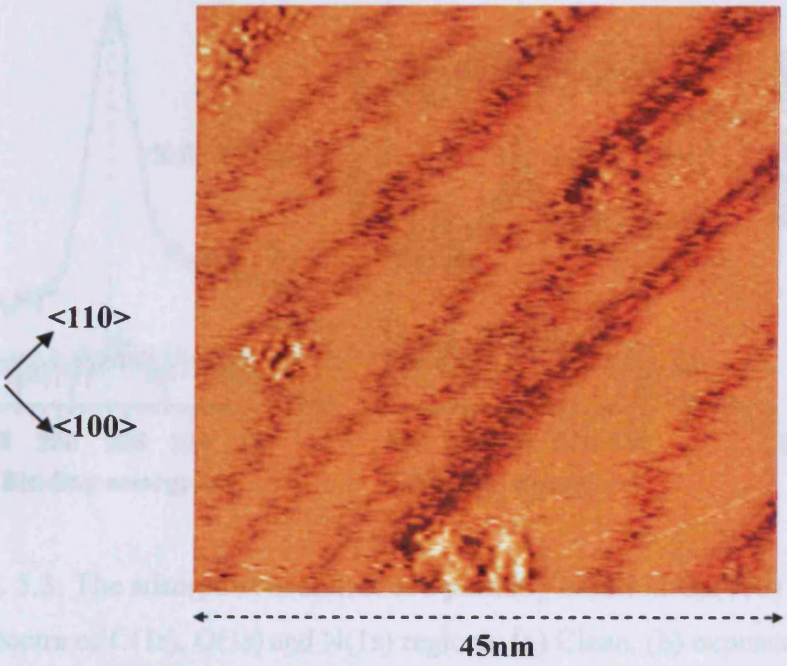

Fig. 5.2: STM image after a dose of 120L of aniline at a Cu(110) surface at 295K.

5.5(a) Aniline adsorption with a pre-oxidised Cu(110) surface at 295K: XPS results

A clean Cu(110) surface was exposed to 2L of oxygen at room temperature. This gave rise to a peak in the O(1s) region at 529.6eV and the calculated coverage was $1.3x10^{14}$ atoms cm^{-2}. Aniline exposure of 20L resulted in removal of this chemisorbed oxygen and peaks became present in the C(1s) and N(1s) region. These peaks had a binding energy of 283.7 eV and 397.5 eV respectively. The final surface concentrations were $1.6x10^{15}$ cm^{-2} carbon, and $2.6x10^{14}$ nitrogen, giving a C:N ratio of approximately 6:1.

This agrees with the composition of the molecule. The ratio of final nitrogen concentration to initial oxygen concentration was 2:1, suggesting an overall reaction stoichiometry of 2 aniline: 1 oxygen.

$$2C_6H_5NH_2(g) + O(a) \rightarrow H_2O(g) + C_6H_5NH(a) \qquad (1)$$

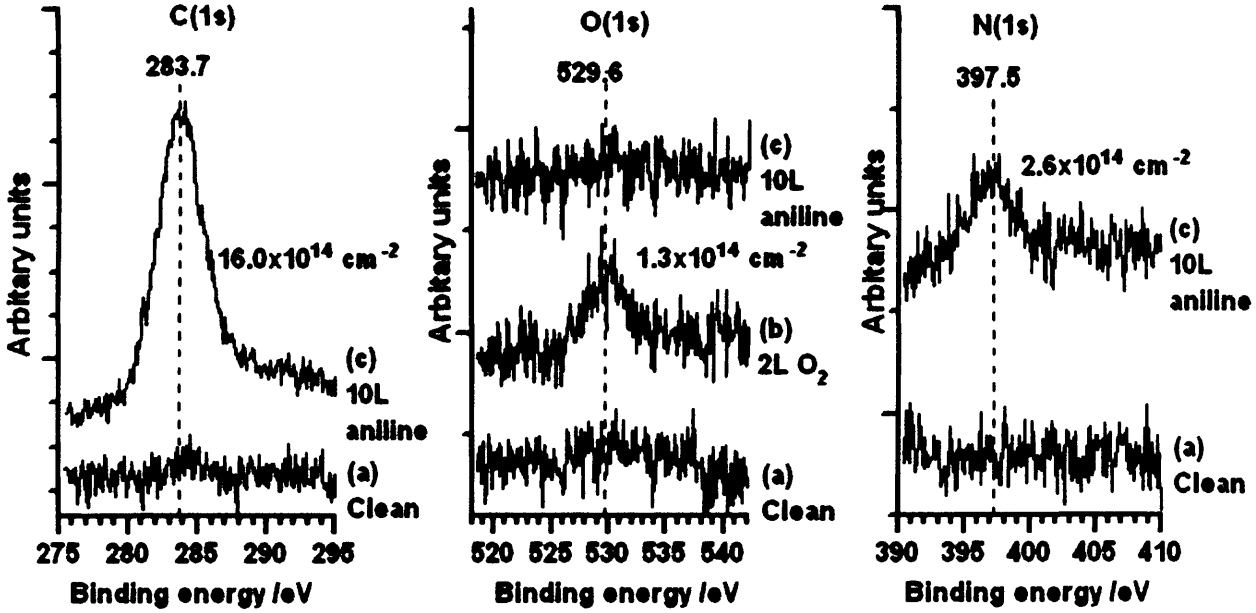

Fig. 5.3: The adsorption of aniline at a partially oxidised Cu(110) surface at 295K. XP spectra of C(1s), O(1s) and N(1s) regions; (a) Clean, (b) exposure of 2L of oxygen, (c) 10L dose of aniline.

5.5(b) Exposure of aniline to a higher oxygen concentration

The surface was exposed to 3L of oxygen. This resulted in a chemisorbed oxygen concentration of 2.9×10^{14} atoms cm^{-2}. This surface was then exposed to several exposures of aniline. This resulted in a C(1s) peak at 283.7eV and an N(1s) peak at 397.6eV. After an exposure of 4L, the reaction stoichiometry was 2 aniline: 1 oxygen removed. Upon further dosing, up to a total of 120L, the stoichiometry changed from 2:1 to 1:1.

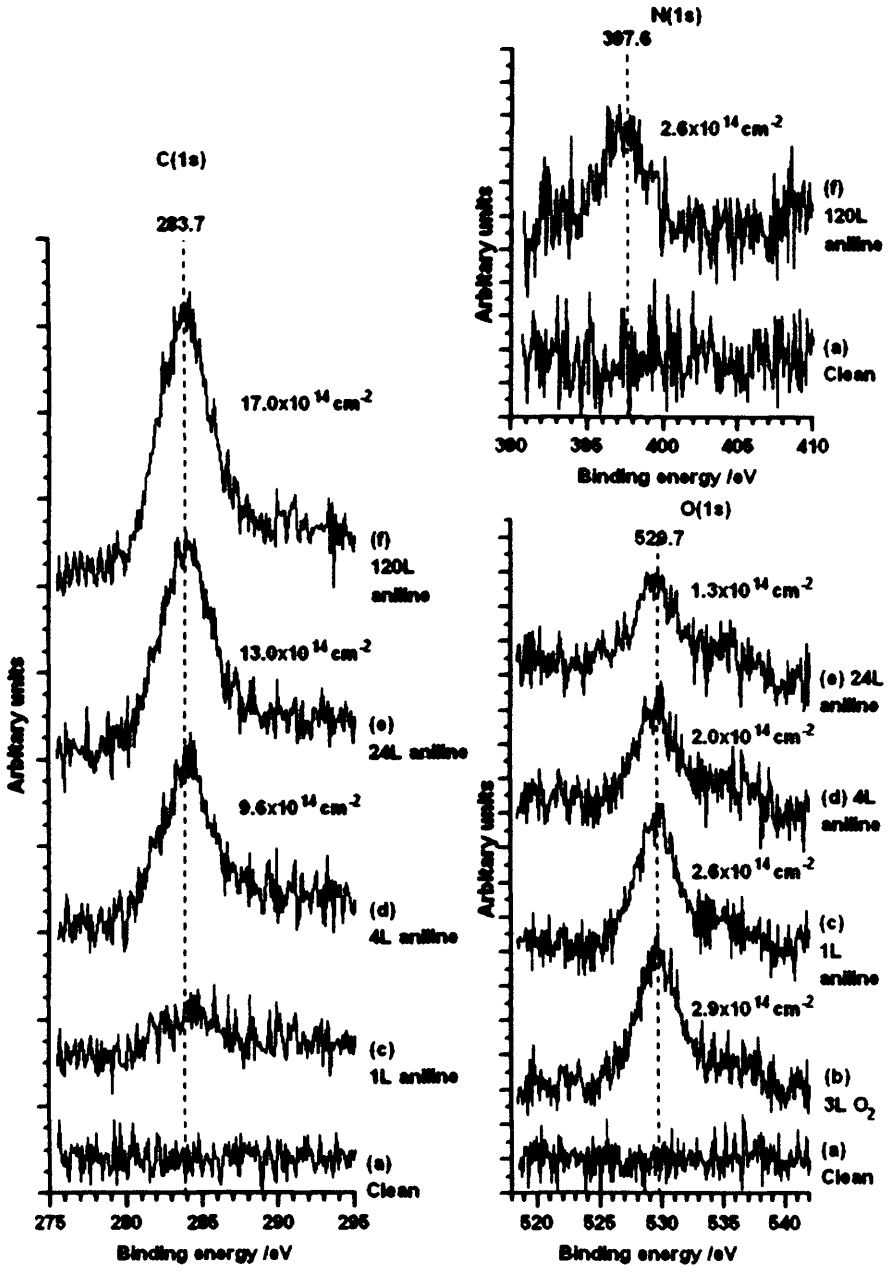

Fig. 5.4: C(1s), O(1s) and N(1s) XP spectra of the reaction of aniline with a partially oxidised Cu(110) surface at 293 K. (a) clean, (b) 3L of oxygen dosed, (c) 1L aniline dosed, (d) 4L aniline dosed, (e) 24L aniline dosed, (f) 120L aniline dosed.

5.5(c) Aniline adsorption with a pre-oxidised Cu(110) surface at 295K: STM results

An initial oxygen concentration of 2.4 x 10^{14} atoms cm^{-2} at a Cu(110) surface was exposed to 20L of aniline. STM images recorded after dosing the aniline showed an adsorbed product surrounding the oxygen islands which is the more reactive area [21]. The image shown in figure 5 shows a p(2x1)O(a) lattice. The size of the structure surrounding the oxygen lattice suggests that a phenyl ring is present. There is no long range order present.

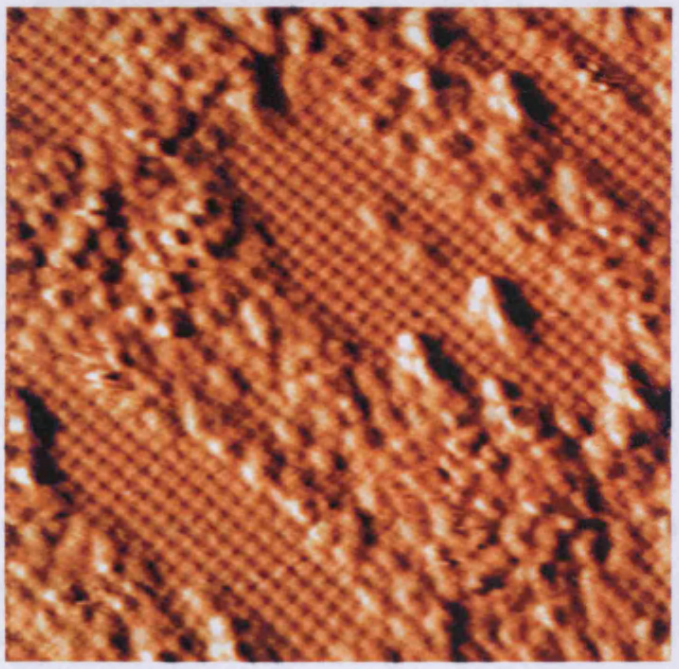

Fig. 5.5: Image of a partially oxidised surface following a 20L exposure of aniline.

A lower oxygen concentration (1.9 x 10^{14} atoms cm^{-2}) resulted in a surface that suggests the reaction has reached completion. The image now shows long range order in the form of 'zig-zags' occurring all over the surface. This zig-zag appearance is a result of at least two domains existing side by side. No oxygen is seen at the surface and this agrees with the XP spectra.

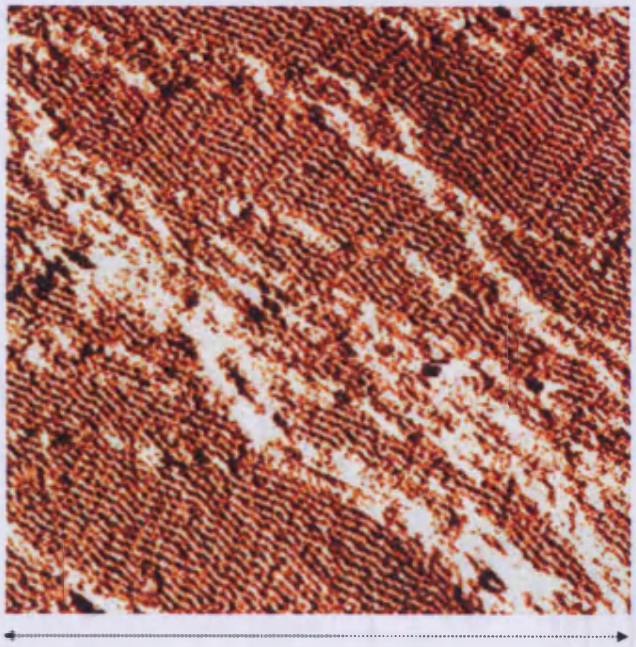

75nm

Fig.5.6: 'zig-zag' structure at the surface after exposing a partially oxidised surface to 100L of aniline.

5.6 Aniline adsorption with a fully oxidised surface.

Exposure of the Cu(110) sample to 10L of oxygen at 295K, yielded a fully oxidised surface, with a characteristic O (1s) binding energy of 529.7 eV. The oxygen concentration was calculated to be 5.38×10^{14} atoms/cm^2. the surface was then exposed to 200L of aniline. This resulted in no change in the oxygen peak and no carbon adsorption was observed.

STM images confirmed the XP results (images not shown). The complete p(2x1)O(a) lattice was unaffected by the aniline dose.

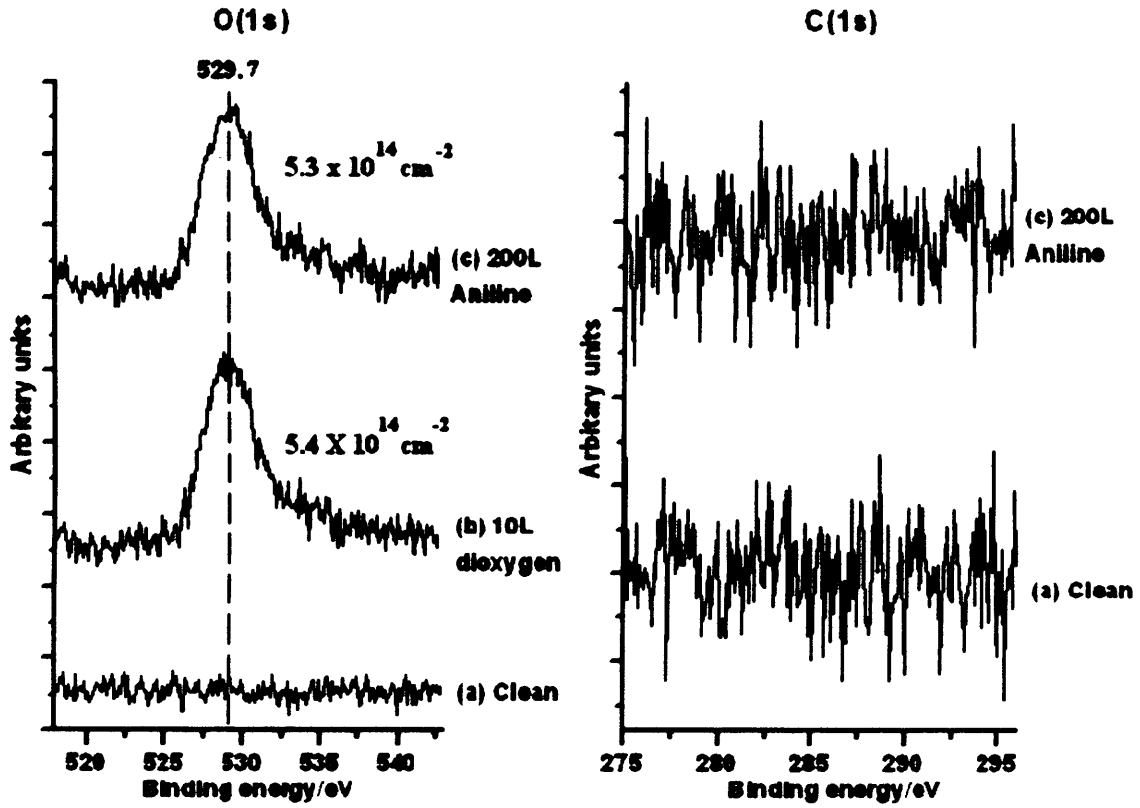

Fig. 5.7: The adsorption of aniline at a preoxidised Cu(110) surface at 290K. XP spectra of the C(1s) region at 100 eV and O(1s) region at 100eV, (a) clean, (b) 10L of oxygen dosed, (c) 200L of aniline dosed.

5.7(a) A co-adsorption of aniline and oxygen at a Cu(110) surface: XPS results.

A clean Cu(110) surface was exposed to a mixture of aniline and oxygen (300:1 respectively) at room temperature. The XP spectra show a peak at 284eV in the C(1s) region and a peak at 397.8eV in the N(1s) region. No oxygen was present at the surface. The surface concentrations of carbon and nitrogen were 2.0×10^{15} cm^{-2} and 3.3×10^{14} cm^{-2} respectively giving a C:N ratio of 6:1.

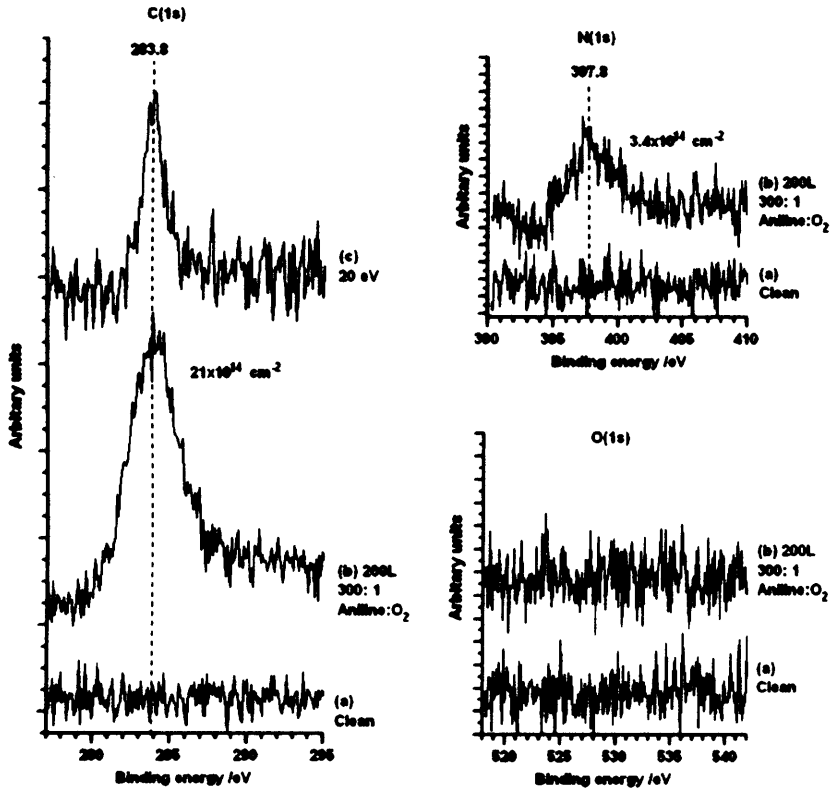

Fig.5.8: C(1s), O(1s) and N(1s) XP spectra of a 300:1 Aniline:oxygen coadsorption at a Cu(110) surface at 293 K. (a) clean, (b) after exposure to 200L aniline/oxygen mixture, (c) 20eV pass energy C(1s) XP spectrum.

5.7(b) Co-adsorption of aniline and oxygen at a Cu(110) surface: STM results.

STM images indicate that there has been a greater amount of surface reconstruction as compared to aniline adsorption at a partially oxidised surface. The 'zig-zag' structure is still visible. The reconstruction has resulted in smaller, less defined terraces, separated by steps of 1.2Å. The STM indicates that no oxygen is present.

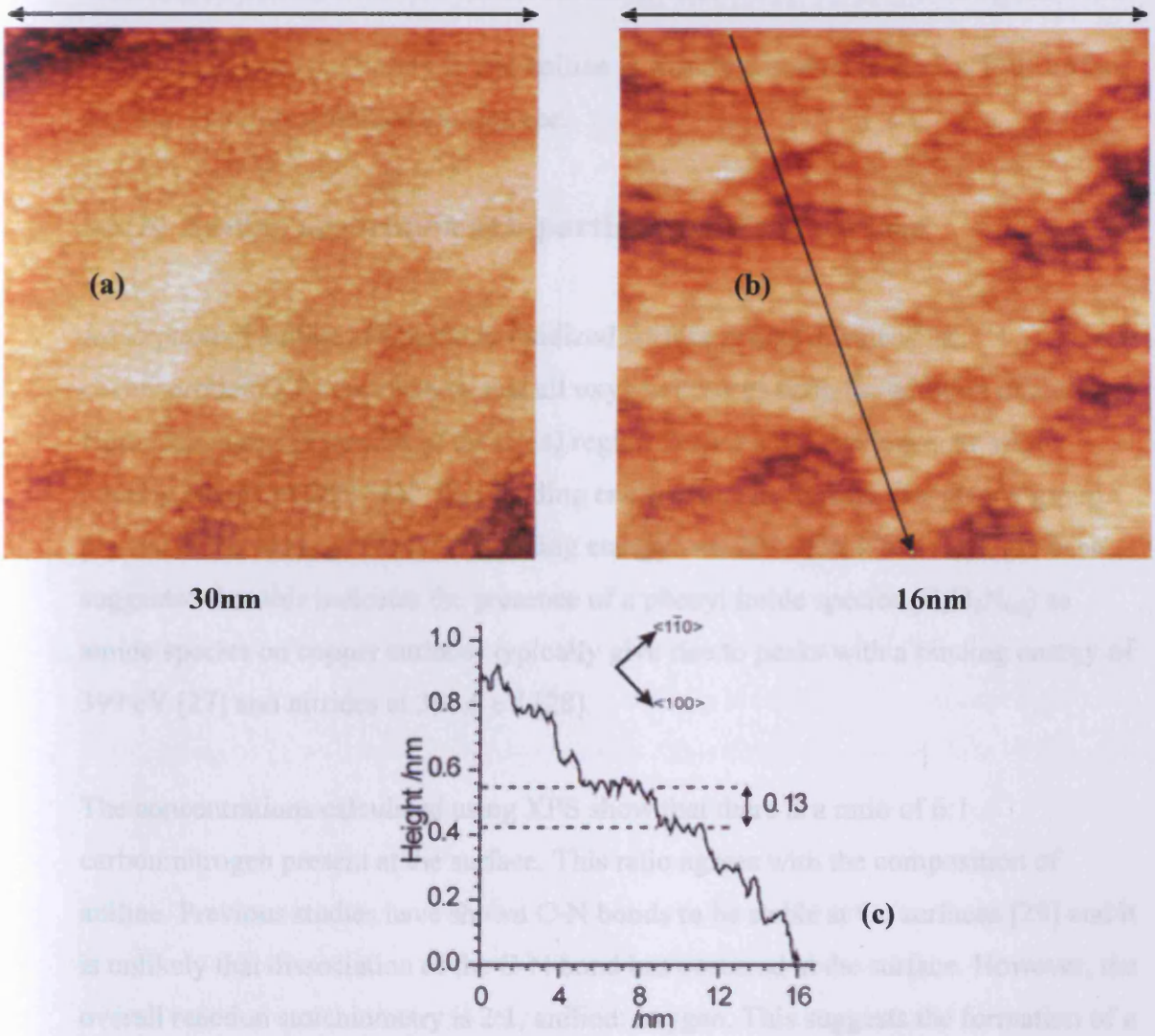

Fig. 5.9: Cu(110) surface after exposure to a 300:1 aniline vapour/oxygen mixture at 293 K, (a) Reconstructed surface, (b) zoomed version of image (a), (c) line profile of the reconstructed surface.

5.8 Discussion

5.8(a) Aniline adsorption at a clean Cu(110) surface.

In contrast to ammonia [22-25] and some other amines, aniline shows some adsorption at a clean surface, ammonia would only adsorb in the presence of oxygen. The C(1s) binding energy was 284eV. The low concentration obtained after a dose of 120L of aniline (5.2×10^{14} atoms cm^{-2}) and the STM images suggest that adsorption only occurred at step edges as there were no visible structures present in the STM

images. The other possibility is that aniline is weakly adsorbed to the Cu(110) surface and was therefore mobile at the surface.

5.8(b) Aniline adsorption at a partially oxidized surface.

Adsorption of aniline at a partially oxidized surface results in extensive chemisorption. XP spectra show that all oxygen desorbs upon the addition of aniline. High resolution XP spectra of the C(1s) region show a single carbon state with a binding energy of 283.7 eV. This binding energy is characteristic of a phenyl group present at the surface. The N(1s) binding energy was 397.8eV. It has therefore been suggested that this indicates the presence of a phenyl imide species ($C_6H_5N_{(a)}$) as amide species on copper surfaces typically give rise to peaks with a binding energy of 399 eV [27] and nitrides at 396.5 eV [28].

The concentrations calculated using XPS show that there is a ratio of 6:1 carbon:nitrogen present at the surface. This ratio agrees with the composition of aniline. Previous studies have shown C-N bonds to be stable at Cu surfaces [29] and it is unlikely that dissociation of the C-N bond has occurred at the surface. However, the overall reaction stoichiometry is 2:1, aniline: oxygen. This suggests the formation of a chemisorbed phenyl amide ($C_6H_5NH_{(a)}$) as shown in equations 2 and 3.

$PhNH_2(g) + O(a) \rightarrow PhNH(a) + OH(a)$ (2)

$PhNH_2(g) + OH(a) \rightarrow PhNH(a) + H_2O(g)$ (3)

However, previous experiments [30] show that in the case of ammonia adsorption at a Cu(110) surface, despite a similar 2:1 stoichiometry, reaction with oxygen gives an imide ($NH_{(a)}$). This was proven using vibrational spectroscopy. In the present case the reaction stoichiometry becomes 1:1 at higher initial oxygen surface concentrations, whilst the XP binding energy indicates that the product remains the same. Since the N(1s) B.E. of the product is typical of an imide we suggest that the imide is the product suggesting dissociation of the imide group ($RNH \rightarrow RN + H$). A proposed mechanism for the reaction of aniline with oxidised Cu(110) surfaces is as follows.

$PhNH_2(g) + O(a) \rightarrow PhNH(a) + OH(a)$ (2)

$PhNH_2(g) + OH(a) \rightarrow PhNH(a) + H_2O(g)$ (3)

$2OH(a) \rightarrow O(a) + H_2O(g)$ (4)

$PhNH(a) \rightarrow PhN(a) + H(a)$ (5)

$2H(a) \rightarrow H_2(g)$ (6)

$PhNH(g) + OH(a) \rightarrow PhN(a) + H_2O(g)$ (7)

At low oxygen coverages equation 7 is slow relative to 2, 3 and 4 but is dominant at high surface coverages. This may be due to steric hindrance between two aniline reactants or the need for two adjacent adsorption sites. The phenyl amide formed from equations 2 and/or 3 must be unstable at the surface in respect to the phenyl imide dissociating to give adsorbed hydrogen which either remains at the surface or desorbs via equation 6.

The p(2x1) structure of oxygen adsorbed at a Cu(110) surface is well understood. The oxygen lattice formed by the reaction of oxygen with Cu(110) surfaces consists of added copper-oxygen chains orientated in the <100> direction. The added copper atoms are situated in the hollow sites of the Cu(110) substrate and it is these atoms that are imaged by STM (fig. 10) [31]. Therefore STM images that show oxygen islands together with chemisorbed phenyl-imide can be used to determine the adsorption site of the imide species.

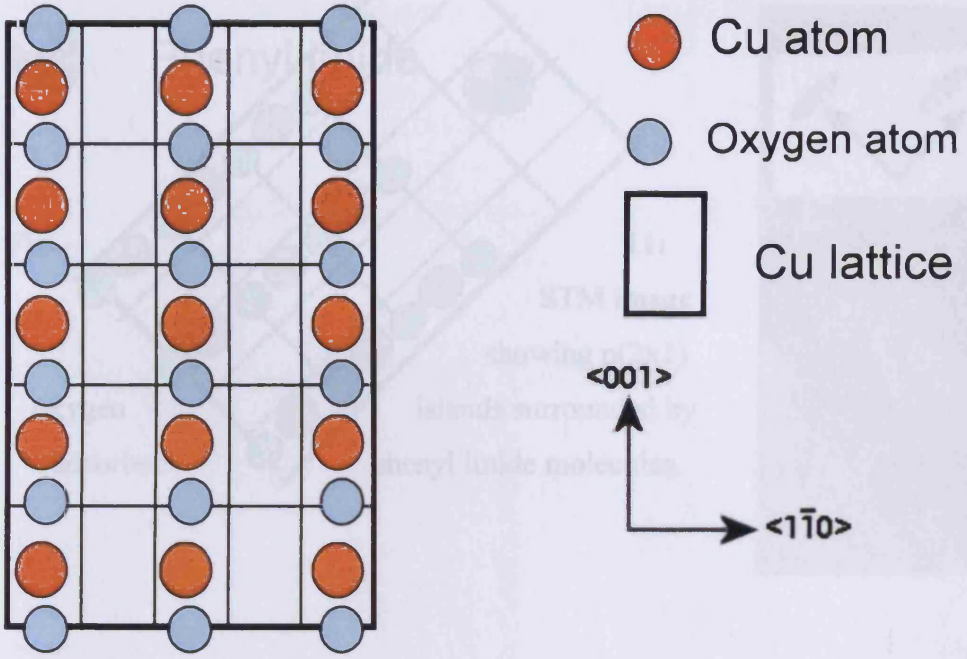

Fig. 10: Structure formed by the dissociative chemisorption of oxygen at a Cu(110) surface.

It has been seen that with benzene [32] and other phenyl containing compounds [33] that adsorption of the phenyl ring occurs in the hollow sites of the Cu(110) substrate. Figure 11 shows a lattice superimposed onto an oxygen island and then extrapolated over areas of adsorbed phenyl imide. The p(2x1)O lattice maxima corresponding to the added copper atoms are directly in line with the amide product maxima in both the <100> and the <110> directions. It is suggested that the features imaged with a ~0.7nm diameter are the phenyl rings due to the high electron density content. Therefore, it is concluded that the phenyl rings of the adsorbed imide molecules are situated in the hollow sites of the Cu(110) substrate.

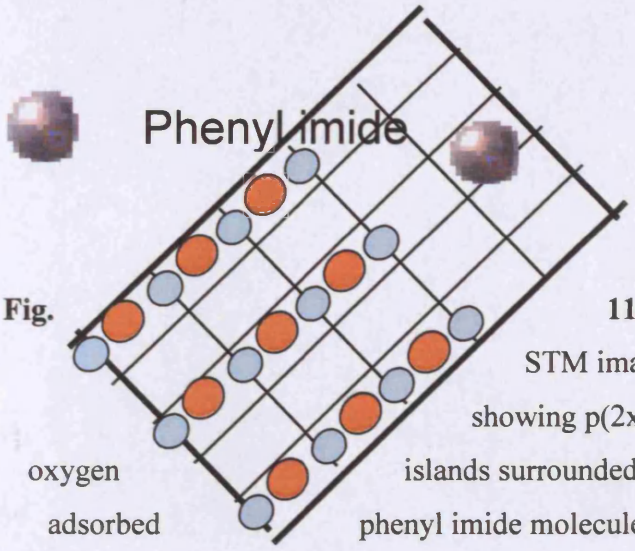

Fig. 11: STM image showing p(2x1) oxygen adsorbed islands surrounded by phenyl imide molecules.

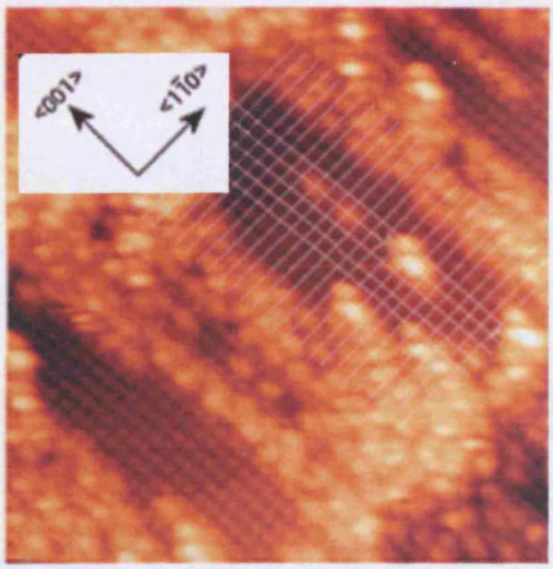

Molecularly resolved STM images show three different domains of the 0.7nm diameter features. These domains are $\begin{pmatrix} 4 & 0 \\ 2 & 2 \end{pmatrix}$(c(4 x 4) Woods notation), $\begin{pmatrix} 4 & 0 \\ -1 & 2 \end{pmatrix}$ and $\begin{pmatrix} 4 & 0 \\ 1 & 2 \end{pmatrix}$. All three are closely related and $\begin{pmatrix} 4 & 0 \\ -1 & 2 \end{pmatrix}$ and $\begin{pmatrix} 4 & 0 \\ 1 & 2 \end{pmatrix}$ are mirror images of each other. The surface concentrations of the imide in each domain are identical.

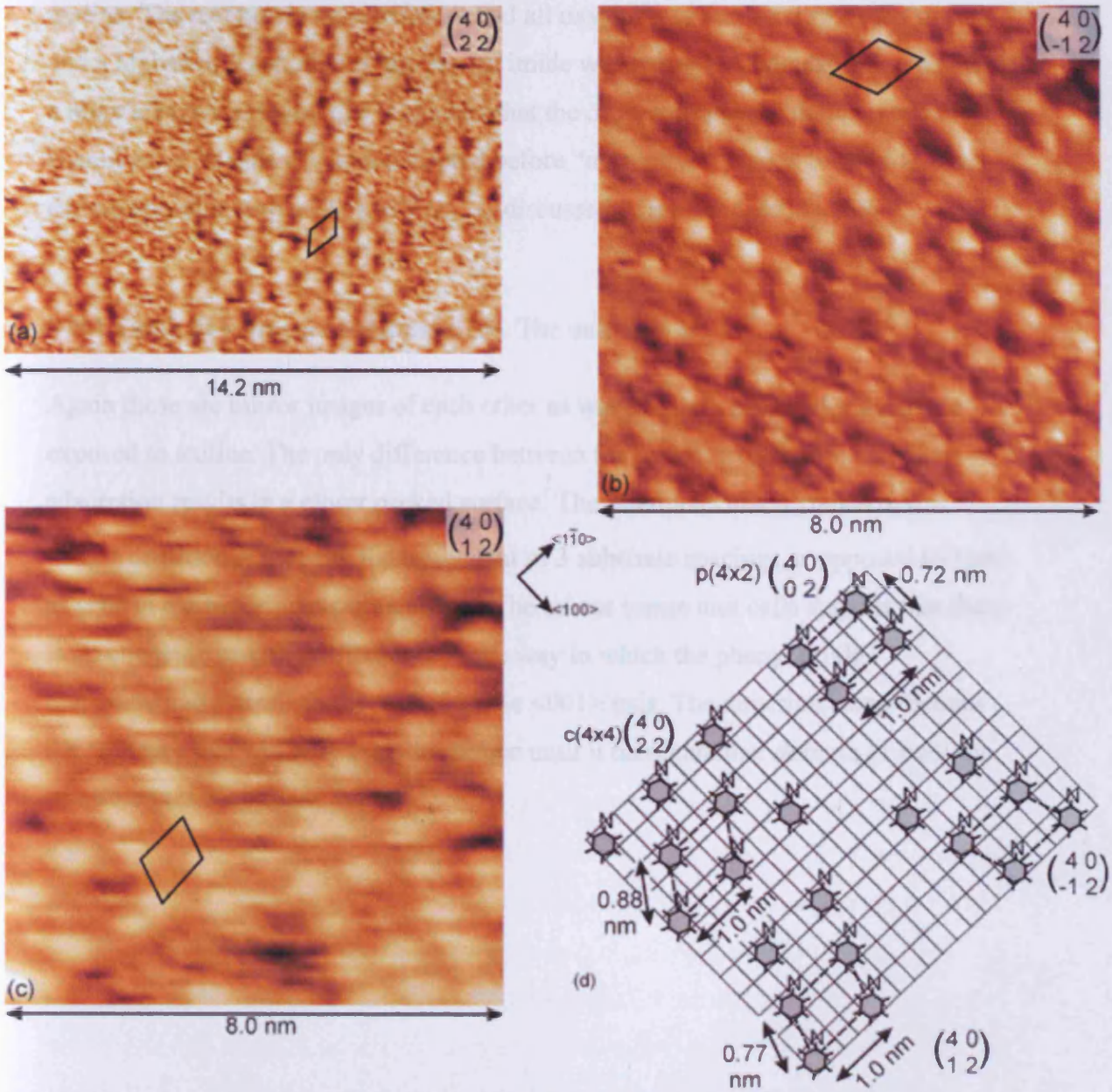

Fig. 12: The three different domains present at the surface.

It is noticeable that p(4x2) is not present at the Cu(110) surface. The reason for this is discussed later.

5.8(c) Coadsorption of aniline and oxygen

Exposure of the surface to an aniline/oxygen mixture (300:1) resulted in XPS peaks at 283.8 eV in the C(1s) region and 397.8 eV in the N(1s) region. The ratio was 6:1 carbon: nitrogen. These results are similar to exposure of a pre-oxidised surface to aniline. The reaction is more efficient and all oxygen was desorbed from the surface and a higher concentration of the phenyl imide was present. A co-adsorption results in a more efficient reaction due to the fact that the oxygen transients that precede the chemisorbed islands can be intercepted before "unreactive" islands form [34]. The carbon concentration of 2.1×10^{15} cm^{-2} is discussed in greater detail in **X.9.**

STM shows two structures at the surface. The unit cells are $\begin{pmatrix} 3 & 0 \\ -1 & 2 \end{pmatrix}$ and $\begin{pmatrix} 3 & 0 \\ 1 & 2 \end{pmatrix}$.

Again these are mirror images of each other as was seen at a pre-oxidised surface exposed to aniline. The only difference between the two structures formed is that co-adsorption results in a closer packed surface. The intermolecular distance in the $<1\bar{1}0>$ direction is 0.76nm, the equivalent of 3 substrate spacings as opposed to 1nm as seen in the experiments in figure 12. The mirror image unit cells suggest that there is no energetic or steric differences in the way in which the phenyl imide perpendicularly bonds to the surface in the <001> axis. The direction taken dictates the structure that will adsorb at the surface until it meets another domain or until the structure meets a surface defect.

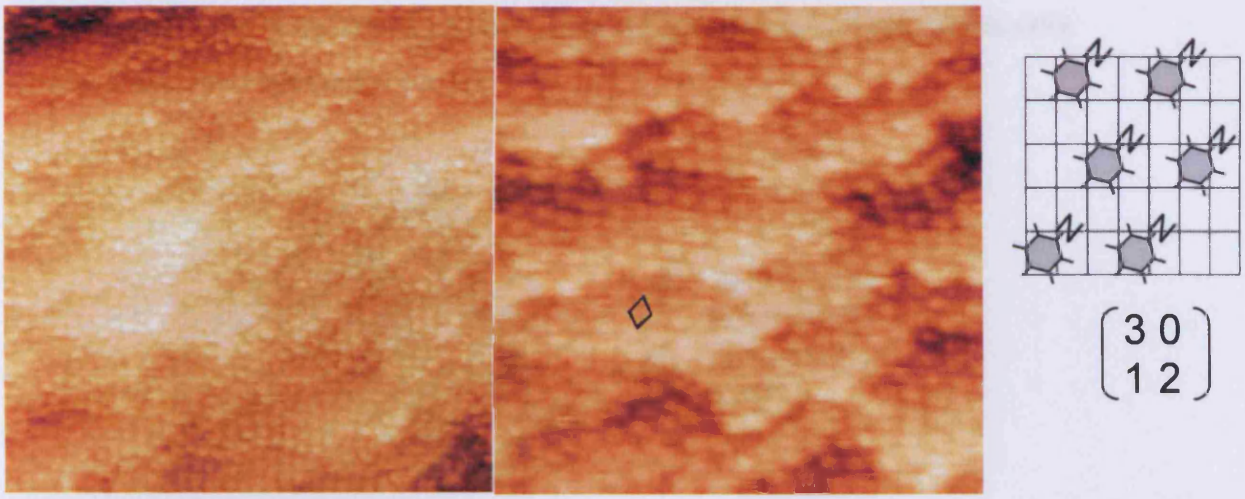

Fig. 13: STM image of the domain at the Cu(110) surface.

5.9 Discrepancies in surface concentrations

The concentrations of phenyl imide adsorbed at a preoxidised surface and from the co-adsorption reaction were calculated using both XPS and STM. If each feature in the STM represents a phenyl imide then the three structures produced from the reaction of aniline with preadsorbed oxygen resulted in a phenyl imide concentration of 1.4×10^{14} cm^{-2}. For the coadsorption, this concentration was calculated to be 1.8×10^{14} cm^{-2}. The actual concentrations determined by XPS were 2.7×10^{14} cm^{-2} and 3.5×10^{14} cm^{-2}, respectively. It can be seen that these concentrations are double that of the calculated concentration using STM. It is therefore concluded that STM is only imaging half the molecules. There are two proposals for this discrepancy of surface concentrations. The first proposal suggests that the phenyl rings are orientated in an edge to face T-shaped structure in which every other phenyl group is orientated perpendicular to the surface as shown in figure 14. This is known to be a favourable structure for close packed aromatic systems. However it is known that phenyl rings generally bond parallel to the surface and even though the interaction between a parallel and perpendicular species may compensate for the reduction in the heat of adsorption that arises from the perpendicular orientation this is the least favourite proposal. It is suggested that steric factors may also restrict this structure forming. Various studies of vibrational spectroscopy of aniline at metal surfaces have always

found the molecule lying almost parallel to the surface. However these studies only looked at low coverages at the surface.

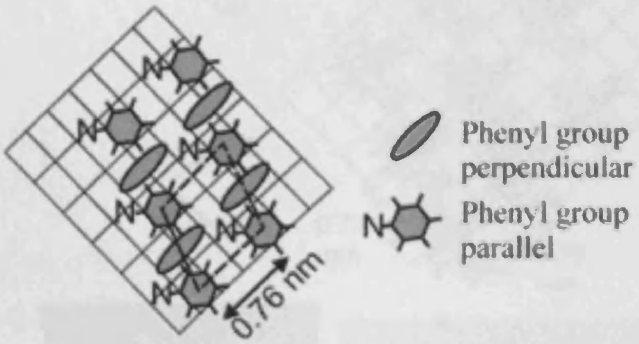

Fig. 14: A model to show the T-shaped structure formed at the surface which would result in only half the aniline molecules being imaged at the Cu(110) surface.

An alternative model involves a form of π stacking. This entails parallel phenyl pairs with the coordination of both nitrogens to the surface achieved by tilting the rings away from the surface plane. Figure 15 shows a detailed model of a possible complex. The lower phenyl ring is situated above a hollow site and the nitrogen atom is at the short bridge site. The second phenyl ring is 0.15nm above it and rotated by 65°. This again places the nitrogen group above a short bridge site. To bring the nitrogen of the upper ring to a similar height of the lower molecule, the rings can be tilted. Tilting them by 15-20° to the surface plane without moving the nitrogen atoms could cause this result. Vibrational spectroscopy studies conclude that the phenyl group lies almost parallel to the surface [36, 37]. However, these studies only concern adsorption at a clean surface. Therefore the surface concentration is lower and may not be high enough to cause the pi-stacked complex.

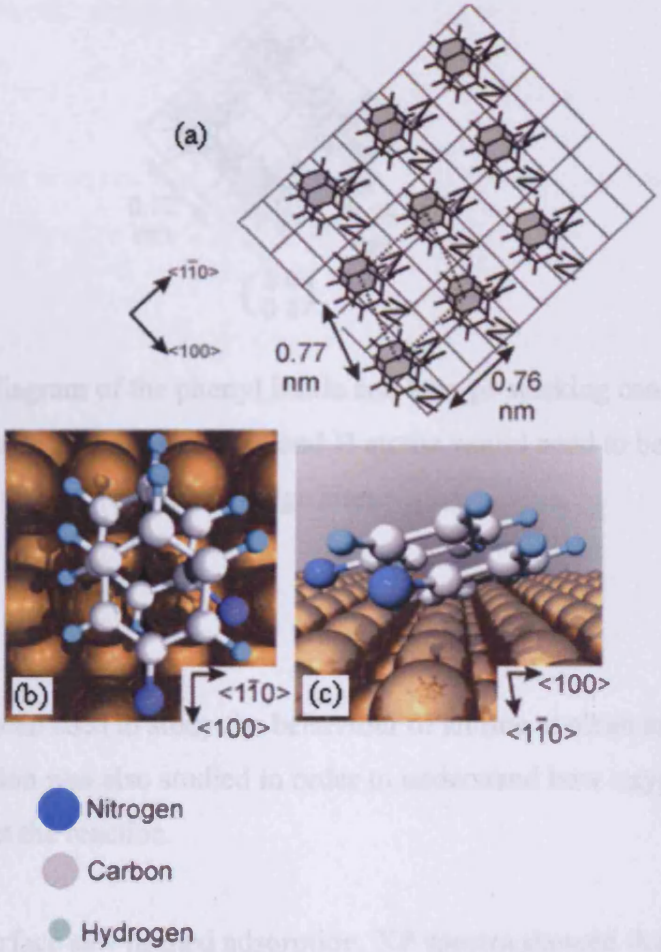

Fig. 15: (a) Pi-stacking model to account for the discrepancy between STM and XPS results, (b) top view of phenyl-imide ball and stick model, (c) side view of ball and stick model showing the tilted rings

The proposed model also offers an explanation as to why the unit cells $\begin{pmatrix} 4 & 0 \\ 0 & 2 \end{pmatrix}$ and $\begin{pmatrix} 3 & 0 \\ 0 & 2 \end{pmatrix}$ (p(4x2) and p(3x2) respectively) are not observed. These structures would result in the overlap of a nitrogen and a hydrogen at a bridge site as shown in figure 16.

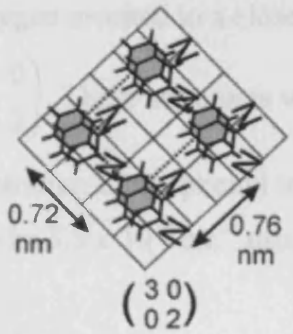

Fig. 16: Schematic diagram of the phenyl imide and how pi-stacking can explain the lack of primitive square unit cells; both N and H atoms would need to be situated at short bridge sites.

5.10 Conclusion.

XPS and STM have been used to study the behaviour of aniline at clean and oxidised surfaces. A coadsorption was also studied in order to understand how oxygen transients would affect the reaction.

Reaction at a clean surface saw limited adsorption. XP spectra showed that only low concentrations of aniline were present. STM studies revealed no adsorbate at the surface indicating mobility and showed no surface reconstruction.

Adsorption occurred more readily at a partially oxidised surface and resulted in a formation of a phenyl imide. By simultaneously imaging the phenyl-imide and the p(2x1)O(a) lattice the phenyl group was shown to lie above the substrate hollow site, in this position the nitrogen atom of the imide can be placed over the short bridge site, the favoured site for NH(a). The maximum concentration of phenyl imide deduced from the XP spectra was 2.7×10^{14} cm^{-2}. Three closely related domains were present at the surface and these can be described by $\begin{pmatrix} 4 & 0 \\ 2 & 2 \end{pmatrix}$, $\begin{pmatrix} 4 & 0 \\ -1 & 2 \end{pmatrix}$ and $\begin{pmatrix} 4 & 0 \\ 1 & 2 \end{pmatrix}$ unit meshes.

Coadsorption of aniline and oxygen resulted in a closer packed surface structure described by $\begin{pmatrix} 3 & 0 \\ -1 & 2 \end{pmatrix}$ and $\begin{pmatrix} 3 & 0 \\ 1 & 2 \end{pmatrix}$. These structures were mirror images. The closer packing lead to a higher concentration of the phenyl imide present at the surface. The concentration was calculated to be 3.5×10^{14} cm^{-2} using XP spectra.

Concentrations calculated using XPS were twice that of concentrations calculated using unit cells determined by STM. Two models were proposed to account for this discrepancy. The first involved alternating parallel and perpendicular phenyl rings with respect to the surface. The favoured proposal on a basis of the steric hindrance involves parallel pi-stacking of the phenyl rings.

5.11 References

[1] P. R. Davies and N. G. Newton, *Surf. Sci.* 546 (2003) 149.

[2] A. F. Carley, P. R. Davies, K. R. Harikumar, R. V. Jones, G. U. Kulkarni and M. W. Roberys, *Top. Catal.* 14 (2001) 101.

[3] P. R. Davies and J. M. Keel, *PCCP,* 1 (1999) 1383.

[4] A. F. Carley, P. R. Davies, R. V. Jones, G. U. Kulkarni and M. W. Roberts, *Chem Commun,* (1999) 1383.

[5] P.R. Davies and N. Shukla, *Surf. Sci,* 322 (1995) 8.

[6] CRC Handbook of Chemistry and Physics; 59 ed.; R. C. Weast, Ed.; CRC Press Inc: Boca Raton, 1979; Vol. 59, p. F215.

[7] E. P. Hunter and S. G. Lias, *J. Phys. Chem.* Ref. Data 27 (1998) 413.

[8] R. V. Plank, N. J. Dinardo and J. M. Vohs, *Surf. Sci.* 340 (1995) L971.

[9] G. Ramsey, D. Rosina and H. Graen, *Surf. Sci.* 232 (1990) 266.

[10] R. Rummel and C. Ziegler, *Surf. Sci.* 418 (1998) 303.

[11] T. J. Rockey, M. Yang and H. Dai, *Surf. Sci.* 589 (2005) 42.

[12] J. L. Solomon and R. J. Madix, *Surf. Sci.* 255 (1991) 12.

[13] C. Bronnimann, Z. Bodnar, R. Aishimann, T. Mallat and A. Baiker, *J. Catal.* 161 (1996) 720.

[14] W. D. Huntsman, N. L. Madison and S. L. Schlesinger, *J. Catal.* 2 (1963) 498.

[15] J. Struijk and J. Scholten, *Appl. Catal. A*, 82 (1992) 277.

[17] E. Lazarova, G. Petkova, R. Raicheff and G. Neykov, *J. Appl. Electrochem.* 32 (2002) 1355.

[18] K. F. Khaled and N. Hackerman, *Electrochem.* Acta49 (2004) 485.

[20] T. B. Du, J. J. Chem and D. Z. Cao, *J. Mater. Sci.* 36 (2001) 3903.

[21] A.F. Carley, P.R. Davies and M.W. Roberts, *Chem. Commun.* (1998) 1793.

[22] P. R. Davies and J. M. Keel, *Surf. Sci.* 469 (2000) 204.

[23] A. F. Carley, P. R. Davies and M. W. Roberts, *Catal. Lett.* 80 **(2002)** 25.

[24] A. F. Carley, P. R. Davies, R. V. Jones, K. R. Harikumar, G. U. Kulkarni and M. W. Roberts, *Top. Catal.* 11 (2000) 299.

[25] A. F. Carley, P. R. Davies, M. W. Roberts and D. Vincent, *Top. Catal.* 1 (1994) 35.

[26] A. F. Carley, M. Coughlin, P. R. Davies, D. J. Morgan and M. W. Roberts, *Surf. Sci. Letts.* 2004.

[27] B. Afsin, P. R. Davies, A. Pashusky, M. W. Roberts and D. Vincent, *Surf. Sci.* 284 (1993) 109.

[28] B. Afsin, P. R. Davies, A. Pashuski and M. W. Roberts, *Surf. Sci.* 259 (1991) L724.

[29] P. R. Davies and J. M. Keel, *Phys.Chem.Chem.Phys.* 1 (1999) 1383.

[30] B. Afsin, P. R. Davies, A. Pashusky, M. W. Roberts and D. Vincent, *Surf. Sci.* 284 (1993) 109.

[31] J. Buisset, H. P. Rust, E. K. Schweizer, L. Cramer and A. M. Bradshaw, *Surf. Sci.* 349 (1996) L147.

[32] B. L. Rogers, J. G. Shapter and M. Ford, *Surf. Sci.* 548 (2004) *548.*

[33] A. F. Carley, M. Coughlin, P. R. Davies, D. J. Morgan and M. W. Roberts, *Surf. Sci.* 555 (2004) L138.

[34] A. F. Carley, P. R. Davies and M. W. Roberts, *Catal. Lett.* 80 (2002) 25.

[35] C. A. Hunter, K. R. Lawson, J. Perkins and C. J. Urch, *J. Chem. Soc.-Perkin Trans. 2* (2001) 651.

[36] M. R. Ashton, T. S. Jones, N. V. Richardson, R. G. Mack and W. N. Unertl, J. Electron Spectrosc, Relat. Phenom. 54 (1990) 1133.

[37] R. V. Plank, N. J. Dinardo and J. M. Vohs, Surf. Sci. 340 (1995) L971.

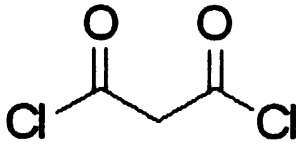

Chapter 6

Interaction of Malonyl dichloride with Cu(110) surfaces

6.1 Introduction

The interaction of gaseous malonyl dichloride ($Cl_2C_3O_2H_2$) with clean Cu(110) and partially oxidised Cu(110) surface has been studied. This investigation aims to enhance the current understanding of halogen containing molecules interaction with a Cu(110) surface. Emphasis is placed on the reaction with a partially oxidised surface.

6.2 Background

The chemisorption of halogen containing atoms is considered to be important in molecular folding and design [1]. Halogens are strong adsorbates and can effectively poison many catalytic reactions. However, in some cases they are used as promoters [2]. Adsorption on metallic surfaces is of particular importance due to its relevance to many industrial processes. Halogens are model adsorbates for studying chemisorption

on covalently bonded materials, such as semiconductors, owing to the simple nature of the bonds that they form. Experimentally, organo-halides are frequently used as precursors to the formation of adsorbed organic groups on metal surfaces [3]. Adsorbed halides are also known to act as promoters for catalytic reactions. An example of this is chlorine which is commonly used as a promoter for silver catalyzed ethylene epoxidation [4]. Using halogens as promoters results in a change in the thermodynamic stabilities of the surface intermediates and transition states with respect to each other and therefore influences the activities of catalytic surfaces and the selectivity to specific products. Adsorption of halogens has also been used to selectively block surface defect sites such as kinks and steps in experiments designed to distinguish between the contributions to molecular desorption from terrace, step and kink sites [5].

As far as we are aware there have been no previous studies of the adsorption of malonyl dichloride adsorption. An investigation of this molecule may help to understand reactions that may occur with other species at the surface. The interaction between the chlorine electron pair and the carbonyl group in malonyl dichloride is ineffective as it requires the overlap of the chlorine 3p orbital and the carbon 2p orbital. This overlap is poor. The polar effect of the chlorine destabilizes the carbonyl group through an unfavourable interaction of the carbon – chlorine bond dipole with a partial positive charge on the carbonyl carbon. The chloride ion is a very weak base and due to this it is a very good leaving group.

Halogen adsorption has been studied at copper surfaces. An STM study of chlorine and bromine chemisorption at a Cu(100) surface reported the appearance of the c(2×2)Cl structure at coverages at and above ~ 70% saturation, with continuous regions appearing by ~ 95% saturation [6]. It was noted that chemisorption of both chlorine and bromine induced step faceting, but while halide formation in the case of Cl_2 was initiated at the corners of the step facets and was proceeded by copper atoms being stripped away in rows parallel to the step edge, for bromination there was no evidence that kinks were more reactive than other sites along the steps. Following bromination, the Cu(100) surface was characterised by peninsulas and channels that the authors attributed to the reaction starting at the steps.

An STM investigation of the Cu(100) surface exposed to Cl_2(g) [7] could not image any of the features typical of adsorbate phases at coverages below a monolayer of c(2×2)Cl. This was attributed to the mobility of the chemisorbed chlorine under the influence of the scanning tip. At a coverage of a monolayer, the chemisorbed chlorine was no longer mobile. AES provided evidence for the formation of CuCl at room temperature after a Cl_2 dose of 400 L. The CuCl film sublimed at 420-480 K, resulting in the restoration of the chlorine monolayer. The chemisorbed chlorine was removed in the form of CuCl molecules at temperatures in the range 770-900 K.

Previous studies of HCl adsorption at clean Cu(110) and partially oxidised Cu(110) surfaces have seen the formation of very large structures at the surface [8]. It was reported that there was no trace of any adsorbate-induced reconstruction observed at the surface until the concentration of Cl exceeded 4.9×10^{14} cm^{-2} (~88% of a monolayer). The appearance of adsorbate features with the STM therefore only occurs when the concentration of Cl approaches that of a monolayer of c(2×2), and mobility is hindered by the volume of adsorbate present at the surface.

6.3 Experimental

The instrument used in this investigation has been discussed previously. The radiation used for the XP data acquisition was the Al(kα) line with a photon energy of 1486.6eV. All XP data was recorded at a pass energy of 50eV unless otherwise stated. All spectra were referenced to the clean Cu($2p_{3/2}$) peak at 932.7eV.

Oxygen (99.99% Argo International), HCl (99.0% Argo International) and malonyl dichloride (98.0% Aldrich) were attached to the gas line. Further purification of the malonyl dichloride liquid was achieved through several freeze-pump-thaw cycles. The purity of all gasses was monitored using in-situ mass spectrometry.

6.4 Malonyl dichloride adsorption on Cu(110) at 295K

6.4 (a)XPS results

Exposure of an atomically clean Cu(110) surface to malonyl dichloride at room temperature (1500L in total) resulted in no carbon (1s), oxygen (1s) or chlorine (2p) peaks in the XP spectra. It can therefore be concluded that malonyl dichloride will not adsorb to a clean Cu(110) surface (spectra not shown).

6. 4(a)i Chemisorptive Replacement of Oxygen by malonyl dichloride at Cu(110) Surfaces, (1L of oxygen) at 295K: XPS results

An initial dose of 1L of oxygen onto an atomically clean Cu(110) surface resulted in a partially oxidised surface with an oxygen atom concentration of 1.84×10^{14} cm^{-2} as measured from XP spectra. The O(1s) binding energy in the XP spectrum was 529.7eV. Exposure of this surface to 5L of malonyl dichloride resulted in a broad peak developing in the C(1s) region at around 285eV and a second species in the O(1s) at 536eV. The original oxygen peak now centred at 530eV has increased in intensity. There is also a Cl(2p) peak at 197.5eV. The carbon, oxygen and chlorine concentrations were 4.2×10^{14}, 3.92×10^{14} and 8.10×10^{13} atoms cm^{-2} respectively. Subtracting the initial oxygen concentration gives a ratio of 5:2.5:1 C:O:Cl. This is not consistent with the ratio expected for molecular adsorption (3:2:2), the carbon concentration is approximate due to the difficulty in quantifying the peak.

A further dose of 20L resulted in the complete removal of carbon. The O(1s) spectra shows some broadening and a decrease in concentration. It also shows a shift from 530eV to 530.5eV. The Cl(2p) shows an increase in intensity of chlorine. All concentrations are tabulated in table 1.

A final dose of 600L of malonyl dichloride resulted again in no carbon present in the C(1s) spectra. The O(1s) region shows a slight decrease in oxygen intensity but the peak remains as broad as previously. The Cl (2p) spectrum shows a significant increase in intensity.

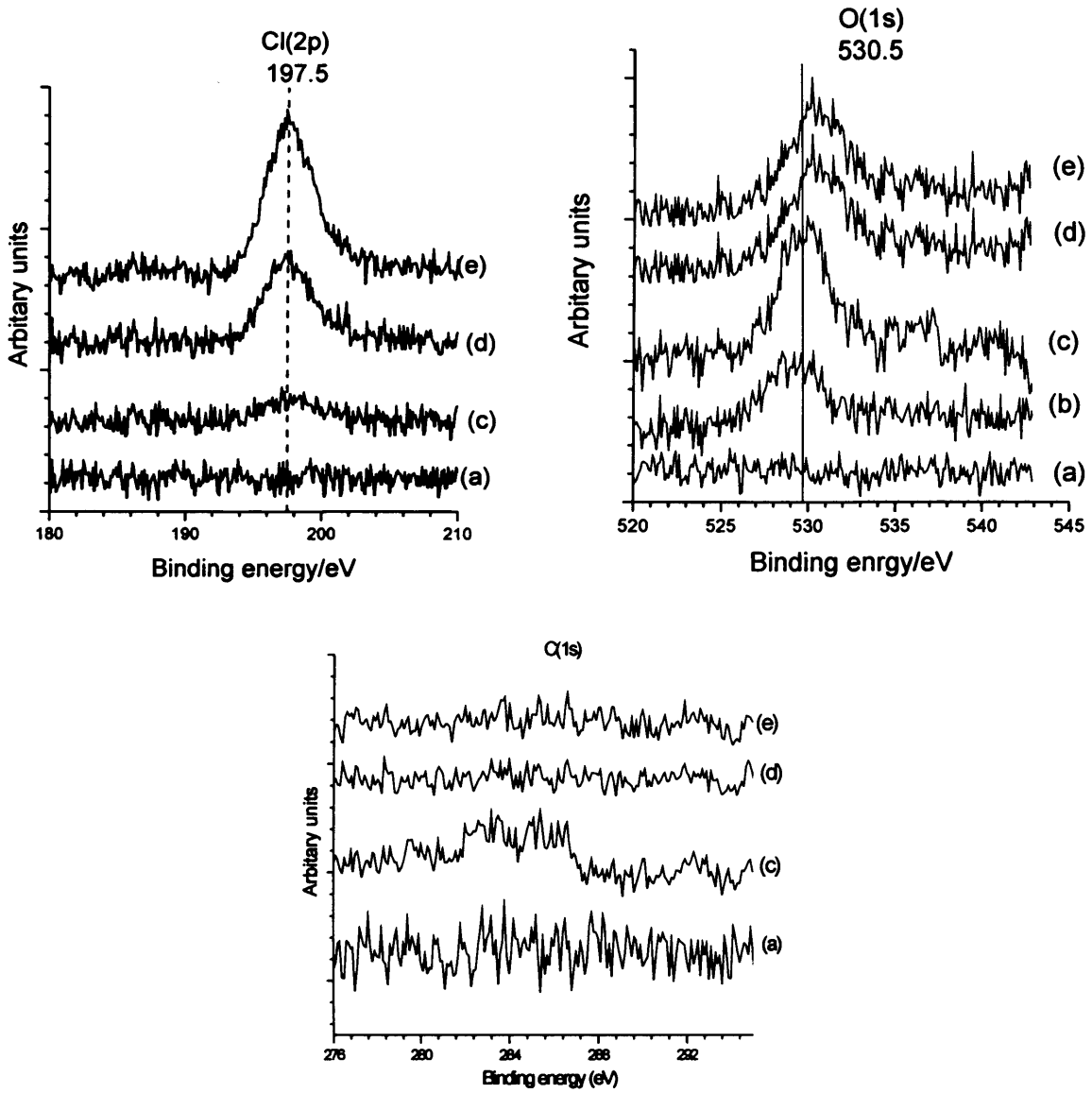

Fig. 6.1: The adsorption of malonyl dichloride at a Cu(110) surface at 290K. XP spectra of the C(1s) region at 20 eV, O(1s) region and Cl(2p) region. (a) clean, , (b) 1L of oxygen dosed, (c) 5L of malonyl dichloride dosed, (d) 20L exposure, (e) 600L exposure.

Exposure of malonyl dichloride (L)	C(1s) Concentration (atoms cm^{-2})	O(1s) Concentration (atoms cm^{-2})	O(1s) Concentration with initial oxygen subtracted (atoms cm^{-2})	Cl(2p) Concentration (atoms cm^{-2})
Oxygen initial dose (1L)		1.84×10^{14}		
5	4.2×10^{14}	3.92×10^{14}	2.08×10^{14}	8.10×10^{13}
20	0	2.88×10^{14}	1.04×10^{14}	3.52×10^{14}
600	0	2.33×10^{14}	4.9×10^{13}	6.25×10^{14}

Table 6.1: Concentrations of species present in fig. 1.

The large FWHM of the O(1s) spectra after the initial dose of malonyl dichloride suggests the presence of two or more oxygen species at a binding energy greater than 529.7eV. The spectra suggest that the chemisorbed oxygen is still present, but there is now an increased number of oxygen species present at the surface at 530.5eV. However the signal to noise ratio is poor.

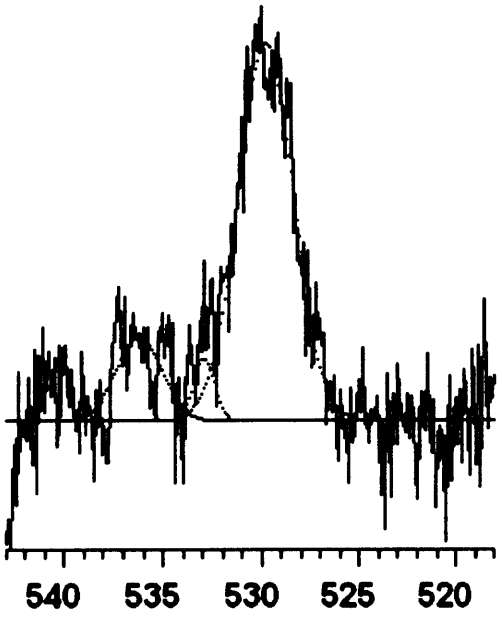

B.E. (eV)

Fig. 6.2: curve fitting of the initial O(1s) peak

Further doses of malonyl dichloride (20L) result in the complete removal of carbon from the surface. The O(1s) spectra also shifts 0.5eV higher. Cl(2p) spectra show an increase in the amount of chlorine at the surface. Subtracting the initial oxygen concentration results in a O:Cl ratio of 1:3.3.

The final dose of malonyl dichloride results in no carbon and a slight decrease in concentration of oxygen (5.5×10^{14} atoms cm^{-2}). The chlorine concentration has increased to 6.25×10^{14} atoms cm^2. The binding energy of the chlorine remains at 197.5eV.

6.5 STM studies of MDC at a partially oxidised surface at 295K

STM images of a Cu(110) surface previously exposed to 4L of oxygen were exposed to a 600L dose of malonyl dichloride. This resulted in images with large structures running in the <110> direction. These structures have a height of approximately 5-8Å. As the images show, some of the structures were imaged as holes in the surface. These structures had a depth of 4-5Å. Both of these structures varied in length but on average they were approximately 50nm long.

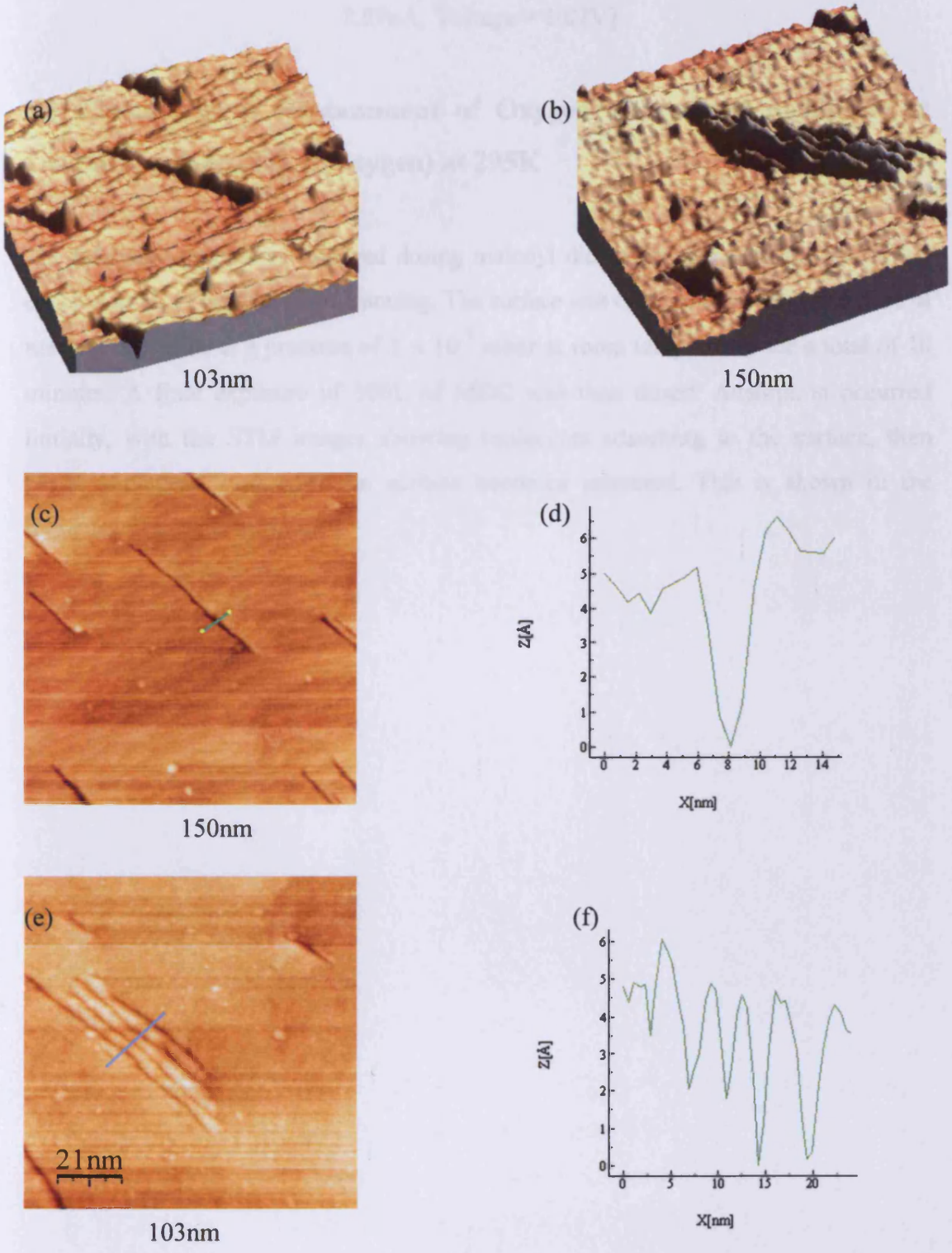

Fig. 6.3: STM images of 600L of malonyl dichloride on a partially oxidised Cu(110) surface; (a) 3d image of a hole in the surface, (b) 3d image of structure on the surface, (c) image of a hole, (d) line profile of the hole, (e) image of the structures, (f) line

profile of the structures [scanning conditions: sample bias negative, Current = 2.89nA, Voltage = 1.02V]

6.6 Chemisorptive Replacement of Oxygen by malonyl dichloride at Cu(110) Surfaces, (3L of oxygen) at 295K

The following experiment involved dosing malonyl dichloride onto a surface previously exposed to 3L of oxygen while scanning. The surface was exposed to a continuous dose of malonyl dichloride at a pressure of 1×10^{-7} mbar at room temperature for a total of 20 minutes. A final exposure of 500L of MDC was then dosed. Adsorption occurred initially, with the STM images showing molecules adsorbing to the surface, then larger structures form until the surface becomes saturated. This is shown in the sequence of images in figure 4.

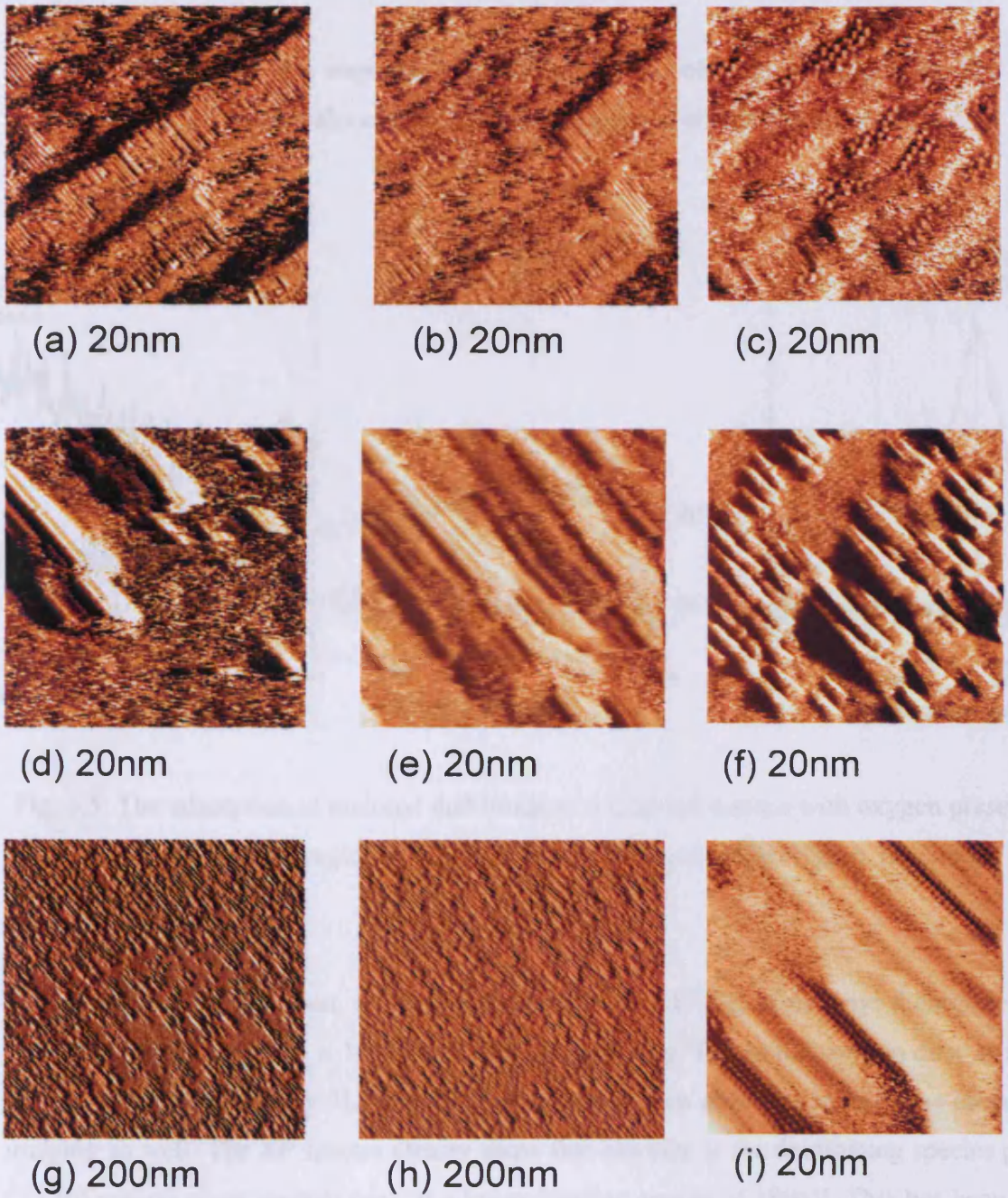

Fig. 6.4: A sequence of images taken while exposing the Cu(110) surface (predosed with 3L of oxygen) to malonyl dichloride at a pressure of 1×10^{-7} mbar at room temperature for a total of 20 minutes [scanning conditions: sample bias negative, Current = 2.66nA, Voltage = 1.12V]

The Cu(110) surface was exposed to a total of 1700L of malonyl dichloride. The corresponding XP spectra show some carbon, oxygen and chlorine to be present.

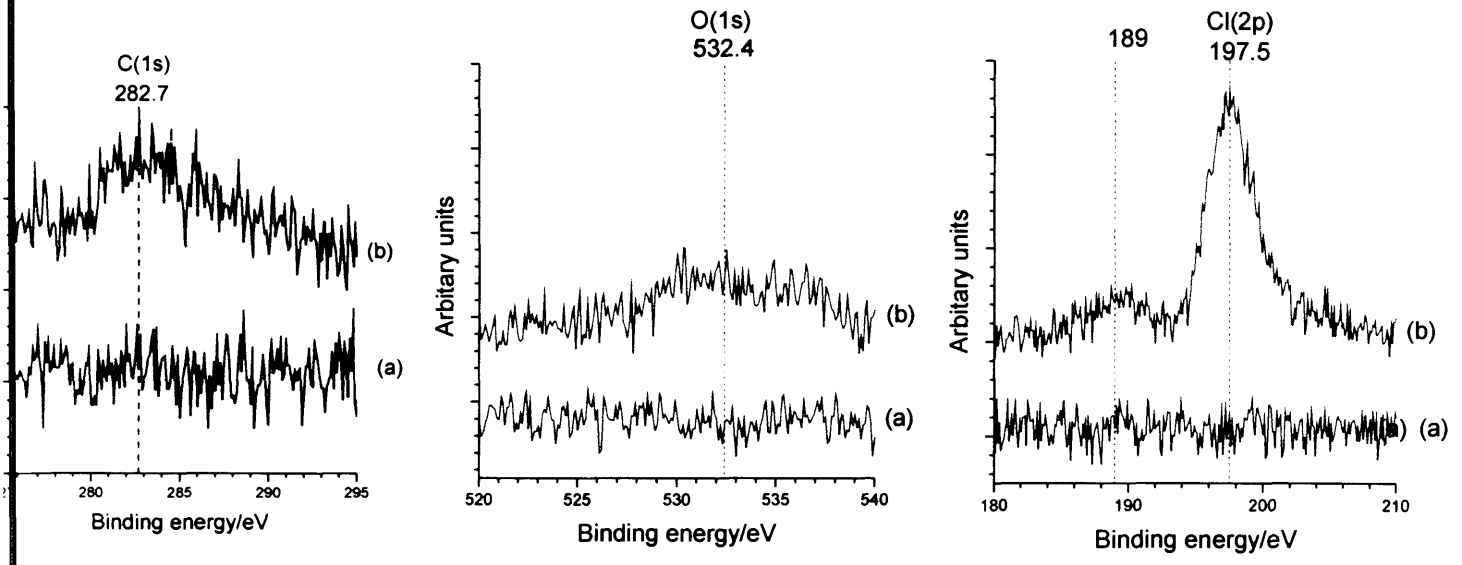

Fig. 6.5: The adsorption of malonyl dichloride at a Cu(110) surface with oxygen present at 290K. XP spectra of the C(1s) region at 100eV, O(1s) region and Cl(2p) region. (a) clean, , (b) 1700L exposure.

The concentration of carbon, oxygen and chlorine after 1700L of malonyl dichloride was 1.47 x 10^{14}, 8.02 x 10^{13} and 7.15 x 10^{14} atoms cm^{-2} respectively. The initial oxygen dose at the Cu(110) surface was approximately 3L. No XP spectra were taken after this initial dose as the STM was imaging so well. The XP spectra clearly show that chlorine is the dominating species present. The Cl (2p) spectra show another peak at a lower binding energy of 189eV. This has been assigned as a Alkβ satellite.

Heating the surface to 600K resulted in a complete loss of carbon and oxygen. Only chlorine was present and this had a concentration of 9.40 x 10^{14} atoms cm^{-2}. The second peak has now diminished.

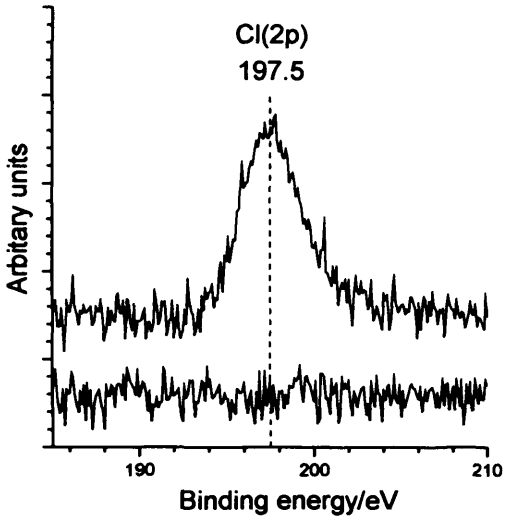

Fig. 6.6: Heating the surface to 600K; Cl (2p) spectra.

6.7 Chlorine 2s studies of chemisorptive replacement of oxygen by malonyl dichloride at Cu(110) surfaces (3L of oxygen).

The following experiment looks at the Cl(2s) region in order to compare binding energies with previous studies of HCl on Cu(110) surfaces.

An initial dose of 3L of oxygen resulted in a concentration of 2.2 x 10^{14} atoms cm^{-2}. A continuous dose 1200L of malonyl dichloride resulted in the following spectra (all spectra were acquired at a pass energy of 100eV).

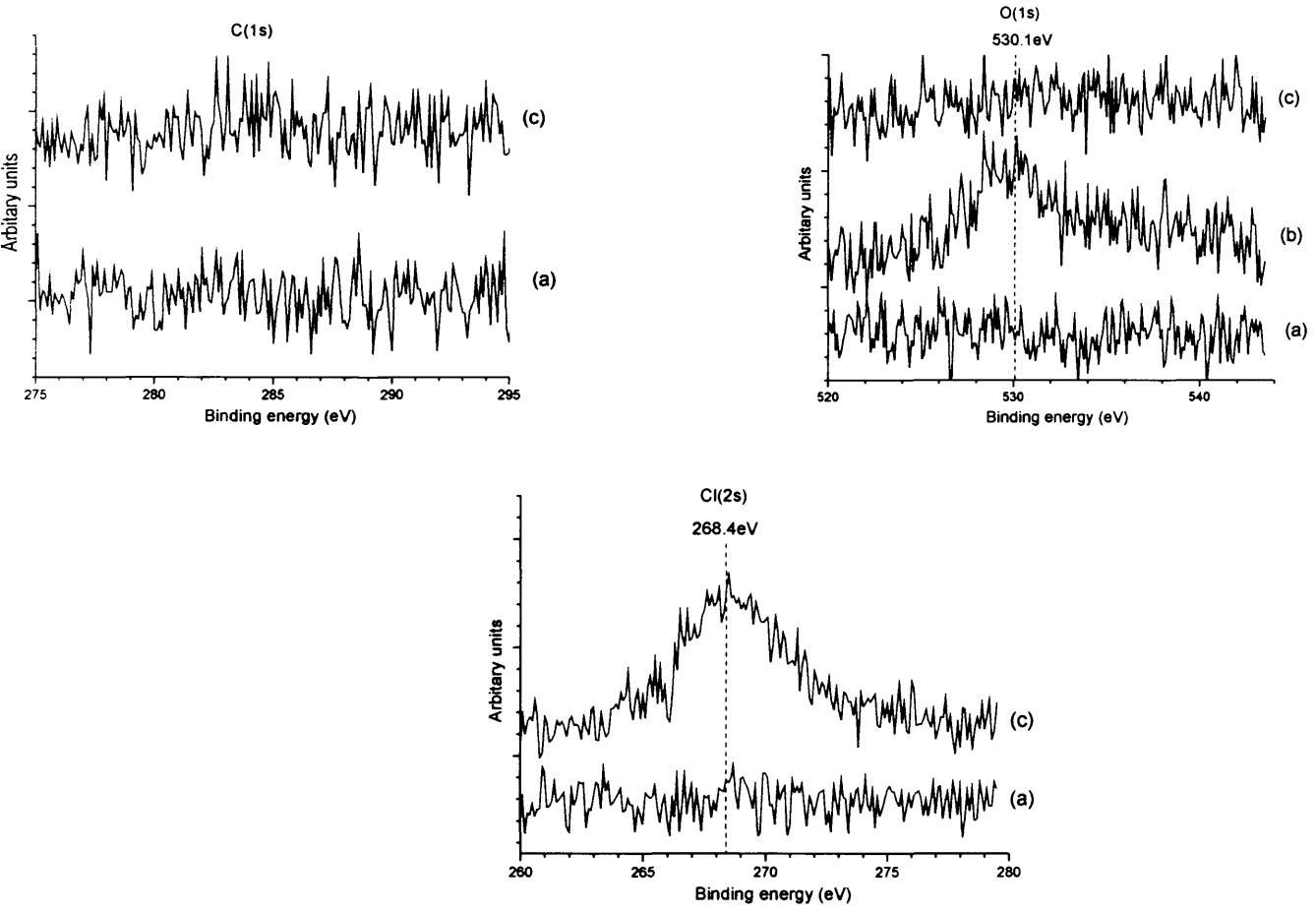

Fig. 6.7: The adsorption of malonyl dichloride at a Cu(110) surface at 290K. XP spectra of the C(1s) region, O(1s) region and Cl(2p) region. (a) clean, , (b) 3L of oxygen dosed, (c) 1200L of malonyl dichloride dosed.

There is no carbon and oxygen present after dosing malonyl dichloride. The chlorine concentration was calculated to be 7.20 x 10^{14} atoms cm^{-2}. This is a similar concentration to the experiment shown in fig. 1. The binding energy of the Cl(2s) spectra (268.4 eV) matches that of HCl exposure to an oxidised Cu(110) surface[8].

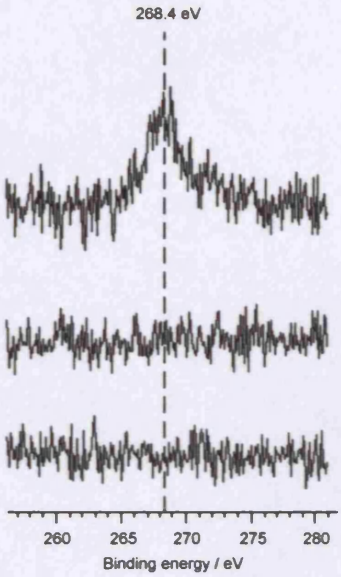

Fig. 6.8: Cl(2s) XP spectra obtained after pre-exposure of a Cu(110) surface to dioxygen, followed by exposure to HCl at 295 K (a) clean; (b) 4 L of O_2; (c) 450 L of HCl (Reproduced from R. V. Jones [8].

The concentration of chlorine on the surface was 6.8 x 10^{14} atoms cm^{-2}. Carbon and oxygen were not present after the 450L dose of HCl. STM images of HCl at a partially oxidised Cu(110) surface were also very similar to malonyl dichloride adsorption as shown in fig. 9.

(a) (b)

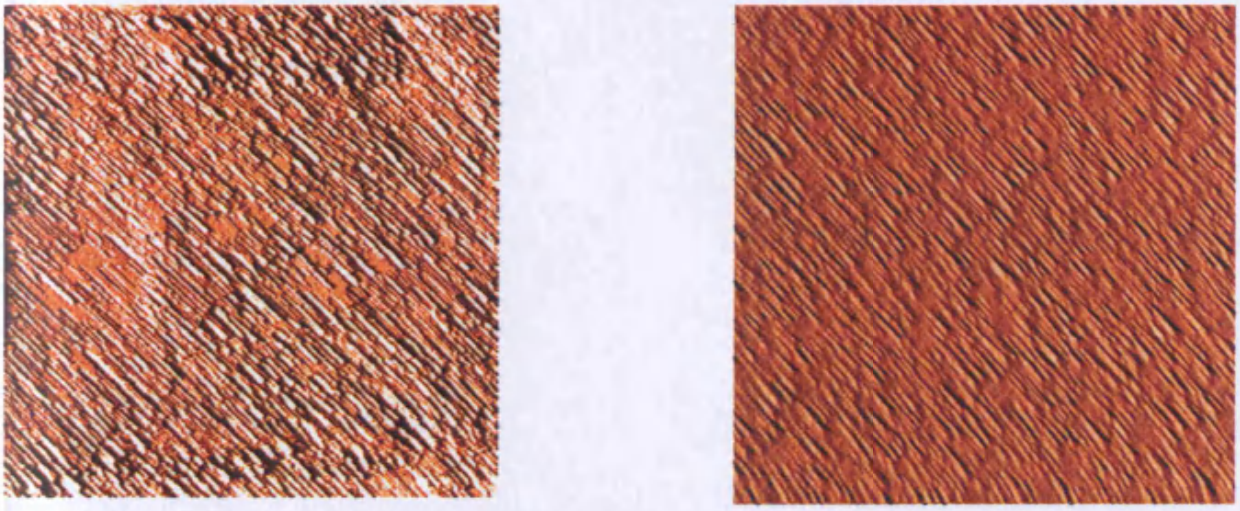

500nm 500nm

Fig. 6.9: STM images (a) HCl on a partially oxidised Cu(110)surface [8], (b) Malonyl dichloride on a partially oxidised surface.

The HCl structures had a maximum height of 13Å, a width of 90Å and a length of 500Å. In comparison, the structures formed when a partially oxidised Cu(110) surface is exposed to 1200L of malonyl dichloride had a maximum height of 20Å, a width of 180Å and a length of 600Å. The structures are bigger that those measured after an exposure of 450L of HCl. However, the dose of malonyl dichloride was larger.

6.8 Physisorption of malonyl dichloride at a clean Cu (110) surface

The following experiment involved cooling the copper sample to below room temperature using liquid nitrogen. The liquid nitrogen was pumped around the probe and therefore resulted in the cooling of the sample. When the sample had cooled, the surface was exposed to 30L of malonyl dichloride.

Exposure to 30L resulted in a carbon, oxygen and chlorine concentration of 7.11 x 10^{14}, 5.84 x 10^{14} and 5.85 x 10^{14} atom cm^{-2} respectively which is close to the 3:2:2 ratio that was expected. The chlorine binding energy was slightly higher than previous at 198eV. All three regions show broad peaks. The carbon binding energy at 284.2eV was much higher than in the previous experiments. This is also the same case for the oxygen.

Allowing the sample to warm to room temperature resulted in a decrease in concentration of carbon and oxygen. The carbon was totally removed whereas the concentration of oxygen was reduced to 1.88 x 10^{14}. The increase of chlorine to 6.23 x 10^{14} atom cm^{-2} was probably due to release of malonyl dichloride from the sample holder as it was allowed to warm to room temperature.

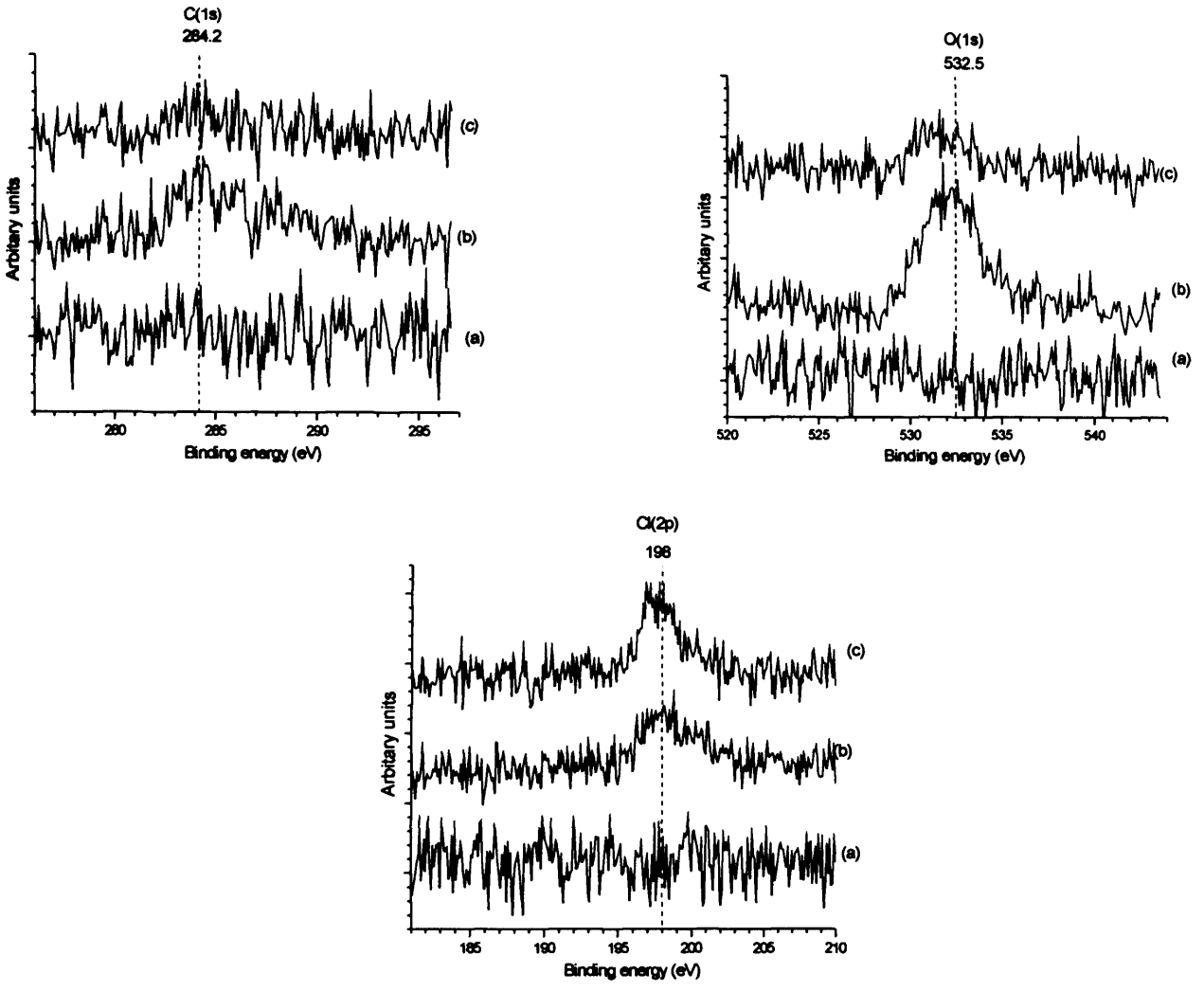

Fig. 6.10: The adsorption of malonyl dichloride at a Cu(110) surface below room temperature. XP spectra of the C(1s) region, O(1s) region and Cl(2p) region. (a) clean, (b) 30L exposure, (c) surface at room temperature.

6.9 Discussion

Malonyl dichloride will only adsorb at a Cu(110) surface in the presence of oxygen at room temperature. This indicates that oxygen activates a reaction with malonyl dichloride at the Cu(110) surface. The decrease in chemisorbed oxygen concentration as the surface is exposed to malonyl dichloride suggests a reaction is occurring which results in the desorption of an oxygen containing species.

From XPS it is clear that the effect of malonyl dichloride is to deposit Cl in the reaction that leads to the desorption of chemisorbed oxygen. It seems that an intermediate may be involved. The surface concentrations calculated from the XP spectra demonstrate that the molecule malonyl dichloride is not chemisorbing at the surface intact. The change in the binding energy of the chemisorbed oxygen suggests that there is an oxygen containing species adsorbed at the surface. Further exposure of malonyl dichloride results in an increase in the binding energy of O(1s). As there is no carbon on the surface after a dose of 20L, the species that contains carbon is no longer at the surface. Comparing the initial carbon concentration to the initial chlorine concentration adds further evidence that the molecule is not intact at the surface. Further dosing results in an increase in only chlorine. The following mechanism accounts for the loss of oxygen and carbon and the adsorption of chlorine.

$$O(a) + C_3H_2O_2Cl_2 \rightarrow 2Cl(a) + CO_2(g) + C_2H_2O(g) \qquad (1)$$

The binding energy of chlorine as seen in the experiments agrees with Cl adsorbed at a Cu(110) surface.

The STM images of the surface after 600L of malonyl dichloride were exposed to 1L of dioxygen on a Cu(110) surface show a number of "hills and valleys" running in the <100> direction. The hills have an average height of 5Å and the valleys have an average depth of 5Å. Walter *et al*[9] reported that beyond saturation of chlorine at a Cu(111) surface, a corrosion reaction occurs which forms a thick copper chloride at the surface. This chloride is reported to contain molecular chlorine trapped within defects in its three dimensional structure. The mechanism is unclear but it can be assumed that reconstruction has occurred due to the adsorbate-substrate interaction. The reconstruction occurs due to the dissociation of the molecule malonyl dichloride. When enough chlorine is present, the reaction with the Cu substrate results in large three dimensional structures present.

The reaction of malonyl dichloride with a partially oxidised surface was imaged using STM. This gave a greater insight into the reaction occurring at the surface. After an exposure of eight minutes of malonyl dichloride (approximately 48L), the roughly circular species seen in fig. 6.4(c) was observed. These individual features have an

average size of 7Å comparable with the expected size of the malonyl dichloride molecule, which has a length of approximately 6.6Å. Further dosing of malonyl dichloride results in the structures mentioned above no longer being present at the surface. A larger structure appears in the <001> direction. These structures have a height of approximately 7Å. The line profile shows that they are triangular in shape.

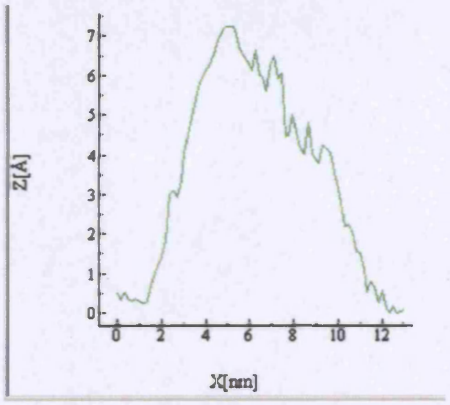

Fig. 6.11: Line profile from fig. 6.4(h)

The length of these structures varies but the average was 45nm. These structures increase in size as more malonyl dichloride is dosed. The structures become taller, broader and increase in length. The final image shows the surface saturated. The height of the structures is now 15Å, and the width is 100Å. The length of the structures was averaged at 600Å. Figure 4 shows that the chemisorptive replacement of oxygen adatoms by the adsorbed species had no preference for the ends of the Cu-O rows, in contrast to the reaction of chemisorbed oxygen at Cu(110) surfaces with hydrogen sulfide [10] and with ammonia [11], which follow a chain unzipping mechanism. Both malonyl dichloride and HCl [8] only form these structures in the presence of oxygen. One proposal is that the p(2x1) oxygen islands which consist of added Cu + O rows act as a source of copper for chlorine as they are reacted away. This would result in the formation of CuCl or $CuCl_2$.

$$Cu\text{-}O\text{-}Cu\text{-}O\text{-}Cu\text{-}O\ldots. + Cl \rightarrow CuCl/CuCl_2 \quad (2)$$

The oxygen offers an alternative route to the formation of CuCl with less energy required than removing Cu atoms from the surface.

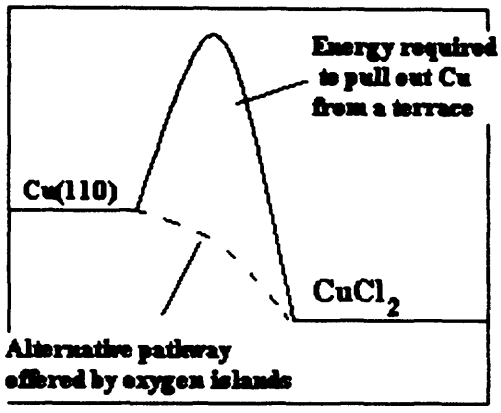

Fig. 6.12: a diagram showing how oxygen allows a reaction to occur

The STM results in figure 6.4(i) show that the random terraces have gone. All that is present at the surface are structures that align in the (001) direction. The Cl concentration calculated by XPS in figure 5 is greater than that of a monolayer of atomically flat c(2x2) at Cu(110) as previous studies have shown [31].

The results presented here have many similarities to the findings of dichlorine adsorption at the clean Cu(100) surface and HCL adsorption at a partially oxidised surface. Elstov *et al* [12] reported that dichlorine adsorption resulted in the reaction proceeding from a monolayer of adsorbed chlorine to the formation of a chloride multilayer. The production of this multilayer was accompanied by the loss of all diffraction spots in the LEED pattern. Halide adsorption has also been studied by Roslinda Ithnin and Robert G Jones [13] and again there was a growth of a halide at a metal surface. A study of halogens adsorbing to Ag(111) showed the formation of multilayers [14]. Most reports of halogen adsorption at single crystal metal surfaces suggest the presence of epitaxially grown metal-halide structures following high halogen exposures [15-20]. These reports also show evidence for the formation of CuCl or $CuCl_2$ at the surface.

The XP spectra of the experiment after dosing 1700L of malonyl dichloride onto a partially oxidised Cu(110) surface showed some difference to the previous

experiment. There is some carbon present. A binding energy of 282.7eV has been measured and this suggests that there could be carbidic carbon present [21]. The Cl (2s) spectrum has the same binding energy as the previous experiment. However there may be a new species with the much lower binding energy of 189eV. However, it is most likely that this has resulted from a kβ satellite. There is also a low oxygen concentration present. Again this peak is very broad and probably differs from the previous experiment due to the increased dose of malonyl dichloride.

Heating the surface results in loss of carbon and oxygen and only chlorine remains. This adds further evidence to the fact that malonyl dichloride is dissociating and chlorine is being deposited at the surface in a similar way to HCl and Cl_2. The Cl(2s) spectra having the same binding energy as HCl at a partially oxidised surface also leads to this same conclusion.

When the surface is cooled below room temperature malonyl dichloride physisorbs to the atomically clean Cu(110). Physisorption resulted in a chlorine – oxygen ratio of 1:1. This agrees with the expected composition of the molecule. Allowing the surface to reach room temperature results in the complete desorption of carbon. The oxygen to chlorine ratio has also changed and it has now become 5:1 chlorine: oxygen. This again shows that there is a reaction occurring that results in the complete removal of carbon and a decrease in oxygen.

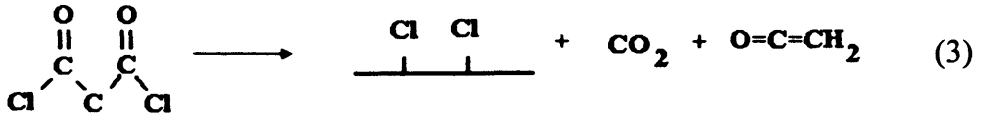

(3)

All that appears to be binding to the surface is chlorine. The formation of the chloride layer is facilitated by low temperatures. The mechanism is not clear from these results, but a relatively high concentration of physisorbed malonyl dichloride appears to be necessary.

The Cl concentration in all experiments goes above that of a monolayer of atomically flat c(2×2) at Cu(110). This suggests that the massive structures observed are caused by a Cl overlayer at a highly reconstructed copper surface.

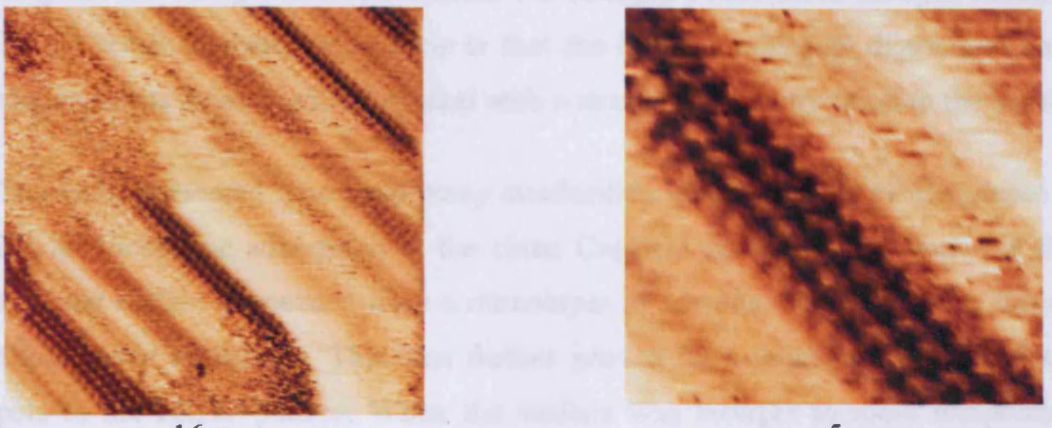

16nm 5nm

Fig. 6.13: A close up of the structure present at the surface as shown in figure 4.

Figure 11 shows a close up of the Cl overlayer. This was observed after the adsorption of malonyl dichloride had ceased. The roughly circular features have a diameter of 3 Angstroms. This is comparable with the diameter of a chlorine atom. The distance between the circular features is 0.4nm. This is comparable with the measurements of the $CuCl_2$ structure.

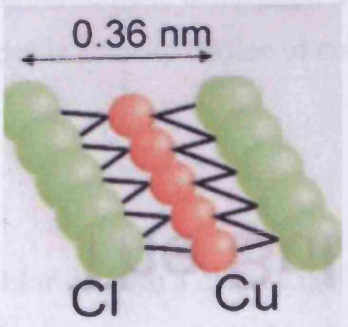

Fig. 6.14: Measurements of the $CuCl_2$ structure

However, XP spectra gave no indication of the presence of $CuCl_2$. This is indicated by no change in the Cu(LMM) Auger peak. This may be due to the fact that $CuCl_2$ is present in such low concentrations.

Halogens chemisorb in a dissociative fashion to give adsorbed halogen atoms. This is due to the fact that if a halogen molecule is interacting with a metal surface then any transferred electron density will enter the π^* antibonding orbital of the molecule, weakening the halogen-halogen bond. At the same time the build-up of negative charge on the halogen atoms enhances the strength of the metal-halogen interaction. The net result of these two effects is that the halogen molecule dissociates and the halogen atoms interact with the metal with a strong ionic contribution to the bonding.

The results presented here have many similarities to the findings of M.Galeotti *et al* [22] for dichlorine adsorption at the clean Cu(100) surface. It was reported that at 160K the surface proceeded from a monolayer of adsorbed chlorine to the formation of a chloride multilayer. This was further proven by a rapid loss of all diffraction spots in the LEED pattern. When the surface was brought to room temperature it contained multilayer thick islands. Many reports of halogen adsorption at single crystal metal surface conclude that there are epitaxially grown metal-halide structures following high halogen exposures [23-25].

Reconstruction occurs more readily at less stable surfaces such as the fcc(110). Copper appears to be an extremely good metal for C-Cl bond cleavage as the XPS shows that all that is left at the surface is a Cu-Cl structure. This was also the case with the adsorption of trans-dichloroethene adsorption at a Cu(110) surface [26]. It can therefore be seen that copper is a cheap choice of component in a dechlorination catalyst.

6.10 Conclusion

The interaction of malonyl dichloride with a clean Cu(110) surface resulted in no adsorption. An oxygen pre treated surface exposed to malonyl dichloride has been investigated using STM and XPS. At low temperatures, malonyl dichloride physisorbed at the surface. However, it is believed that even at low temperatures, malonyl dichloride undergoes dissociation and a carbon species is desorbed from the surface. Warming results in only chlorine being present at the surface.

Reacting malonyl dichloride with a partially oxidised surface results in corrugated rows orientated in the <100> direction appearing. There is an increase in the mobility

of the substrate atoms and this is seen with the STM as step rearrangements. The concentration of chlorine is greater than that of a $Cl_{(a)}$ c(2x2) structure. This increase in concentration may be due to the formation of $CuCl_2$. XPS does not show evidence to distinguish between CuCl and $CuCl_2$ contrary to previous literature; however this could be due to the fact that there is such a low concentration present. The presence of oxygen allows a reaction to occur. The reason for this being that oxygen acts as a source of copper.

6.11 References

[1] P. Auffinger, E. Westhof, and P. Shing Ho, *Proc. Natl. Acad. Sci. USA.* 101 (2004) 16789–16794.

[2] R. G. Jones, *Prog. Surf. Sci.* 27 (1988) 25-160.

[3] A. J. Gellman, *J. Phys. Chem.* 106 (2001) 10509-10517.

[4] S. L. Barteau, *J. Vac. Sci. Technol.* (2003) 200-212.

[5] J. D. Horvath and P. Kamakoti, *J. Am. Chem. Soc.* 126 (2004) 14988.

[6] C.Y. Nakakura, G. Zheng and E.I. Altman, *Surf. Sci.* 401 (1998) 173.

[7] K.N. Elstov, A.N. Klimov, V. Yu. Yurov, V.M. Shevlyuga, U. Bardi and M. Galeotti, *JETP Lett.* 62 (1995) 444.

[8] R. V. Jones, PhD Thesis, University of Wales, Cardiff, 2001.

[9] W. K. Walter, D. E. Manolopoulos and R. G. Jones, *Surf. Sci.* 348 (1996) 115-132.

[10] C. Bai, "*Scanning Tunnelling Microscopy and its Application*", Springer Series in Surface Sciences Vol 32, Springer, Berlin (1995) 204.

[11] A.F. Carley, P.R. Davies, M.W. Roberts and D. Vincent, *Top. Catal.* 1 (1994) 35.

[12] M.Galeotti, B. C., U. Bardi, B.V. Andryushechkin, A.N. Klimov and K.N. Eltsov, *Surf. Sci.* 76 (1995) 91.

[13] R. I. Jones, *J. Phys. Condens. Matt.* 8 (1996) 3285–3295.

[14] J. H. White, *Lang.* 10 (1994) 486-491.

[15] K.N. Elstov, V. Yu. Yurov, V.M. Shevlyuga, U. Bardi and M. Galeotti, *Surf. Sci.* 62 (1995) 444.

[16] K.N. Elstov, *Surf. Sci.* 753 (1991) 251-252.

[17] Y. Nakakura, *Phys. Rev. B.* 401 (1998) 173.

[18] Z. Shuxian, J. M., W. Jianxin and K. Wandelt, *Surf. Sci.* 759 (1991) 251-252.

[19] T.W. Fishlock, F.H. Jones, R.G. Egdell and J.S. Foord, *Surf. Sci.* 629 (1997) 377-379.

[20] K. Swamy, P. Sandl and E. Bertel, *Surf. Sci.* 466 (2000) 11.

[21] K. Thomas, *PhD Thesis* University of Cardiff, 1994.

[22] M.Galeotti, B. Cortigiani, U. Bardi, B.V. Andryushechkin, A.N. Klimov and K.N. Eltsov, *J. Electron Spec. Rel. Phen.* 76 (1995) 91.

[23] K.N. Elstov, G.Ya. Zueva and A.N. Klimov, *Surf. Sci.* 251-252 (1991) 753.

[24] Y. Nakakura, G. Zheng and E.I. Altman, *Surf. Sci.* 401 (1998) 173.

[25] C.Y. Nakakura, G. Zheng and E.I. Altman, *Surf. Sci.* 401 (1998) 173.

[26] Y. Jugnet, N.S. Prakasha, J.C. Bertolini, S.C. Laroze, and R. Raval, *Catal. Lett.* 56 (1998) 17–21.

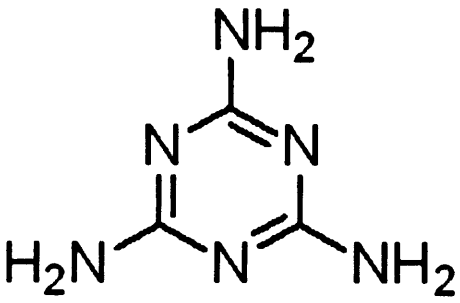

Chapter 7

Interaction of Melamine with Cu(110)and Ag(111) surfaces

7.1 Introduction

The interaction of melamine with clean and oxidised Cu(110) has been studied using x-ray photoelectron spectroscopy and scanning tunnelling microscopy. Adsorption at a clean Ag(111) surface has also been studied. The investigation focuses on the different structures formed at the two surfaces.

7.2 Melamine chemisorption at metal surfaces

The interaction of melamine with Cu(110) has been studied in order to further the previous work of amines at Cu(110) surfaces (aniline, pyridine etc). Amines not only have a direct involvement as reactants in catalytic reactions but also modify the

selectivity and activity of many other reactions. For example, amines are used as modifiers for palladium based hydrogenation catalysts [1]. The aim of the present study was to find out how the Cu(110) substrate would affect the structures produced after exposing the surface to melamine and how much the intermolecular hydrogen bonding between melamine molecules would play a part in the structures formed at this surface.

To the best of our knowledge the literature shows no study of melamine at a Cu(110) surface. However, many other amines have been studied. Ammonia being the simplest possible amine gives an idea how amines adsorb at a Cu(110) surface. It has been shown that the behaviour of ammonia is similar at the majority of single crystal metal surfaces and is therefore independent of the metal involved[2]. Ammonia was found to adsorb molecularly at Cu(110) at low temperature (80 - 120 K) and desorb upon warming to room temperature (298K)[3]. No dehydrogenation reaction occurs for ammonia adsorbed at a clean copper surface. However, in the presence of chemisorbed oxygen, water formation results and a nitrogen species identified as $NH_{(a)}$ from its XP binding energy, formed as the surface is exposed the ammonia.

$$NH_3(g) + O_{(a)} \rightarrow H_2O(g) + NH(a) \quad (1)$$

Table 1 below shows some binding energies for NH_x species at a Cu(110) surface.

Species	NH_3(a)	NH_2(a)	NH(a)	N(a)
B.E. / eV	400.8	398.0	397.5	396.8

Table 7.1: N(1s) binding energies for NH_X species at Cu(110)[4].

Various other amines adsorbed at a Cu(110) surface have also been studied. It was found that nitrobenzene adsorbed at a clean Cu(110) surface. It decomposed to form a phenyl species[5]. In contrast, it was found that nitroaniline did not decompose at the surface. It had the ability to form multilayers and this was attributed to intermolecular hydrogen bonding.

Previous studies have shown aniline adsorption at a clean Cu(110) surface results in limited dissociation. However, in the presence of chemisorbed oxygen, a reaction occurs which results in the formation of chemisorbed phenyl imide[6,7]. This is discussed in greater detail in chapter 5. The binding energy of the imide was 397.5eV. It was found that the adsorption site of the phenyl group was the two fold hollow.

Molecular self-assembly at surfaces occurs due to the intermolecular forces and the surface interactions. Melamine has the ability to hydrogen bond at three sites. The use of copper and silver will contrast adsorbate-substrate and adsorbate-adsorbate interactions. Fabrication of supramolecular assemblies using hydrogen bonding is useful because it provides both high selectivity and directionality [8]. Supramolecular structures formed by the self assembly of molecular building blocks show many uses for future technologies. The ability to engineer distinct 1, 2, or 3 dimensional patterns at a supramolecular scale is a crucial step towards nanosized technology. The possibility of regulating size and shape of nanostructures in relation to function is a challenge.

The approach to controlling surface structures using adsorbed molecular monolayers to create preferential binding sites that accommodate individual target molecules has been studied previously [9]. Previous studies have used hydrogen bonding to guide the assembly of two types of molecules into a two dimensional open honeycomb network that controls and templates new surface phases formed by deposited metal atoms [10]. Pores might also prove useful in achieving controlled co-location of a wider range of guest species. This could lead to the promotion of chemical interactions, polymerization and the formation of complex supramolecular surface structures.

Hydrogen-bonded architectures are abundant in biological systems. Nature uses non-covalent interactions to put together large assemblies of molecules. It is these factors that have motivated their exploitation in supramolecular chemistry. This has been demonstrated particularly for systems in solution. Hydrogen bonds have been used as crystal design elements for the preparation of solid state supramolecular organisations [11]. The rules of nanopatterning of organic molecules can play a major role in future technologies [12,13].

The concepts of supramolecular organisation have been applied to two-dimensional assemblies on surfaces and Hetch [14] emphasises how organic molecules will serve as functional building blocks of molecular construction sets. Self organisation has been stabilised using di-polar coupling and metal co-ordination. Takashi Yokoyama *et al* [15] formed surface supported supramolecular structures whose size and aggregation pattern were controlled by tuning the non-covalent interactions between individually adsorbed molecules.

A study by Theobald *et al* [10] looked at the hydrogen bonding of melamine with perylene tetra-carboxylic di-imide at a silver terminated silicon surface. It was discovered that the two dimensional open honeycomb networks could act as a template for deposited fullerene molecules. Packing and growth within the created pores has also been studied (Growth induced reordering of fullerene clusters trapped in a two dimensional supramolecular network). It was found that the interaction between molecule-substrate and molecule-network interactions which control the configuration of the clusters in the pores of a supramolecular network leads to the stabilization of a range of nanophases.

A hydrogen-bonded bimolecular network formed between cyanuric acid and melamine has been studied by Perdiago *et al* [16]. The authors proposed that the highly symmetric molecules cyanuric acid and melamine could be used in the rational design of a supramolecular template. It was shown that adsorbed organic molecules diffuse readily at room temperature on an Ag-Si(111) $\sqrt{3}$ x $\sqrt{3}$ *R*30° surface. The large organic molecules can form extended structures with long range order governed mainly by intermolecular interactions. Attempts to prepare hydrogen bonded arrays of melamine on the Ag-Si(111) $\sqrt{3}$ x $\sqrt{3}$ *R*30° surface at room temperature were unsuccessful. The probable cause of this was the high mobility of the molecule. A co-adsorption of cyanuric acid and melamine lead to a higher surface coverage of the supramolecular network. The pore area created by the interaction of melamine and cyanuric acid was smaller that that created by Theobald *et al* [10] using melamine and perylene tetra-carboxylic di-imide. This pore area changed from ~700 $Å^2$ to 20 $Å^2$.

An STM study of 3,4,9,10-perylene-3,4,9,10-tetracarboxylic-dianhydride (PTCDA) and it interaction with melamine has been studied on an Ag-Si(111)$\sqrt{3}$x$\sqrt{3}$ R30° surface[17]. The anhydride-melamine hydrogen bonding was examined and it was found that a hexagonal network phase was formed that was partly stabilized by PTCDA anhydride groups interacting with two amine groups of the melamine via two N-H····O hydrogen bonds. The configuration was stable despite the expected repulsive interaction between the central dianhydride oxygen atom and the nitrogen atom contained in the melamine ring. Two distinct phases were shown to exist: a double row phase and a hexagonal network.

7.3 Experimental

The instrument used in this investigation has been discussed previously. The radiation used for the XP data acquisition was the Al(kα) line with a photon energy of 1486.6eV. All XP data was recorded at a pass energy of 50eV unless otherwise stated. All spectra were referenced to the clean Cu($2p_{3/2}$) peak at 932.7eV.

Melamine (>99% Aldrich) was deposited from a k-cell that was attached to the chamber and outgassed extensively before use. Malonyl dichloride (97% Aldrich) was purified by several cycles of freeze pump thawing and dosed to the chamber through a variable leak valve. Purity was monitored with in situ mass spectrometry.

7.4(a) Melamine ($C_3H_9N_3$) adsorption at clean Cu(110) at 295K: XPS results

A clean Cu(110) surface was exposed to a two minute dose of melamine from the k-cell equilibrated at 145°C. This gave rise to peaks in the C(1s) and N(1s) regions at 285 and 397 eV respectively (fig. 1). The carbon concentration was calculated to be 1.20×10^{14} atoms/cm^2 and the nitrogen concentration was 2.68×10^{14} atoms/cm^2.

Because of the low concentrations both have an error of approximately 1.0 x 10^{14}. This gives a ratio of approximately 1: 2.3, carbon to nitrogen. This ratio is close to the 1:2 ratio expected for molecular melamine. The weakness of the C(1s) signal was due to experimental issues with the XPS. This increased the percentage error and therefore made the concentration more difficult to calculate accurately.

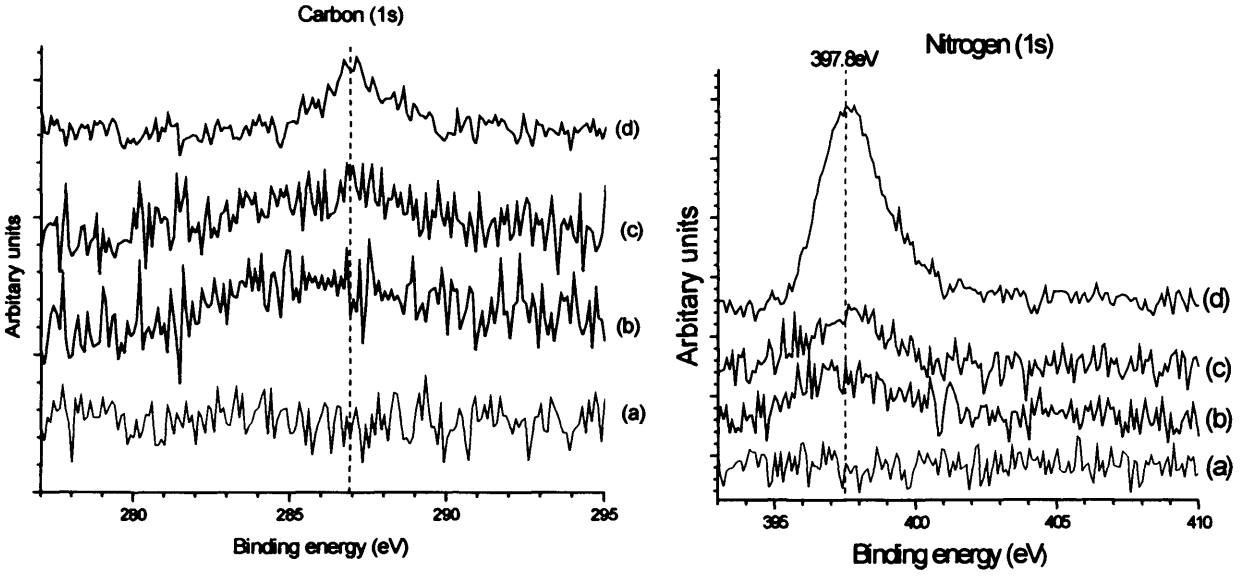

Fig. 7.1 Adsorption of melamine at a Cu(110) surface at 290K. (a) Clean surface; (b) 120 second dose at 145°C, (c) 300 second dose and (d) 480 second dose at a Cu(110) surface at 290K.

Adsorption of a 5 minute dose at 145°C, on an atomically clean Cu(110) surface, results in carbon and nitrogen present. The binding energy of the carbon was around 287eV. An increase in the broad peak suggests that there is more than one species present. The binding energy of the N(1s) peak was 398eV which is 1eV higher than the low concentration shown in figure 1. The concentrations for each species were 1.4 x 10^{14} and 3.52 x 10^{14} of carbon and nitrogen.

As in the case of the previous experiment, the ratios (1:2, C:N) suggest that molecular adsorption of melamine has occurred. The binding energy of the nitrogen is consistent

with that for an NH_2 group being present at the surface[18]. The broadness of the carbon spectra makes it difficult to distinguish an exact binding energy.

The surface concentrations were still below a monolayer. The dosage was therefore increased to 480 seconds at 145°C. The concentrations from this dose exceeded a monolayer ($\sigma_C = 7.45 \times 10^{14}$, $\sigma_N = 1.26 \times 10^{15}$ atoms cm^2). The carbon and nitrogen binding energy also increased. However the nitrogen binding energy still falls into the NH_2 range. The asymmetry of the nitrogen suggests the presence of two chemically inequivilent nitrogens. The ratio of carbon to nitrogen (1:2) agrees with melamine molecularly bound to the Cu(110) surface.

7.4(b) Melamine adsorption at clean Cu(110) at 295K: STM results

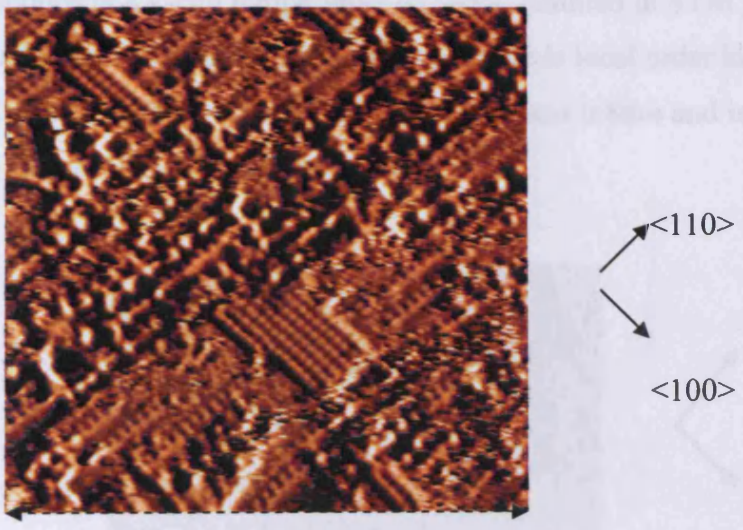

Fig. 2 STM image after a dose of 120 seconds of melamine at a Cu(110) surface at 290K [bias: negative, voltage = 1.24V, current = 2.89nA].

The STM images (fig. 2 and 3) corresponding to the XP spectra in Fig 1.a show that there are two species present. Measurements suggest that $O_{(a)}$ is present and islands of the well-documented p(2x1)O(a) lattice can be seen in the <100> direction. This is present due to contamination. The larger feature present is assigned to melamine on the basis of the XPS results. The features have a diameter of 0.9nm. There is some local order in the <110> direction.

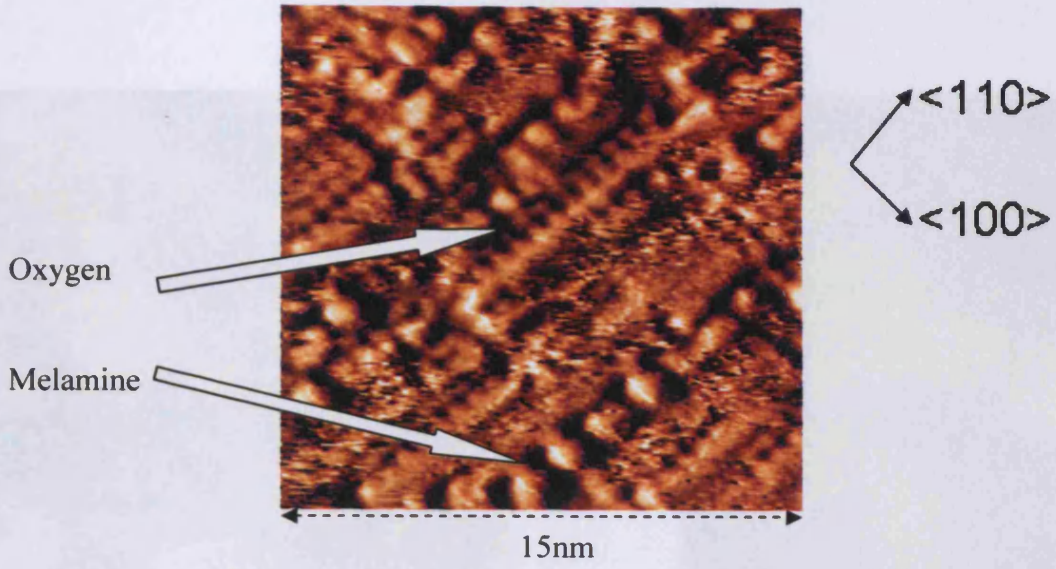

Fig. 7.3 Close up of surface shown in Fig. 2.

A dose of 300 seconds at a k-cell temperature of 145°C resulted in STM images with similarities to the lower concentration experiment. There is local order in the <110> direction. The diameter of the molecules on the surface was 0.8nm and is agreement with the size of the molecule shown in figures 2 and 3.

Fig. 7.4 STM image after a dose of 300 seconds of melamine at a Cu(110) surface at 290K [bias: negative, voltage = 0.99V, current = 3.32nA].

The STM images shown in Fig. 5 correspond to a concentration exceeding a monolayer ($\sigma_{C=}$ = 7.45 x 10^{14}, σ_N = 1.26 x 10^{15} atoms cm^2). A more ordered part of the surface can be seen. The apparent height of the ordered island is 0.3nm relative to the rest of the surface. The concentrations of nitrogen and carbon exceed a monolayer.

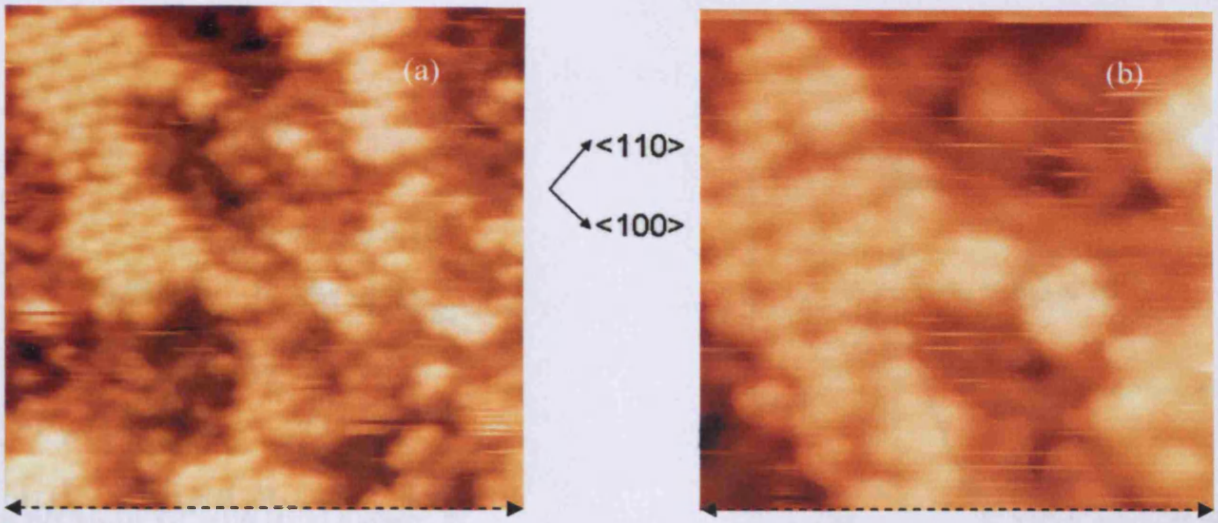

Fig. 7.5 STM image after a dose of 480 seconds of melamine at a Cu(110) surface at 290K, (a) ordered island, (b) close up of ordered island [bias: negative, voltage = 1.03V, current = 2.21nA].

The STM image shows a hexagonal structure. The fact that the substrate has less interaction with melamine at a second or even third layer could be the reason why melamine is able to form the hexagonal structure instead of (as the lower concentrations show) forming rows in the <110> direction.

7.5 The effect of temperature (400K): XPS and STM results.

The surface was annealed to encourage ordering of the molecules at the surface. The XP spectra show the carbon and nitrogen binding energies decreasing by 0.3 and 0.4eV respectively. The concentration of carbon and nitrogen lost from the surface was 1.15×10^{14} and 2×10^{14} atoms/cm^2. The concentrations shown in figure 6 suggest that melamine is molecularly desorbing, probably due to the less strongly interacting second layer desorbing. The ratio of carbon to nitrogen that was left on the surface was 1:1.68 respectively. Taking errors into account this is still consistent with molecularly adsorbed melamine.

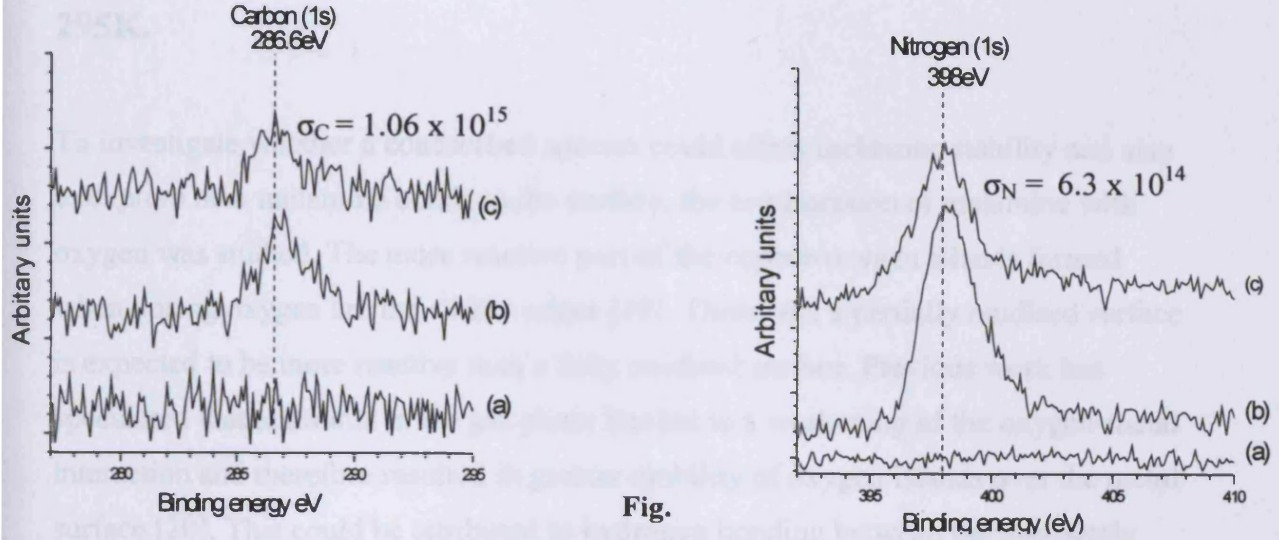

Fig. 6 The adsorption of melamine at a Cu(110) surface. (a) Clean surface; (b) Melamine adsorption at 295K then heating the surface to 450K.

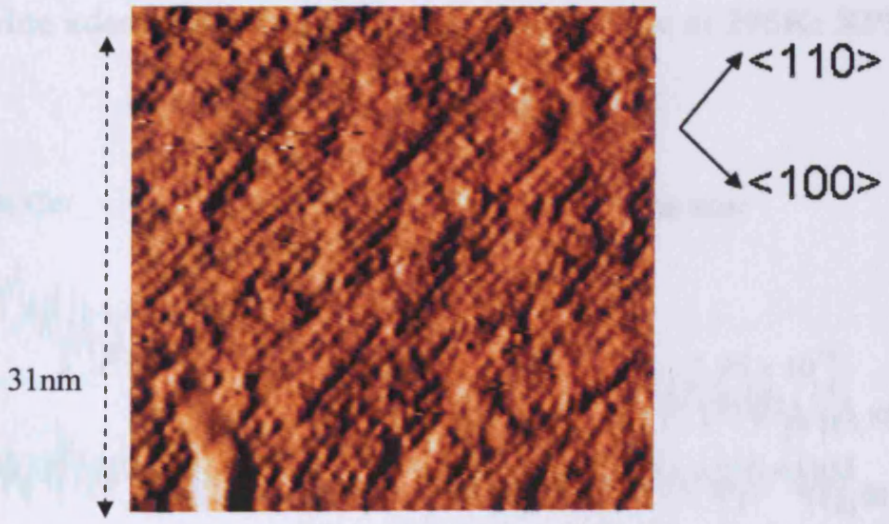

Fig. 7.7 STM image after heating the Cu(110) surface to 450K [bias: negative, voltage = 1.00V, current = 2.49nA].

Comparing figures 5 and 7 the ordered "islands" have now gone. The concentrations do not exceed a monolayer. The image of the surface (fig. 7) shows similarities to figures 2 and 4 where there is some local order in the <110> direction.

7.6 Exposure of a fully and partially oxidised surface to melamine at 295K.

To investigate whether a coadsorbed species could affect melamine stability and also to explore how melamine bonds to the surface, the coadsorption of melamine with oxygen was studied. The more reactive part of the copper-oxygen islands formed when dosing oxygen are the <100> edges [19]. Therefore, a partially oxidised surface is expected to be more reactive than a fully oxidised surface. Previous work has speculated that ammonia in the gas phase has led to a weakening of the oxygen-metal interaction and therefore resulted in greater mobility of oxygen islands over the metal surface [20]. This could be attributed to hydrogen bonding between the transiently adsorbed ammonia molecules. The nature of melamine oxygen interaction was studied in detail to see if the presence of the nitrogens would have a greater interaction with adsorbed oxygen.

7.6(a) Melamine adsorption at a fully oxidised surface at 295K: XPS results.

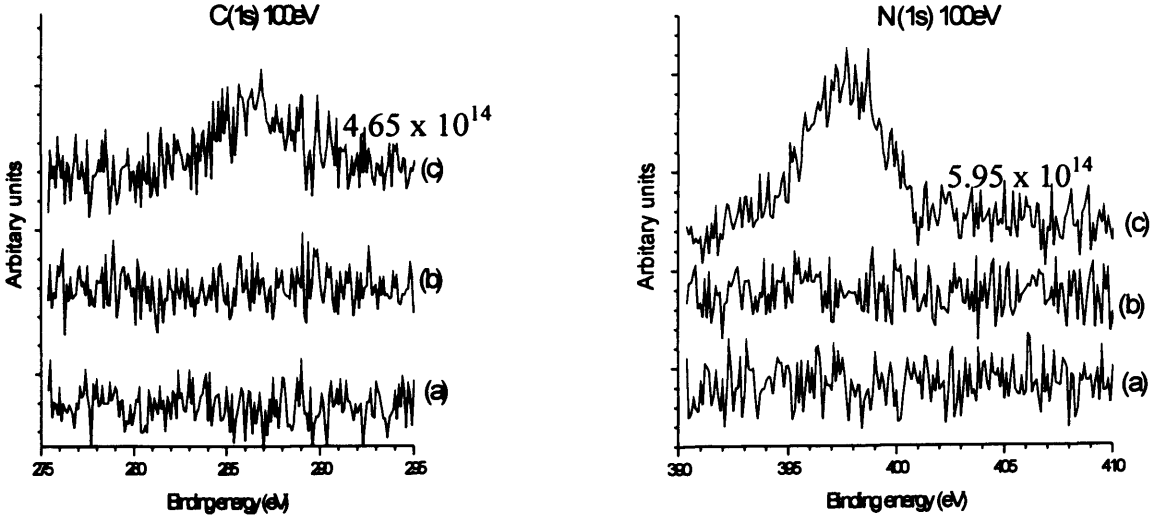

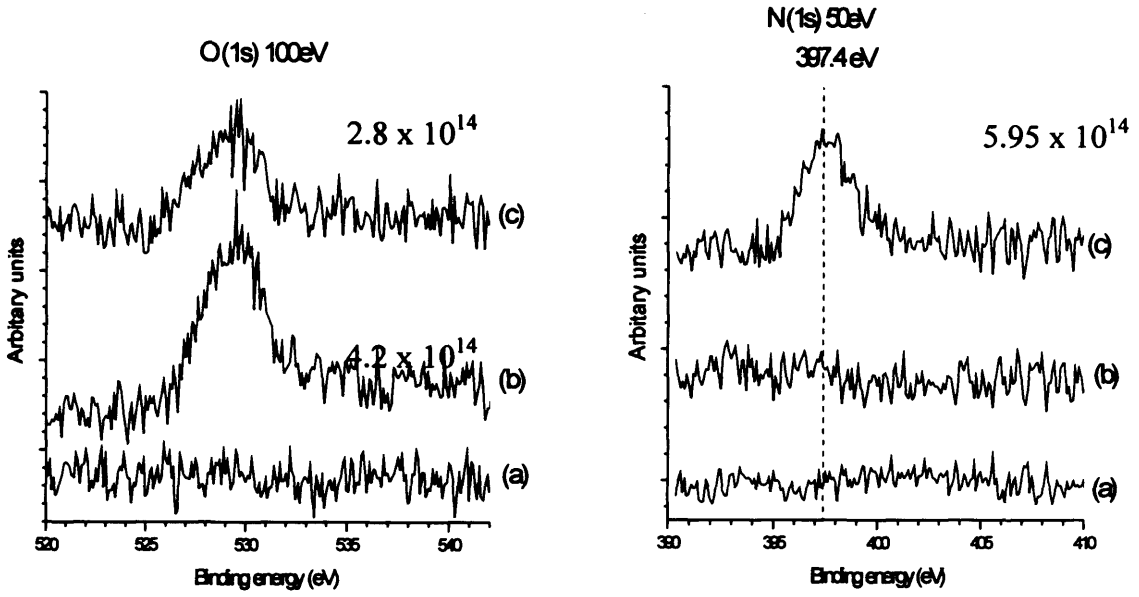

Fig. 7.8 The adsorption of melamine at a preoxidised Cu(110) surface at 290K. XP spectra of the C(1s) region at 100 eV, O(1s) region at 100eV and N(1s) region at 100 and 50eV. (a) clean, (b) 30L of oxygen dosed, (c) 180 second dose of melamine at 140°C.

Exposure of the Cu(110) sample to 30L of oxygen at 295K, yielded a fully oxidised surface, with a characteristic O (1s) binding energy of 529.7 eV. The oxygen concentration was calculated to be 4.2 x 10^{14} atoms/cm^2.

A 180 second exposure of melamine resulted in spectral features in both C(1s) and N(1s) regions. The binding energy of the carbon spectra stayed roughly the same as the binding energy observed for the clean surface. The nitrogen binding energy has decreased by 0.6eV.

The concentration of the chemisorbed oxygen has decreased by 1.4 x 10^{14} atoms/cm^2. The binding energy of the remaining oxygen is unchanged. The fact that the concentration decreased and the nitrogen binding energy decreased suggests a reaction has occurred.

7.6(b) Melamine adsorption at a fully oxidised surface at 295K: STM results.

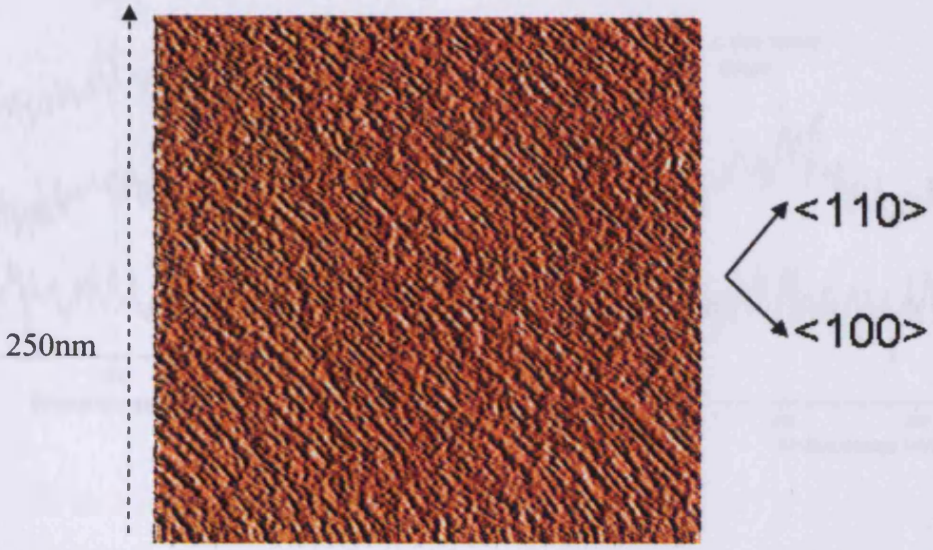

Fig. 9 STM image after a dose of 180 seconds of melamine at a fully oxidised Cu(110) surface at 290K [bias: negative, voltage = 1.33V, current = 1.87nA].

The image shows a different surface as compared to studies with melamine chemisorbed at a clean Cu(110) surface. There are now large structures in the <100> direction. STM images showing a closer look at these structures were unobtainable. However, it is obvious that oxygen has had an effect on the direction that melamine forms rows. It is suspected that the reaction that has taken place has resulted in the adsorbed species taking an oxygen and therefore adsorbing in the place of the p(2x1) rows.

7.6(c) Melamine adsorption at a partially oxidised surface at 295K: XPS results

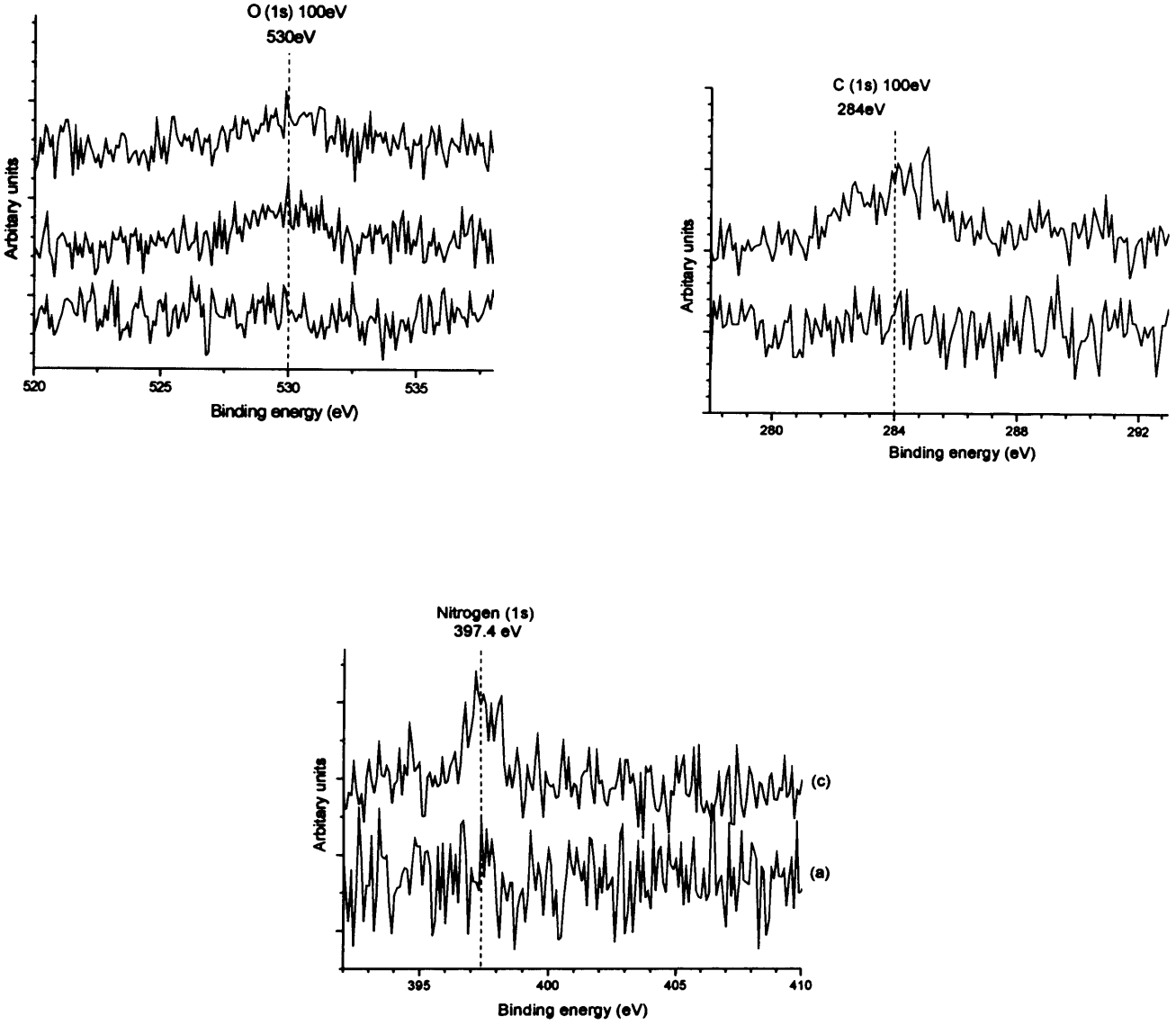

Fig. 7.10 The adsorption of melamine at a partially oxidised Cu(110) surface at 290K. XP spectra of the C(1s) region at 100 eV, O(1s) region at 100eV and N(1s) region at 100. (a) clean, (b) 4L of oxygen dosed, (c) 3 minute dose of melamine at 137°C.

Exposure to 10L of oxygen resulted in a surface with chemisorbed oxygen (530 eV), the concentration of which was 2.6 x 10^{14} atoms/cm^2. Exposure to a 180 second dose of melamine at a k-cell furnace temperature of 137°C resulted in a marked change in the oxygen spectra as shown in fig 11. The chemisorbed oxygen peak decreased

slightly in intensity. The carbon and nitrogen concentrations were 2.3 x 10^{14} and 2.48 x 10^{14} atoms/cm^2 respectively. This produces a ratio of 0.92:1 which differs from the previous melamine experiments. Melamine molecular adsorption is no longer occurring. The binding energy of the nitrogen is no longer in the NH_2 region, it is now characteristic of a $NH_{(a)}$ at a Cu(110) surface. The carbon peak is broad and this suggests that there is more than one species present.

7.6(d) Melamine adsorption at a partially oxidised surface at 295K: STM results

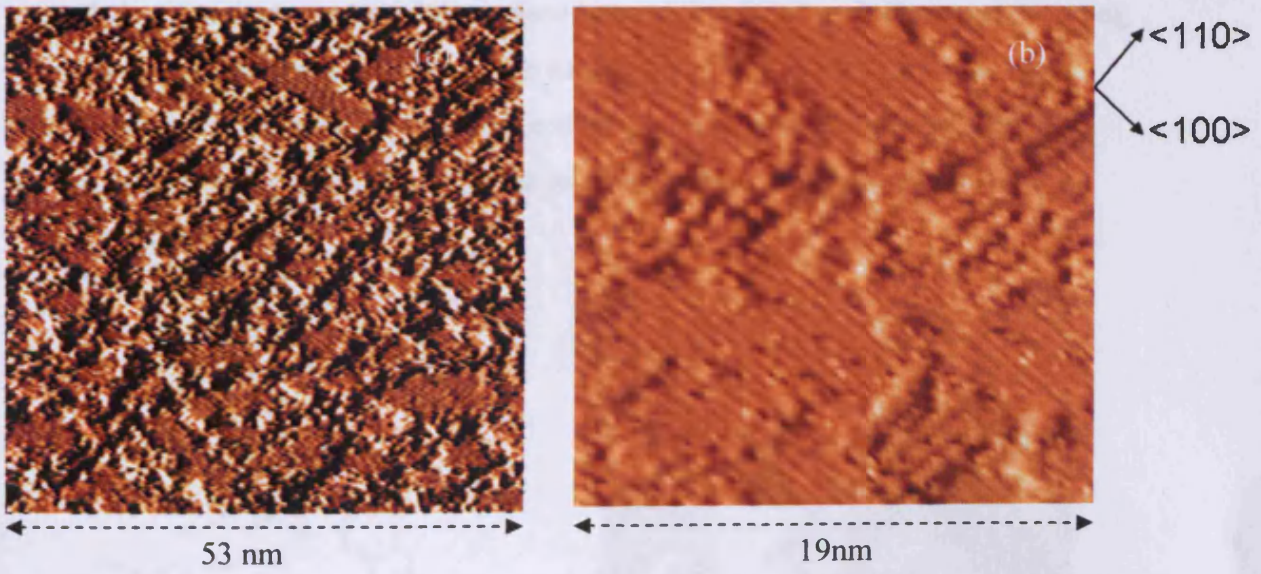

Fig. 7.11 STM image after a dose of 180 seconds of melamine at a partially oxidised Cu(110) surface at 290K [bias: negative, voltage = 1.11V, current = 2.75nA].

The STM image differs from a fully oxidised surface. Rows of oxygen can be seen in the <100> direction. There is also a larger structure present that clusters around the oxygen islands. The quality of the image makes it difficult to measure the size of the structures present.

7.7 Discussion

7.7(a) Melamine adsorption at a clean Cu(110) surface

At 295K melamine molecularly adsorbed at a Cu(110) surface. Heating the surface resulted in molecular desorption. The binding energy of the N(1s) region at medium and high concentration agrees with there being an NH_2 group at the surface. The low concentration (with oxygen contamination) N(1s) region gave a binding energy of 397eV. This would signify an NH group present. Therefore, further studies of an oxygenated surface and how it interacts with melamine were undertaken.

STM images show local order in the <110> direction. However, when concentrations exceeded a monolayer, parts of the surface became more ordered. Hydrogen bonding is believed to account for this order. The multilayer which arises due to the high concentration dose results in melamine ordering on adsorbed melamine. The following diagram proposes how melamine would interact in order to form the ordered structures.

(a) (b)

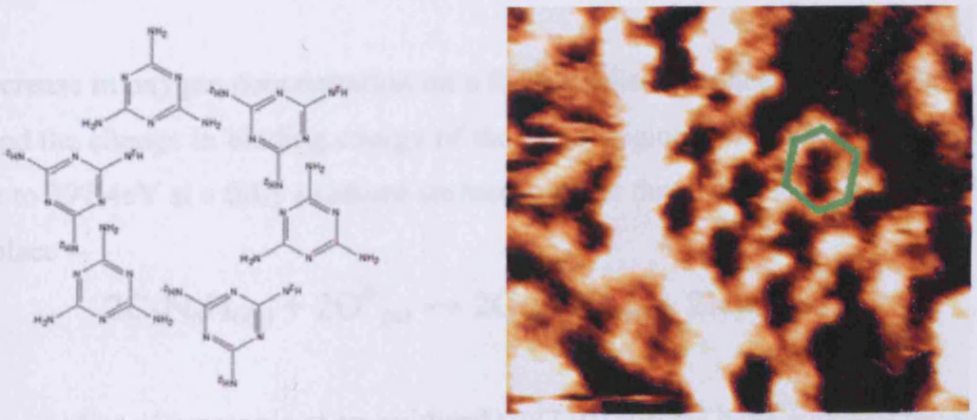

Fig. 7.12 (a) Model of a hexagonal structure formed by melamine via intermolecular bonding, (b) the second layer structure that exhibits a hexagonal structure.

Heating the surface results in the loss of the multilayer and melamine behaves as the previous experiments have shown with some local order in the <110> direction.

At low concentrations, XP spectra of carbon (1s) and nitrogen (1s) show a very high FWHM of 8eV and 6eV respectively. As the concentration increased, exceeding a monolayer, this broadness decreased to 4eV. There are two possibilities for this decrease. The two non-equivalent nitrogen atoms contained in melamine should cause some broadness in the N (1s) region. The fact that this broadness decreases may suggest that hydrogen bonding is causing the nitrogen atoms to become more equivalent. This same reason could not be used to explain the decrease in broadness of the C (1s) region as all three carbons contained in melamine are equivalent. This leads to the second possibility where at the lower concentrations the hydrogen bonding of melamine is causing a build up of layers. XP spectra would then see melamine bonded at the Cu(110) surface and melamine bonded to melamine result in a range of environments for the carbons. As the concentration is increased, the multi layer builds all over the surface and XP spectra records only the top layer of melamine and therefore there is a decrease in the broadness of the nitrogen (1s) and carbon(1s) regions. However the broad peak is very weak. It could therefore be drowned out by the more intense narrow peak.

7.7(b) Melamine adsorption at a fully oxidised surface.

The decrease in oxygen concentration on a fully oxidised surface (4.2×10^{14} to 2.8×10^{14}) and the change in binding energy of the N(1s) region from 398eV at a clean surface to 397.4eV at a fully oxidised surface suggest that the following reaction has taken place –

$$2C_3N_6H_{6(g)} + 2O^{\delta-}{}_{(a)} \rightarrow 2C_3N_6H_{3(ad)} + 2H_2O_{(g)} \quad (2)$$

Previous studies of ammonia at an oxidised Cu(110) surface have revealed the same reaction [21]. However, the above reaction does not affect the carbon as shown by the binding energy of 287eV which is the same as at a clean Cu(110) surface. The

broadness of the N(1s) peak suggests that there are at least 2 nitrogen species present at the surface. This would agree with the two non equivalent nitrogen's present in $C_3N_6H_3$, NH and N. Not all of the oxygen reacted as the XPS shows that there is still chemisorbed oxygen present (2.8×10^{14} atoms/cm^2). STM images of the surface resulted in some large structures with local order in the <110> direction. These structures have an average height of 1nm above the maxima. The STM was not able to image a close up of these structures. It is suggested that the adsorption of melamine at a fully oxidised surface has resulted in the formation of an imide.

7.7(c) Melamine adsorption at a partially oxidised surface.

The binding energy of the nitrogen again suggests that melamine has reacted and an imide has been produced. This would result in the desorption of water. Previously it has been seen that where oxygen is preadsorbed, the reaction occurs with the <100> ends of the Cu-O chains [6]. The nature and role of oxygen transients has been discussed in detail elsewhere for a number of different systems [20]. The adsorption site cannot be determined as atomic imaging of the oxygen islands was not possible. However it is known that phenyl rings have been located over a hollow site on the substrate lattice. This has also proven the case with phenyl species [21] and benzene [22] on a Cu(110) surface. The adsorption site of NH(a) at Cu(110) surfaces is the short bridge site [23][24].

7.8 Summary

Low coverage melamine adsorption at a clean Cu(110) surface results in a structure that is dictated by interactions of melamine with the surface. At higher concentrations a second layer structure is dictated by hydrogen bonding between melamine molecules. Adsorption of melamine at oxidised Cu(110) surfaces results in the formation of an imide.

7.9 Melamine adsorption at clean Ag(111) at 295K: XPS results

Exposure of a clean Ag(111) crystal to a 120 second dose of melamine at 140°C resulted in a carbon peak developing in the C(1s) region centred at 286.8 eV and a peak in the N(1s) region at 398.1 eV. The carbon and nitrogen concentrations were calculated to be $\sigma_C = 4.16 \times 10^{14}$ and $\sigma_N = 7.03 \times 10^{14}$ atoms cm^{-1}. Taking errors into account this is consistent with the 1:2 C:N ratio expected for melamine adsorption.

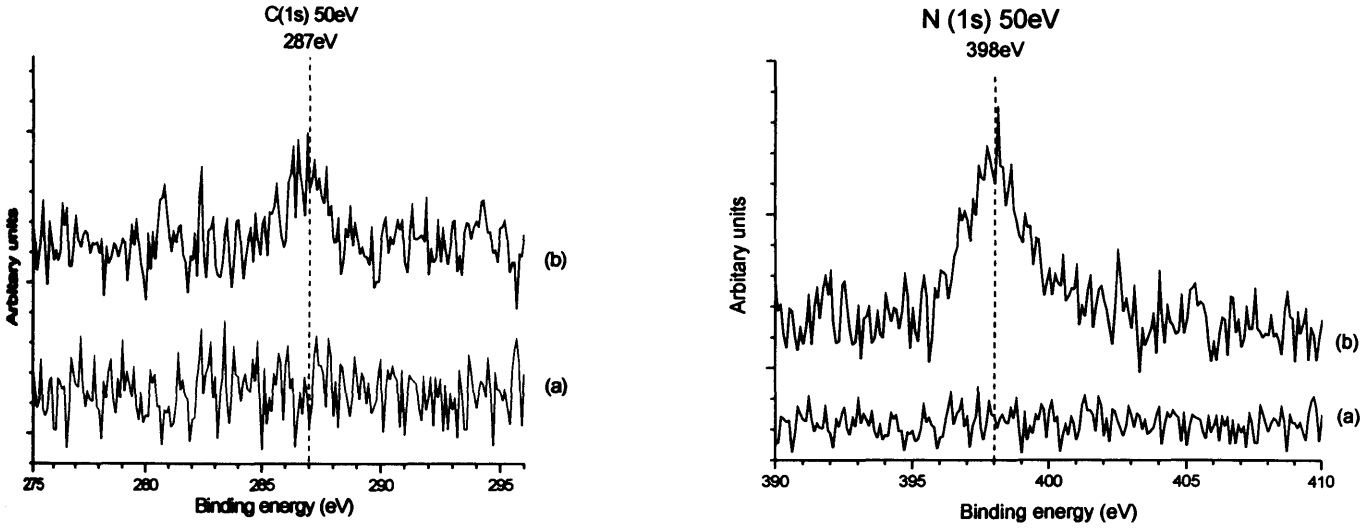

Fig. 7.13 Melamine absorption on Ag(111), (a) clean surface, (b) 120 second dose at 140°C.

The broad asymmetry of the N(1s) signal (in figure 13) suggests the presence of two N(1s) components consistent with the two different nitrogen atoms present in melamine. A curve fit of the N(1s) spectrum (fig, 14) shows the two states have a ratio of 2:1 consistent with the melamine structure. (NB. The binding energy scale is in the opposite direction to the XP spectra shown above due to the software used). The single carbon peak is also consistent with the equivalent carbons in melamine.

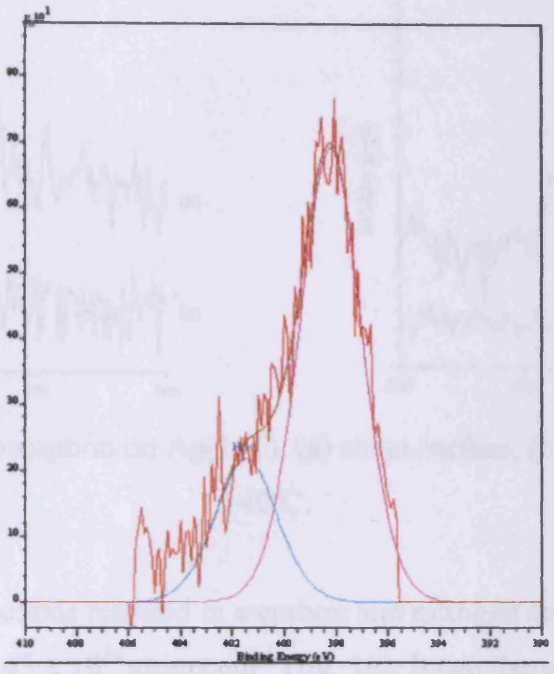

Fig. 7.14 A curve fit of the N(1s) spectra shown in figure 13 representing the two N(1s) components.

Increasing the dose of melamine to 240 seconds resulted in an increase in both carbon and nitrogen present at the surface: $\sigma_C = 3.0 \times 10^{15}$ and $\sigma_N = 5.03 \times 10^{15}$ atoms cm^{-1} as shown in figure 15. The binding energies have remained the same. Again allowing for errors, this adsorption is consistent with the 1:2 C:N ratio expected. The concentrations calculated suggest that there is now more than a monolayer present. This can be seen by the increase in FWHM in the C(1s) spectra. The three equivalent carbons contained in the melamine molecule would result in a single peak present. The broadness of the C(1s) spectra is the result of multilayers present at the Ag(111) surface. The N(1s) spectra also shows an increase in FWHM.

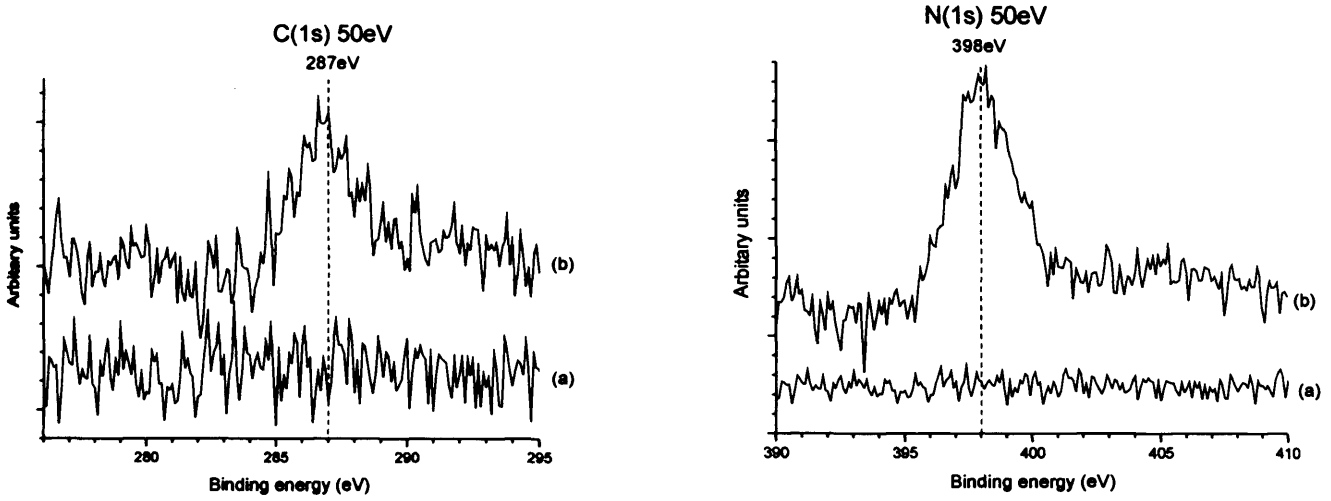

Fig. 7.15 Melamine absorption on Ag(111), (a) clean surface, (b) 240 second dose at 140°C.

A larger dose of 480 seconds resulted in a carbon and nitrogen concentration of σ_C = 8.46×10^{15} and $\sigma_N = 1.45 \times 10^{16}$ atoms cm^{-1} (fig. 16). It can therefore be suggested that melamine can form an indefinite number of layers on Ag(111), similar to standard physisorption. The broadness of the C(1s) and N(1s) peaks has increased further. This is caused by the increase in the amount of layers present at the surface.

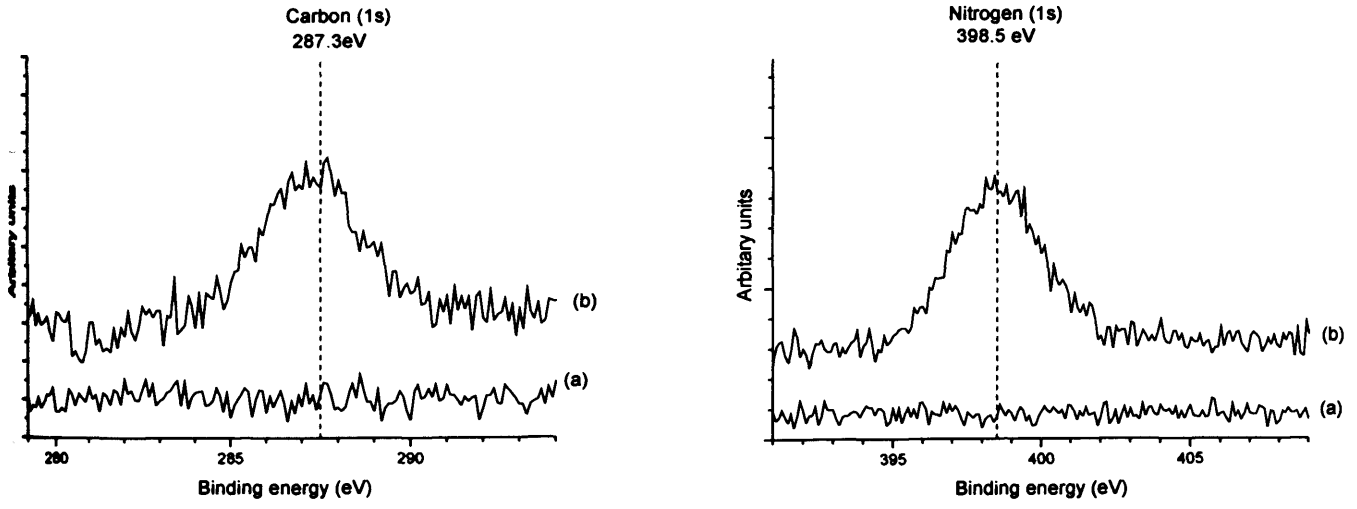

Fig. 7.16 Melamine absorption on Ag(111), (a) clean surface, (b) 480 second dose at a furnace temperature of140°C.

Heating the surface to 400K results in a complete loss of both carbon and nitrogen. However, the fact that there is almost a complete removal of melamine from the substrate at 400K suggests that the interaction with melamine and Ag(111) is weak and therefore the hydrogen bonding between molecules will probably dictate the structure at the surface.

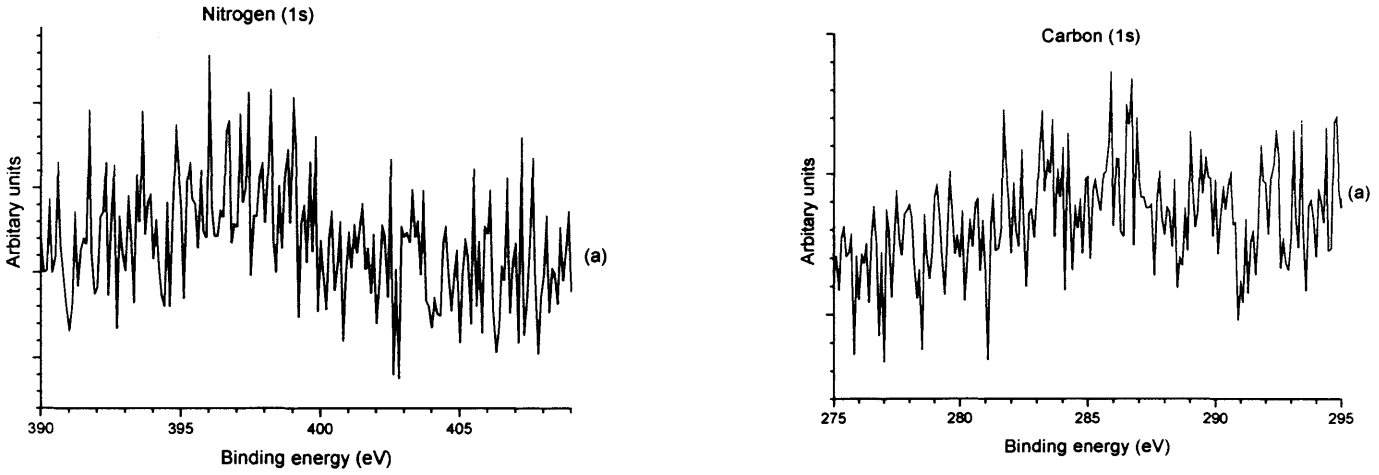

Fig. 7.17 Melamine absorption on Ag(111), (a) After heating the surface to 400K

7.10 Melamine adsorption at clean Ag(111) at 295K: STM results

From the XP data an exposure of 120 seconds at a furnace temperature of 140°C resulted in a carbon and nitrogen concentration of $\sigma_C = 4.16 \times 10^{14}$ and $\sigma_N = 7.03 \times 10^{14}$ atoms cm^{-1}. The STM images (fig. 18) suggests that large portions of the surface are clean but on smaller terraces with more restricted mobility a well ordered ad-layer is present.

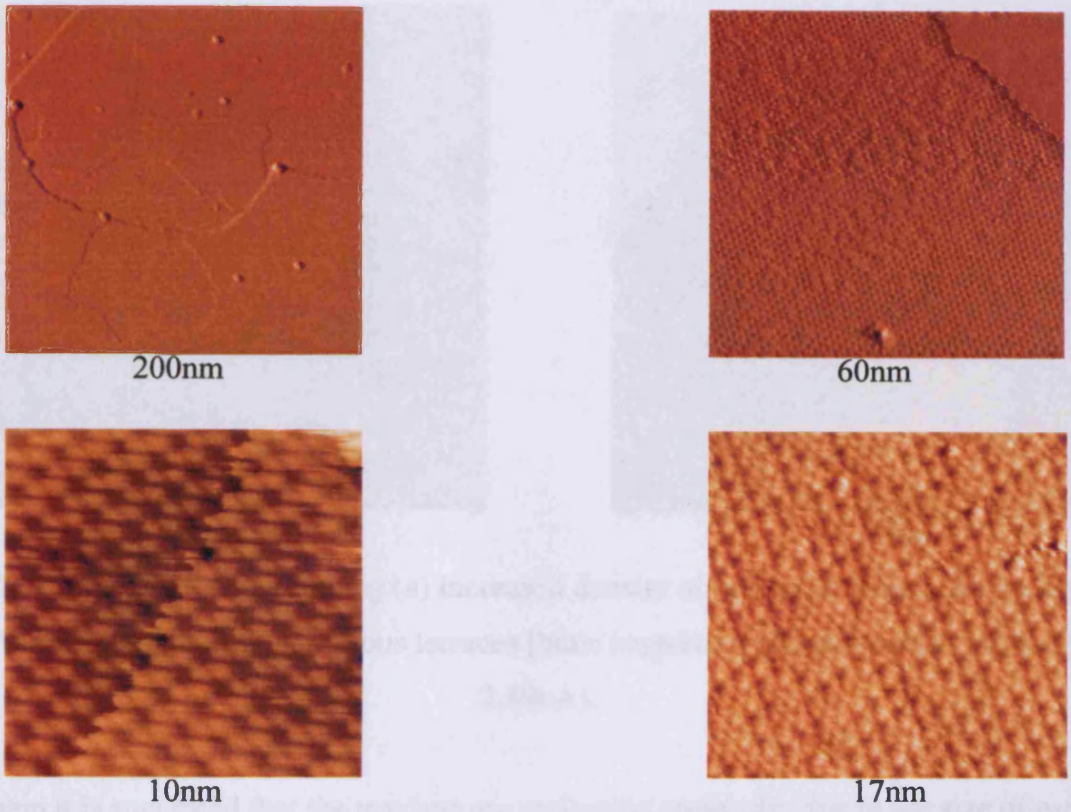

Fig. 7.18 STM images of (a) large terraces of melamine adsorbed at Ag(111), (b) zoomed image of the structures present, (c) pairs of melamine molecules forming the distorted hexagonal structure and (d) melamine and the substrate present [bias: negative, voltage = 1.55V, current = 3.21nA].

The size of each feature (0.5nm) is consistent with the expected diameter of the melamine molecule.

7.10(a) Increased concentration

XP spectra show that an exposure of the Ag(111) surface to melamine dosed from the k-cell for 240 seconds at a furnace temperature of 140°C resulted in a surface concentration of $\sigma_C = 3.0 \times 10^{15}$ and $\sigma_N = 5.03 \times 10^{15}$ atoms cm^{-1} corresponding to more than a monolayer present (STM images shown in fig. 19).

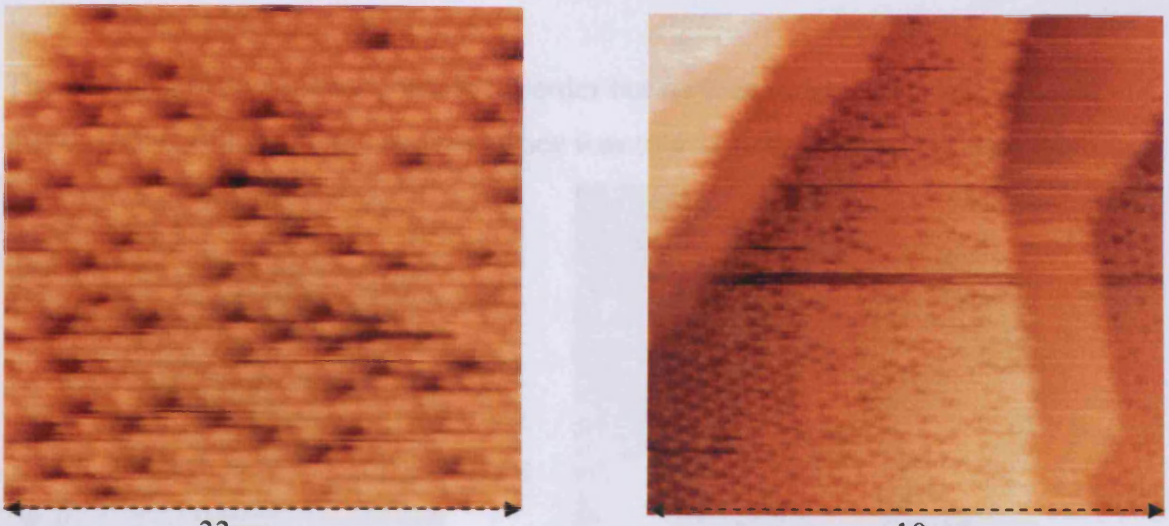

Fig. 7.19 STM image showing (a) increased density of melamine molecules present, (b) structures imaged at various terraces [bias: negative, voltage = 1.24V, current = 2.89nA].

Again it is suggested that the maxima are melamine molecules due to the size of each molecule; 0.53nm. The hexagon structure is now more symmetric probably due to the substrate having less of an impact on the structure of a second or third layer.

7.10(b) Concentration => ~ 3 x 10^{14} molecules cm^{-2}

A further dose of 480 seconds at a furnace temperature of140°C results in a surface concentration of σ_C = 8.67 x 10^{14} and σ_N = 1.45 x 10^{16} atoms cm^{-1}. STM reveals large circular structures with a height averaging 4nm.

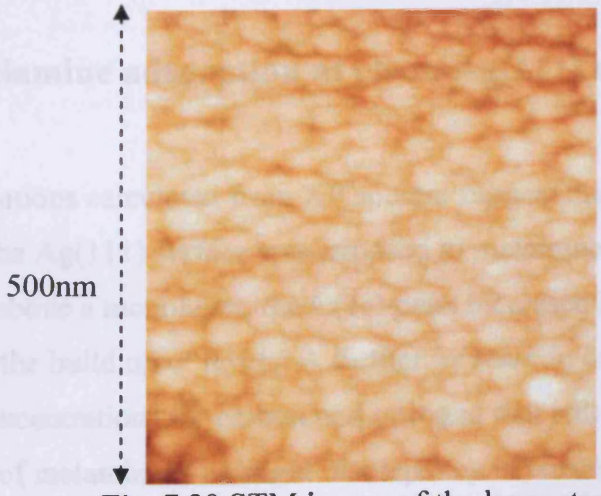

Fig. 7.20 STM image of the large structures.

These large structures show some local order but no long range order. XPS showed that the effect of heat on the above surface was to desorb the majority of melamine.

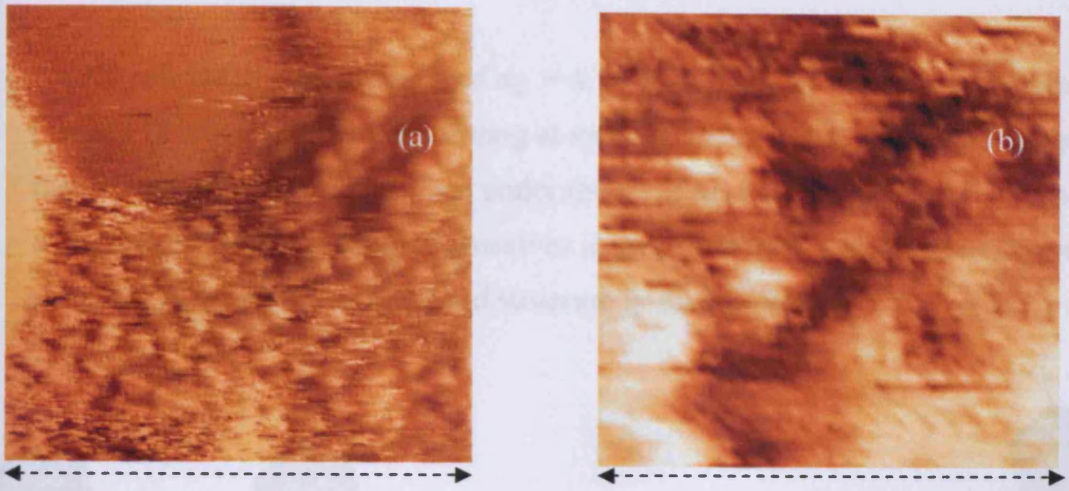

Fig. 7.21: (a) image of the structure present after heating the surface to 400K, (b) A zoomed picture of image (a) [bias: negative, voltage = 0.88V, current = 2.89nA].

The XPS concentrations could not be calculated as there is little melamine present. However as the STM shows, there are some structures present that are comparable to the higher concentration structures. This adds to the evidence that this less distorted hexagonal structure can create the large structures shown in figure 20. An increase in concentration results in a three dimensional structure being built.

7.11 Discussion

7.11 (a)Melamine adsorption at clean Ag(111) surfaces

The concentrations calculated from XP spectra suggest that molecular adsorption occurred as the Ag(111) surface was exposed to melamine. As the concentration was increased to above a monolayer, the C(1s) peak increased in FWHM. This was indicative of the build up of layers. A further increase in concentrations resulted in calculated concentrations for carbon and nitrogen that still agreed with the composition of melamine. The slight discrepancy in concentration ratios could be due to desorption of melamine during XP scans. The chance of this occurring would

increase as more layers are added to the surface. Heating the surface to 400K resulted in complete desorption of melamine. This signifies a weak interaction between melamine and the surface.

An XP calculated concentration of $\sigma_C = 4.16 \times 10^{14}$ and $\sigma_N = 7.03 \times 10^{14}$ atoms cm^{-1} resulted in ordered structures forming at small terraces. The STM images suggest that melamine is mobile at the surface under the STM tip until a monolayer is formed. The melamine molecules position themselves in pairs and form a distorted hexagonal structure. A model of the proposed structure is shown below.

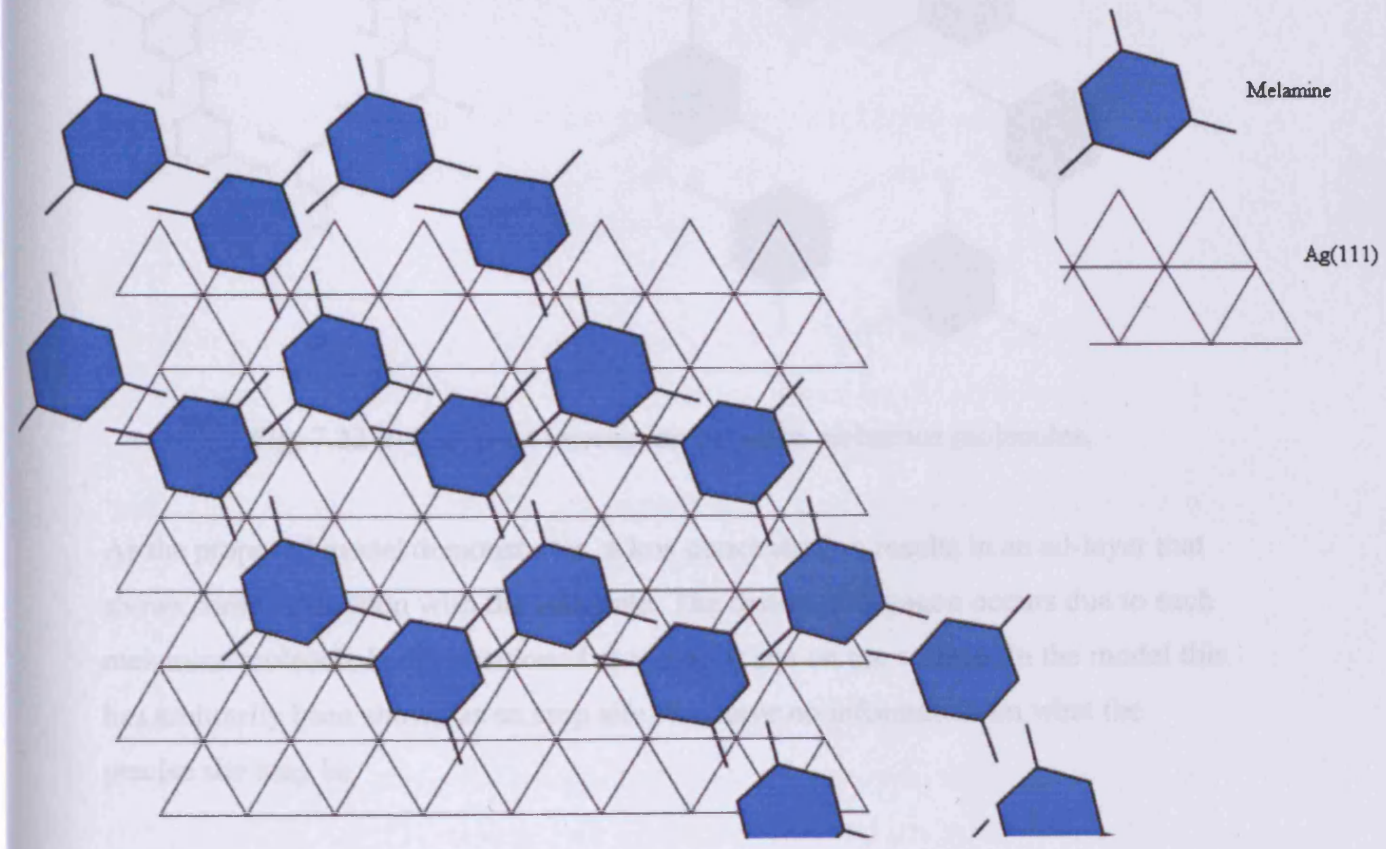

Fig. 7.22 a: Proposed model for the structure of melamine at an Ag(111) surface.

The threefold symmetry of melamine would lead to the symmetric structure depicted in Fig. 7.22b. The distorted hexagon observed suggests an influence from the substrate.

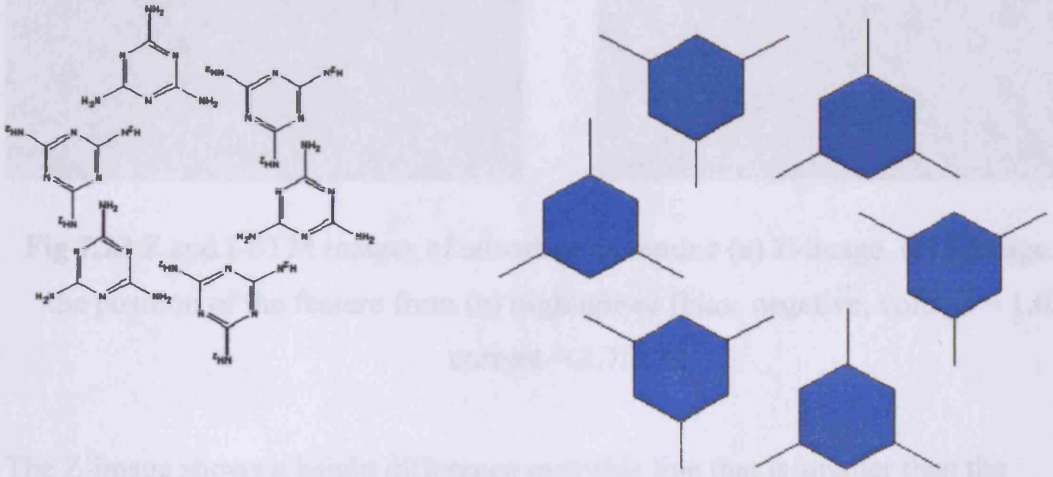

Fig. 7.22 b: Proposed interaction between melamine molecules.

As the proposed model demonstrates, a low concentration results in an ad-layer that shows some interaction with the substrate. The distorted hexagon occurs due to each melamine molecule being positioned at a similar site on the surface. In the model this has arbitrarily been shown as an atop site. We have no information on what the precise site may be.

The Z image of figure 23 shows a line intersecting the adsorbed melamine molecules (concentration – $\sigma_C = 4.16 \times 10^{14}$ and $\sigma_N = 7.03 \times 10^{14}$ atoms cm^{-1}). The I-image (differential current image) is shown in Fig. 23b with the position of the line on the Z-image highlighted.

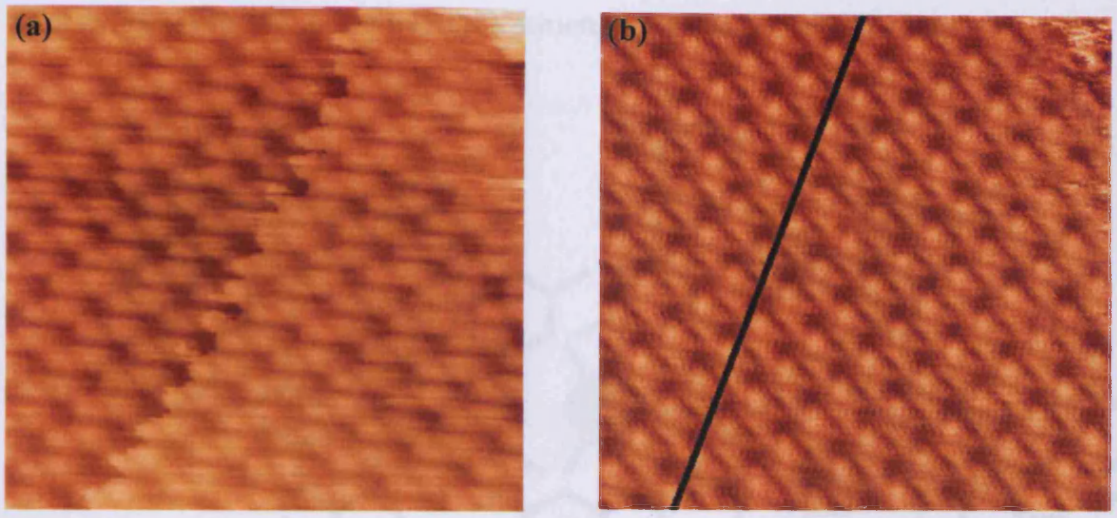

Fig 7.23 Z and I-STM images of adsorbed melamine (a) Z-image, (b) I-image, with the position of the feature from (a) highlighted [bias: negative, voltage = 1.03V, current = 1.75nA].

The Z-image shows a height difference over this line that is smaller than the measurement error of the STM (~0.2 Angstroms). It can also be seen that melamine molecules lie across the boundary. No change in brightness is observed in the I-image. This suggests that the line is a consequence as a bulk defect. The most likely being a dislocation which forms a 'micro-step' and hence a contrast in the height image.

The concentration of melamine molecules present at the surface at this stage corresponds to a coverage of a monolayer. STM images would suggest that there is still some clean Ag(111) present. This is attributed to the mobility of the adsorbed melamine molecules which readily diffuse across the surface. A small terrace will limit this surface diffusion.

Concentration of σ_C = 3.0 x 10^{15} and σ_N = 5.03 x 10^{15} atoms cm^{-1}

At this higher concentration, melamine formed a more symmetrical structure at the surface. This can be attributed to second layer melamine where the substrate has less

influence on the structure formed by melamine as it is most probable that a second layer is being imaged. A model of the structure formed is proposed below.

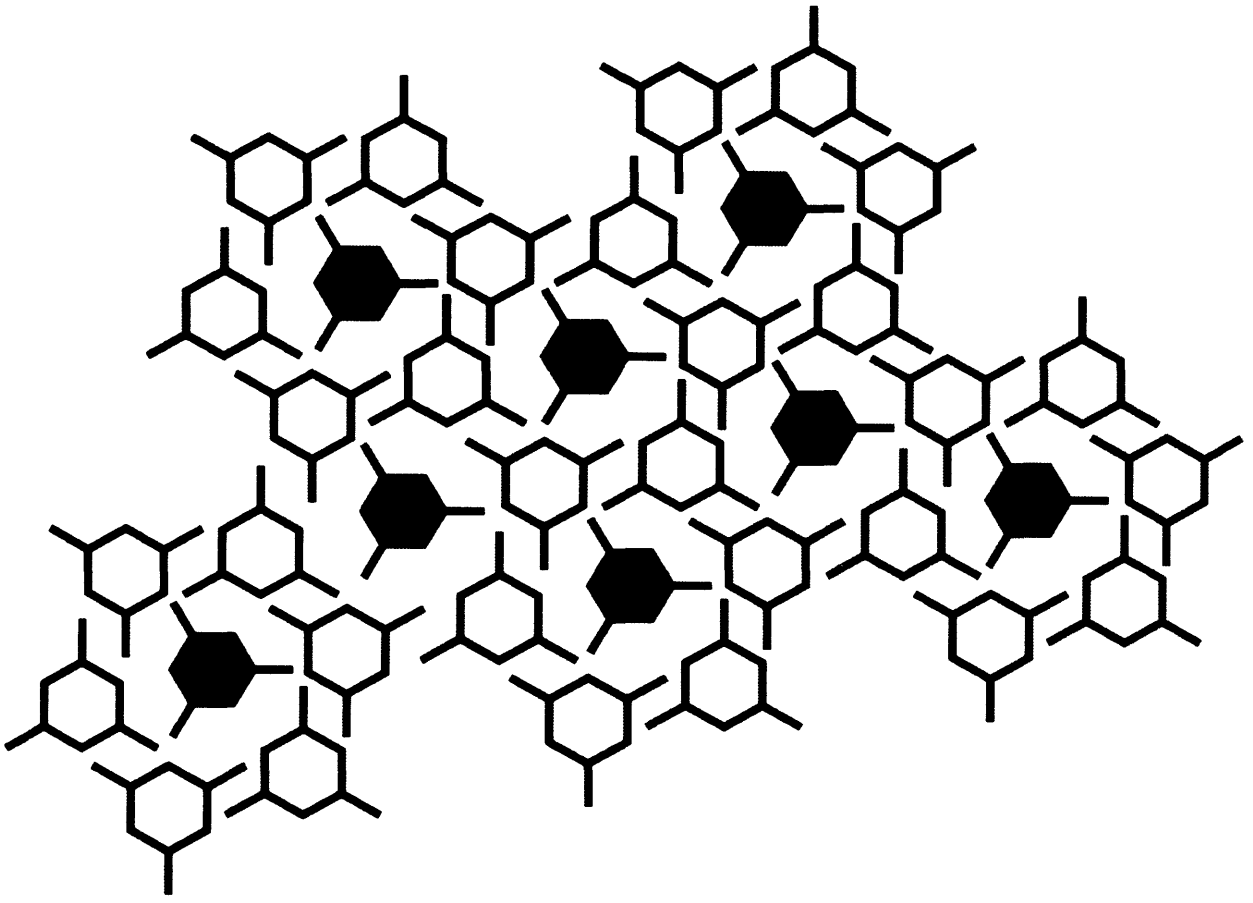

Fig. 7.24 Pictorial representation of adsorbed melamine at an Ag(111) surface.

The molecules highlighted in figure 25 are significantly smaller than the other molecules which may be due to a difficulty in H-bonding with other melamine molecules laterally. These are identified in the mode structure above. It can therefore be suggested that the highlighted molecules are tilted and therefore form a hydrogen bond between two layers. This would promote three dimensional growth.

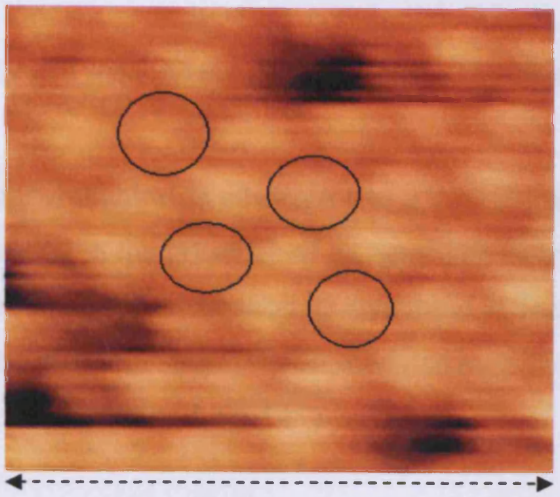

Fig. 7.25 STM image of adsorbed melamine, smaller molecules highlighted.

Concentration => ~ 3 x 10^{14} molecules cm^{-2}

A greater concentration of melamine at the surface results in a build up of many layers. These are imaged as large structures with a diameter of around 40nm. There are some much larger and much smaller structures present. The effect of heat (400K) on these structures resulted in removal of almost all melamine. The structures left at the surface are comparable to the structures formed at a concentration of σ_C = 3.0 x 10^{15} and σ_N = 5.03 x 10^{15} atoms cm^{-1}.

7.12 Summary

Melamine molecularly adsorbs at an Ag(111) surface. At concentrations of a monolayer and below, STM images ordered structures at smaller terraces. Increasing the concentration results in a more symmetrical structure. This is due to the substrate having less influence. Increasing the concentration further results in a build up of layers. These layers build up indefinitely.

7.13 Malonyl dichloride and Melamine at a Cu(110) surface

Chapter 6 discussed malonyl dichloride adsorption at a Cu(110) surface. It was shown that adsorption only occurred in the presence of oxygen. The following section looks at the co-adsorption and sequential adsorption of melamine and malonyl dichloride. Emphasis is placed on the different structures formed due to the co-adsorption and the reactions that occur at the Cu(110) and Ag(111) surfaces.

7.14 Sequential adsorption at a Cu(110) surface at 295K: XPS results.

A clean Cu(110) surface was exposed to a 300 second dose of melamine at 145°C from a k-cell. This gave rise to peaks in the C(1s) and N(1s) regions at 287 and 398.1 eV respectively (figure 13a & d) The carbon concentration was calculated to be 1.06 x 10^{15} atoms/cm^2 and the nitrogen concentration was 2.0 x 10^{15} atoms/cm^2. This gives a ratio of approximately 1: 2, carbon to nitrogen. This ratio suggests that melamine is molecularly bound to the surface. A 500L dose of malonyl dichloride resulted in a slight broadening of the N(1s) peak. The C(1s) spectra remained the same with no additional carbon present. As shown in figure 26 there is no oxygen present at the surface. The only change in the surface is the presence of chlorine with a calculated concentration of 2.10 x 10^{14} atoms/cm^2. The binding energy of the chlorine is 198eV. Comparing this with previous experiments at Cu(110) where malonyl dichloride was dosed on a partially oxidised surface, this binding energy is 0.5eV higher. It is not known what state this chlorine is. However the binding energy is comparable with chemisorbed chlorine at a Cu(110) surface[25].

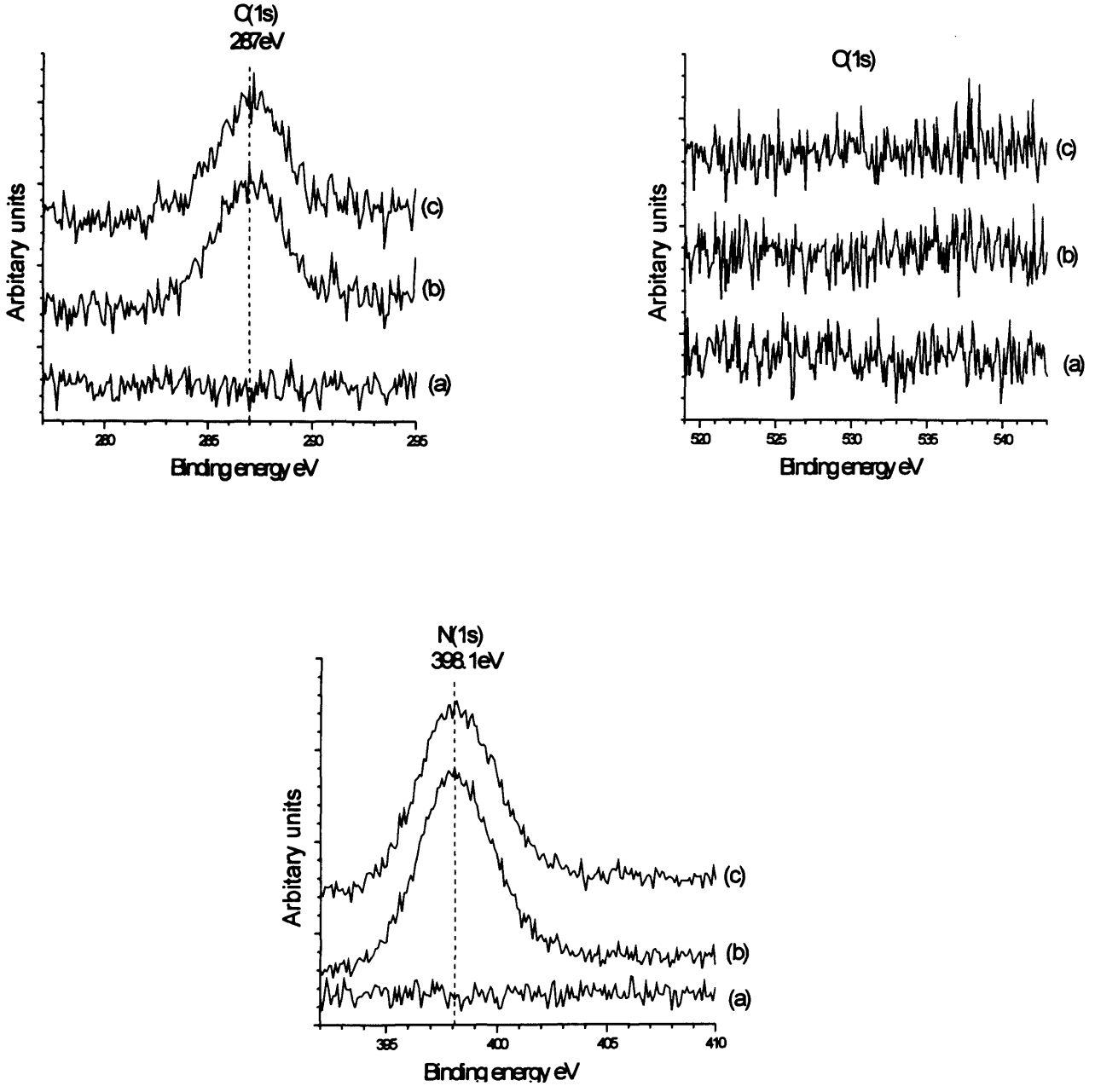

Fig. 7.26 The adsorption of melamine at a Cu(110) surface followed by dosing malonyl dichloride. XP spectra of C(1s), N(1s), O(1s) and Cl(2p) regions; (a) Clean surface; (b) 5 min exposure to melamine at 145°C; (c) exposure to 200L of malonyl dichloride

7.15 Co-adsorption at a Cu(110) surface at 295K: STM results.

The STM revealed a structure different from the previous studies of melamine at a Cu(110) surface. The surface now shows local order in the <100> direction. Previous studies of HCl adsorbed at a Cu(110) surface [25] resulted in similar structures as shown in fig. 27.

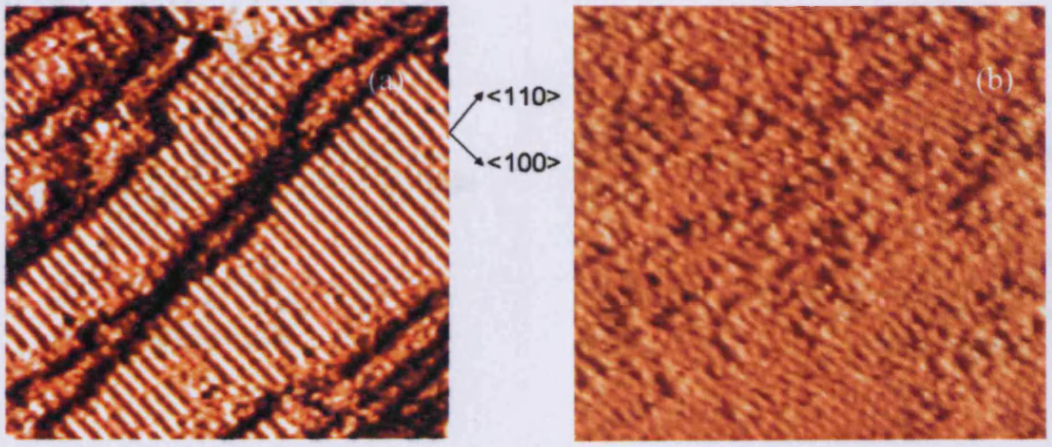

Fig. 7.27 STM images of (a) The reconstructed Cu(110) surface saturated with rows aligning in the ⟨001⟩ direction after a large dose of HCl at a Cu(110) surface, (b) image after a dose of 5 minutes of melamine at a Cu(110) surface at 290K and then exposure to 200L of malonyl dichloride [bias: negative, voltage = 1.35V, current = 1.8nA].

7.16 The effect of heat at the surface (450K): XPS results.

Heating the surface to 450K resulted in the following XP spectra.

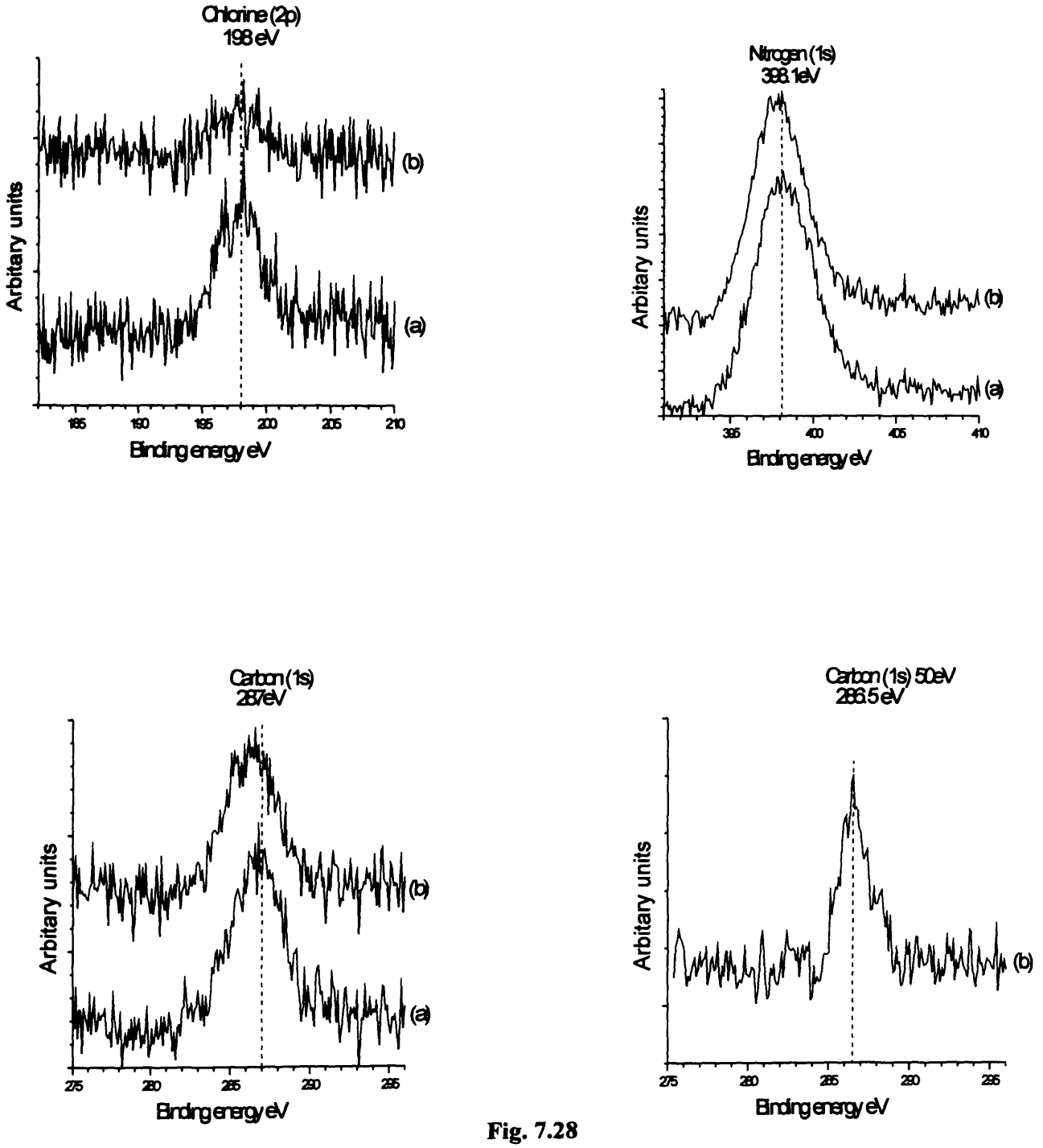

Fig. 7.28

The adsorption of melamine at a Cu(110) surface and then dosing malonyl dichloride. XP spectra of C(1s) at 100ev, C(1s) at a pass energy of 50eV, N(1s) and Cl(2p) regions; (a) Surface as left overnight; (b) Heating the surface to 450K.

After heating the concentrations of the three elements have decreased. The concentrations of carbon, nitrogen and chlorine are now 8.63 x 10^{14}, 1.83 x 10^{15} and 6.3 x 10^{13} atoms/cm^2. The ratio of carbon to nitrogen is still 1:2 the peak suggesting that melamine is desorbing molecularly. The binding energy of N(1s) has decreased slightly to 398eV. The carbon binding energy has also decreased to 286.5eV.

7.17 The effect of heat at the surface (450K): STM results.

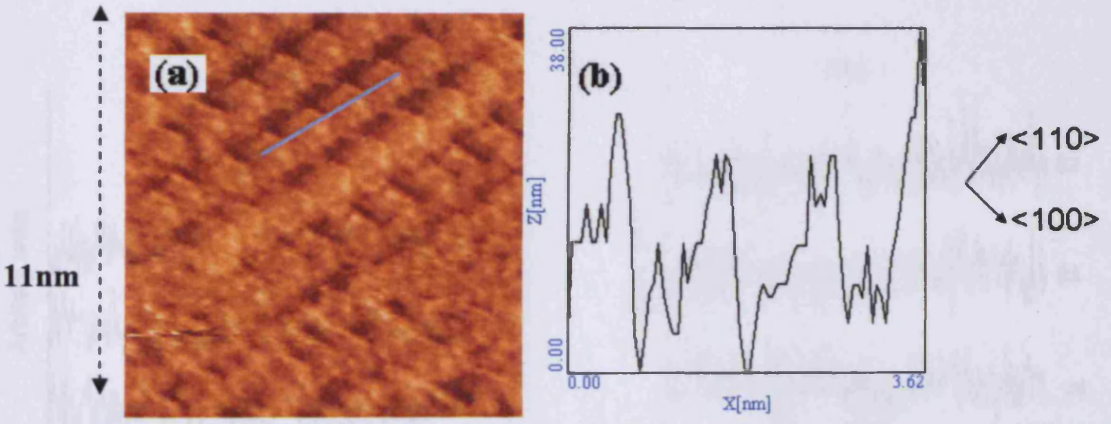

Fig. 7.29 STM image after heating the surface shown in figure 28, (a) two different structures shown, (b) line profile of structure shown in (a) [bias: negative, voltage = 1.09V, current = 1.75nA].

A line profile of the structures (figure 29b) suggests that each molecule is tilted. This would agree with other studies of other amines at copper surfaces such as aniline[6] [26]. The STM images indicate interaction between the hexagonal structures. Each hexagonal structure has a light strand connecting it to a parallel molecule. It is suggested that this interaction is caused by the intermolecular attraction between the hydrogen attached to the nitrogen and the negative nitrogen contained in the ring of the adjacent molecule.

7.18 Co-adsorption of melamine and malonyl dichloride at an Ag(111) surface: XPS results.

A clean Ag(111) was exposed to melamine from a k-cell at 145°C for 240 seconds. This resulted in chlorine, carbon and nitrogen. The binding energies are shown in fig. 30. The calculated concentrations suggest that molecular adsorption occurred (1.06 x 10^{15} : 2 x 10^{15} atoms cm^2 C:N). The surface was then exposed to 200L of malonyl dichloride. The concentrations of carbon and nitrogen remained the same. However, there is now chlorine present. The chlorine concentration was calculated to be 2.10 x 10^{14} atoms cm^2. The binding energy is indicative of chemisorbed Cl [25].

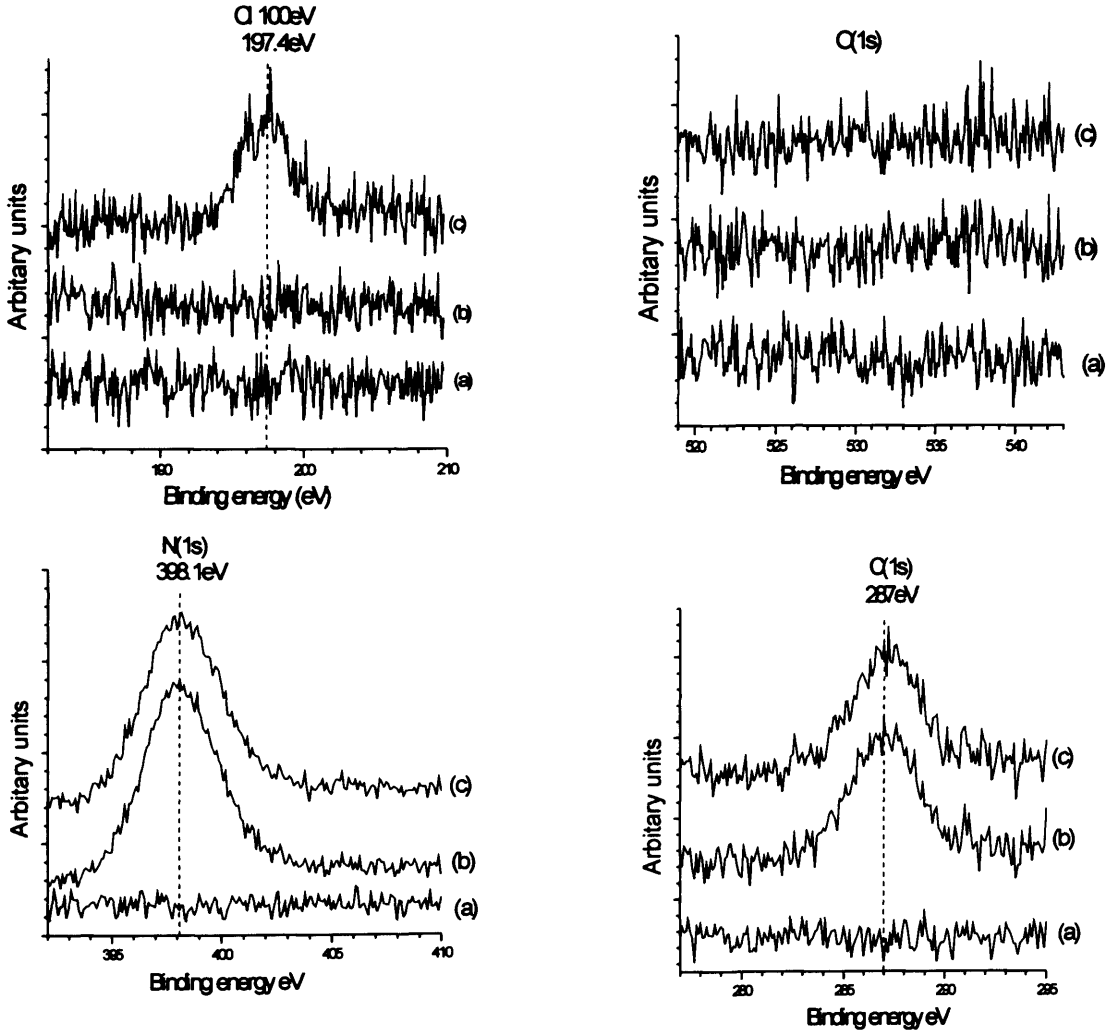

Fig. 7.30 The adsorption of melamine at a Ag(111) surface followed by exposure to malonyl dichloride. XP spectra of C(1s), N(1s), O(1s) and Cl(2p) regions; (a) Clean surface; (b) 5 min exposure to melamine at 145°C; (c) exposure to 200L of malonyl dichloride.

7.19 Co-adsorption of melamine and malonyl dichloride at an Ag(111) surface: STM results.

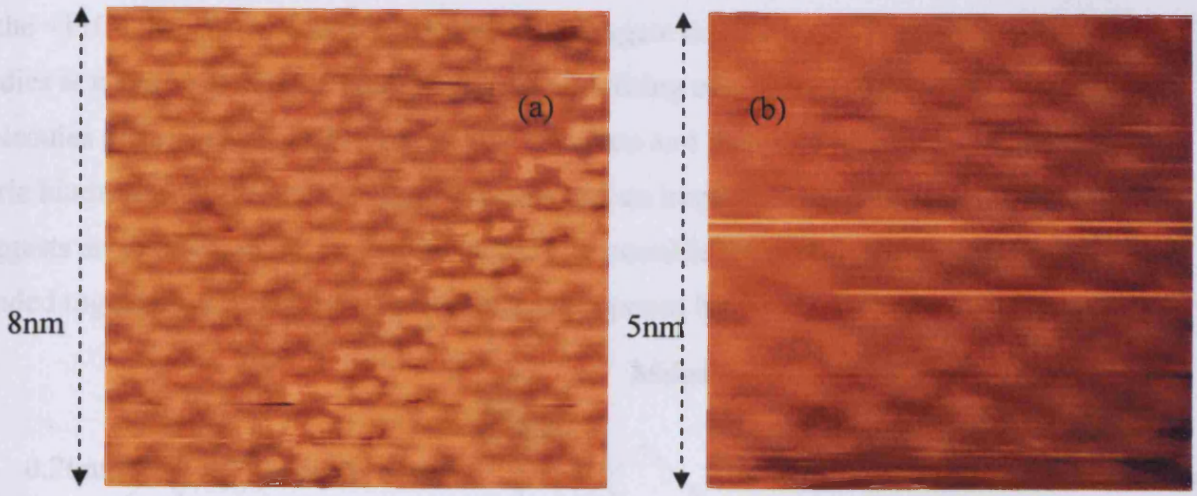

Fig. 7.31 STM images of (a) melamine and chlorine and (b) chlorine at an Ag(111) surface [bias: negative, voltage = 1.65V, current = 1.59nA].

The STM reveals two different structures present. The first structure shown in figure 31a shows a hexagonal structure centred around a feature of 3 angstroms in size after melamine was exposed to malonyl dichloride. The hexagonal structure appears to consist of six melamine molecules with a diameter of 6 angstroms. This agrees with the earlier studies of melamine on Ag(111). The second structure shows smaller features present at the surface. These features have a diameter of 3 angstroms.

7.20 Discussion

7(a)Co-adsorption of melamine and malonyl dichloride at a Cu(110) surface

The N(1s) binding energy of 398eV suggests that there is an NH_2 group present [27]. The fact that the ratios remain consistent for melamine suggests that it is molecularly adsorbed at the Cu(110) surface. However as the previous chapter shows, malonyl dichloride will not react with a clean copper surface. Melamine has therefore catalysed the reaction of malonyl dichloride at the surface, and resulted in adsorption of chlorine. The adsorbed

chlorine has resulted in an increase in the ordering of melamine. The STM images show hexagonal shaped molecules consistent with the hexagonal structure of one melamine molecule. The calculated concentration using STM was consistent with the concentration calculated using XPS. The Cu(110) surface has had an impact on the structure with order in the <110> direction. Height measurements suggest that each ring is tilted. Previous studies at a Cu(110) surface have also observed tilting of a phenyl ring [6, 26]. The molecules are closer packed in the <110> direction and therefore tilting would decrease steric hindrance. Hydrogen bonding has also had an impact on the structure. Figure 17 suggests an interaction between molecules. It is possible the molecules are hydrogen bonded together. A model of this structure is proposed below.

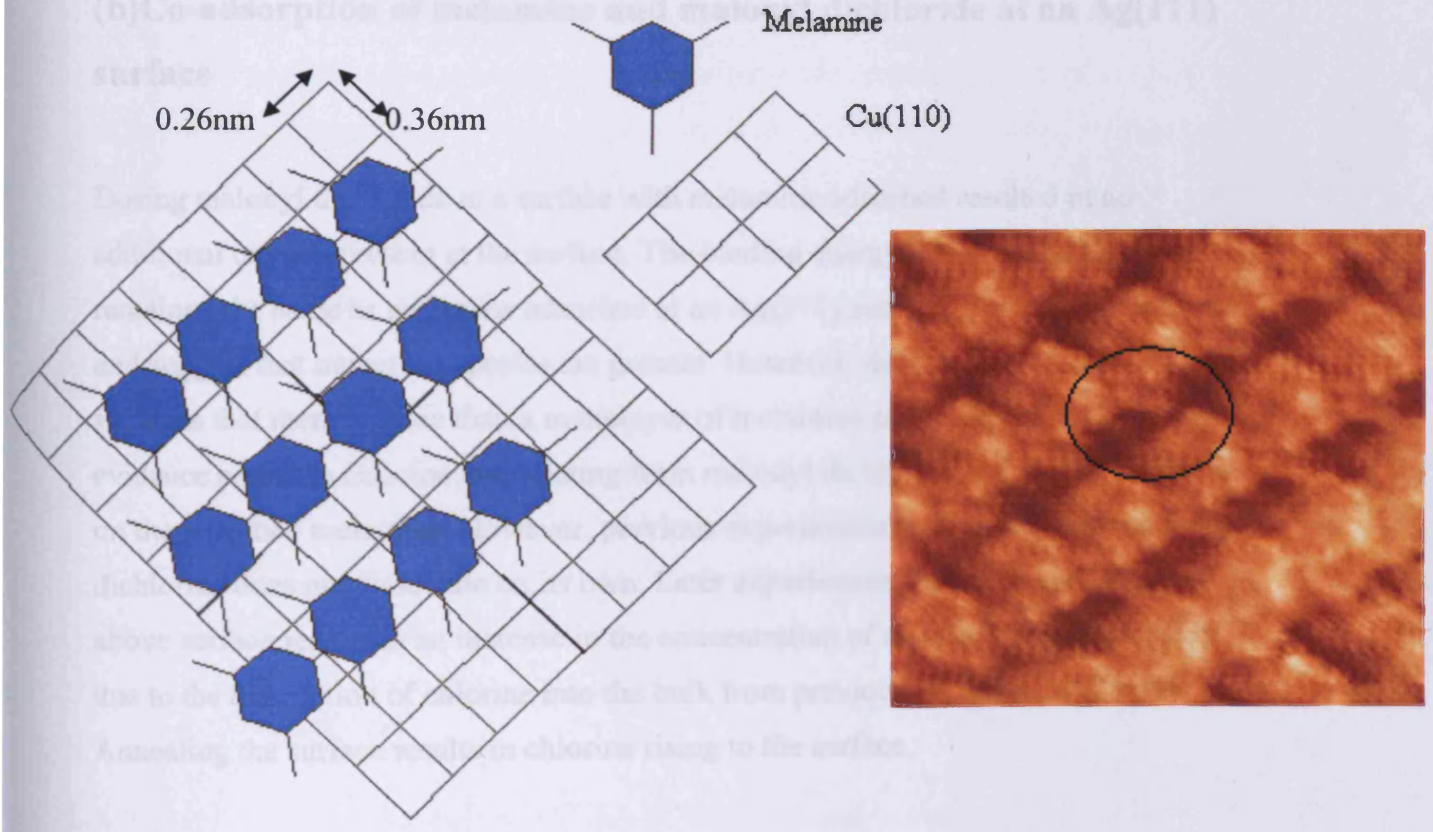

Fig. 7.32 The interaction between molecules

The model suggests there may be a conjugated system created. This system results in a general delocalization of the electrons, which increases stability and thereby lowers the overall energy of the molecule. Steric effects would cause the tilting. This in turn would increase π-π interactions and increase stability.

XPS would suggest that an amide link was not produced between melamine and malonyl dichloride. However it was found that chlorine has had an effect on the adsorption of melamine. A reaction must have occurred between melamine and malonyl dichloride in order for the adsorption of chlorine to occur. This reaction may have caused the structuring at the surface but the ratios and binding energies suggest that melamine has molecularly adsorbed at the surface. Chlorine is not imaged by the STM. This could be due to the fact that chlorine is underneath the melamine structure and therefore having an impact on the adsorption. The structure present is due to the interaction with the Cu(110) surface and the intermolecular forces between molecules.

(b)Co-adsorption of melamine and malonyl dichloride at an Ag(111) surface

Dosing malonyl dichloride to a surface with melamine adsorbed resulted in no additional oxygen present at the surface. The binding energy of C(1s) and N(1s) has remained the same as melamine adsorbed at an Ag(111) surface. Both peaks are broad and suggest that numerous species are present. However, the calculated concentration suggests that there is more than a monolayer of melamine present at the surface. All evidence points to chlorine dissociating from malonyl dichloride and having no effect on the adsorbed melamine. However, previous experiments have shown that malonyl dichloride does not dissociate on its own. Later experiments show that annealing the above surface results in an increase in the concentration of chlorine. This is probably due to the dissolution of chlorine into the bulk from previous experiments [28-31]. Annealing the surface results in chlorine rising to the surface.

The second structure shown in figure 32b is too small to be melamine. This is therefore believed to be chlorine and the measurements taken using STM images agree with previous studies of chlorine adsorption [25]. Chlorine has been studied previously at an Ag(111) surface. It was found that initial concentrations give rise to a ($\sqrt{3}$ x $\sqrt{3}$)-R30° pattern [32] [33]. This evolves to a (17 x 17) saturation structure at higher doses [34]. The structure shown in figure 32b has an interatomic distance of 4.9 angstroms. This agrees with the interatomic distance of a ($\sqrt{3}$ x $\sqrt{3}$)-R30° pattern. A low concentration of chlorine has been observed at an Ag(111) surface. Melamine

may be the factor that allows it to be imaged at such a low concentration. It can be seen in figure 32a that melamine and chlorine are both imaged. The STM is only imaging some of the chlorine atoms and the chlorine has the structure of ($\sqrt{3}$ x $\sqrt{3}$)-R30°.

Figure 32a shows that the melamine molecules are not individually imaged. It is suspected that this is due to the chlorine interaction with melamine. The electron density appears stronger between molecules. This suggests a stronger hydrogen bond.

7. 21 Caesium adsorption at an Ag(111) surface

The objective of the present work was to investigate how caesium adsorption would affect the melamine structure at an Ag(111) surface. Alkali covered metal surfaces are of practical interest in a number of ways such as cathodes and promoters in heterogeneous catalysis [35]. Cesium has previously been studied at a Cu(111) surface. It was found that cesium atoms take the on top site relative to the copper substrate [36]. At an Ag (110) surface it was found that that 0.1 ML Cs coverage converts the entire surface to a mixture of (1 x 2) and (1 x 3) reconstructed structures, indicating that Cs atoms exert a long range cooperative effect on surface structures [37]. Theoretical treatments [38] have shown that the surface can undergo a missing-row reconstruction as a small amount (~0.05 electron per surface atom) of excess charge is transferred to the surface.

7. 22 Experimental

An Ag(111) surface was exposed to cesium using a Getter source made by SAES. This was initially outgassed extensively in order to lower contamination of the surface. The dose was controlled by the amount of current applied.

7.23 Caesium adsorption at an Ag(111) surface at 295K: XPS results

An Ag(111) surface was exposed to Caesium for 150 seconds at a current of 5A. This initial dose resulted in a concentration of 6.25 x 10^{14} atom/cm^2. The binding energy of the Cs($3d_{5/2}$) photoelectron peak at a clean silver surface was 726eV + or – 0.2eV.

This was invariant with coverage. This binding energy agrees with previous studies of Cs adsorption at a clean Cu(110) surface [39]. A further dose at 500 seconds resulted in a concentration of 1.13×10^{15} atoms/cm^2.

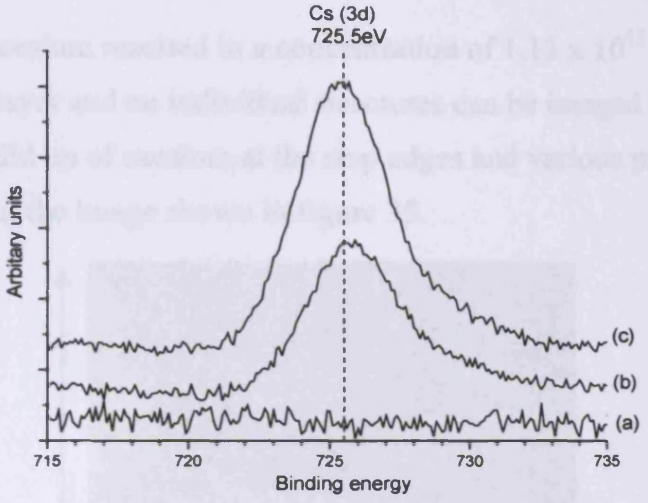

Fig. 7.33 An Ag(111) surface exposed to Cesium, (a) clean surface, (b) caesium exposed at 5A for 150seconds and(c) 5A for 500 seconds.

7.24 Caesium adsorption at an Ag(111) surface at 295K: STM results

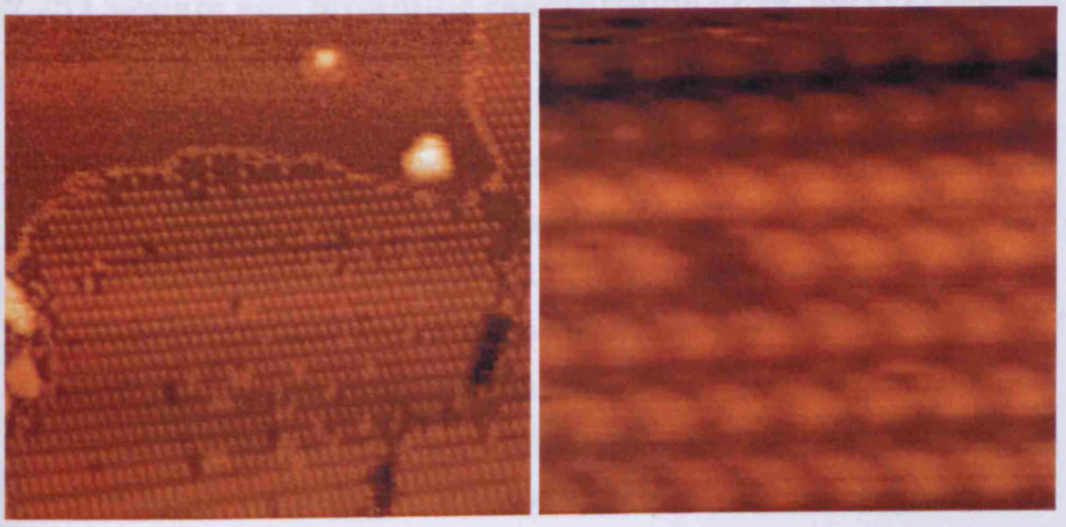

50nm 8nm

Fig. 7.34 (a)Cs at an Ag(111) surface, (b) zoom in of image (a) [bias: negative, voltage = 1.22V, current = 2.55nA].

From XP data an exposure of 150 seconds resulted in a coverage of 6.25 x 10^{14} atom/cm^2. At this coverage the STM revealed an oblique structure at various terraces. There is spacing between atoms of 1nm in all directions.

A further dose of cesium resulted in a concentration of 1.13 x 10^{15} atoms/cm^2. This is now over a monolayer and no individual structures can be imaged at the surface. There is now a build up of caesium at the step edges and various parts of the terraces. This can be seen in the image shown in figure 35.

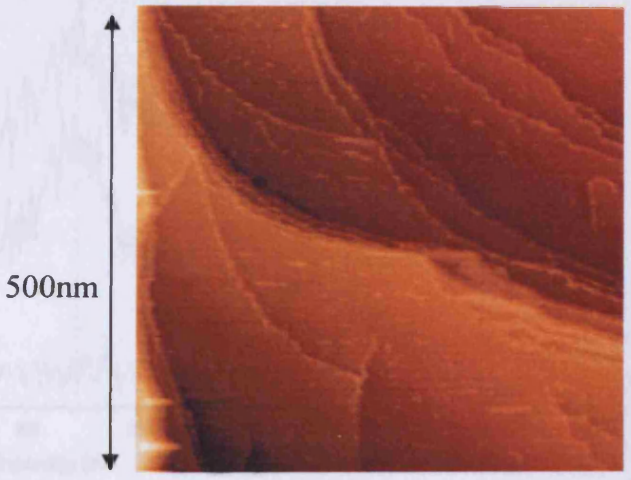

Fig. 7.35 : STM image of caesium at an Ag(111) surface [bias: negative, voltage = 1.24V, current = 2.32nA].

7.25 Caesium and melamine coadsorption at an Ag(111) surface at 295K: XPS results

Caesium was exposed to preadsorbed melamine at an Ag(111) surface. A clean Ag(111) surface was exposed to a two minute dose of melamine at 145° from a k-cell. This gave rise to peaks in the C(1s) and N(1s) regions at 287 and 398.5 eV respectively (figure 36) The carbon concentration was calculated to be 1.5 x 10^{15} atoms/cm^2 and the nitrogen concentration was 2.8 x 10^{15} atoms/cm^2. Both concentrations have an error of approximately 1.0 x 10^{14}. This gives a ratio of approximately 1: 1.8, carbon to nitrogen. This ratio suggests that melamine is molecularly bound to the surface. Caesium was dosed at a current of 5 amps for 1.5 minutes. This resulted in no change in carbon and nitrogen concentration. The binding

energies have also remained the same. There is now a peak is the Cs 3d region with a concentration calculated to be 5.48 x 10^{14} atoms/cm^2.

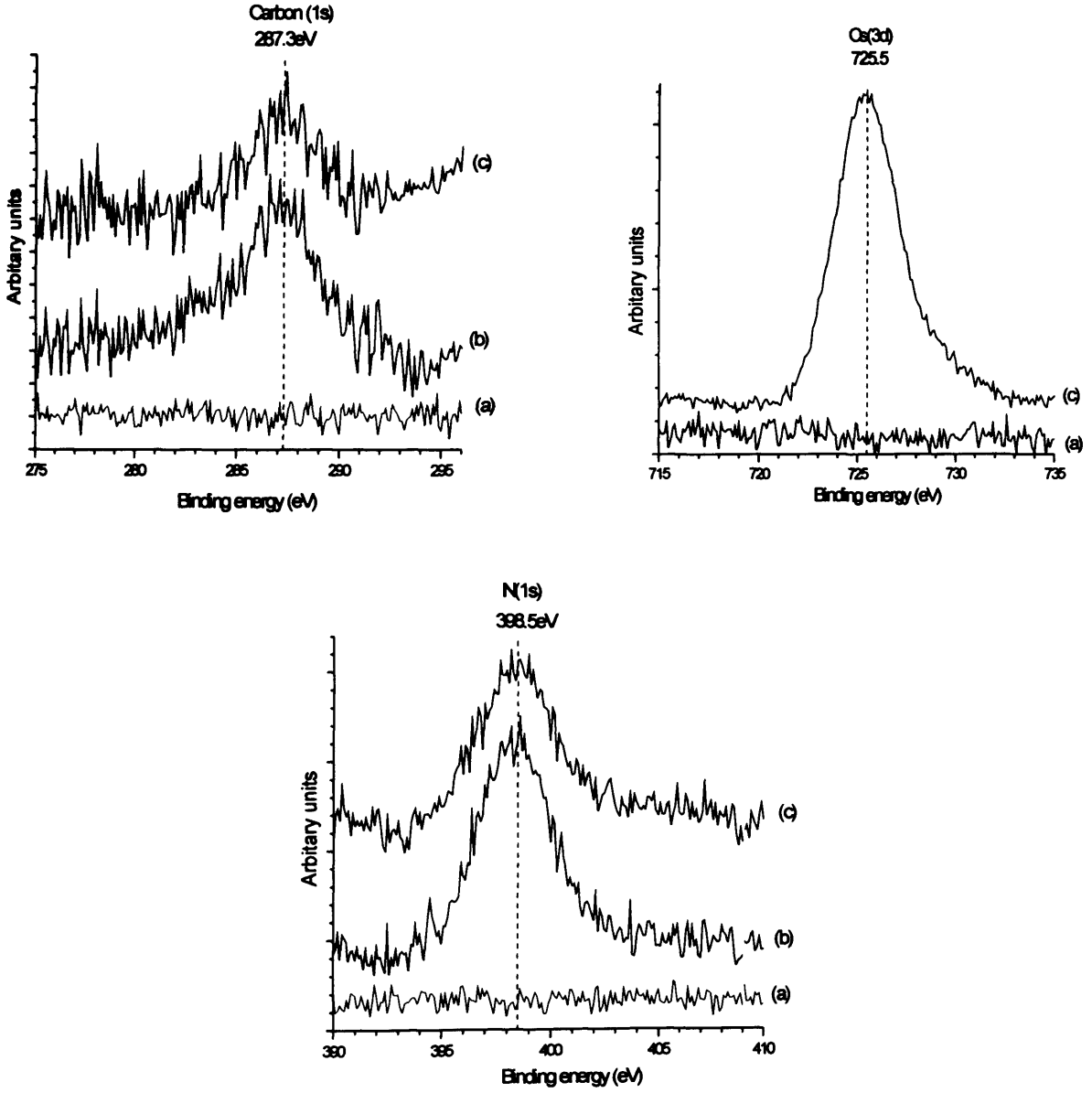

Fig. 7.36 The adsorption of melamine at a Ag(111) surface followed by dosing caesium. XP spectra of C(1s), N(1s) and Cs(3d) regions; (a) Clean surface; (b) 5 min exposure to melamine at 145°C; (c) exposure to caesium at 5A for 1.5 minutes.

7.26 Caesium and melamine coadsorption at an Ag(111) surface at 295K: STM results

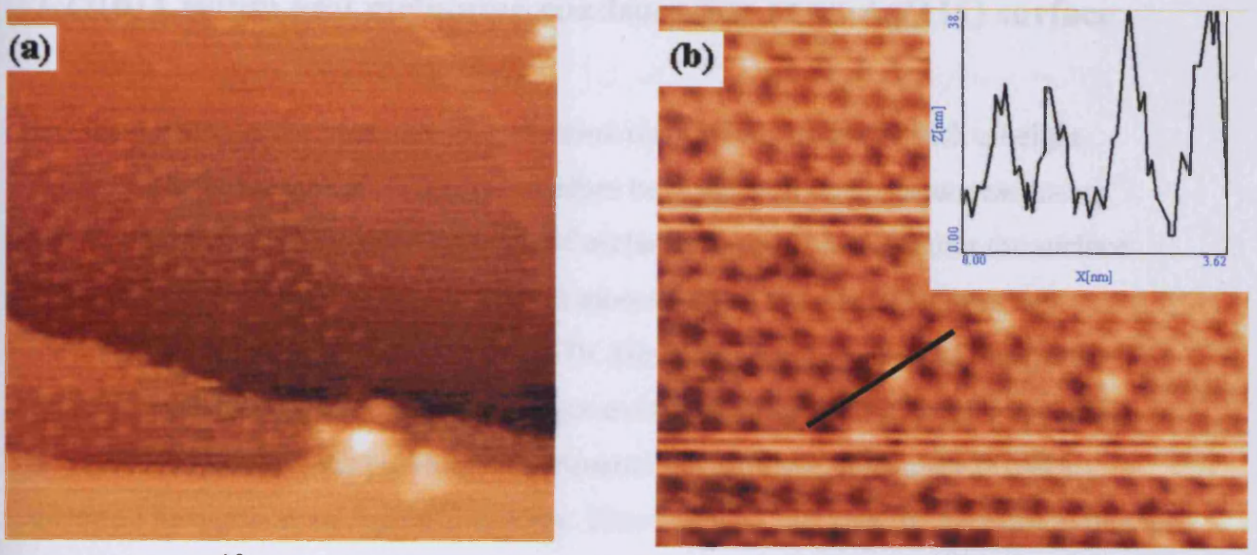

Fig. 7.37 Sequential adsorption of melamine and cesium adsorbed at an Ag(111) surface, (a) two structures at the surface, (b) cesium adsorbed on melamine (with a line profile) [bias: negative, voltage = 1.78V, current = 3.15nA]

STM studies show the presence of melamine and a larger structure on top of melamine. The size of this second structure is 1.4 nm in diameter and has a height of approximately 1 angstrom. The height difference compared to melamine was 0.5 angstroms.

7. 27 Discussion

7.27(a) Caesium adsorption at an Ag(111) surface

One distinct structure has been found at the Ag(111)-Cs interface at 295K. Increasing the concentration to beyond a monolayer resulted in multilayer decoration at the step edges. Bond lengths of different concentration were unable to be measured due to difficulty in STM imaging at different concentrations. Previous work by G. M. Lamble *et al* [40] found that as the concentration of cesium increased on an Ag(111)

surface, the bond length decreased by 0.3Å. This was attributed to a change from a largely ionic state towards a more covalent status in the Cs over layer. .

7.27(b) Cesium and melamine coadsorption at an Ag(111) surface

Dosing cesium in the presence of melamine resulted in structures with a height difference of 0.5 angstroms. It can therefore be suggested that caesium atoms are sitting on the supramolecular network of melamine molecules. Heating the surface resulted in the removal of these caesium atoms and all that remained was the melamine network as shown in figure 37b. However, the distortion as seen in the previous melamine experiments no longer exists. Melamine now forms a regular honeycomb network. As previous experiments have shown, melamine forms a distorted hexagon at an Ag(111) surface. Therefore the fact that the network is regular could be attributed to cesium being present at the surface. It has been seen previously that caesium takes the on top site at a (111) surface. The melamine molecules may have shifted on order to accommodate the caesium atoms.

7. 28 Conclusion

Melamine adsorption at a Cu(110) surface resulted in molecular adsorption. The STM imaged features that showed order in the <110> direction. It can therefore be concluded that substrate-adsorbate interactions were stronger than molecular interactions. This is supported by the more ordered second layer structure. The hexagonal structure formed due to intermolecular interactions between melamine molecules. The fact that it is at least a second layer structure would result in a weaker interaction with the substrate. These islands were not stable above 400K.

Adsorption at an oxidised surface did result in a reaction and the formation of an amide at the surface. The structure at the surface also changed. Predominantly, melamine adsorbed in the <100> direction as opposed to the <110> direction. It can be concluded that reaction with preadsorbed oxygen resulted in an amide adsorbing in its place.

Adsorption of melamine and malonyl dichloride at a Cu(110) surface resulted in a reaction occurring leading to Cl adsorption but no effect on melamine. The binding energies do suggest that melamine is adsorbed molecularly at the surface but chlorine was also present. The STM revealed rows aligned in the <001> direction. This was similar to chlorine at a Cu(110) surface. The effect of heat created an ordered ad layer. XPS shows some chlorine present but this is not imaged by the STM. The ordered structure was possibly formed from melamine molecules tilting at the surface. This lead to an increase in order due to π-π interactions. Intermolecular forces, probably caused by hydrogen bonding, resulted in a lateral interaction.

A decrease in adsorbate-substrate interactions would allow the structure formed to be dominated by intermolecular forces. Adsorbed melamine at Ag(111) surfaces is not imaged probably because it is mobile. Higher concentrations or terraces with restricted mobility resulted in imaging the structure. The substrate had some effect on the structure as a distorted hexagon was formed. Increasing the concentration to more than a monolayer resulted in a less distorted hexagonal structure. The model proposed portrayed how steric factors caused various melamine molecules to be perpendicular to the others. This promoted layer growth.

A co-adsorption of melamine and malonyl dichloride at an Ag(111) surface produced a surface with melamine molecularly adsorbed and also chlorine present. Again it was seen that chlorine and melamine interacting. However, the STM was able to image both chlorine and melamine. Various islands were found consisting of a ($\sqrt{3}$ x $\sqrt{3}$)-R30° pattern. This agrees with previous studies of low concentrations of chlorine. Another structure formed was a distorted hexagon structure formed by melamine surrounding a chlorine atom. Again this chlorine takes a ($\sqrt{3}$ x $\sqrt{3}$)-R30° pattern. The STM suggests that the interaction between melamine molecules may be stronger due to the inability to image single melamine molecules.

Pre-adsorbed melamine was exposed to cesium. Cesium atoms adsorbed on the supramolecular network created by melamine. There was no change in the binding energy of C(1s) and N (1s) spectrum. Cesium had a binding energy 0.3eV lower than that at a clean Ag(111) surface. The stability of cesium was not as great as that of the

network created by melamine molecules as the effect of heat at the surface resulted in the removal of the cesium atoms or diffusion of caesium through to the substrate.

7.29 References

[1] W. D. Huntsman, N. L. Madison and S. I. Schlesinger, *J. Catal.* 2 (1963) 249.

[2] R. M. Lambert & M. E. Bridge, *The Chemical physics of solid surfaces and heterogeneous catalysis,* 3B, 1984.

[3] D. Lackey, M. Surman, & D. A. King, *Vac.* 33 (1983) 867.

[4] B. Asfin, P. R. Davies, A. Pashusky, M. W. Roberts and D. Vincent, *Surf. Sci,* 284 (1993) 109.

[5] Q. Chen, S. Haq, B. G. Frederick, N. V. Richardson, R. E. Palmer, J. Schmidt, D. M. Bird, *International Conference on Vibrations at surfaces n° 8,* 368 (1996) 310-317.

[6] P. R. Davies, D. Edwards, and D. Richards, *J. Phys. Chem. B.* 108 (48), (2004) 18630 -18639.

[7] A. F. Carley, P. R. Davies, D. Edwards, R. V. Jones and M. Parsons, *Chem. & Material Sci.* 36 (2005) 1-4.

[8] G. A. Jeffrey, "An introduction to Hydrogen bonding", Oxford University Press, 1997.

[9] J.K. Gimzewski , M.T. Cuberes, R.R. Schlittler, *Nature,* 49 (1996) 101-114.

[10] J. A. Theobald, M. A. Phillips, N. R. Champness, P. H. Beton, *Nature,* 424 (2003) 2038.

[11] J. Veciana, J. C., C. Ravira, E. Malins and J-J- Novoa, *J. Phys. Chem.* 6 (1996) 1967-1986.

[12] G. M. Whitesides, J. P. Mathias, & C. T Seto, *Sci.* 254 (1991) 1312–1319.

[13] S. I. Stupp, V. LeBonheur, K. Walker, K. E. Huggins, M. Keser, & A. Amstutz, *Chem. Int. Ed. Engl*, 276 (1997) 384–389.

[14] S. Hetch, *J. Phys. Chem. B* 42 (2003) 24-26.

[15] Takashi Yokoyama, S. Y., Toshiya Kamikado, Yoshishige Okuno & Shinro Mashiko, *J. Phys. Chem. B.* 413 (2001) 619-621.

[16] L. M. A. Perdiago, N. R. Champness & P.H. Beton, *Chem. Commun.* (2006) 538-540.

[17] J. C. Swarbrick, B. L. Rogers, N. R. Champness, and P. H. Beton, *J. Phys. Chem. B.* 110, (2006) 6110-6114.

[18] B. Afsin, P. R. Davies, A. Pashusky, M. W. Roberts and D. Vincent, *Surf. Sci.* 284 (1993) 109.

[19] A.F. Carley, P.R. Davies and M.W. Roberts, *Chem. Commun.* (1998) 1793.

[20] A. F. Carley, P.R. Davies, M. W. Roberts, *Catal. Lett.* (2002) 80.

[21] A. F. Carley, M. Coughlin, P.R. Davies, D. J. Morgan, M. W. Roberts, *Surf. Sci.* 555 (2004) L138.

[22] B. L. Rogers, J. G. Shapter, M. Ford *Surf. Sci.* 548 (2004) 29.

[23] P.R Davies, J. M. Keel, *Phys. Chem. Chem. Phys.* 1 (1999) 1383.

[24] C. J. Hirschmugl, K. M. Schindler, O. Schaff, V. Fernandez, A. Theobald, P. Hofmann, A. M. Bradshaw, R. Davis, N. A. Booth, D. P. Woodruff, V. Fritzsche, *Surf. Sci.* 352 (1996) 232.

[25] R. V. Jones, PhD Thesis, University of Wales, Cardiff, 2001.

[26] P. R. Davies, D. Edwards, and D. Richards, *Surf. Sci.* 573 (2004) 284-290.

[27] B.E. B. Afsin, P. R. Davies, A. Pashusky, M. W. Roberts and D. Vincent, *Surf. Sci.*, 284 (1993) 109.

[28] B.V. Andryushechkin, K.N. Eltsov, V.M. Shevlyuga, V.Yu. Yurov, *Surf. Sci.* 431 (1999) 96–108.

[29] M. Bowker, K.C. Waugh, *Surf. Sci.* 134 (1983) 639.

[30] M. Bowker, K.C. Waugh, *Surf. Sci.* 155 (1985) 1.

[31] M. Bowker, K.C. Waugh, B. Wolfindale, G. Lamble, D.A. King, *Surf. Sci.* 179 (1987) 254.

[32] P. J. Goddard and R. M. Lambert *Surf. Sci.* 67 (1977) 180.

[33] M. Bowker and K. C. Waugh *Surf. Sci.* 99 (1980) 639.

[34] B. V. Andryushechkin, K. N. Elstov, V. M. Shevlyuga and V. Yu Yurov *Surf. Sci.* 407 (1998) L633.

[35] K. Aika, H. Hori, and A. Ozaki, *J. Catal.* 27 (1972) 424.

[36] S. A. Lindgren and L. Walldén, J. Rundgren, P. Westrin, and J. Neve, *Phys. Rev. B.* 28 (1983) 6707–6712.

[37] C. Guo, R.J. Madix, *Surf. Sci.* 550 (2004) 81–92.

[38] C.L. Fu, K.M. Ho, *Phys. Rev. Lett.* 63 (1989) 1617.

[39] Albert F. Carley, Philip R. Davies, K. R. Harikumar, Rhys V. Jones, and M. Wyn Roberts, *J. Phys. Chem. B.* 108 (38) (2004) 14518 -14526.

[40] G. M. Lamble, R. S. Brooks, and D. A. King, *Phys. Rev. Lett.* 61 (1988) 1112–1115.

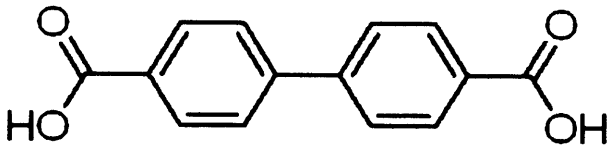

Chapter 8

Interaction of Biphenyl dicarboxylic acid with clean and oxidised Cu(110) and Ag(111) surfaces

8.1 Introduction

The interaction of biphenyl dicarboxylic acid (BPDCA) with clean and oxidised Cu(110) and Ag(111) surfaces has been studied. The investigation focuses on the different structures formed at the two surfaces.

8.2 BPDCA chemisorption at metal surfaces

8.2 (a) Cu(110)

The bonding of carboxylic acids to copper surfaces plays an important role in catalytic processes. For example, the rate determining step in methanol synthesis over $Cu/ZnO/Al_2O_3$ catalysts, is believed to be the hydrogenation of adsorbed formate (HCOO-) species [1]. The adsorption of carboxylic acids on metal surfaces has been studied extensively as they provide model systems for intermediate steps in heterogeneous catalysis.

The adsorption of di-carboxylic acids at metal surfaces provides an opportunity to investigate the competition between surface-adsorbate and adsorbate-adsorbate interactions. Suitably tailored carboxylic acids offer a flexible route to the nano-scale engineering of chemically functionalised surfaces with a wide range of applications requiring specific molecular or nano-particle recognition.

It is known that the adsorption of simple monocarboxylic acids onto the Cu(110) surface leads to the deprotonation of the acid group into the carboxylate functionality. Surface saturation results in the carboxylate plane orientated perpendicular to the Cu surface with the oxygen atoms interacting with adjacent close packed Cu atoms along the <110> direction [2-3].

Studies of formic acids adsorbed on copper surfaces have resulted in interesting results where reconstruction and roughening has occurred [4-5]. Formic acid decomposes at temperatures around 450K via the formate to produce $H_{2(g)}$ and $CO_{2(g)}$ [6].

The adsorption of oxalic acid onto the Cu(110) surface was investigated using reflection absorption infrared spectroscopy (RAIRS) in order to determine orientation at the surface [7]. It was found that the molecule adsorbs as a mono-oxylate species. Increasing the concentration results in change in the molecule's orientation to the upright position. The upright orientation results in a carboxylic group at the vacuum interface and therefore creates a chemically functionalised surface. At lower temperatures (370K), the formation of dimers occurs between oxalic acid molecules.

The molecule trimesic acid (TMA, 1,3,5-benzenetricarboxylic acid, $C6H3(COOH)_3$) has been studied at a less reactive Cu(100) surface [8]. It was found that at low temperatures, TMA adsorbed parallel to the surface. As the temperature was increased, a bonding transition occurred which lead to an upright geometry due to carboxylate formation. Aromatic carboxylic acids adopt a flat-lying geometry on account of the ring surface interactions.

8.2 (b) Ag(111)

Surface-supported systems are promising materials for many applications, e.g., in nanopatterning, surface templating, heterogeneous catalysis, and sensing or molecular recognition. Research on

self assembled monolayers has played an important role in surface science for some time. Redox, optical and electronic properties have been studied using self-assembly [8-11]. There are three kinds of intermolecular interactions that play an important role in self assembly. These are hydrogen bonding, metal-ligand interaction and dipole-dipole interaction. Hydrogen bonding has high selectivity and directionality and is one of the key factors in many biological systems. The hydrogen bond can be used to form surface nanostructures through the self assembly process. When supramolecular organisation occurs at surfaces, self assembled structures will be stabilized by intermolecular and adsorbate-substrate interactions.

Ag(111) is a closer spaced and less reactive surface than Cu(110). It provides small atomic corrugation and low chemical reactivity. At room temperature the carboxylic acid groups will be preserved instead of forming the carboxylate. This is unlike the case for reactions of carboxylic acids at a copper surface [12].

The carboxyl group is known to be the most fundamental hydrogen bonding system [13]. It is known that carboxylic acids adsorb at Ag(111) surfaces to form well packed monolayers [14-15] The bond distances and angles are shown below. These would only be accurate in the gas phase.

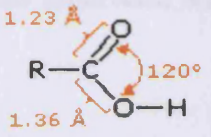

An extensive literature search has found no investigations of the adsorption of BPDCA at Ag(111) surfaces. However, there are similar molecules that have been used in creating a supramolecular structure at an Ag(111) surface. 4-[trans-2-(pyrid-4-yl-vinyl)]benzoic acid (PVBA) and 4-[(pyrid-4-yl-ethynyl)]benzoic acid (PEBA) adsorption at an Ag(111) surface have been studied using STM [16]. As both species were rigid it was found that the carboxylic group and the pyridyl moiety formed head to tail hydrogen bonds. The molecules adsorbed in a flat geometry and the balance of intermolecular and adsorbate-substrate interactions allowed arrangements with long range order. The subtle differences in molecular shape results in drastic changes in the 2 dimensional network created by hydrogen bonding. A change in stereo chemistry can change the balance between molecule substrate and lateral intermolecular interactions.

1,4-benzene-dicarboxylic acid C_6H_4-$(COOH)_2$ has been studied by STM at an Au(111) surface [17]. It was found that two dimensional supramolecular structures evolved through hydrogen bonding. The supramolecular ordering extended over several substrate reconstruction domains. It was able to do this due to the fact of the versatility of hydrogen bridges in molecular engineering at surfaces.

The adsorption of acridine-9-carboxylic acid at an Ag(111) surface resulted in different structures present at the surface [18]. These structures changed with terrace size. XPS was used to quantify and analyse the surface. It was found that like other fused ring systems, ACA adsorbed on the Ag(111) surface via π-surface interactions. At large terraces, ACA molecules nucleate from the step edge to form two-dimensional structures spanning the terrace width. On narrow terraces, molecules form a distinct dimer phase which results in a lower density of the molecules present.

8.3 Experimental

The instrument used in this investigation has been discussed previously. The radiation used for the XP data acquisition was the Al(kα) line with a photon energy of 1486.6eV. All XP data was recorded at a pass energy of 50eV unless otherwise stated. All spectra were referenced to the clean $Cu(2p_{3/2})$ peak at 932.7eV.

1g of BPDCA (>99% Aldrich) was placed into a k-cell that was attached to the chamber. Oxygen (99.99%) obtained from Argo International was attached to the gas line. It was exposed via a leak valve into the chamber; the purity of the reagents was checked using mass spectrometry.

8.4 BPDCA adsorption at clean Cu(110) at 295K: XPS results

A clean Cu(110) surface was exposed to a dose of BPDCA for 120 seconds at a cell temperature of 290°C. This resulted in the formation of peaks in the C(1s) and O(1s) regions at a B.E. of 283.4eV and 530.2eV respectively. The calculated concentrations were $\sigma_C = 1.89 \times 10^{15}$ atoms per cm^2 and $\sigma_O = 5.26 \times 10^{14}$ atoms per cm^2. Continued, sequential exposures served to increase the carbon and oxygen intensities. Concentrations above a monolayer resulted in a second peak in the O(1s) region with a binding energy of 533eV. The concentrations are given in table X.1.

Exposure (seconds at 290°C)	Total C(1s) concentration ($x10^{15}$ atoms cm^{-2})	Total O(1s) concentration (atoms cm^{-2})	Ratio (C:O)
120	1.89	$5.26 x10^{14}$	3.6:1
240	1.24	$4.10 x10^{14}$	3:1
540	3.63	$1.20 x10^{15}$	3:1
740	4.7	$1.47 x10^{15}$	3:1

Table 8.1: Concentrations of carbon and oxygen.

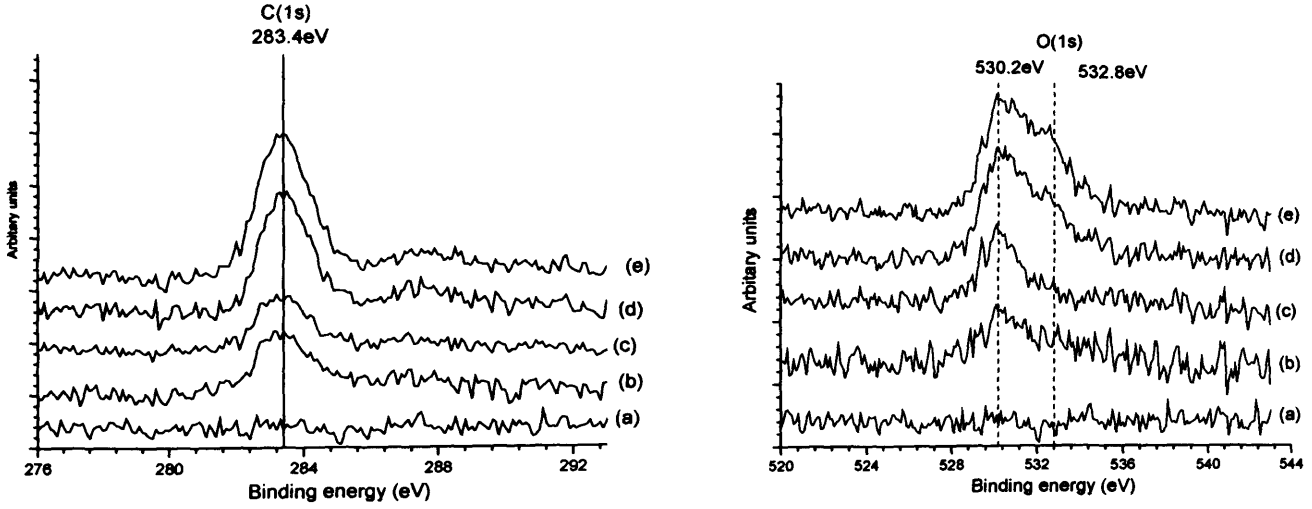

Fig. 8.1: BPDCA at a Cu(110) surface, (i) C(1s) region, (ii) O(1s) region, (a) Clean, (b) 120 second exposure at 290°C, (c) 240 second exposure at 290°C, (d) 540 second exposure at 290°C, (e) 740 second exposure at 290°C.

The maximum carbon surface concentration obtained was $4.7 x10^{15}$ atoms cm^{-2}. The concentration of the corresponding O(1s) peak was calculated to be $1.47 x10^{15}$ atoms cm^{-2}. The O(1s) spectra shown in figure 1 clearly show the presence of two oxygen species.

Annealing the surface to 450K (Fig. 2) resulted in a loss of both carbon and oxygen. The second oxygen species at 532.8eV has now also been removed. The remaining concentrations were calculated as $\sigma_C = 1.78 \times 10^{15}$ and $\sigma_O = 4.86 \times 10^{14}$ atoms cm^{-2} which gives a ratio of 3.6:1 respectively. It is speculated that the second oxygen species is due to there being more than a monolayer present at the surface. Further annealing to 550K resulted in the total loss of oxygen from the surface. The carbon was seen to remain with some evidence for an increase in intensity at a B.E. of 285eV. This suggests the presence of carbonaceous species at the surface.

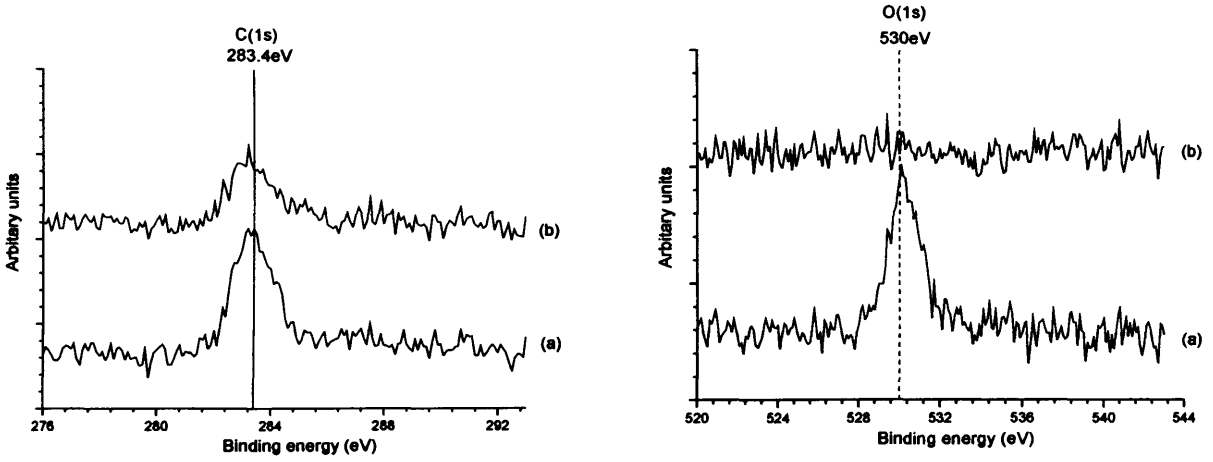

Fig. 8.2: BPDCA at a Cu(110) surface, (i) C(1s) region, (ii) O(1s) region, (a) heated to 450K, (b) Heated to 550K,

8.5 BPDCA adsorption at a partially oxidised Cu(110) surface at 295K: XPS results

A clean Cu(110) surface was exposed to 4L of oxygen. This resulted in a surface concentration of oxygen of 2.13×10^{14} atoms cm^{-2}. Exposure to 180 seconds of BPDCA resulted in peaks developing at a B.E. of 284eV and 531eV. The chemisorbed oxygen peak appears to remain the same. The carbon and oxygen concentrations were $\sigma_C = 8.43 \times 10^{14}$ and $\sigma_O = 2.29 \times 10^{14}$ atoms cm^{-2} respectively. Annealing the surface to 450K resulted in a drop in both carbon and oxygen concentrations to 3.75×10^{14} and 2.01×10^{14} atoms cm^{-2} respectively.

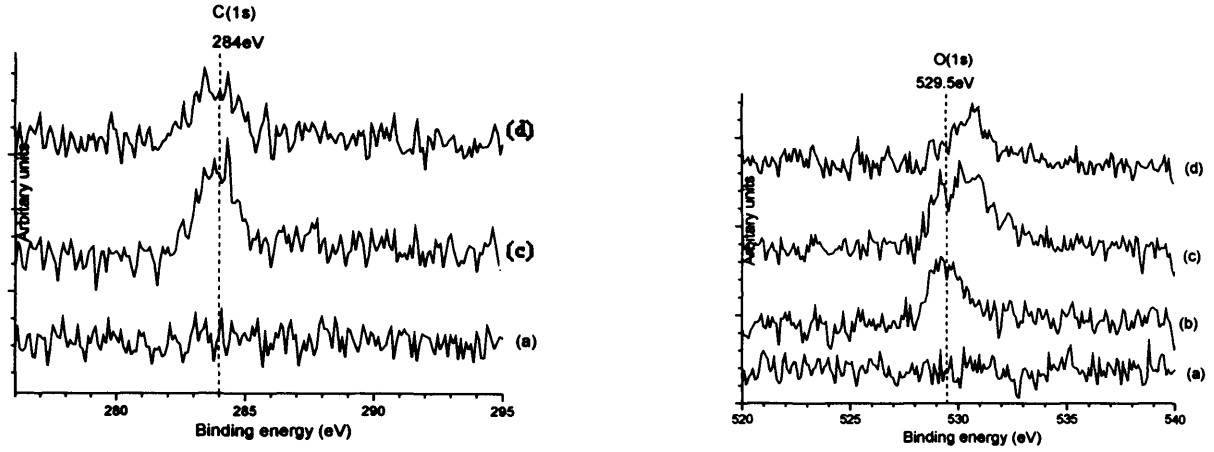

Fig. 8.3: BPDCA at a partially oxidised Cu(110) surface, (i) C(1s) region, (ii) O(1s) region, (a) Clean, (b) 4L of oxygen, (c) 180 second exposure at 290°C, (d) heated to 400K.

The carbon 1(s) spectra show a peak at 284eV. This is a slightly higher binding energy than BPDCA at a clean Cu(110) surface. Preadsorbed oxygen does have some effect of the adsorption of BPDCA. Upon addition of BPDCA the O(1s) spectra show an additional peak at 530.3eV. This is in agreement with the binding energy of oxygen in BPDCA at the clean Cu(110) surface.

Heating the sample to 400K results in a decrease in both the carbon and oxygen concentrations. The fact that only the oxygen species with the lower binding energy remains suggests that a reaction did occur with the pre adsorbed oxygen and this resulted in the carboxyl species present at the surface with a similar binding energy to that of chemisorbed oxygen. The surface composition of carbon and oxygen is now 2:1. The loss of chemisorbed oxygen can be attributed to a reaction involving the hydrogen of the acid moiety with the preadsorbed oxygen to produce water. This would subsequently be desorbed.

$$\text{At room temperature - } RCO_2H_{(a)} + O_{(a)} \rightarrow \text{No reaction} \qquad (1)$$

$$\text{At 400K } 2RCO_2H_{(a)} + O_{(a)} \rightarrow H_2O + 2RCO_2^-{}_{(a)} \qquad (2)$$

8.6 BPDCA adsorption at a fully oxidised Cu(110) surface at 295K: XPS results

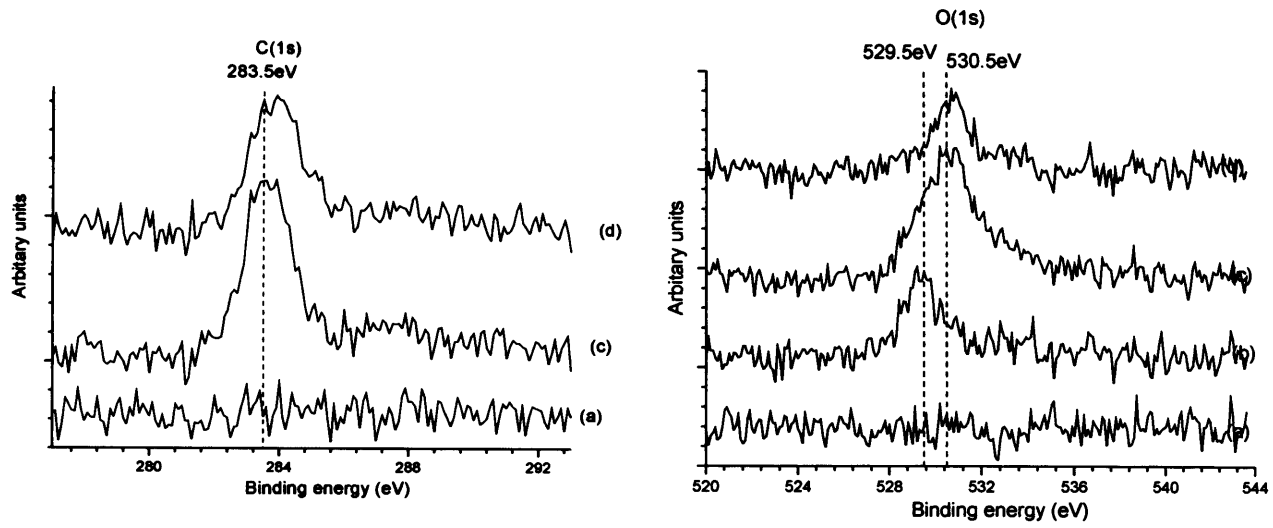

Fig. 8.4: BPDCA at a partially oxidised Cu(110) surface, (i) C(1s) region, (ii) O(1s) region, (a) Clean, (b) 40L of oxygen, (c) 180 second exposure to BPDCA at 290°C, (d) heated to 400K.

A clean Cu(110) surface was exposed 40L of oxygen. This resulted in a chemisorbed oxygen concentration of 4.0×10^{14} atoms cm^{-2}. The binding energy was 529.5eV. Exposure to 180 second of BPDCA resulted in a carbon peak developing at 283eV. The concentration was $\sigma_C = 2.15 \times 10^{15}$ atoms cm^{-2}. The oxygen peak has shifted to 530.2eV and the concentration was $\sigma_O = 8.88 \times 10^{14}$ atoms cm^{-2}. The broadness of the peak suggests that there are two species present. Subtracting the initial chemisorbed oxygen results in an oxygen concentration of 4.88×10^{14} atoms cm^{-2}. This gives a ratio of 4.4 : 1 carbon : oxygen respectively. Although not in agreement with the composition of the molecule, the ratio is much closer than that at a partially oxidised surface.

Warming the sample to 450K resulted in a loss of the chemisorbed oxygen. The carbon (C1s) concentration has decreased slightly. The binding energy has remained the same. The concentrations were $\sigma_C = 1.61 \times 10^{15}$ atoms cm^{-2} and $\sigma_O = 4.20 \times 10^{14}$ atoms cm^{-2}. This results in a ratio of 3.8:1 C:O. This ratio agrees with the composition of the molecule. It is therefore suggested that the unreacted BPDCA molecules physisorbed to the oxidised surface. Heating removed the chemisorbed oxygen and all remained was BPDCA chemisorbed to the Cu(110) surface.

8.7 Discussion

The adsorption of BPDCA on a Cu(110) crystal gave rise to two distinct oxygen species. The first signal at 530.2 is characteristic of a carboxylate species. The second peak, at 532.8eV appears as adsorption goes above a monolayer. The second oxygen species can be attributed to an unbound carbonyl group binding energy. Previous carboxylate structures on Cu(110) are given in the table below.

Adsorbed structure	C(1s) energy (eV)	O(1s) energy (eV)	Reference
Formate $HCOO_{(a)}$	288.1	531.1	[19]
Acetate $CH_3COO_{(a)}$	284.46 287.51	530.83	[20]
Glycine $NH_2CH_2COO_{(a)}$	286.23 288.25	531.57	[21]
Acrylate $H_2C{=}CHCOO_{(a)}$	285.0 287.9	531.5	[22]
Chemisorbed oxygen	N/A	529.7	[23]

Table 8.2: Binding energies of previous carboxylate structures at a Cu(110) surface

An initial dose of BPDCA resulted in a broad C(1s) peak. These peaks can be attributed to the numerous carbons present in the molecule. Increasing the dose resulted in a loss of concentration. This is due to more than a monolayer of BPDCA being present. It is suggested that the second layer decreases in concentration as more is dosed due to the weaker interaction at the surface. More BPDCA molecules hitting the surface results in the removal of the second layer BPDCA molecules. Further doses resulted in an increase in intensity with the FWHM remaining the same.

The initial dose resulted in a ratio (3.6:1 C:O) consistent with the molecule BPDCA. However, further doses resulted in a ratio of 3:1 carbon: oxygen. The B.E. suggests carboxylate formation but discriminating between CO_2H and CO_2 + H is not definitive. However the fact that O(a) is not

affected suggests no dissociation. Carboxylate formation is a typical finding at a Cu surface. This is observed in the adsorption of benzoic acid at a Cu(110) surface [24].

The ratios suggest that heating the surface resulted in desorption of BPDCA. The concentrations of carbon and oxygen remaining can be accounted as a monolayer coverage. Therefore the initial heating removed the other layers present. In view of the chemical reactivity of the substrate and the elevated temperature, it is expected that deprotonation of the carboxylic acids occur. This is analgous to findings for other carboxylic acids on Cu surfaces under comparable conditions [25-27]. Futher heating resulted in a complete desorption of all oxygen. Some carbon remained. Decarbonylation to yield CO_2 is a well established decomposition pathway [28-29]. The loss of oxygen and most carbon can therefore be attributed to this.

XP spectra suggests that the adsorption of BPDCA on a partially oxidised surface resulted in no reaction. Curve fitting shows that the initial chemisorbed oxygen concentration remained the same. Comparison of the binding energies of C(1s) and O(1s) with the previous experiment at a clean Cu(110) surface also suggest that no reaction has occurred as the binding energies have remained the same. Heating the surface results in the removal of almost all the chemisorbed oxygen with some BPDCA being removed. The concentrations suggest that molecular desorption occurred.

Adsorption of BPDCA at a fully oxidised surface resulted in no removal of chemisorbed oxygen. It is therefore suggested that BPDCA is physisorbing to the chemisorbed oxygen layer. Heating the surface results in desorption of the chemisorbed oxygen probably as water. The equations below show some possibilities of the desorption reaction.

$$RCO_2H_{(a)} + O_{(a)} \rightarrow H_2O + 2RCO_2^-{}_{(a)} \qquad (3)$$

$$RCO_{2(a)} \rightarrow R_{(a)} + CO_{2(g)} \qquad (4)$$

The remaining carbon and oxygen at a composition of 3.8:1 suggest that molecular desorption has occurred. The binding energies also agree with this as both the C(1s) and O(1s) agree with BPDCA adsorption at a clean Cu(110) surface.

8.8 BPDCA adsorption at a clean Cu(110) surface at 295K: STM results

Exposure to a 120 second dose of BPDCA resulted in the observation of structures of 1nm in length and a height of 1.4 Angstroms.

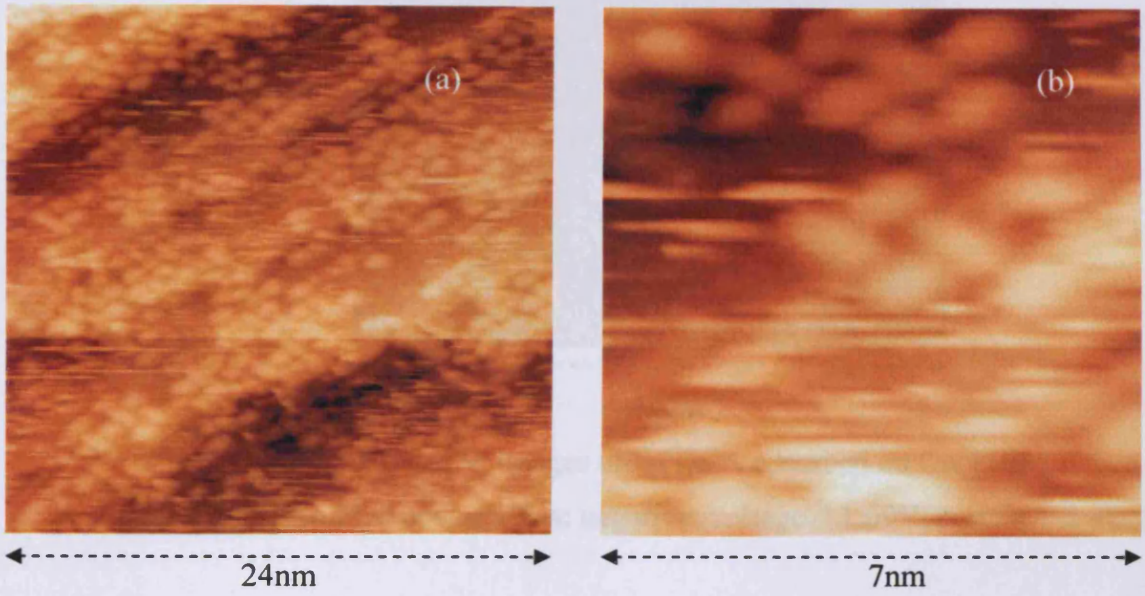

Fig. 8.5: STM images of BPDCA adsorbed on Cu(110)
(a) After 120second exposure, (b) enlargement of a section from (a) [bias: negative, voltage = 1.03V, current = 2.21nA]

The images obtained in fig.5 show that no long range ordering at the surface has occurred. The features agree with the size of the molecule BPDCA. The molecules show some order in the <110> direction. A closer inspection shows that some of the molecules form small areas of order. Figure 5(b) shows a structure obviously influenced by the Cu(110) surface, but intermolecular forces are also playing a factor. An increase in dose to 240 seconds results in a similar image as shown above. However as fig.6 shows, there are now more molecules present.

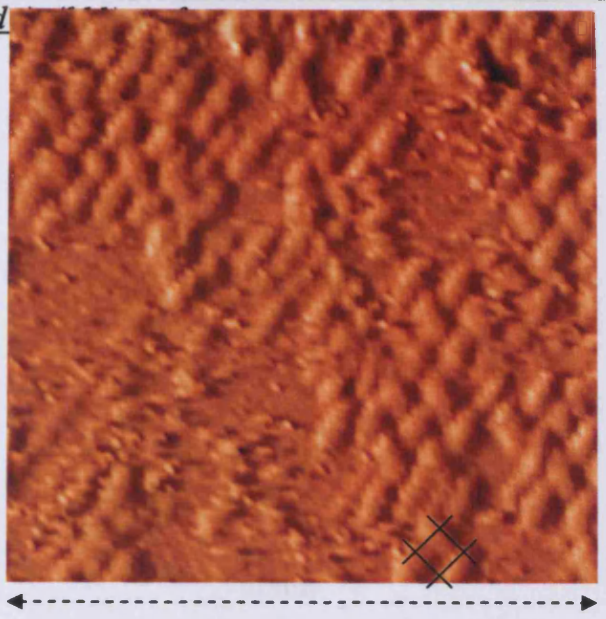

Fig. 8.6: STM images of BPDCA adsorbed on Cu(110)
after 240 second exposure [bias: negative, voltage = 1.09V, current = 2.32nA].

The structures shown are the same size as previously shown in figure 5. Again, some of the molecules form a square structure.

Further dosage results in more molecules present. The following images were taken after a dose of 300 seconds of BPDCA.

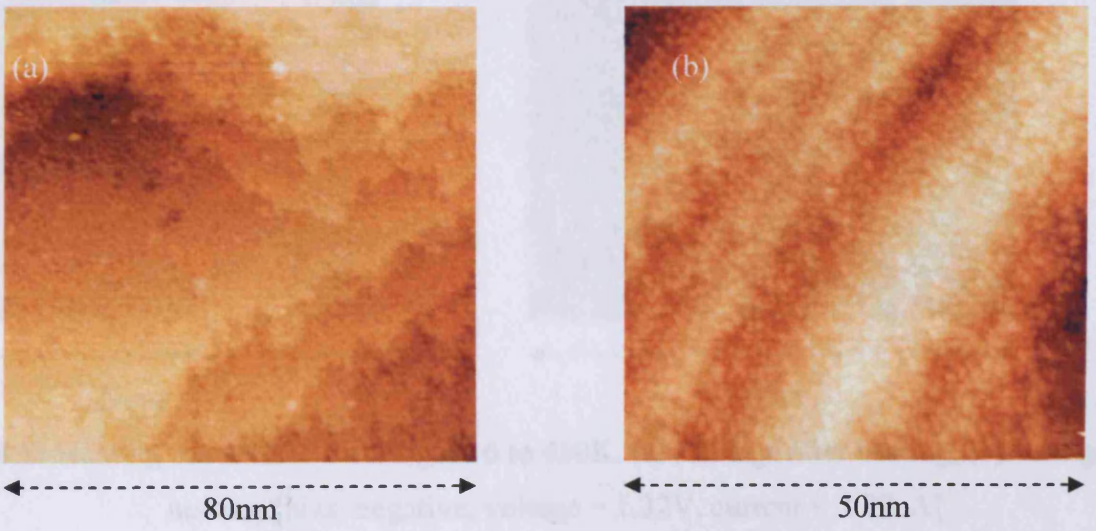

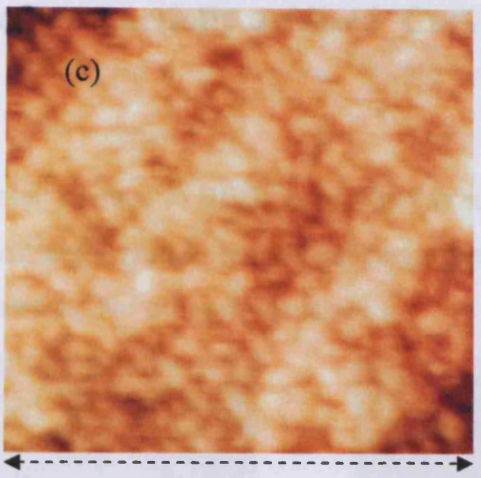

Fig. 8.7: STM images of BPDCA adsorbed on Cu(110)
(a) After 300 second exposure, (b) enlargement of a section from (a), enlargement of a section from (b) [bias: negative, voltage = 1.23V, current = 3.33nA].

Increasing the dosage has increased the surface concentration of the BPDCA structures. Some of the structures are randomly arranged while others form an ordered square structure. The pseudo square contains four molecules, 2 orientated in <100> direction and 2 in the <110> direction.

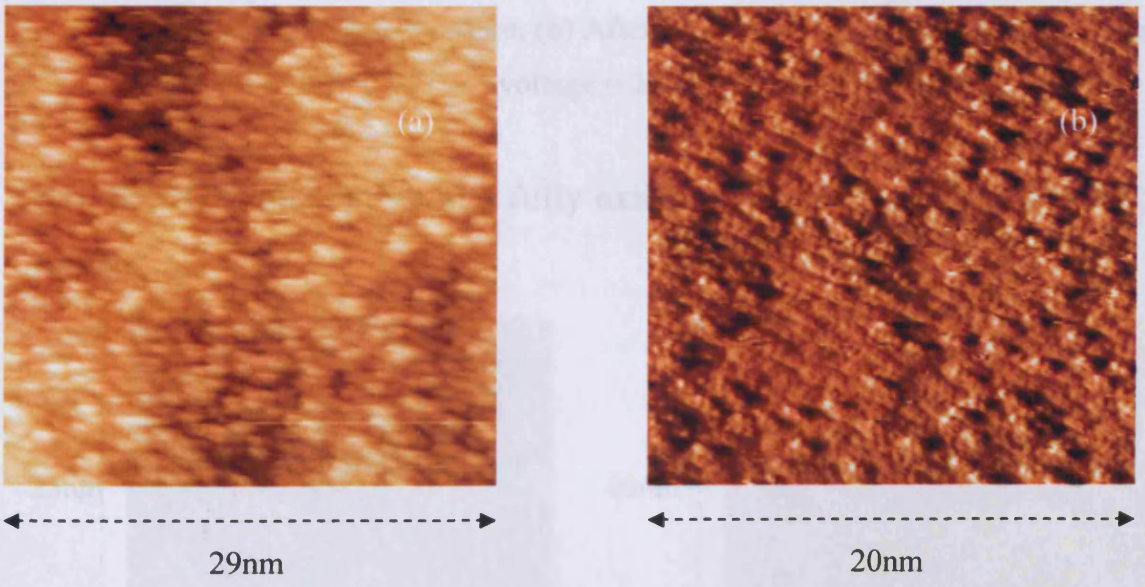

Fig. 8.8: Heating the surface from figure 6 to 450K. (a) Z image after heating, (b) I image after heating [bias: negative, voltage = 1.32V, current = 2.89nA].

Heating the surface removes all ordered structures. The most predominant order is now in the <001> direction. The length of the molecules are still approximately 1nm in length.

8.9 BPDCA adsorption at a partially oxidised Cu(110) surface at 295K: STM results

Exposure of the oxygen treated surface to BPDCA resulted in no reconstruction. The larger structures shown are approximately 1nm in length and reside predominantly on the step edges and around the oxygen p(2x1) islands. No other order is seen.

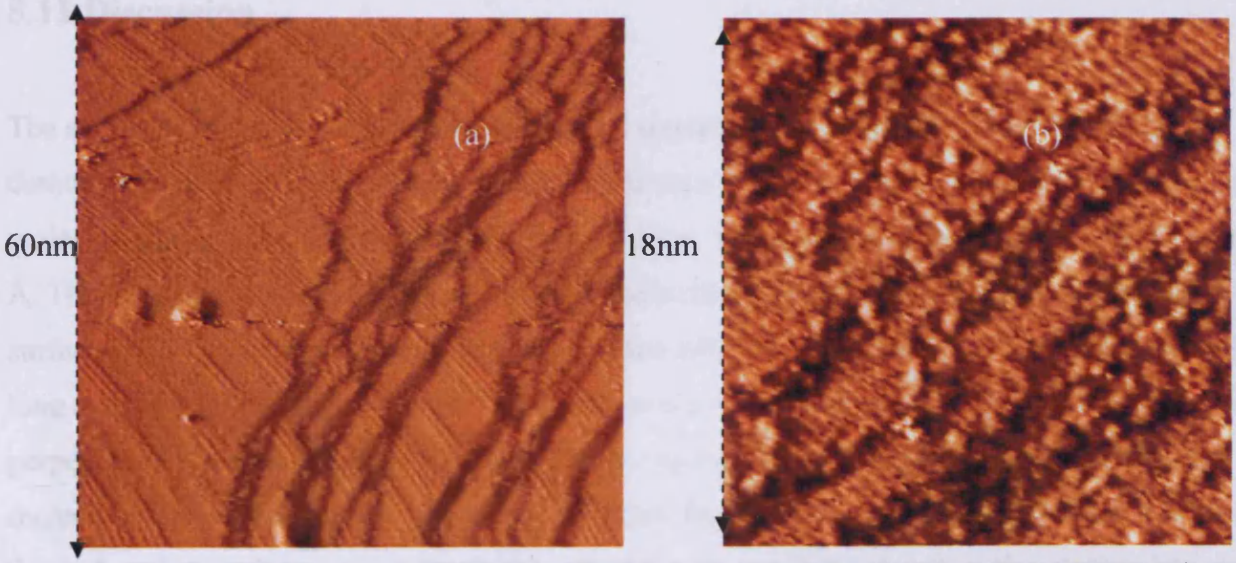

Fig. 9: STM images of BPDCA adsorbed on a partially oxidised Cu(110) crystal (a) After 4L oxygen exposure, (b) After 180 second exposure of BPDCA [bias: negative, voltage = 1.00V, current = 2.99nA].

8.10 BPDCA adsorption at a fully oxidised Cu(110) surface at 295K: STM results

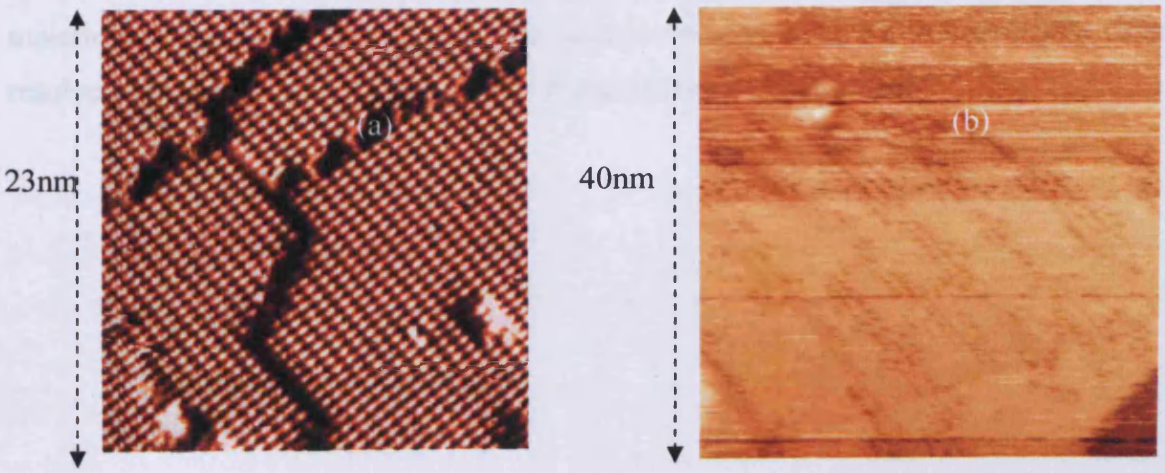

Fig. 8.10: STM images of BPDCA adsorbed on a partially oxidised Cu(110) crystal (b) After 40L oxygen exposure, (b) After 180 second exposure of BPDCA

Exposure to 40L of oxygen resulted in a monolayer of p(2x1) oxygen present at the Cu(110) surface as shown in figure 10a. Dosing BPDCA resulted in images of poor quality. This is probably caused by the mobility of BPDCA molecules at the surface due to there being more than one layer present.

8.11 Discussion

The sequence of images showing the increased concentration of BPDCA at the Cu(110) demonstrate the degree of ordering at the surface as a function of increasing concentration. Each molecule shown has a length of approximately 1nm. The apparent height of the molecule was 1.4 Å. This is a typical value for planar aromatic molecules with a π-system orientated parallel to the surface [30-31]. These measurements suggest that BPDCA adsorb in a flat lying geometry. The long axis of BPDCA align in either the <100> or the <110> directions. Adjacent molecules are perpendicular to each other surprisingly with the end group pointing to the centre of the next molecule. The suprising observation suggests that the intermolecular interactions occur between the carboxylate end group and the C-H bond of the phenyl ring rather than the carboxylate group. This supprising result is probably due to the domination of substrate-molecule interactions over molecule-molecule interactions.

This agrees with the size of the molecule using calculated bond lengths. A more ordered structure is observed on larger terraces. This order occurs due to hydrogen bonding and π interactions. The lateral intermolecular coupling is mediated by the unusual hydrogen bonding between carboxylate moieties and aromatic rings. As substrate atomic structure and adsorbed molecules could not be resolved simultaneously, the adsorption site could not be determined.

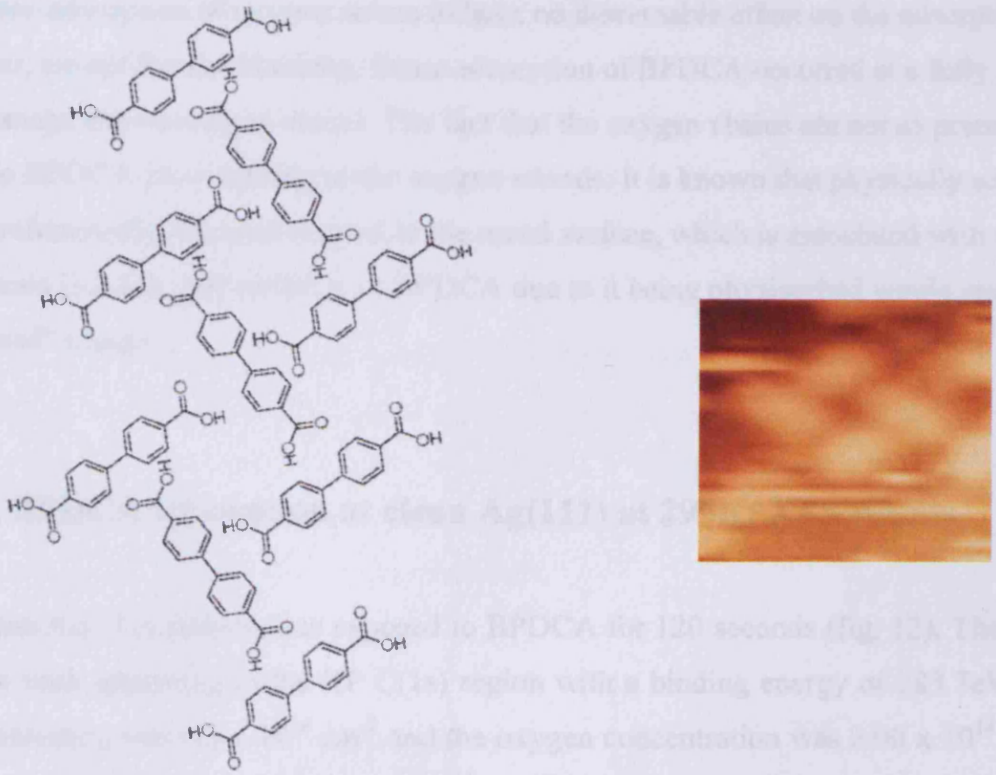

Fig. 8.11: A model of proposed structure at a clean Cu(110) surface.

Increasing the concentration does not result an increase in the height measured for the molecule. This is unlike the results of Frederick et al [32] who observed benzoic acid initially adsorb in flat lying configuration on Cu(110) and then converts to the upright position as it gets closer to the saturation point. This produces a reduced bonding area which allows more molecules to adsorb. The difference here is that BPDCA has two phenyl rings and two CO_2 groups holding it flat.

Heating the surface to 450K resulted in a loss of the order resulting from H-bonding and π interactions. BPDCA is now adsorbed in the <100> direction. The surface has reduced long range order. All that remains is local order in the <100> direction.

For the partially oxidised system, ($\sigma_O = 2.13 \times 10^{14}$ atoms cm^{-2}), the STM reveals the co-existence of both chemisorbed oxygen and BPDCA on the surface. The oxygen displays a p(2x1)-O adlayer and therefore appears unaffected by BPDCA adsorption. BPDCA adsorption occurs mainly on the

step edges and around the oxygen p(2x1) islands. Adsorption of BPDCA occurred as for a clean surface but in lower concentration.

The pre-adsorption of oxygen seems to have no discernable effect on the adsorption of BPDCA on copper, except for site blocking. Some adsorption of BPDCA occurred at a fully oxidised surface. The image shows oxygen chains. The fact that the oxygen chains are not as pronounced may be due to BPDCA physisorbing to the oxygen islands. It is known that physically adsorbed π-systems are preferentially oriented parallel to the metal surface, which is associated with π-bonding to the substrate [33-34]. The mobility of BPDCA due to it being physisorbed would result in the "blurred" image.

8.12 BPDCA adsorption at clean Ag(111) at 295K: XPS results

A clean Ag(111) surface was exposed to BPDCA for 120 seconds (fig. 12). The exposure led to a single peak appearing in the XP C(1s) region with a binding energy of 283.7eV. The carbon (1s) concentration was 6.5 x 10^{14} cm^{-2} and the oxygen concentration was 2.00 x 10^{14} cm^{-2}. This gives a ratio of 3.25:1 C:O suggesting that it is molecularly adsorbing at the Ag(111) surface. Both the binding energies of the carbon and oxygen are similar to studies at a Cu(110) surface. Increasing the exposure results in an increase in both carbon and oxygen (carbon concentration = 2.12 x 10^{15} cm^{-2}, oxygen concentration = 7.6 x 10^{14} cm^{-2}). The ratios remain the same. Heating the surface resulted in molecular loss of BPDCA (spectra not shown) leaving a clean surface.

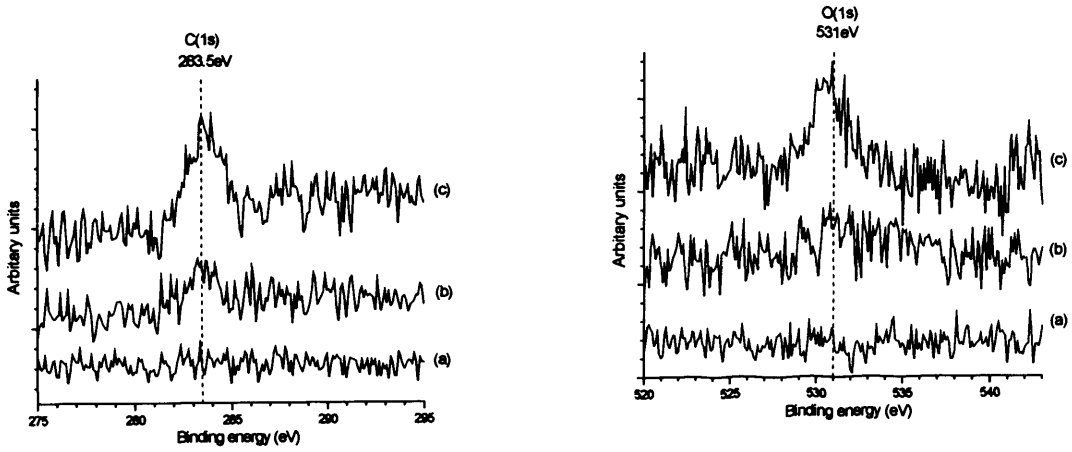

Fig. 8.12: BPDCA adsorption at a clean Ag(111) surface; (a) clean surface, (b) 120 second dose of BPDCA, (c) 240second dose of BPDCA

The $Ag3d_{5/2}$ core level (not presented here) is located at 368.4eV. This remains the same before and after the doses of BPDCA. This close agreement with the reported value for clean Ag excludes the possibility of metal-ligand formation [35]. However it is unlikely that a change would be seen as such a small percentage of Ag would have been affected.

8.13 STM of lower concentration adsorption.

At low concentrations, BPDCA adsorbs at the step edges. The molecule is approximately 10Å in length and has a width of 5Å. This is a good correlation with the calculated size of the molecule. The distance between the molecules is 0.6nm. the ordering at the terrace is probably dominated by the silver lattice as such low concentrations would require interactions with the substrate otherwise the molecule would be mobile at the surface.

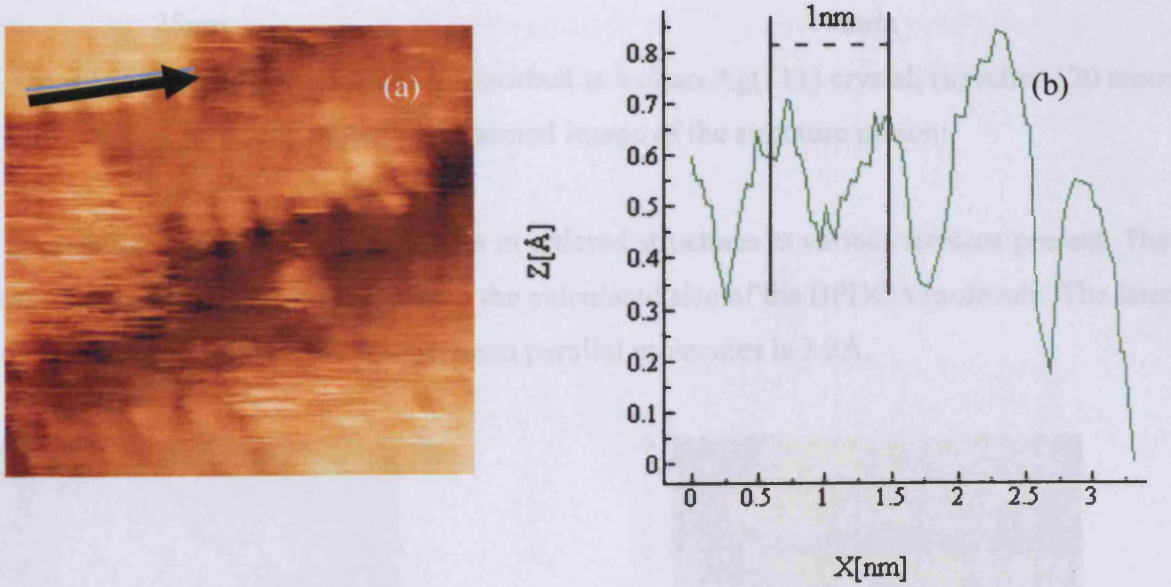

Fig. 8.13: STM images of BPDCA adsorbed at a clean Ag(111) crystal, (a) After 120 second exposure. (b) Line profile of the structure

Various terraces show some adsorption of BPDCA. As figure 13 shows, there is no long range order at the substrate. The size of the adsorbed species suggests that BPDCA adsorbs flat on the

Ag(111) surface. This can be associated with π-bonding orbitals pointing towards the substrate. This has been the case with the molecule 4-[(pyrid-4-yl-ethynyl)] benzoic acid on the Pd(110) surface [36] and other large organic molecules with extended π-systems such as oligothiophenes on Ag(111) [37-38]. The 3.2Å spacing of the ordered rows shown in the lower left hand corner of figure 14 (a) suggest that it is a terrace of clean Ag(111). This adds to the conclusion that only a small concentration is present.

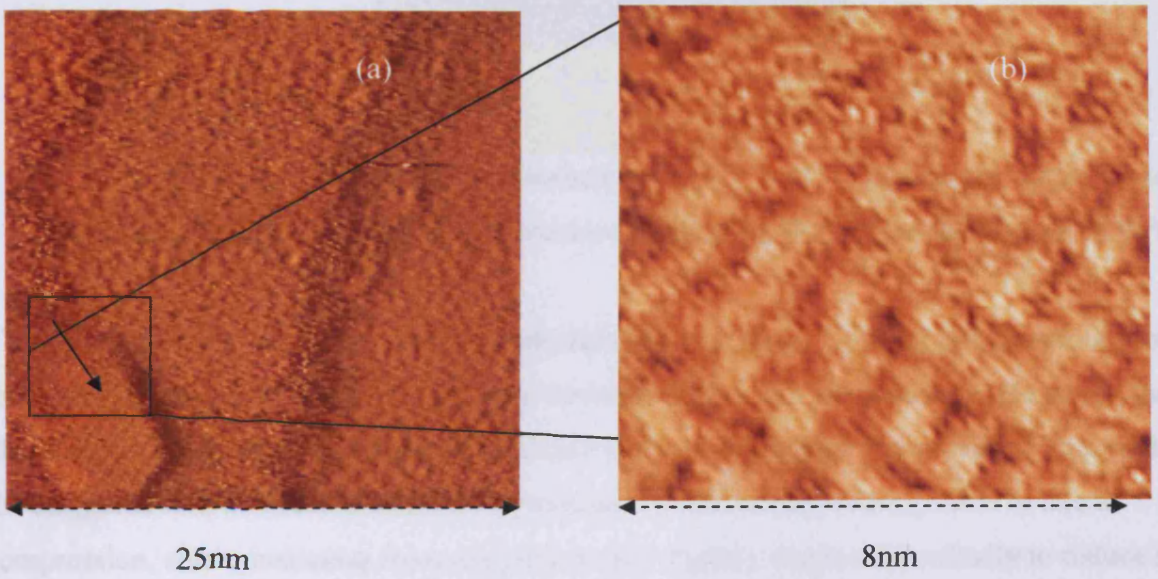

Fig. 14: STM images of BPDCA adsorbed at a clean Ag(111) crystal, (a) After 120 second exposure. (b) Zoomed image of the structure present.

An intermediate dose of BPDCA results in ordered structures at various terraces present. The measured size of the feature agree with the calculated size of the BPDCA molecule. The lateral spacing is 0.8nm and the distance between parallel molecules is 7.2Å.

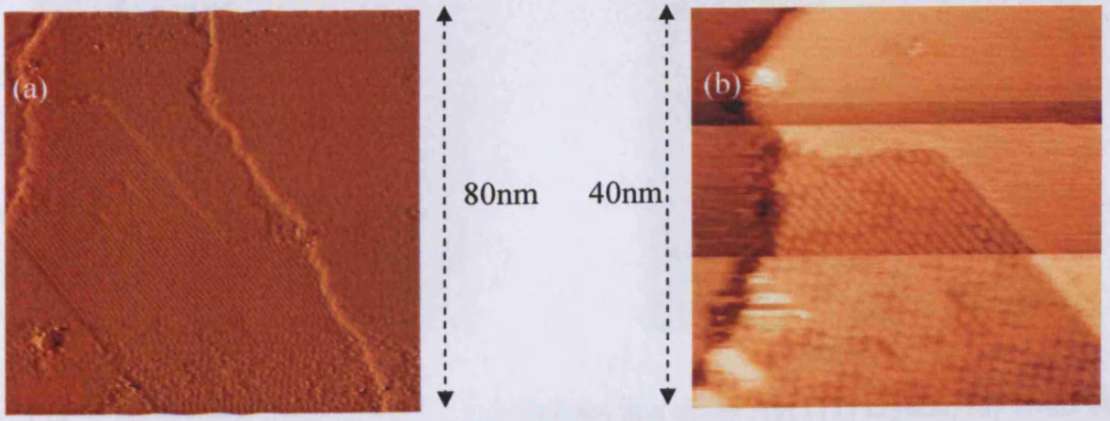

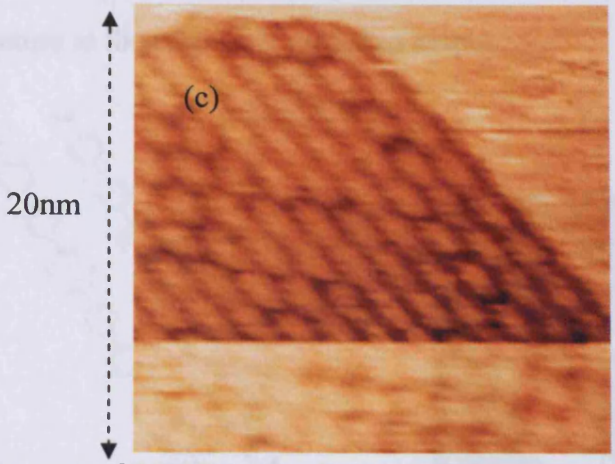

Fig. 8.15: STM images of BPDCA adsorbed at a clean Ag(111) crystal, (a) After 200 second exposure, (b) Zoomed image of the structure present, (c) Further zoomed image of BPDCA.

The parallel orientation of the acid prevents saturation of lateral bonding and therefore promotes 2 dimensional growth. H-bonding can occur between OH....O of the molecule. However, there is also the possibility of $\pi - \pi$ interactions occurring between parallel phenyl rings. This could cause the staggered lateral interaction but still promote 2 dimensional ordering. Due to lateral compression, some molecular rows are presumably slightly displaced vertically to reduce strain and therefore appear brighter in the STM images. The borders of the islands are usually straight; this is due to the fact that kinks are energetically unfavourable [39].

The structures were found occurring at directions that alternated at 60°. This follows the symmetry of the Ag(111) lattice.

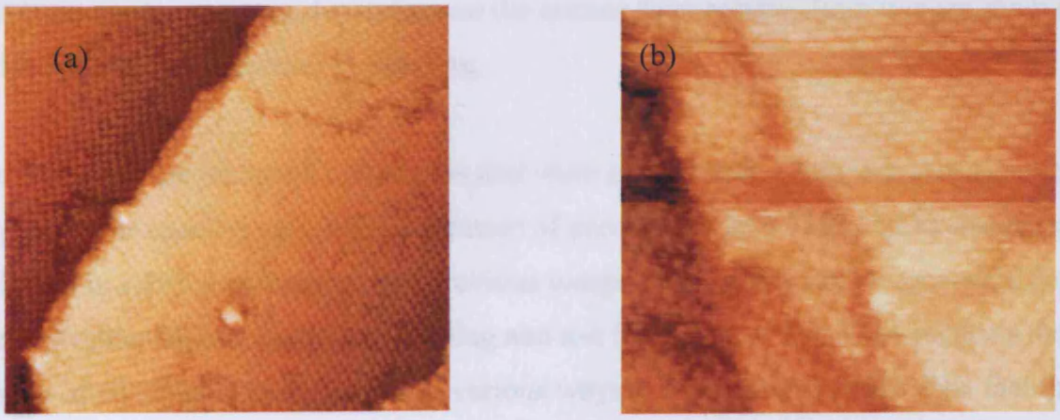

Fig. 8.16: STM images of BPDCA adsorbed at a clean Ag(111) crystal, (a) After 200 second exposure, (b) closer look at a terrace

A model of the structure at the surface is proposed below.

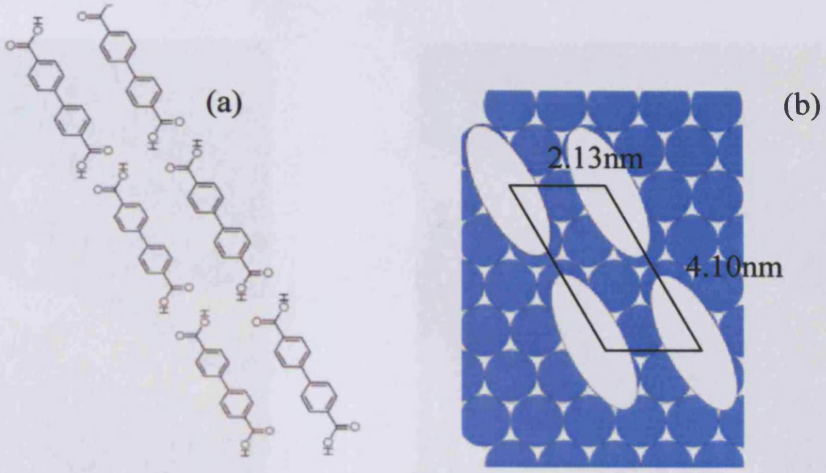

Fig. 8.17: A model of BPDCA at an Ag(111) surface; (a) H-bonded structure, (b) structure at an Ag(111) surface.

The proposed structure has many variations on the surface. In the above example, the benzene rings are placed at the on top site since several studies show this is preferred. However other possibilities such as bridging and hollow are possible but cannot be distinguished in this study.

8.14 STM of Higher concentration adsorption.

A coverage of a monolayer revealed two different structures present at the surface. These structures appear to occur depending on the terrace they occupy. Both images show a strong indication of intermolecular H-bonding.

The first structure occurred on terraces that were smaller than 12nm. An average of the lateral and perpendicular spacing gave a measurement of approximately 0.75nm. STM images show that the molecule is a different shape to the previous images. This shape can be accounted for the strongest intermolecular forces; hydrogen bonding and π-π interactions. The STM suggests that the electron density of BPDCA is being pulled in various ways to adjacent molecules. The fact that this is imaged gives an idea of the strength of the intermolecular forces at a weaker substrate. However, the structure was also found to be occurring at 60° angles consistent with the surface symmetry.

Again this suggests that even though the structures formed seem to totally depend on the intermolecular forces, the substrate still has some interaction.

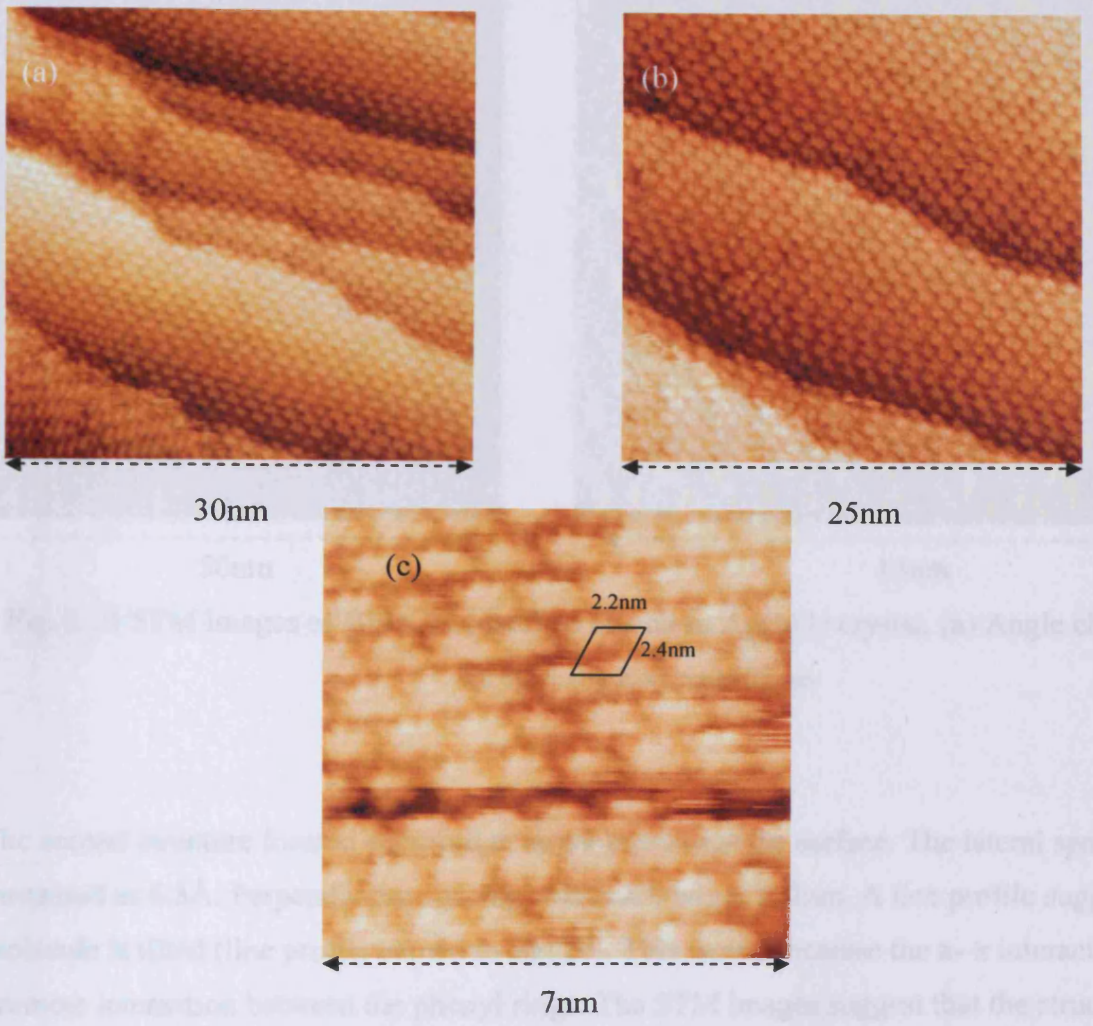

Fig. 8.18: STM images of BPDCA adsorbed at a clean Ag(111) crystal, (a) After 400 second exposure, (b) Zoomed image (c) indication of structure at a different angle.

The change in angle of adsorption at the substrate can occur at different terraces. However, STM has shown at numerous cases that an angle change can occur at the same terrace. The following image shows numerous changes in angle of adsorption. Height measurements suggest that this occurs on the same terrace. It is therefore suggested that some defect at the substrate causes the change, such as a screw dislocation or just the way islands develop. The angle changes occur at 60° intervals. Again this is due to the interaction of the substrate. Another possibility of the change in angles could be caused by two domains growing together. This would also result in an angle change as is seen in the STM images.

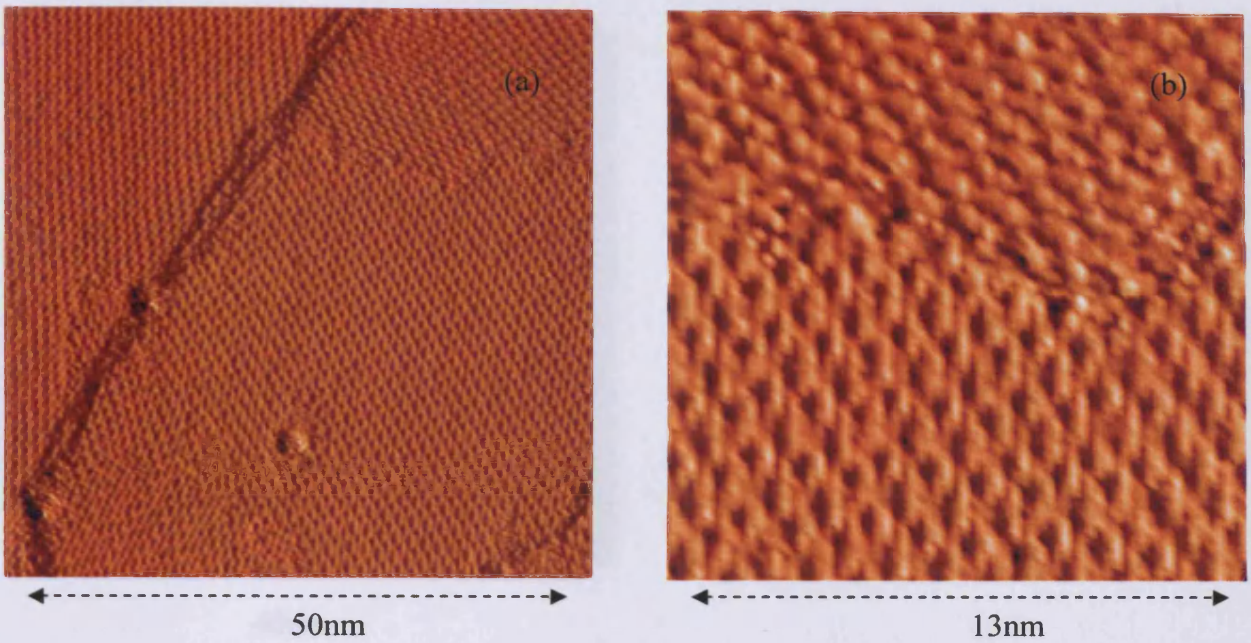

Fig. 8.19 STM images of BPDCA adsorbed at a clean Ag(111) crystal, (a) Angle changes at the surface, (b) Zoomed image

The second structure formed occurred at larger terraces at the surface. The lateral spacing was measured as 6.5Å. Perpendicular spacing was much larger at 2nm. A line profile suggests that the molecule is tilted (line profile shown in fig. 20). This would increase the π- π interactions and promote interaction between the phenyl rings. The STM images suggest that the structure is dominated by hydrogen bonding. This is indicated in the images as there appears to be electron density between molecules. This is shown clearly on numerous images. The length of this proposed hydrogen bond is 2.7Å. This is comparable with calculated hydrogen bond lengths.

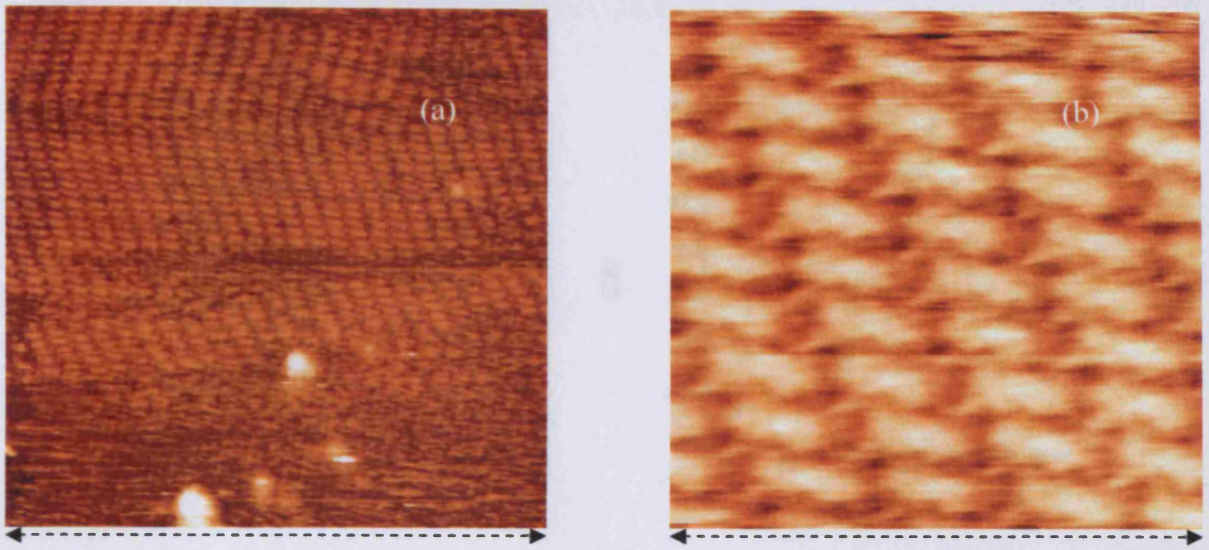

Fig. 8.20: STM images of BPDCA adsorbed at a clean Ag(111) crystal, (a) After 350 second exposure, (b) Zoomed image.

A model of the proposed structure is shown below. The lateral spacing has increased between molecules. However, STM suggests that the interaction between molecules is stronger due to the imaging of the electron density. π-π interactions are occurring between the phenyl rings of the molecule BPDCA.

STM allowed a closer look at the molecule at the surface. The image below shows the two phenyl rings contained in the molecule. A line profile shows that one phenyl ring is 0.15Å higher than the other. This would add to the evidence that the molecule is tilted to allow stronger π-π interactions and therefore promote a three dimensional structure. Again, the substrate affects the structure as it occurs at the surface at 60° intervals.

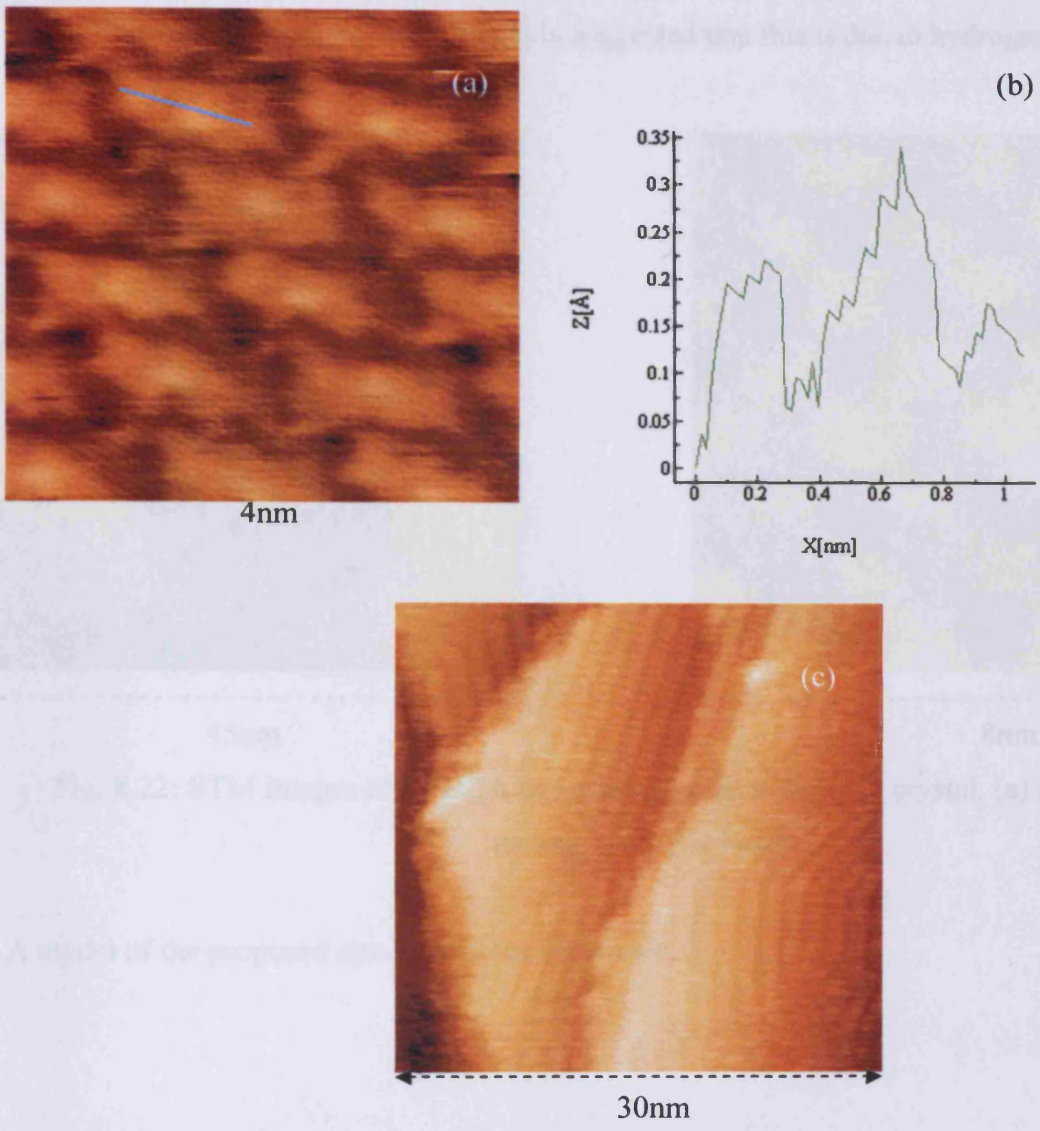

Fig. 8.21: STM images of BPDCA adsorbed at a clean Ag(111) crystal, (a)BPDCA molecule, (b) Line profile of BPDCA molecule, (c) direction of structures at the surface.

8.15 The effect of heating the surface to 500K

The XPS suggests that heating the surface results in molecular desorption. In the STM image heating coverages sub monolayer to 500K resulted in a slight change in the surface composition. The structure formed takes a "zig-zag" appearance. This may be due to substrate defects. The spacing between molecules has decreased and is the same in all directions. The effect of heat may

have caused the loss of a proton and resulted in a carboxylate adsorbed at the surface. However, the XPS saw no change in binding energy. The effect of heat has resulted in one BPDCA molecule interacting with four others, and again it is suggested that this is due to hydrogen bonding.

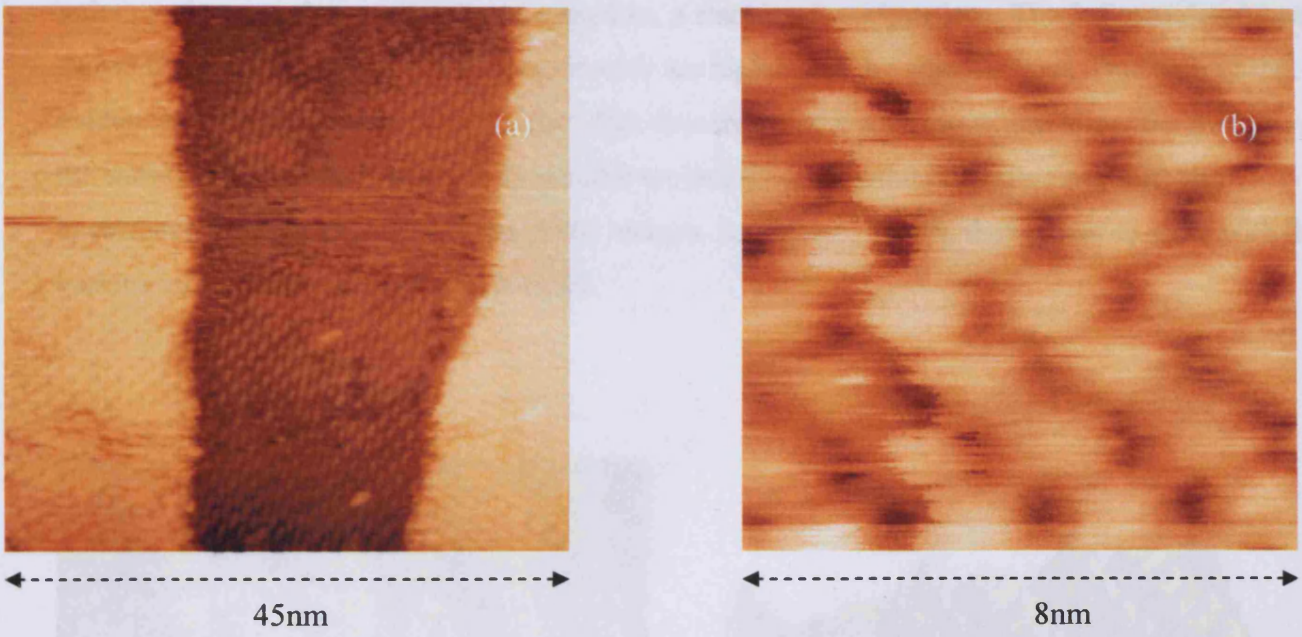

Fig. 8.22: STM images of BPDCA adsorbed at a clean Ag(111) crystal, (a) Structure before heating, (b) After heating.

A model of the proposed structure is shown below.

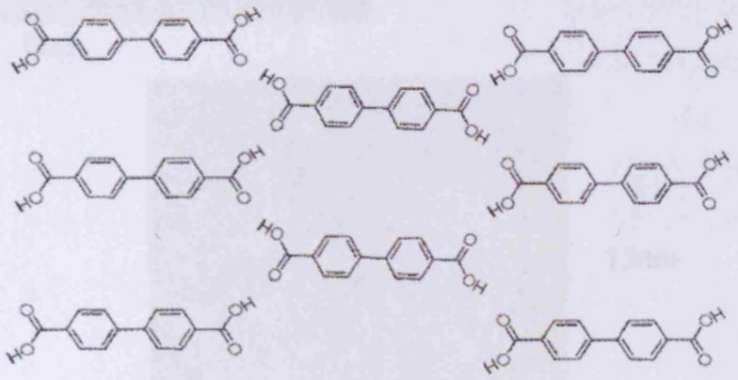

Fig. 8.23: A model of BPDCA at an Ag(111) surface; (a) H-bonded structure after heating the surface.

An intermittent structure was seen during the various experiments. This structure did not seem to be related to coverage, nor did it occur through the effect of heat. It seems that BPDCA is also able to form rows. The spacing between perpendicular atoms is very low. This would suggest that in order to accommodate a higher concentration, π stacking is taking place. The 3 dimensional image shows that the one row of BPDCA molecules are higher that the adjacent row. This adds to the evidence that π stacking is taking place. The occurrence of π stacking would allow the freedom of the carboxyl groups to interact with parallel molecules. This would therefore promote the occurrence of rows as is seen in the STM images. As figure c shows, these rows co-exist with the various more common structures formed.

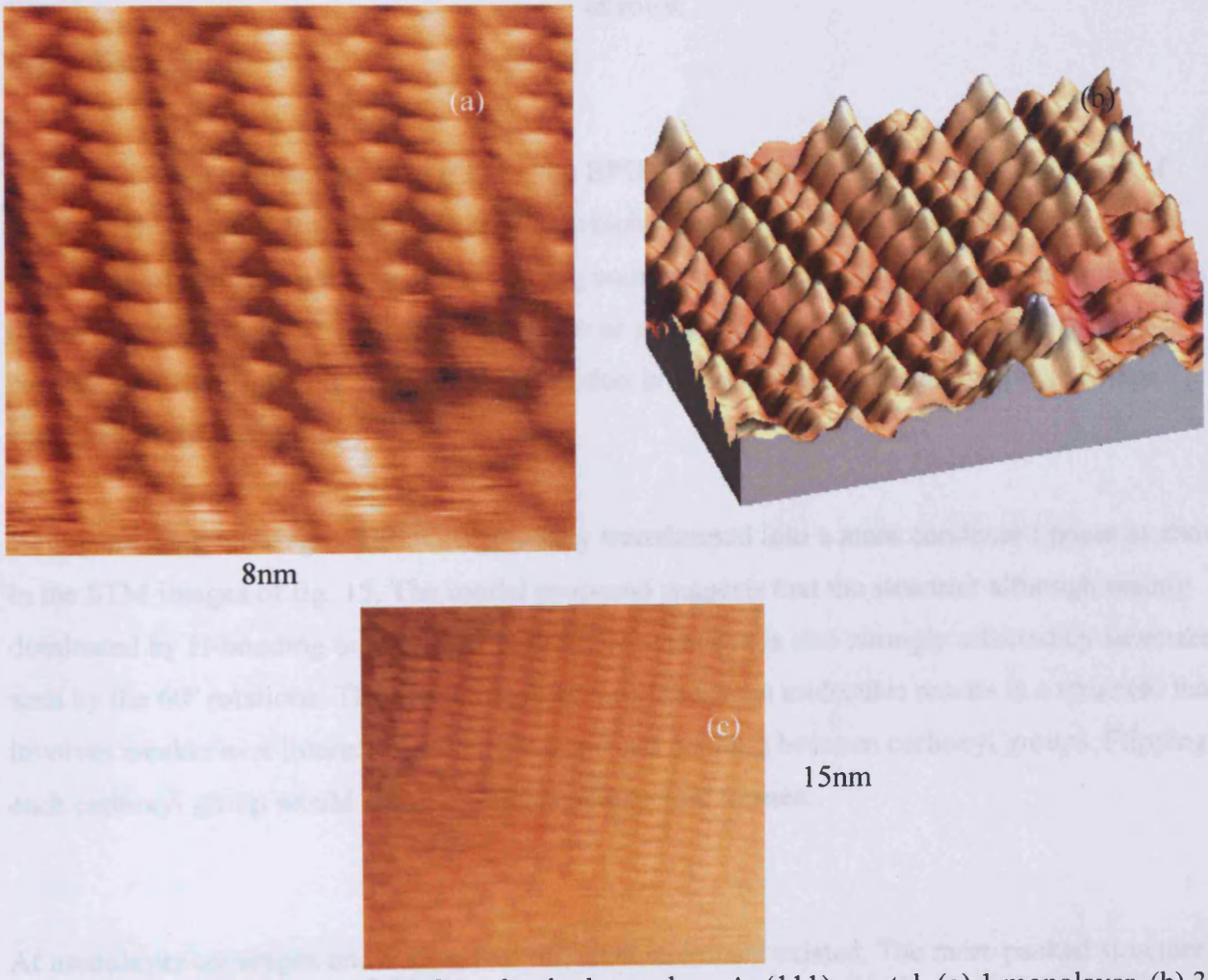

Fig. 8.24: STM images of BPDCA adsorbed at a clean Ag(111) crystal, (a) 1 monolayer, (b) 3D image of (a), (c) both structures present.

A model of this structure is shown below.

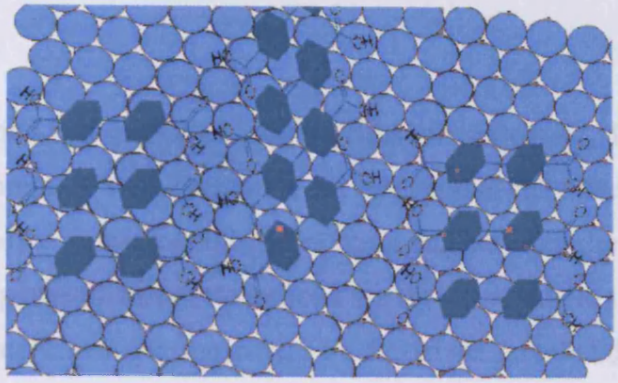

Fig. 8.25: A model of BPDCA at an Ag(111) surface; (a) Structure which results in the formation of rows.

8.16 Discussion

At sub monolayer coverages on Ag(111), the BPDCA molecules formed at the step edges of terraces. There were also molecules imaged which showed no order at certain terraces. The interaction of BPDCA with Ag(111) is strong enough to allow the STM to image the molecules at the surface regardless of whether a monolayer or a packed small island is present. This is in contrast to melamine. This increase in interaction is due to the presence of two phenyl rings contained in the molecule.

With increasing coverages, BPDCA gradually transformed into a more condensed phase as shown in the STM images of fig. 15. The model proposed suggests that the structure although mainly dominated by H-bonding between the carboxylic acids and is also strongly affected by substrate as seen by the 60° rotations. The intermolecular forces between molecules results in a structure that involves weaker π- π interactions, and head to head bonding between carboxyl groups. Flipping each carboxyl group would result in the linear structure formed.

At monolayer coverages and above, two different structures existed. The more packed structure shown in figure 17 was the result of six intermolecular bonds. It is proposed that these interactions occur due to the two negative oxygen atoms and the positive carbon contained in the carbonyl

group. This would occur on each end of the molecule and result in a total of 6 intermolecular bonds. This could promote delocalization in the molecule and therefore would decrease the π interactions. This is seen in the structure as the adsorption results in the molecules flat at the surface.

The second structure formed had increased spacing between molecules. This may have been due to the fact that it was only found on larger terraces. On each end of the molecule, the electron density is imaged and suggests only one hydrogen bond is occurring between the head of each molecule. It can be suggested that the perpendicular interactions are therefore due to the π interactions between adjacent molecules. The increased spacing would be due to the fact that the π interactions are much weaker that the hydrogen bond. The imaged electron density was also slightly larger than in figure 17 and therefore the molecule did not delocalise as much as previously. A model of the structure is proposed below.

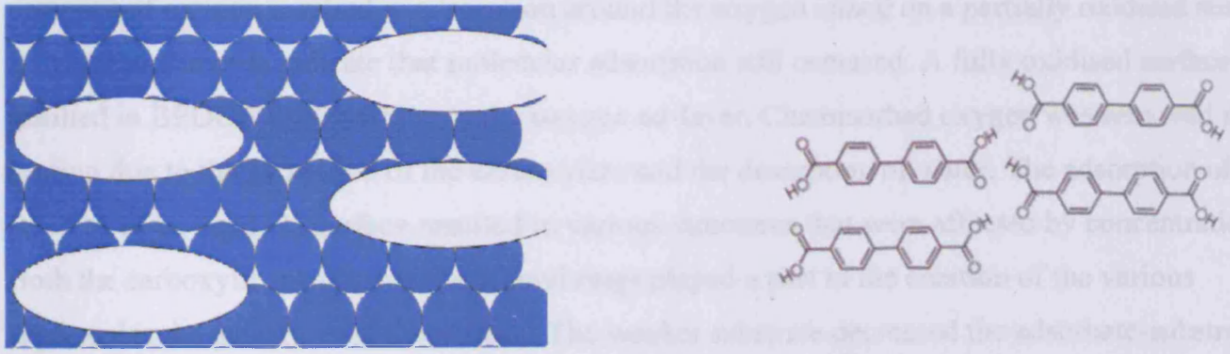

Fig. 8.26: A model of BPDCA at an Ag(111) surface on a larger terrace.

The XPS concentrations suggested that heating the surface resulted in molecular desorption. The STM resulted in a structure that was different to the previous concentrations. The closer packed structure resulted from the interaction of one carbonyl group with the other. It is suggested that this is the most energetically stable structure present at the surface.

It was seen that BPDCA also formed rows. This structure allowed the greatest concentration at the surface. However, due to the fact it was the rarest structure found at the surface suggests that it is the most energetically unstable. It is proposed that the structure is the result of one row of BPDCA molecules being stood up at the surface instead of lying perpendicular. This results in π-stacking

with the adjacent flat lying row. This π-stacking allows the freedom of the carbonyl groups and therefore promotes the formation of rows. It is unknown why this structure forms at the surface. The most probable cause is concentration. In order to allow more BPDCA molecules to adsorb at the surface, the molecules adopt a more densely packed structure which allows for a greater concentration.

8.17 Conclusion

The room temperature interaction of BPDCA with clean, partially oxidised and fully oxidised Cu(110) single crystal, and clean Ag(111) single crystal surfaces have been investigated using STM and XPS. Chemisorption occurred at a clean Cu(110) surface. The XPS indicated a second layer species. This was removed using heat. The STM saw some order created by intermolecular forces between the carboxyl groups and the phenyl rings. Predominantly, the substrate-adsorbate interaction was too strong for any supramolecular structures to be formed. Exposure in the presence of oxygen resulted in adsorption around the oxygen island on a partially oxidised surface. STM measurements indicate that molecular adsorption still occurred. A fully oxidised surface resulted in BPDCA physisorbing to the oxygen ad-layer. Chemisorbed oxygen was removed upon heating due to the formation of the carboxylate and the desorption of water. The adsorption of BPDCA at an Ag(111) surface resulted in various structures that were affected by concentration. Both the carboxylic groups and the phenyl rings played a part in the creation of the various supramolecular structures at the surface. The weaker substrate decreased the adsorbate-substrate interactions and allowed more freedom for intermolecular interactions. Upon warming, a different structure was formed. The model suggests that heating removes the π-π interactions.

8.18 References

[1] T. S. Asgaard, *J. Catal.*, 156 (1995) 229-242.

[2] S. Bao, G. Liu, D.P. Woodru., *Surf. Sci.* 203 (1998) 89.

[3] M. Pascal, C.L.A. Lamont, M. Kittel, J.T. Hoeft, R. Terborg, M. Polcik, J.H. Kang, R. Toomes, D.P. Woodru ., *Surf. Sci.* 492 (2001) 285.

[4] F. M. Leibsle, S. Haq, B. G. Frederick, M. Bowker, and N. V. Richardson, *Surf. Sci.*, 343 (1995) 1175.

[5] M. Bowker, E. Rowbotham, F. M. Leibsle, and S. Haq, *Surf. Sci.* 349 (1996) 97.

[6] M. Bowker and R. J. Madix, *Surf. Sci.* 102 (1981) 542.

[7] D.S. Martin, R.J. Cole, S. Haq, *Surf. Sci.* 539 (2003) 171–181.

[8] A. Dmitriev, N. Lin, J. Weckesser, J. V. Barth, and K. Kern, *J. Phys. Chem. B* 106 (2002) 6907-6912.

[9] C. D. Bain, E. B. Troughton, Y. T. Tao, J. Evall, G. M. Whitesides, R. G. Nuzzo, *J. Am. Chem. Soc.* 111(1989) 321.

[10] L. Scudiero, D. E. Barlow, U. Mazur, K. W. Hipps, *J. Am. Chem.Soc.* 123 (2001) 4073.

[11] R. W. Wagner, J. S. Lindsey, J. Seth, V. Palaniappan, D. F. Bocian, *J. Am. Chem. Soc.* 118 (1996) 3996.

[12] N. Lin, A. Dmitriev, J. Weckesser, J. V. Barth, K. Kern, *Angew. Chem., Int. Ed.* 41 (2002) 4779.

[13] G. A. Jeffrey,. "An introduction to Hydrogen bonding", oxford university press, 1997.

[14] J. Lipkowski, P. N. Ross, Eds,. " Adsorption of Molecules at Metal Surfaces", VCH Publishers: New York, 1992.

[15] D. L. Allara, R. G. Nuzzo, *Langmuir,* 1 (1985) 45.

[16] Johannes V. Barth, Jens Weckesser, Giancarlo Trimarchi, Masha Vladimirova, Alessandro De Vita,Chengzhi Cai, Harald Brune, Peter Gunter, □and Klaus Kern, *J. AM. Chem. Soc,* 124 (2002) 7991-8000.

[17] Sylvain Clair, Stephane Pons, Ari P. Seitsonen, Harald Brune, Klaus Kern, and Johannes V. Barth, *J. Phys. Chem. B* 108 *(2004)* 14585-14590.

[18] Bo Xu, Bindhu Varughese, Diane Evans, and Janet Ruett-Robey, *J. Phys. Chem. B*, 110 (2006) 1271-1276.

[19] R. W. Joyner and M. W. Roberts, *Proc. R. Soc. Lond. A.* 250 (1976) 107.

[20] M. Bowker and R. J. Madix, *Surf. Sci.* 116 (1982) 549.

[21] J. Hasselstrom, O. Karis, M. Weinelt, N. Wassdahl, A. Nilson, M. Nyberg, L. G. M. Patterson, M. G. Samant and J. Stohr, *Surf. Sci.* 407 (1998) 221.

[22] D. J. Morgan, PhD Thesis, University of Wales, Cardiff, 2002.

[23] A. F. Carley, P. R. Davies, M. W. Roberts, *Proc. R. Soc. Lond. A.* 250 (1976) 107.

[24] B. G. Frederick, F. M. Leibsle, S. Haq, N. V. Richardson, *Surf. Re*V. *Lett. 3* (1996) 1523.

[25] N . Lin, A. Dmitriev, J. Weckesser, J. V. Barth, K. Kern,. Angew. *Chem. Int. Ed* , 114 (2002) 4973.

[26] P . Messina, A. Dmitriev, N. Lin, H. Spillmann, M. Abel, J. V. Barth, K. Kern, *J. Am. Chem. Soc.* 124 (2002) 14.

[27] C. Perry, S. Haq, B. G. Frederick, N. V. Richardson, *Surf. Sci.* 409 (1998) 512.

[28] R. W. Joyner and M. W. Roberts, *Proc. R. soc. Lond. A.* 250 (1976) 107.

[29] M. Bowker and R.J. Madix, *Surf. Sci.* 95 (1980) 190.

[30] J. Weckesser, J. V. Barth, K. Kern, *J. Chem. Phys.* 10 (1999) 5351.

[31] P. Sautet, *Chem. ReV.* **1997**, 97 (1997) 1097.

[32] B. G. Frederick, F. M. Leibsle, S. Haq, N. V Richardson, *Surf. ReV. Lett.* 3 (1996) 1523.

[33] J. Stohr, *NEXAFS Spectroscopy*; Springer-Verlag, 25 (1991).

[34] A. F. Lee, K. Wilson, R. M. Lambert, A. Goldoni, A. Baraldi, G. Paolucci, *J. Phys. Chem. B* 104 (2000) 11729.

[35] H. M. Liao, R. N. Sodhi, T. W. Coyle, *J. Vac. Sci. Technol., A,* 11 (1993) 2681.

[36] J. Weckesser, J. V. Barth, K. Kern, *J. Chem. Phys.* 110 (1999) 5351-5354.

[37] E. Umbach, M. Sokolowiski, R. Fink, *R. Appl. Phys. A* 63 (1996) 565-576.

[38] A. Soukopp, K. Glocker, P. Kraft, S. Schmitt, M. Sokolowiski, E. Umbach, E. Mena-Osteritz, P. Bauerle, E. Hadicke, *Phys Rev B* 58 (1998) 13882-13894.

[39] J. V. Barth, J. Weckesser, N. Lin, A. Dmitriev, K. Kern, *Appl. Phys. A* 76 (2003) 645-652.

Thesis Summary

Aniline reacts with a partially oxidised Cu(110) surface which results in the desorption of water. An ordered phenyl imide layer is formed at the surface. This can be described by three unit meshes - $\begin{pmatrix} 4 & 0 \\ 2 & 2 \end{pmatrix}$, $\begin{pmatrix} 4 & 0 \\ -1 & 2 \end{pmatrix}$ and $\begin{pmatrix} 4 & 0 \\ 1 & 2 \end{pmatrix}$. A co-adsorption of aniline and oxygen results in two structures, described by $\begin{pmatrix} 3 & 0 \\ -1 & 2 \end{pmatrix}$ and $\begin{pmatrix} 3 & 0 \\ 1 & 2 \end{pmatrix}$ unit meshes. In both cases it was seen that the XPS concentration was double the concentration as predicted by STM. It is proposed that this was due to pi-stacking of the phenyl rings.

The interaction of malonyl dichloride with a clean Cu(110) surface resulted in no adsorption. Reacting malonyl dichloride with a partially oxidised surface results in corrugated rows orientated in the <100> direction appearing. The concentration of chlorine is greater than that of a $Cl_{(a)}$ c(2x2) structure. This increase in concentration may be due to the formation of $CuCl_2$. XPS does not show evidence to distinguish between CuCl and $CuCl_2$ contrary to previous literature; however this could be due to the fact that there is such a low concentration present.

Melamine was adsorbed at both an Ag(111) and a Cu(110) surface. At a Cu(110) surface the STM imaged features that showed order in the <110> direction. It can therefore be concluded that substrate-adsorbate interactions were stronger than molecular interactions. This is supported by the more ordered second layer structure.

At an Ag(111) surface the substrate had some effect on the structure as a distorted hexagon was formed. Increasing the concentration to more than a monolayer resulted in a less distorted hexagonal structure. Cesium was exposed to the structure formed at an Ag(111) surface. Cesium atoms adsorbed on the supramolecular network created by melamine. The stability of cesium was not as great as that of the network created by melamine molecules as the effect of heat at the surface resulted in the removal of the cesium atoms or diffusion of caesium through to the substrate.

The room temperature interaction of BPDCA with clean, partially oxidised and fully oxidised Cu(110) single crystal, and clean Ag(111) single crystal surfaces have been investigated using STM and XPS. Chemisorption occurred at a clean Cu(110) surface. Predominantly, the substrate-adsorbate interaction was too strong for any supramolecular structures to be formed. Exposure in the presence of oxygen resulted in adsorption around the oxygen island on a partially oxidised surface.

At an Ag(111) surface resulted in various structures that were affected by concentration. Both the carboxylic groups and the phenyl rings played a part in the creation of the various supramolecular structures at the surface.